IfE Schriftenreihe · Heft 58

Tino Aboumahboub

Modeling and Optimization of the Global Electricity Generation System with High Shares of Fluctuating Renewable Energy Sources

Herausgegeben von:
Lehrstuhl für Energiewirtschaft und Anwendungstechnik
Technische Universität München
Ordinarius: Prof. Dr.-Ing. Ulrich Wagner
Komm. Leiter: Prof. Dr. rer. nat. Thomas Hamacher

TECHNISCHE UNIVERSITÄT MÜNCHEN

Lehrstuhl für Energiewirtschaft und Anwendungstechnik

Modeling and Optimization of the Global Electricity Generation System with High Shares of Fluctuating Renewable Energy Sources

Tino Aboumahboub

Vollständiger Abdruck der von der Fakultät für Elektrotechnik und Informationstechnik der Technischen Universität München zur Erlangung des akademischen Grades eines

Doktor-Ingenieurs

genehmigten Dissertation.

Vorsitzender: Univ.-Prof. Dr.-Ing. Josef S. Kindersberger

Prüfer der Dissertation:

1. Univ.-Prof. Dr.-Ing. Ulrich Wagner
2. Univ.-Prof. Dr. Reinhard Haas, Technische Universität Wien / Österreich

Die Dissertation wurde am 05.10.2011 bei der Technischen Universität München eingereicht und durch die Fakultät für Elektrotechnik und Informationstechnik am 17.02.2012 angenommen.

ISBN 978-3-933283-54-2

1. Auflage 2012

Vertrieb: E & M Energie & Management Verlagsgesellschaft mbH
Schloss Mühlfeld 20, 82211 Herrsching
www.emvg.de, info@emvg.de

Druck: Uni-Druck, www.uni-druck.com

Acknowledgements

I am very grateful to Prof. Ulrich Wagner because of giving me the opportunity to do this Ph.D. project. This opportunity has opened me new perspectives. It has led to the development of my scientific knowledge and my social involvements. I am always indebted to him for what I could learn, develop and contribute to the scientific world in these three very good years as well as the entire positive influences on my prospective life.

I would like to thank my other supervisors at TU München: Prof. Thomas Hamacher and Dr. Peter Tzscheutschler. I am very thankful to Prof. Hamacher and Dr. Tzscheutschler because of their continuous and insightful feedback on my Ph.D. project. I am very indebted to Dr. Peter Tzscheutschler because of providing me with the solar irradiation data and evaluating the global potential of solar thermal electricity production that enabled me to start my own research project. I furthermore acknowledge the highly insightful feedback of my advisors at KU Leuven: Prof. William D'haeseleer and Dr. E. Delarue. I am very thankful to Erik because of his kindness during my stay as a visiting scholar at KU Leuven and his innovative suggestions for the improvement of my optimization model. I am very thankful to Dr. Markus Biberacher because of his kindness as well as the valuable insights that I got from his Ph.D. thesis. I would like also to thank Dr. Frank Voß at the Center for Environmental Systems of the University of Kassel because of providing me with the water availability data and his help to gain access to the results of the WaterGAP model.

I furthermore acknowledge the highly useful and detailed feedback of all members of the examination committee on the thesis manuscript.

Then, I would like to thank everyone at the Institute for Energy Economy and Application Technology (IfE). My special thanks go to Mr. Heinrich Kleeberger for providing me with the facilities to perform the calculations, Ms. Merling-Walter, Ms. Gretz, Dr. Tobias Massier, and Dr. Isabell Nemeth. I am thankful to my fellow Ph.D. students and colleagues for the nice working environment and the pleasure moments: Philipp Kuhn, Max Kühne, Roman Burhenne, Johannes Dorfner, Matthias Huber, Karl Janker, Milica Grahovac, and Christian Heilek.

And last, best...I would like to thank my mother because of her true love and support. I would like also to thank my aunts and my cousin Himan because of their true love.

Abstract

The proposed emissions reduction targets and the scarcity of fossil fuel resources necessitate the transition of the fossil-fuel based electricity generation system of today towards a renewable-based electricity supply. Technical potential for electricity production from solar and wind energy is adequately high to cover the worldwide electricity demand. However, due to fluctuating patterns and geographical dispersion of the primary energy source, challenges arise when integrating a high share of solar and wind power into the electricity system.

To analyze worldwide influences of large-scale integration of solar and wind power into the electricity generation system and to investigate the required adaptations, a global multi-regional electricity system investment and production optimization model is developed in this thesis, deploying the linear programming optimization method. The modeling approach is a combination of an adequately precise geographical coverage with a high temporal resolution. The model properly mimics geographical dependencies of energy supply and demand as well as short-term intermittent patterns of fluctuating renewable energy sources (FRES), i.e. solar and wind energy. Technical restrictions of dispatchable power plants are modeled at a technology level. These allow a detailed, realistic analysis of the utilization of FRES in a prospective global electricity generation system.

Through minimization of overall system costs, promising sites for renewable power production, optimal generation capacities and power production mix, and operation schedule of power plants on a technology level are determined. The required capacities for energy storage and for inter-regional transmission of electricity and hydrogen are quantified under different framework conditions. CO_2 emissions and the certificate price are also determined by this optimization model. Examination of the simulation results versus a real power generation mix and comparison of the obtained results with the solution proposed by different methodologies and electricity system models validate the developed optimization model.

Through applying the developed methodology, optimal configuration of a prospective global electricity supply system adapted to an increasing generation from FRES is investigated under various framework conditions. The influence of an ideal globally-interconnected electricity supply structure and the role of energy storage systems to mitigate negative consequences of solar and wind integration on the operation of power system are studied. Furthermore, this work includes a detailed analysis of influencing factors of CO_2 emissions of the world electricity supply sector. While the potential for reducing CO_2 emissions in the short-term, i.e. by means of fuel switching, is evaluated, long-term CO_2 emissions abatement and required structural adaptations towards a low-carbon electricity supply system are studied while a special focus is laid on the influences caused by the integration of solar and wind power and the role of an ideal global grid.

Contents

1 Introduction

1.1 Towards an emission free electricity generation system

The world is confronting challenging issues of climate change. CO_2 is one of the main contributors in the global warming phenomenon; its concentration has risen from a pre-industrial level of about 280 ppmv to more than 380 ppmv [1]. Although industrialized world regions have initiated climate policies, scenario studies indicate that greenhouse gas (GHG) emissions are likely to increase in the future in most world regions [2]. To ensure that carbon dioxide concentrations stabilize at target levels proposed in [1, 3], a significant reduction of global emissions is required. This can only be achieved if efficient economical and political incentives are set up. It has been shown that without a near-term introduction of supportive and effective policy actions by governments, annual global GHG emissions are projected to rise from 9.7 Gt CO_2-eq in 2000 to 36.7 Gt CO_2-eq in 2030 [3]. The energy-related CO_2 emissions, mainly from fossil fuel combustion, are projected to grow 40-110% between 2000 and 2030 [3].

The electricity sector can play an important role in the reduction of anthropogenic GHG emissions. Around 40% of global GHG emissions fall on the electricity sector [4, 5]. Today, the electricity system is mainly fossil-fuel based and centralized while power transmission and energy storage play a minor role. Regarding the considerable contribution of the power sector, substantial changes must be made in its present structure. Promotion of low emitting or emission-free technologies is of high priority to meet the proposed emissions reduction targets and to deal with the scarcity of fossil fuel resources. Projections of the global energy mix in integrated assessment models show that within the coming century a significant share of renewable energies is required to achieve stabilization targets of 400 and 450 ppm CO_2-eq; there, mostly solar and wind energy are proposed as well as biomass as promising energy resources [6].

The Photovoltaic (PV) sector has been continuously developing over the last decade and is forecasted to follow this trend in the future coming years. The worldwide cumulative capacity reached to 23 GW with an additional increase of about 7.2 GW in 2009 [7, 8]. Today, Europe is leading the way with a total capacity of around 16 GW by the end of 2009. Germany with a cumulative capacity of 10 GW remains the world's largest market. Outside Europe, Japan positions itself as the third largest market with a cumulative capacity of 484 MW while the U.S. with around 475 MW installed capacity in 2009 is considered as a potential leading market in the future. China and India are also expected to show impressive growth in the next five years [8].

After almost 20 years of silence, in the early years of the new millennium, Concentrating Solar Power (CSP) gained interest again, and new solar thermal power plants have been built in Europe and USA. At present, the total worldwide capacity is approximately 655 MW and is producing 1400 GWh of electricity through a year. Apart from USA and Spain, other countries, where CSP plants are going to be built, include Australia, India, Central Asia, Mexico, and the Mediterranean countries like Italy, France, Greece, Turkey, Morocco, Libya, Algeria, Egypt, and Israel [9].

Wind power has become the fastest growing renewable technology, and this development is expected to continue. The total installed capacity reached to 158 GW with an additional

increase of 37.5 GW in 2009 [10]. Europe is leading the way with a total capacity of 76 GW by the end of 2009; USA with a total installed capacity of 35 GW followed by Germany with a cumulative capacity of 26 GW and China with 25 GW installed capacity include the world's largest markets [10]. This high growth rate is forecasted to continue in the coming years. According to the reference scenario of the Global Wind Energy Council (GWEC), the total installed capacity of wind power is projected to reach 415 GW in 2020 and rise to 573 GW by 2030. This is correspondent to an electricity production of 1019 TWh and 1405 TWh through a year, respectively [11]. In OECD Europe, the total capacity is forecasted to reach 184 GW in 2020 and rise to 234 GW by 2030 [11].

Technical potential of electricity production from renewable energy sources is adequately high to cover the worldwide electricity demand [12-17]. Biomass is geographically flexible; it can be transported to the regions, having a high level of electricity demand [18]. However, other renewable energy sources such as wind and solar energy are only available at specific sites and time slices. These sites are not necessarily located in proximity to densely populated areas, where the demand for electricity is high [12, 13, 19]. Thus, competitiveness of these resources in electricity markets depends on one hand on the distance between the areas of high potential and the load centers as well as the accessible technologies for energy transport. Additionally, temporal fluctuations of these energy resources challenge their integration into the power system even further as these cannot be controlled and dispatched at the same level of conventional generation technologies. Indeed, variability of fluctuating renewable energy sources (FRES), i.e., solar and wind energy, has raised concerns about their impacts on power system's reliability and costs. However, smoothening effects on their short-term variations, which can be realized within a dispersed generation structure, may provide a competitive framework for their deployment. A well interconnected network is thus a precondition to make an optimal usage of spatial de-correlations of FRES. Cross-border exchange of electricity enables capturing smoothening effects of geographical aggregation on variations of wind power generation and increases the capacity credit of wind power. Furthermore, bulk energy storage systems provide further balancing requirements and facilitate integrating a high share of solar energy into the electricity generation system of future. Another raised scenario is that of a future hydrogen economy. This vision implies that all energy needs are satisfied with hydrogen as a secondary energy carrier. For instance, in [20], an energy economy is proposed, which is dominated by hydrogen.

1.2 Research objective and scope of investigation

Large-scale integration of FRES into the power system introduces a wide range of challenges for the design and operating the power system. System impacts of these energy resources comprise different time scales ranging from a short-time scale, which includes balancing the system during the operational time scale (minutes to hours), and the long-term, which includes providing enough power and energy at peak load. The aspects of wind power that challenge operating the power system and are related to its variable output and limited predictability have been addressed in various studies (for instance, [21, 22]).

On a long-term horizon, however, integration of FRES affects investment decisions in electricity markets. Hence, structure of the power generation system and deployed technologies differ from the centralized, fossil-fuel based electricity generation system of today.

In this thesis, the focus is mainly laid on the capacity effects of FRES. The central objective is to analyze the influences of large-scale integration of solar and wind power on the structure of the electricity generation system. Regarding the concern about contribution of all parts of the world in an international movement towards an emission-free electricity supply system, it is relevant to study this issue on the worldwide scale. Interesting questions that are going to be addressed include:

- What is the optimal share and combination of FRES that can be integrated into a prospective global electricity generation system under different framework conditions?
- What is the optimal geographic distribution of solar and wind power plants?
- How much new capacity of dispatchable power plants must be installed?
- How does an ideal global grid look like and what are its benefits?
- How much energy storage capacity is required to facilitate integrating a high share of FRES into the power system?
- What are the influences of integrating different shares and combinations of solar and wind energy on the costs and environmental aspects of the global electricity generation system?

In this study, the structure of a prospective global electricity generation system, which integrates a high share of solar and wind energy, is to be optimized under different framework conditions. The influences of an ideal globally-interconnected electricity supply structure and the impacts of energy storage systems to mitigate negative consequences caused by the power system integration of FRES are analyzed and quantified. According to the aspects of interconnected power systems, integrating a high share of FRES, the design of a future global electricity supply system is a complex optimization problem. Supply of electricity must be equal to the demand at all time steps; physical links are required to transport electricity and hydrogen between the regions. Technical restrictions on the operation of power generation and storage systems must be addressed as well. Furthermore, regarding the temporal variations and geographical dependencies of FRES, a realistic analysis of their utilization can only be accomplished at a high temporal and geographical resolution. Thus, the applied methodology must allow a chronological simulation of short-term variations of FRES and of the electricity load. Geographical dependencies must also be taken into account. The role of all these system components has to be addressed within the entire power system and analyzed through an integrated approach instead of an isolated analysis of a system component at a detailed level.

1.3 Thesis outline

This thesis is divided into five parts. The thesis' overall structure is presented in Fig. 1.1. In chapter 2, an overview is given on different modeling techniques of electricity generation systems. Afterwards, the model, developed in this study to optimize investment and production in electricity generation systems with a high share of FRES, is elaborated. A new methodology is proposed to include technical details in linear investment planning models. A comparison of this methodology with a short-term operation optimization model is then presented.

Different data sources, used as input to the global electricity system optimization model, and approaches applied for their estimation are described in chapter 3.

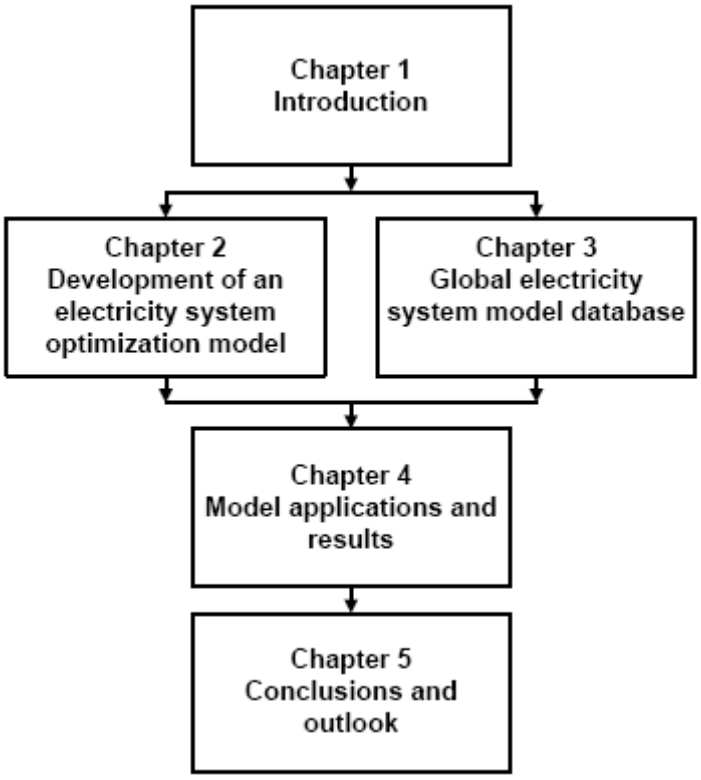

Fig. 1.1: Overview of chapters and thesis' structure

In chapter 4, applications of the developed methodology and the results of different scenarios are presented. The model is applied to investigate optimal configuration of a prospective global electricity supply system, integrating a high share of FRES. Represented questions are addressed under different framework conditions.

The starting point to analyze the system's behavior is the so-called "full renewable supply" scenario. This is to have a vision about the structure of an ideal, emission-free electricity generation system of future at global scale. The model is applied to investigate how in a prospective electricity supply structure, transporting electricity and hydrogen over long distances allows gaining profit from spatial de-correlations of fluctuating patterns of solar and wind power production. Influences of energy storage are studied as well.

Regarding the important debates on climate change issues and the potential role of the power sector, in the next step, a detailed analysis is performed on the influencing factors of CO_2 emissions of the global electricity supply system. At first, the global model is examined versus a real power generation mix and is calibrated through steps. Afterwards, while the potential for reducing CO_2 emissions in the short-term, i.e. by means of fuel switching, is evaluated, long-term abatement in the power sector and required adaptations are studied.

Finally, a two dimensional parameter study is performed by varying the penetration share of FRES and the renewable energy mix. The model is applied to investigate optimal configuration of a prospective, low emitting electricity supply system of the world adapted to an increasing

power production from FRES. Feasible integration shares and optimal combinations of solar and wind power are determined under different framework conditions. Capacity expansions of inter-regional power transmission lines, required investments in conventional power generation technologies and energy storage systems are studied at various shares and combinations of solar and wind power. Possible CO_2 emissions abatement due to an increasing power generation from FRES is then evaluated.

The last chapter includes a summary, conclusions, and recommendations for future research.

2 Development of an electricity system optimization model

2.1 Introduction

Starting in the 1990s, electricity markets around the world have been restructured, transforming the former monopolized sector into partially decentralized competitive market segments. Moreover, integration of FRES into the power system results in additional challenging issues due to their short-term variability and limited predictability. In pace with the liberalization process and the growing share of FRES, various modeling techniques have been developed and applied to simulate and optimize the behavior of electricity generation systems.

In this chapter, at first, there is an overview on different modeling techniques of electricity generation systems; contribution of this thesis to the development of such tools and approaches is then stated. Afterwards, the model, developed in this study to optimize investment and production in electricity generation systems with a high share of FRES, is described in detail.

2.2 Classification of modeling techniques

According to the classification made in [23], electricity system models can be categorized according to their structure into three types: optimization-based models, equilibrium models, and market simulation models. These can further be categorized according to the assumed market environment: perfect or imperfect competition.

Optimization models maximize or minimize a single objective subject to technical and economical constraints. On a single-firm level, the objective is typically a single firm's profit. If perfect competition exists, the market price is an exogenous variable while under imperfect competition the firm can influence market prices. The entire market can also be addressed by maximizing the total welfare or by minimizing the total system costs given a fixed level of demand. Obtained marginal prices are then representative for commodity price levels in perfect competitive markets. This problem can be formulated by employing optimization methods such as linear programming (LP) or mixed integer linear programming (MILP). This model type can further be differentiated into deterministic and stochastic models. Uncertainty of prices, of the power produced by FRES, and of the electricity load profile can be addressed, for instance, by multi-stage stochastic programming approach. The main advantage of optimization models is the availability of efficient optimization algorithms that are capable of solving large-scale problems with a multitude of technical and economical constraints. However, the focus on a single objective inhibits taking into account market behaviors of different players. On the other hand, in equilibrium and simulation models, an imperfect market environment is assumed, considering interactions of different competitors within the market. Market simulation models such as agent-based models represent market agents via specific assumptions and rules; thus, they allow a wide variety of strategic behaviors and market representations.

A trade-off exists for preferring one modeling approach to another, inspired by the required level of technical detail versus the desired degree of market competition. Regarding the focus of the present work on the impacts of large-scale integration of FRES on the structure of the electricity generation system, optimization models are of special interest as equilibrium approaches and

market simulation models are incapable of representing technical aspects of the power system at the required level.

The main distinction between optimization models can be made according to the considered time frame and the level of technical detail. Short-term models mainly focus on the operational aspects of the power system while in long-term planning models investment decisions are the main focus. Unit commitment and economic dispatch optimization models lie in the first category. They optimize activation levels of power plants over time to satisfy the demand at the lowest cost while technical restrictions of power plants are respected on a unit-basis and at a detailed level [21, 22]. However, capacity expansion planning and optimization of investment decisions are not covered in such models. On the other hand, long-term investment planning models aim at analyzing the evolution of the electricity supply sector under various boundary conditions. Different models of this kind have been developed so far, having different levels of geographical and temporal resolution [24, 25]. In this category of models, investment decisions are treated endogenously while operational constraints and technical restrictions of power plants and of the power transmission network are simplified or even neglected. The model typically runs over periods from 20 up to 40 years and is intended for long-term scenario analysis. However, temporal resolution of the model is mostly limited to a number of typical winter and summer days, which may be disaggregated into peak and non-peak periods. Hence, such models are incapable of a chronological simulation of short-term variations of the power produced from FRES and of the electricity demand. Furthermore, their coarse geographical resolution does not allow a detailed representation of the power transmission network structure and the growing need for capacity expansion of transmission lines in pace with an increasing generation from FRES.

The next criterion, which is proposed to distinguish between optimization models, is with regard to the approach applied to simulate the power transmission network. Transmission constraints can be modeled as follows: single-node, trade-based interconnections, direct current (DC) load flow, and alternative current (AC) load flow. A single-node model in fact neglects the grid; trade-based interconnection models take into account a limited interconnection capacity between the nodes, but do not account for Kirchhoff's and Ohm's laws. A full load flow describes both active and reactive power flows. A simplified variant of a full load flow is called DC load flow. This approach has been widely applied in electricity system optimization models as it assumes that a linear relationship exists between the flows over lines and the injections in nodes [21].

Different mathematical approaches are applied in long-term investment planning and short-term operation optimization models. For an overview of algorithms see [21-31]. These approaches are mainly differentiated into mathematical programming approaches and heuristics.

Heuristic methods are characterized with a low calculation time. They have been applied to solve large unit commitment (UC) problems [28-30]. However, with applying such methods, optimality of the solution cannot be guaranteed. Heuristic methods are in general not suitable for solving sophisticated problems with complex interactions between system components [21, 27]. Enhancements are fuzzy logic approaches, artificial neural networks, and genetic algorithms [31].

In contrast, mathematical programming approaches guarantee the optimality. Mathematical programming (or optimization theory) is that branch of mathematical approaches for maximizing

or minimizing an objective function subject to linear, non-linear and integer constraints on variables. In general, two groups of methodologies exist, either generating a consistent solution (e.g. linear programming) or using a decomposition of the optimization problem, where partial problems are solved separately in order to reduce the overall complexity. Widely used approaches include linear programming, mixed integer linear programming, dynamic programming, and Lagrangian relaxation.

Linear programming (LP) is concerned with maximization or minimization of a linear objective function subject to linear equality and inequality constraints [32]. The simplex algorithm, developed by George Dantzig in 1947, is initiated with a system of equations in canonical form with respect to basic variables; it solves LP problems by moving along the boundaries from one vertex (extreme point) to the next. The simplex method, which is used in all commercial LP solvers, is not a polynomial-time algorithm. The calculation time grows exponentially with the size of the input [33]. An Interior-point algorithm is a polynomial-time algorithm that improves a feasible interior solution point of the linear problem by steps through the interior, rather than improving by steps around the boundary of the feasible region, as the classical simplex algorithm does. In general, LP method is suitable for formulating large-scale sophisticated problems. If it is well-defined in the sense that it is feasible and does not have unbounded optimal value, the optimal solution is guaranteed. However, solving linear programming problems is memory intensive. This method has been widely used in large-scale electricity system investment planning models [24, 25, 26, 27, 34, 35].

Mixed integer linear programming (MILP) is a powerful approach that uses binary variables to approximate non-linear functions in a discrete form [33]. This operational research method consists of an objective function (typically a cost minimization) as a function of parameters and variables subject to several constraints on these variables. Some of the variables are constrained to integer (e.g. binary) values. This method gained interest recently because of the drastic improvement in numerical solution times of commercial mixed integer programming (MIP) solvers [29]. The UC problem is highly suited to be formulated as a MILP problem. It makes the problem easily and clearly accessible for adaptation. MILP has been put in use recently by independent system operators in several markets including the Pennsylvania, New Jersey and Maryland (PJM) market [36]. Examples of the application of a MILP approach to formulate a UC problem are represented in [21, 28, 37, 38]. One way to solve mixed integer problems is to enumerate all the integer solutions in the feasible region and individually check each for optimality as it is done in branch and bound method. However, as the dimension of the problem grows, the number of feasible integer solutions grows exponentially. Therefore, as a single mixed integer problem generates many subproblems, even small mixed integer problems can be very compute intensive and require significant amounts of physical memory.

Dynamic programming (DP) method starts from the theorem of optimality. Several ways exist to implement a DP algorithm to find an optimal solution for a UC problem [22, 39]. The DP method, however, tends to be difficult for large power systems [40]; it is often used in combination with other methods [41, 42, 43].

Lagrangian relaxation (LR) is a well-known and frequently used method to deal with the UC problem. It is based on a dual optimization. The Lagrangian of the optimization problem is considered together with the given constraints. By moving to the dual problem, the coupling

constraint (supply equals demand) is relaxed. This way, the Lagrangian is split for all generation units. The method moves iteratively towards an overall solution, where the demand equals supply. This approach is able to handle large sets of power plants. However, with LR, nor convergence is guaranteed neither there is a guarantee that the obtained solution is feasible [44, 45, 46].

2.3 Contribution of this thesis

In this thesis, the main task is to develop a methodology, which is adequate to properly mimic geographical dependencies of energy supply and demand as well as intermittent patterns of FRES and of the electricity load. The model must be able to mimic complex interactions within a multi-regional, interconnected electricity supply system. Inherent characteristics of renewable energy sources and exogenous boundary conditions must be included as well. While investment decisions are treated endogenously, operational constraints of dispatchable power plants must be taken into account. Capacity expansions of power generation and energy storage systems as well as the energy transport infrastructure are to be optimized, taking into account the development of electricity demand, technical restrictions of power plants, variability of FRES, and influences of exogenous boundary conditions.

Regarding the complexity of the problem, addressed here, heuristic approaches are not taken into account as a suitable methodology. In the addressed problem, not only the produced power is to be optimized but also investment decisions in power generation, energy storage and transport as well as inter-zonal energy flows comprise the main decision variables, which are to be optimized under different framework conditions. Linear optimization methods for discrete optimization problems (branch and cut and branch and bound methods), LR, and DP are not either evaluated as promising approaches due to the complexity of the problem and the large number of variables. Therefore, in order to optimize investment and production in a multi-regional electricity supply system at a high temporal and geographical resolution, linear programming is selected here as a suitable methodology.

In order to analyze impacts of the variability of FRES on the optimal structure and operation of the global electricity supply system, a global multi-regional electricity system optimization model is developed in this thesis. A brief overview of model's structure is provided in Fig. A.1.

To perform the optimization, the model uses a deterministic approach based on linear programming. Model formulation and optimization process are realized by applying the General Algebraic Modeling System (GAMS) software package [47], and the commercial solver Cplex is used. As results, optimized capacities of power plant technologies and energy storage systems as well as inter-regional capacities for energy transport are determined at a given set of boundary conditions. The power produced from each of the power plant technologies, inter-zonal energy flows, CO_2 emissions, and the marginal price of electricity are determined for each region at every hour of the simulation period. The cost of avoiding one ton of CO_2, i.e. marginal price of CO_2 emissions, can also be concluded from this optimization model.

2.4 LP Investment and Production Optimization Model (LPIPOM)

In this section, formulation of the investment and production optimization model is described. This is an extension of the methodology applied in studies [34, 35].

The total system costs serve as objective function and are given in equation (2.1). These are composed of total investment costs, fixed costs and variable operation costs of all types of power plants (*PrPG*), energy transport technologies (*PrTr*), energy storage facilities (*PrSto*), and other generation processes (*PrOt*) such as hydrogen production technologies. The last sum represents the total emissions costs. From a macroeconomic perspective, minimization of overall costs, which corresponds to the maximization of producers' and consumers' surplus, defines an ideal operation of the energy system through a central planner.

Here, *x* and *y* represent the model region while *t* is the simulation time step; *i* is a set comprising all types of processes. In equation (2.1), k^{Inv} is the specific annual investment costs while k^{Fix} and k^{Var} represent specific fixed and variable operation costs, respectively. *CN* is the new capacity installed to produce electricity or hydrogen while *C* represents the cumulative capacity. E^{in} is the energy input to the generation process at each hour, either thermal energy for power production or electricity for electrolytic production of hydrogen. *CNTr(x,y)* and *CTr(x,y)* are the new capacity and the cumulative capacity of a transport interconnection between regions *x* and *y*, respectively. ETr^{in} represents the energy input to the transmission line at each hour, and *r(x,y)* is the distance between regions *x* and *y*. *CNStin*, *CNStout*, and *CNSt* are the new capacity of storage input, storage output, and storage reservoir, respectively; *CStin*, *CStout*, and *CSt* are the corresponding cumulative capacities. ESt^{in} and ESt^{out} represent the energy input to the storage system and the output energy at each hour, respectively; *EStTot* is the total stored energy in the reservoir. *kemf* is the emission factor of fossil-fired power plants while *kCO2e* is the assumed CO_2-price. *w(t) is* the weighting factor of simulated time steps.

$$
\begin{aligned}
z = \sum_{x} \{ & \sum_{i \in \mathrm{Pr}\, PG} [k_i^{Inv}.CN_i(x) + k_i^{Fix}.C_i(x) + \sum_t k_i^{Var}.E_i^{in}(x,t).w(t)] \\
& + \sum_{y} \sum_{i \in \mathrm{Pr}\, Tr} [\frac{1}{2}.r(x,y).(k_i^{Inv}.CNTr_i(x,y) + k_i^{Fix}.CTr_i(x,y)) + \sum_t k_i^{Var}.ETr_i^{in}(x,y,t).w(t)] \\
& + \sum_{i \in \mathrm{Pr}\, Sto} [k_i^{Inv}.CNStin_i(x) + k_i^{Fix}.CStin_i(x) + \sum_t k_i^{Var}.ESt_i^{in}(x,t).w(t)] \\
& + \sum_{i \in \mathrm{Pr}\, Sto} [k_i^{Inv}.CNStout_i(x) + k_i^{Fix}.CStout_i(x) + \sum_t k_i^{Var}.ESt_i^{out}(x,t).w(t)] \\
& + \sum_{i \in \mathrm{Pr}\, Sto} [k_i^{Inv}.CNSt_i(x) + k_i^{Fix}.CSt_i(x) + \sum_t k_i^{Var}.EStTot_i(x,t)] \\
& + \sum_{i \in \mathrm{Pr}\, Ot} [k_i^{Inv}.CN_i(x) + k_i^{Fix}.C_i(x) + \sum_t k_i^{Var}.E_i^{in}(x,t).w(t)] \\
& + \sum_{i \in \mathrm{Pr}\, PG} \sum_t [E_i^{in}(x,t).kemf_i.kCO2e.w(t)]\}
\end{aligned}
\tag{2.1}
$$

Minimization of overall system costs is subject to different restrictions, describing the energy system. The electricity demand satisfaction constraint, given in (2.2), has to be respected for each region at every hour of the simulation period. This restriction certifies that at each hour, power production of all power plants available at each region minus the power used as input to electrolysis systems plus the import-export balance and storage input-output balance is equal to the electricity demand (*D*) of that region at the corresponding hour. Overproduction is allowed when there is excess production from FRES. In constraint (2.2), E^{out} is the output power of a power plant while E^{in} represents the power used as input to electrolysis systems. $ETr^{out}(x,y)$ is the imported electricity in region *x* from region *y* while $ETr^{in}(x,y)$ is the exported electricity from region *x* to region *y* at this hour.

A dual variable is attributed to any constraint in the primal problem according to the property of primal/dual systems in linear programming [32]. According to this, here, the dual variable of the demand satisfaction constraint represents the marginal price of electricity in perfect competitive markets.

$$\sum_{i\in \Pr PG} E_i^{out}(x,t) - \sum_{i\in \Pr Ot} E_i^{in}(x,t) + \sum_{y}\sum_{i\in \Pr Tr}[ETr_i^{out}(x,y,t) - ETr_i^{in}(x,y,t)]$$

$$+ \sum_{i\in \Pr Sto}[ESt_i^{out}(x,t) - ESt_i^{in}(x,t)] \geq D(x,t) \quad (2.2)$$

According to equation (2.3), total capacity of each technology (*C*) is the sum of the previously installed capacity, given as a parameter (*C0*), and the new capacity (*CN*), which is determined through the optimization.

$$C_i(x) = C0_i(x) + CN_i(x) \quad (2.3)$$

The capacity constraint, given in (2.4), certifies that the total installed capacity of each generation technology at each region is lower than the corresponding upper limit (*cUp*). The total capacity of each renewable power plant technology is restricted according to a region-specific upper limit, which is determined from the geographic information system (GIS)-based data of available area for renewable electricity production using the corresponding technology (see chapter 3). Equation (2.5) represents the losses, occurring through energy conversion processes, using the conversion efficiency factor (η).

$$C_i(x) \leq cUp_i(x) \quad (2.4)$$

$$E_i^{out}(x,t) = E_i^{in}(x,t).\eta_i \quad (2.5)$$

The energy-capacity balance of dispatchable power generation technologies and non-dispatchable renewable power plants is given in equations (2.6) and (2.7), respectively. In the simulation methodology, it is assumed that a dispatchable power plant has a maximal output at each hour, which is equal to its rated output multiplied by its standard availability factor. The availability factor (*AVF*) is a technology-specific parameter to downscale the capacity of a power plant due to periodic maintenance and forced outages. However, for non-controllable energy sources, additionally, a time- and region- specific capacity factor (*Supim*) is used as input to determine the available energy from weather dependent renewable sources such as solar, wind, and hydro at every hour of the simulation period.

$$E_i^{out}(x,t) \leq C_i(x).AVF_i \quad (2.6)$$

$$E_i^{out}(x,t) = C_i(x).AVF_i.Supim_i(x,t) \quad (2.7)$$

The following equations describe the energy storage systems. Equations (2.8)-(2.10) calculate the total energy storage capacity (input, output, and the reservoir), using the sum of the previously installed capacity and the new capacity.

$$CStin_i(x) = C0Stin_i(x) + CNStin_i(x) \quad (2.8)$$

$$CStout_i(x) = C0Stout_i(x) + CNStout_i(x) \quad (2.9)$$

$$CSt_i(x) = C0St_i(x) + CNSt_i(x) \quad (2.10)$$

The storage capacity (input, output, and the reservoir) is restricted in (2.11)-(2.13) according to the corresponding upper limit.

$$CStin_i(x) \le cUpStin_i(x) \quad (2.11)$$

$$CStout_i(x) \le cUpStout_i(x) \quad (2.12)$$

$$CSt_i(x) \le cUpSt_i(x) \quad (2.13)$$

The following three constraints limit the maximum input, output, and stored energy according to the total available capacity.

$$ESt_i^{in}(x,t) \le CStin_i(x) \quad (2.14)$$

$$ESt_i^{out}(x,t) \le CStout_i(x) \quad (2.15)$$

$$EStTot_i(x,t) \le CSt_i(x) \quad (2.16)$$

Restrictions (2.17)-(2.18) represent the relationship between the input and output storage capacity using a constant parameter *(β).*

$$CStout_i(x) \ge \beta.CStin_i(x) \quad (2.17)$$

$$CStout_i(x) \le CStin_i(x) \quad (2.18)$$

The balance equation, given in (2.19), defines the energy content of the reservoir at each time step by taking into account the output power and energy inflow of storage systems. The energy content at the initial time step can be assumed at zero as it is given in equation (2.20).

$$ESt_i(x,t) = ESt_i(x,t-1) + ESt_i^{in}(x,t).\eta_i^{in} - \frac{ESt_i^{out}(x,t)}{\eta_i^{out}} \quad (2.19)$$

$$ESt_i(x,t0) = 0 \quad (2.20)$$

Equation (2.21) defines the inter-seasonal energy storage (*EStints*). This is to distinguish between the amount of energy, which is inter-seasonally stored, and the energy, which is stored and applied through the same seasonal period. This has to be taken into account when a number of weeks are selected to represent the whole year in order to reduce the calculation time and complexity of the problem. In such cases, the reservoir capacity must be scaled using the parameter (*w)* according to the equation (2.21) to take account of the non-simulated time steps. In equation (2.21), *ts* is the first time step while *tf* is the last time step of the simulated seasonal period.

$$ESt\,\mathrm{int}\,s_i(x,t) = ESt\,\mathrm{int}\,s_i(x,ts(t)-1) + w(t).[ESt_i(x,tf(t)) - ESt_i(x,ts(t))] \quad (2.21)$$

Equation (2.22) is the cyclic equation, which certifies that the amount of inter-seasonally stored energy at initial time step (*t0*) and at final time step (*T*) is equal. Equation (2.23) defines the total stored energy (*EStTot*) at each time step using the sum of the energy that is inter-seasonally stored up to the actual seasonal period and the part, which is stored at the actual time step.

$$EStInt_i(x,t0) = EStInt_i(x,T) \tag{2.22}$$

$$EStTot_i(x,t) = ESt_i(x,t) + EStInt_i(x,ts(t)-1) \tag{2.23}$$

The inter-zonal energy transport lines are modeled as trade-based interconnections. The first equation below defines the total inter-zonal transport capacity as a sum of the previously installed capacity and the new capacity. The restriction (2.25) limits the transport capacity between each two of the model regions according to the given upper limit (*cUpTr*). The restriction (2.26) limits the inter-zonal energy flow according to the total available capacity. Equation (2.27) represents the energy balance by taking into account the transport losses (*Trl*).

$$CTr_i(x,y) = CTr0_i(x,y) + CNTr_i(x,y) \tag{2.24}$$

$$CTr_i(x,y) \le cUpTr_i(x,y) \tag{2.25}$$

$$ETr_i^{in}(x,y,t) \le CTr_i(x,y) \tag{2.26}$$

$$ETr_i^{out}(x,y,t) = ETr_i^{in}(x,y,t).(1 - Trl_i.r(x,y)) \tag{2.27}$$

The secondary energy carriers are used to produce end-use commodities through different processes. For the end-use commodity (electricity), the final demand is given as an input parameter, and it is to be satisfied at each hour of the simulation period at each model region according to the restriction (2.2). However, for secondary commodities, the final demand is not taken into account. For instance, hydrogen can be classified as a secondary energy carrier if it is only used for stationary power production. The energy balance equation, given in (2.28), certifies that at each hour, the total secondary commodity produced by different processes at each region plus the import-export balance and storage input-output balance is equal to the amount, which is used as input to power generation processes to produce electricity at the corresponding region.

$$\sum_{i \in \Pr Ot} E_i^{out}(x,t) - \sum_{i \in \Pr PG} E_i^{in}(x,t) + \sum_{y} \sum_{i \in \Pr Tr} [ETr_i^{out}(x,y,t) - ETr_i^{in}(x,y,t)]$$

$$+ \sum_{i \in \Pr Sto} [ESt_i^{out}(x,t) - ESt_i^{in}(x,t)] \ge 0 \tag{2.28}$$

The following restrictions are additional system boundary conditions, which may be additionally included according to the purpose of scenario analysis. The CO_2 emissions constraint is given in (2.29). It is defined as an overall system constraint, given the total CO_2 emissions limit (*co2Up*). The total CO_2 emitted from all power plants must be lower than the given CO_2-limit. The dual variable of this constraint is the marginal price of CO_2 emissions. It represents how much the system costs would increase if CO_2 emissions would be mitigated by another one unit.

$$\sum_{x} \sum_{i \in \Pr PG} \sum_{t} E_i^{in}(x,t).kemf_i.w(t) \le co2Up \tag{2.29}$$

Restriction (2.30) is used to certify that a specific share of the global electricity demand *(a)* is satisfied with FRES. In restriction (2.30), (*PrFRES)* represents power plants that produce electricity from FRES, i.e. wind onshore, wind offshore, PV, and CSP. The share of different

energy resources in total renewable electricity can also be specified. For instance, in restriction (2.31), contribution of wind power is defined using a constant parameter (*b)*.

$$\sum_{x}\sum_{i\notin \Pr FRES}\sum_{t}E_i^{out}(x,t)=(1-a).\sum_{x}\sum_{t}D(x,t) \tag{2.30}$$

$$\sum_{x}\sum_{i\in \Pr WIND}\sum_{t}E_i^{out}(x,t)=b.\sum_{x}\sum_{i\in \Pr FRES}\sum_{t}E_i^{out}(x,t) \tag{2.31}$$

2.5 Inclusion of technical details in LPIPOM

In such an investment and production optimization model based on LP, investment decisions in electricity generation systems are optimized while operational constraints of power plants are neglected. However, technical restrictions in operational terms, which can be directly formulated, for instance, by employing the MILP approach, must be respected as well.

Therefore, the aim of this part is to identify additional linear constraints that can be incorporated in LPIPOM to bring its solution in operational terms closer to the technically-feasible solution, found by the MILP approach.

At first, it is shown that the obtained results from LPIPOM in its basic form without inclusion of technical constraints are identical to the results of the classical screening curve methodology. Then, the power system operation optimization model developed based on the MILP approach is described. A comparison is made between LP results and MILP solution for an illustrative case in terms of output power, discarded wind power, and total operational costs. In order to reduce the deviation of the LPIPOM results from the technically-feasible solution, found by the MILP approach, additional linear constraints are then identified and incorporated in LPIPOM. It is demonstrated that with inclusion of ramping constraints on a technology level, optimal power generation capacity mix and curtailment of wind power is changed. Consequently, the deviation of LP solution in terms of operation from MILP results is reduced. Finally, a methodology is proposed to include technology start-up costs in LPIPOM. The results obtained from LPIPOM are then compared with the results of the MILP optimization model. This finally leads to an electricity generation system, which is economically optimized while it is feasible with respect to operational restrictions of power plants.

2.5.1 LPIPOM versus screening curve methodology

2.5.1.1 Screening curve methodology

The screening curve methodology can be used as a first approximation to determine the cost-optimal power generation capacity mix for a given profile of electricity load. In this methodology, a load duration curve (LDC) is used, which is built by sorting the load from the highest level in a descending order at hourly intervals for a one-year period. As wind power is generated at zero marginal costs and is not dispatchable, it is subtracted from the original hourly load, resulting in the so-called residual load curve. If wind power output is greater than electricity demand, wind power is discarded to eliminate negative load levels.

As it is shown in Fig. 2.1, the number of hours that the load exceeds a certain level or lies within a specific range can be determined from the LDC. In the screening curve methodology, total specific annual costs of power plants in combination with the LDC are a basis to determine the

capacity mix of power plants. The operation time of each power plant technology is determined based on relative levels of total specific annual costs, i.e. fixed costs and variable operation costs. Annual fixed costs consist of annual investment costs and fixed O&M costs, expressed in terms of [$/(MW$_{el}$.a)]. Variable costs consist of fuel costs and variable O&M costs; these are expressed in terms of [$/MWh$_{el}$] and are summed over the whole year to get the total annual operation costs. The cost-optimal generation capacity mix is then determined by selecting the cheapest technology for each level of electricity load using the sum of fixed and variable costs.

Fig. 2.1 shows the schematic representation of this screening curve methodology. The load levels, which have exceeded more than *M* hours, are fully covered by a base load capacity of MW_B. *M* is referred to as the technology switching point. For higher levels of load, occurring at *M-P* hours, a mid-load capacity of MW_M is installed. Correspondingly, the capacity of peak (MW_P) and high peak (MW_{HP}) generation technology is determined.

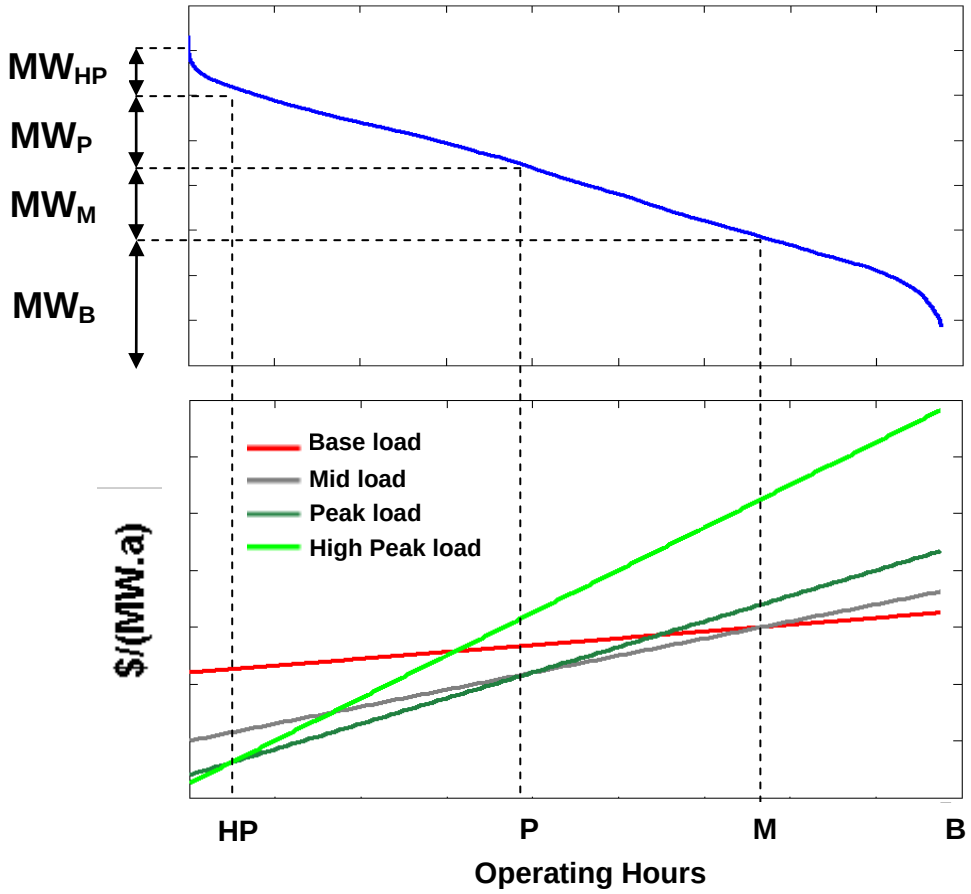

Fig. 2.1: Schematic representation of screening curve methodology

2.5.1.2 Data and assumptions

Five power plant technologies are considered: nuclear fission (“URA-ST”), coal-fired (“COAL-ST”), gas combined-cycle (“GAS-CC”), gas turbine (“GAS-GT”), and wind onshore (“WIND”). Techno-economic parameters are given in Table 2.1. Fuel prices are based on data from [48]. The investment costs are annualized assuming a discount rate of 5% p.a. and using an expected economic lifetime for each power plant technology. Availability is assumed at 100%

for all power generation technologies. Total specific annual costs of different power plants are shown in Fig. 2.2 as a function of operating hours.

Table 2.1: Techno-economic parameters of power plants. Data source: [24, 48, 49] (All costs are in US$ (2008).)

Technology	Lifetime (a)	Efficiency (%)	Fuel price ($/MWh$_{th}$)	Investment ($/kW$_{el}$)	Fixed O&M ($/kW$_{el}$/a)	Variable O&M ($/kWh$_{el}$)
COAL-ST	40	43	12.96	2134	35	0.004
GAS-CC	30	58	35.14	1069	15	0.003
GAS-GT	30	38	35.14	520	10	0.003
URA-ST	60	33	3.08	4102	65	0.0007
WIND	25	100	-	1300	20	0

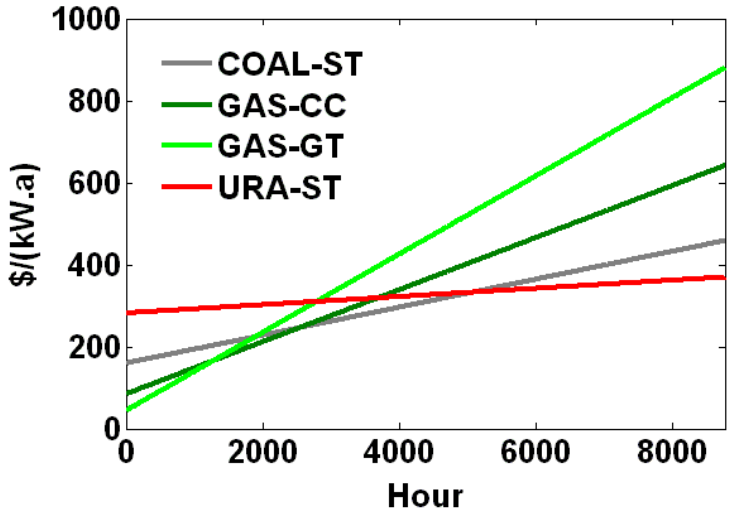

Fig. 2.2: Specific annual costs of power plants. Data Source: [24, 48, 49]

Optimization is performed over a one-year period with an hourly temporal resolution for a single region. The load profile and time series of wind power capacity factor are based on data from [50] for a specific region in Germany. In scenario “WND0”, installation of wind power is not allowed while in scenarios “WND30”, “WND40”, and “WND50” the penetration share of wind power is 30%, 40%, and 50% of annual electricity demand, respectively. The residual load duration curves, representative for different shares of wind power, are shown in Fig. 2.3.

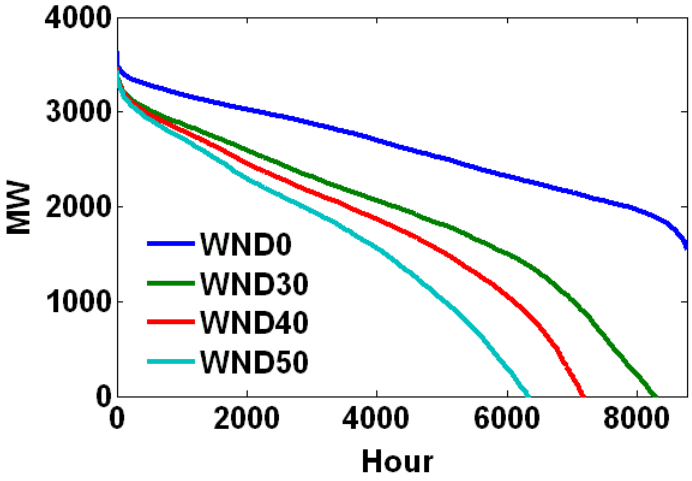

Fig. 2.3: Residual load duration curves. Data Source: [50] (for region D.EON.M in Germany)

2.5.1.3 Results

Fig. 2.4.b and Fig. 2.4.c show the power generation capacity and production mix optimized by LPIPOM for scenarios, differing in the integration share of wind power. This is identical to the optimal capacity mix based on the screening curve methodology, illustrated in Fig. 2.4.a. This is an expected outcome as technical constraints of dispatchable power plants are not respected; hence, both methodologies optimize the capacity mix based on the economics of power generation while technical details of thermal power plants are not taken into account.

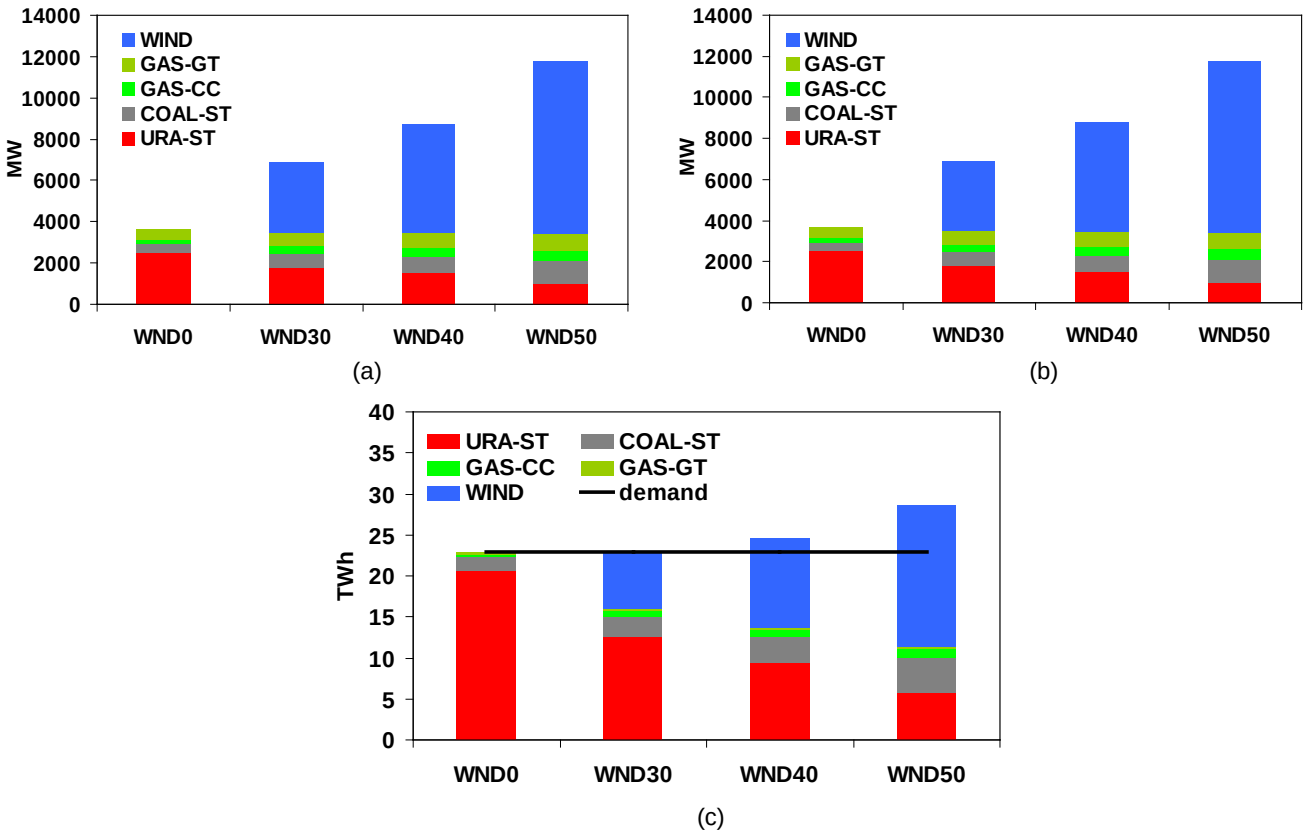

Fig. 2.4: LPIPOM vs. screening curve methodology (a) Optimized capacity mix by screening curve methodology; (b) Optimized capacity mix by LPIPOM; (c) Optimized power production mix by LPIPOM

The operation schedule of thermal power plants optimized by LPIPOM in scenario “WND30” is shown in Fig. 2.5 over a one-week period in winter. The electrical load profile and wind power production are shown as well. It is seen that nuclear power plants are completely shut down during specific hours to allow a full integration of wind power. They are again started up while the minimum required down time is not respected. Furthermore, hourly variations of output power from nuclear and coal-fired power plants exceed actual technical restrictions.

A new methodology needs to be developed to represent different flexibility levels of power generation technologies. This forces the LP optimization model to distinguish between different power plant technologies regarding the level of flexibility. This becomes even more important if increasing the integration share of FRES into a power generation system, which has a high capacity of non-flexible, base load power plants.

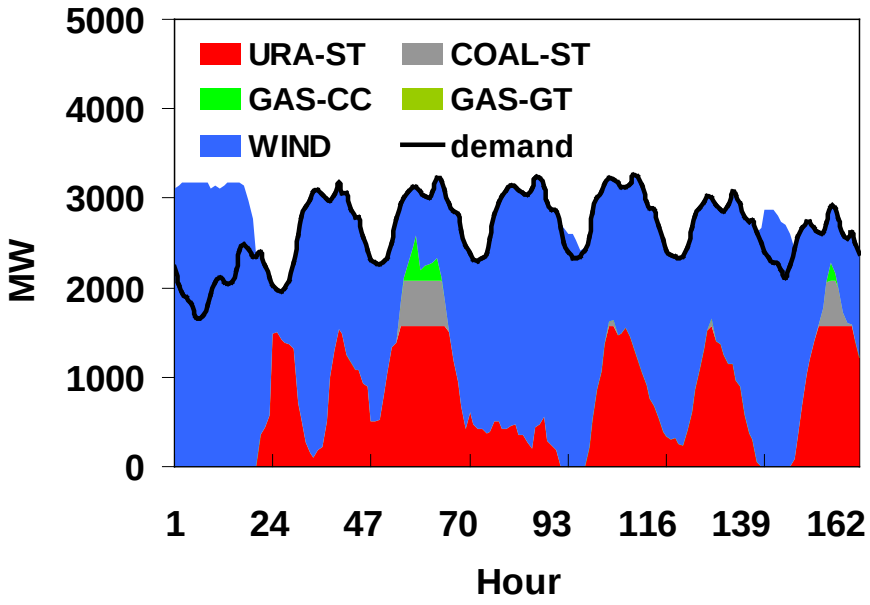

Fig. 2.5: Optimal dispatch in scenario “WND30” over one week in Jan.

2.5.2 LPIPOM versus MILP Operation Optimization Model (MILPOPM)

The feasible share of FRES in an electricity generation system needs to be evaluated by taking into account technical restrictions of power plants. Thus, the simulation methodology must allow representing technical limits, which have impacts on the integration of wind power, specifically during low load periods. For this purpose, operational characteristics of conventional power plants such as must-run status, minimum power level, minimum up and down time, and start-up costs need to be taken into account. These can suitably be formulated using the MILP approach.

In the following, at first, the MILP Operation Optimization Model (MILPOPM) is described. A comparison is then made between the results obtained from MILPOPM, which respects technical restrictions of thermal power plants on a unit-basis, with the results of the LPIPOM in its basic form, which neglects these constraints.

2.5.2.1 MILPOPM Setup

Technical restrictions of thermal power plants, which are implemented on a unit-basis using the MILP approach, are described in this section. The formulation has been inspired by the unit commitment and economic dispatch optimization model developed in [21]. It has been programmed in GAMS, and the commercial solver Cplex is used.

The objective function, given in equation (2.32), is the sum of total variable operation costs (k^{Var}) and start-up costs (k^{st}) of all generation units summed over the total simulation period. In equation (2.32), *j* is a set, which comprises of all power generation units.

$$obj = \sum_{t} \sum_{j} [k^{Var}(j,t) + k^{st}(j,t)] \tag{2.32}$$

Minimization of overall system costs is subject to restrictive equations. The demand satisfaction constraint, given in (2.33), has to be respected at every hour of the simulation period. This restriction certifies that at each hour, power production summed over all generation units is equal to the residual electricity demand. As wind power is generated at zero marginal costs and is non-dispatchable, it is subtracted from the original hourly load profile. This results in the so-called residual electricity load (*ResL*) as it is represented in equation (2.34). The second term on the left hand side of equation (2.33) is the discarded wind power (*windcurt*), which is determined by MILPOPM. If wind power output is greater than electricity demand at a specific hour, curtailment of wind power also referred to as discarded or wasted wind energy is applied to eliminate negative load levels. It is worth mentioning that due to the technical restrictions implemented in MILPOPM, discarded wind power is higher than the curtailment of wind power determined by LPIPOM. Without inclusion of this decision variable *(windcurt)*, which allows further curtailment of wind power, the optimal solution of LPIPOM may lead to technical infeasibility at specific time steps when it is examined in the MILP setup.

$$\sum_{j} E^{out}(j,t) - windcurt(t) = \mathrm{Re}\,sL(t) \tag{2.33}$$

$$\mathrm{Re}\,sL(t) = D(t) - E^{out}_{WIND}(t) \tag{2.34}$$

According to equation (2.35), hourly production of wind power is a multiplication of the wind power capacity factor and the total installed capacity. The wind power capacity is optimized by LPIPOM and is used here as an input parameter.

$$E^{out}_{WIND}(t) = C_{WIND}.Supim_{WIND}(t) \tag{2.35}$$

The following restriction certifies that discarded wind power at each time step is lower than the total produced wind power at the corresponding hour.

$$windcurt(t) \le E^{out}_{WIND}(t) \tag{2.36}$$

In MILP formulation, the quadratic cost curve of a power plant can be approximated by a piecewise-linear function [21, 39]. However, the aim, here, is to evaluate the deviation of the results of LPIPOM from the results of MILPOPM, which are caused by technical restrictions of power plants such as start-up conditions and minimum up and down time requirements. Thus, similar assumptions with respect to economical parameters of power plants are made in both

methodologies. This allows specifically checking upon the influence of technical limits on differences between the obtained results from the two methodologies. For this purpose, a one-step cost function is used in MILP formulation similar to what is assumed in LPIPOM.

To incorporate the cost function of a power plant and to set the minimum operating point, the following constraints are included. The state variable *s(j,t)* is binary; it takes the value of 1 in case the plant *j* is committed in hour *t* and 0 otherwise. In equation (2.37), the minimum operating point is set. Equations (2.37)-(2.38) enforce the generation from plant *j* to lie within the range between the minimum operating level *(Pmin)* and the maximum capacity *(Pmax).* The total variable cost function is given in equation (2.39); *A* is the total variable operation costs at the minimum output of plant *j*, and *F* is the corresponding specific variable operational costs.

$$E^{out}(j,t) = delta(j,t) + P\min(j).s(j,t) \tag{2.37}$$

$$dalta(j,t) \le [P\max(j) - P\min(j)].s(j,t) \tag{2.38}$$

$$k^{Var}(j,t) = A(j).s(j,t) + F(j).delta(j,t) \tag{2.39}$$

The start-up costs are given in equation (2.40). Start-up costs are considered as a fixed block correlated to the minimum output capacity in the hour of start-up. In equation (2.40), *SC* is the specific start-up costs, which is given for each power generation technology.

$$k^{st}(j,t) \ge SC_j.[s(j,t) - s(j,t-1)].P\min(j) \tag{2.40}$$

The minimum up and down time constraints are given in (2.41)-(2.42). The first terms between the brackets reflect a start-up or a shutdown, respectively; the second guarantees that the plant remains on-line or off-line during the required number of hours. According to restriction (2.42), the possibility to start a plant is subject to the status of the plant in the previous periods. If a plant goes offline in hour *t*, it is not able to start again for the next *k* hours defined by the minimum down time of the plant *(mdt)*. The same situation exists when a plant is started up due to the minimum up time of the plant *(mut)*.

$$[s(j,t) - s(j,t-1)] + [s(j,t+k-1) - s(j,t+k)] \le 1 \qquad \forall k \in [1,2,...,mut_j - 1] \tag{2.41}$$

$$[s(j,t-1) - s(j,t)] + [s(j,t+k) - s(j,t+k-1)] \le 1 \qquad \forall k \in [1,2,...mdt_j - 1] \tag{2.42}$$

2.5.2.2 Data and assumptions

Fuel costs, variable operation costs, and conversion efficiency of power plants are given in Table 2.1. Other techno-economic parameters, which are used in the unit commitment problem, are represented in Table 2.2.

Table 2.2: Techno-economic parameters of power plants. Data source: [21, 22, 51]

Technology	Minimum load (%of maximum capacity)	Minimum up/down time (h)	Start-up costs ($/MW$_{el}$)
COAL-ST	35	10	7
GAS-CC	30	4	5
GAS-GT	50	1	0
URA-ST	60	100	10

An optimization is performed over a one-year period with an hourly temporal resolution for scenario “No RAMP”. In this scenario, 30% of the electricity demand is to be satisfied with wind power. The capacity of each power plant technology, resulting from the optimization by LPIPOM, is downscaled according to the corresponding availability factor and is disaggregated based on the unit size levels, given in Table 2.3. These are used as input to MILPOPM to represent the available capacity of each power generation unit. The operation schedule of power plants on a unit-basis is then optimized by MILPOPM for subsequent 24-hour periods while technical restrictions of thermal power plants such as minimum operating point, minimum up and down time requirements, and start-up costs are taken into account.

Table 2.3: Unit size levels and availability factors of power plants. Data source: [52, 53]

Technology	Minimum unit size (MW_{el})	Maximum unit size (MW_{el})	Availability (% of maximum capacity)
COAL-ST	400	800	75
GAS-CC	400	800	90
GAS-GT	10	250	95
URA-ST	800	900	80

2.5.2.3 Results

If the power generation capacity mix, optimized by LPIPOM, is used as input to MILPOPM to represent the available capacity of each generation unit, technical restrictions of thermal power plants lead to a different optimal operation schedule. This results in a higher level of wind power curtailment as compared to the level determined by LPIPOM. The following figures focus on a number of time steps, when the LPIPOM solution is evaluated as an infeasible case if technical restrictions of dispatchable power plants are taken into account.

For instance, Fig. 2.6 compares the optimal dispatch of thermal power plants and discarded wind power, resulting from LPIPOM, with the results of MILPOPM at a typical autumn week-day. In the optimal dispatch of LPIPOM, nuclear power plants are shut down during hours 10-13 to have a full integration of wind power. However, this is not feasible in MILPOPM due to the minimum up and down time constraints. Furthermore, during hours 7-9 and 14-15 we see a low production from nuclear power plants in the LPIPOM solution, which is not allowed in MILPOPM due to the minimum operating level. Thus, during the specified hours, curtailment of wind power is higher in MILPOPM than in LPIPOM.

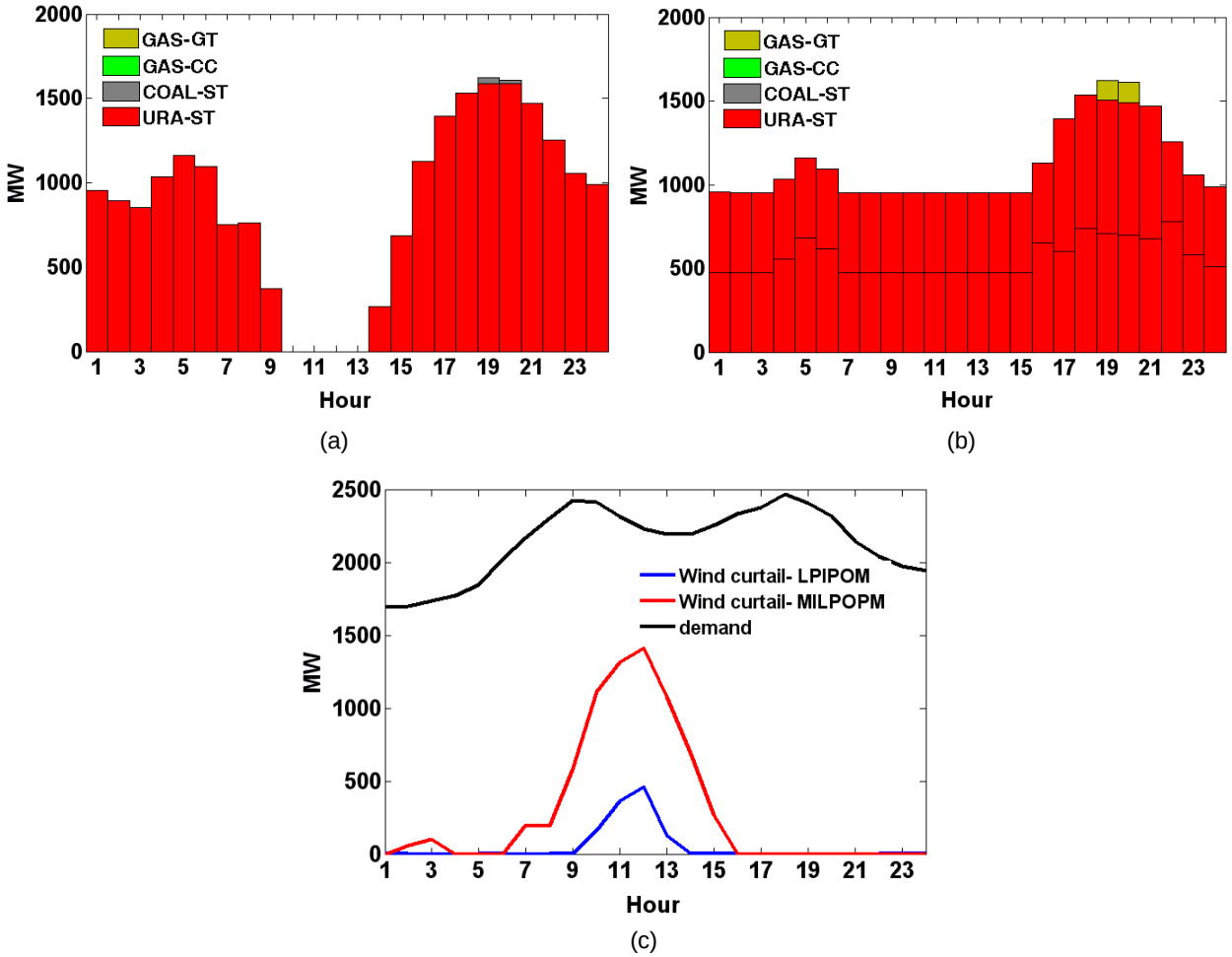

Fig. 2.6: Optimal dispatch of thermal power plants and wind power curtailment at a typical week-day in Sept. in scenario "No RAMP" (a) Produced power from each technology by LPIPOM; (b) Produced power from each unit by MILPOPM; (c) Wind curtailment in LPIPOM vs. wind curtailment in MILPOPM

Fig. 2.7 demonstrates another comparison between the optimal dispatch of thermal power plants at a typical week-day in spring obtained from the two methodologies. Based on the LPIPOM solution, during hours 1-5, nuclear power plants are offline. However, in the MILP approach, due to the minimum operating level and minimum up and down time constraints, both nuclear units are online and operate at the minimum output level. Correspondingly, during the specified hours, curtailment of wind power is higher based on the MILPOPM solution.

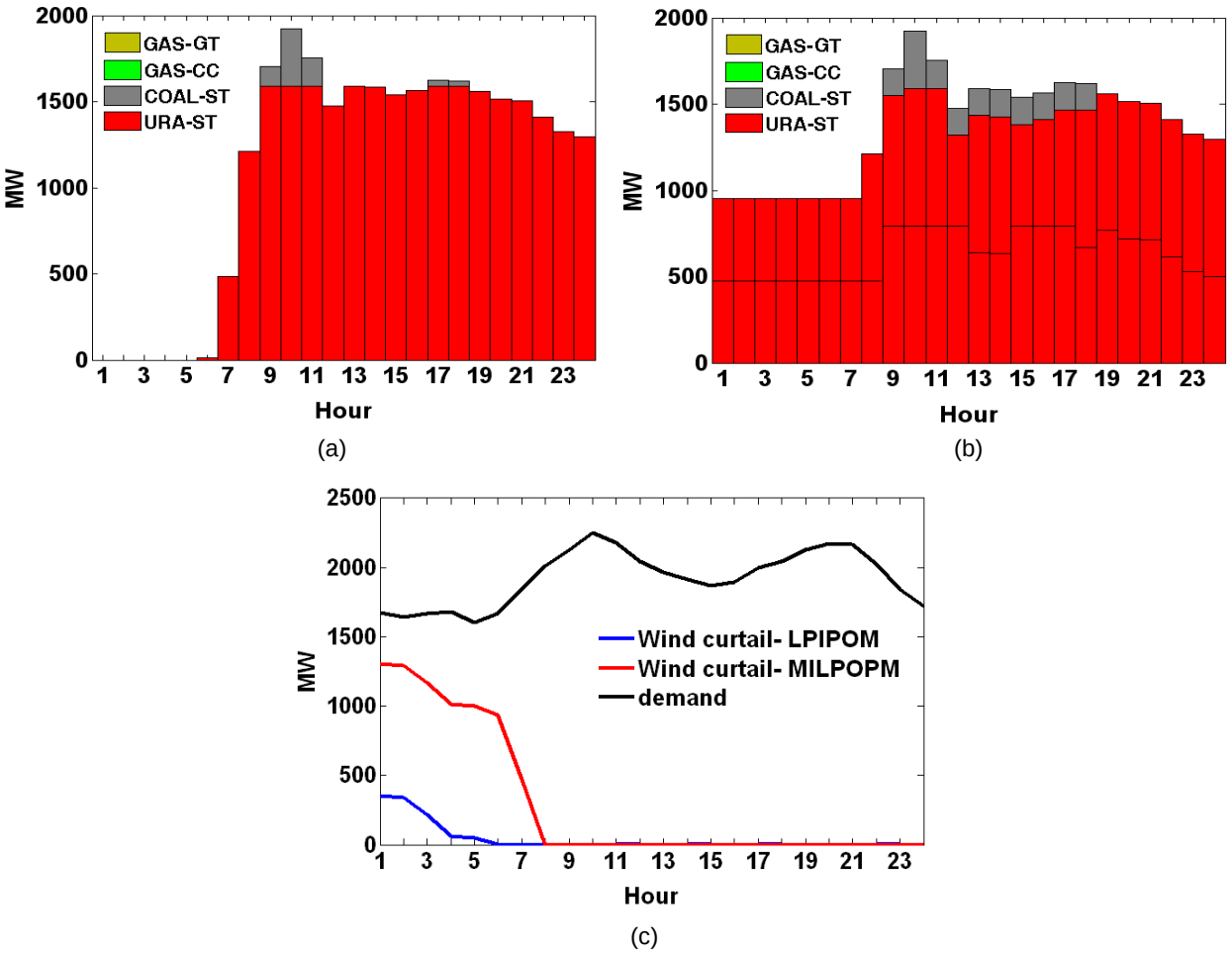

Fig. 2.7: Optimal dispatch of thermal power plants and wind power curtailment at a typical week-day in April in scenario "No RAMP" (a) Produced power from each technology by LPIPOM; (b) Produced power from each unit by MILPOPM; (c) Wind curtailment in LPIPOM vs. wind curtailment in MILPOPM

2.5.3 Incorporation of technical constraints in LPIPOM

To reduce the deviation of LPIPOM results from the MILPOPM solution in operational terms, additional linear constraints are now set up and included in LPIPOM to reflect operational characteristics of thermal power plants. Deviation of the results of LPIPOM from the MILPOPM solution in terms of power production by different technologies, curtailment of wind power, and total operational costs with and without inclusion of technical constraints are compared to demonstrate the influence of these restrictions on the improvement of the LPIPOM solution.

2.5.3.1 Technology ramping

Ramping constraints at a technology level are included in LPIPOM to restrict the hourly variation of output power of dispatchable power plants. The ramp rate expresses the flexibility of a power generation technology as a percentage of the total installed capacity. A more stringent ramp rate is attributed to a base load technology to reflect its lower level of flexibility. Correspondingly, a less stringent ramp rate is assumed for mid- and peak- load power plants [54].

Ramp rates are included in a unit commitment problem in [55], allowing to ramp up or down coal-fired generation units in 4 hours. Full ramp up and down time of 3 hours is used in [56] for coal and nuclear power plants while a full ramp up and down time of 2 hours is assumed for oil-fired and gas combined-cycle power plants. Full ramp up and down time of 4 hours is used for nuclear power plants in a unit commitment problem in [22]; coal and lignite-fired units are allowed to fully ramp up and down in 2.5 hours while a full ramp up and down time of 1.3 hours is assumed for gas combined-cycle and oil-fired units.

As the model works on a technology-aggregated level, rather than on a power plant basis as in a unit commitment problem, the introduced ramp rates may not be directly compared with the ramp rates of individual power plants. The ramp rates, implemented at a technology level, must be considered as a methodology to reflect different levels of flexibility of power generation technologies in the LP investment planning model. These restrictions impose a more realistic behavior of power plants, accounting not only for the ramp rates of individual generation units but also for the minimum operating point and minimum up and down time requirements. As these latter technical restrictions can not be directly implemented within a non-mixed integer problem, more stringent ramp rates are assumed in LPIPOM as compared to the ramp rates of individual power plants, used in a unit commitment problem. Consequently, the aggregated generation output flexibility is lower than the individual ramp rates. Furthermore, ramp rates depend on plant loading. In order to reduce the generation output flexibility when a plant is operated at a lower output level, distinction is made between the committed capacity and the non-committed capacity. A lower ramp rate is thus assumed for the non-committed generation capacity than the committed capacity.

It is worth mentioning that in the MILP formulation, no individual power plant ramp rates are taken into account. With a time step of one hour, it is assumed that all power plants can fully ramp up and down in such a period. This is correspondent to the assumptions made in other studies [21, 52].

2.5.3.1.1 Inclusion of ramping constraints in LPIPOM

Upward and downward flexibility of each power plant technology is limited at each hour according to the restriction (2.43). Here, *rampc* is the ramp rate of the committed capacity, and *rampnc* is the ramp rate of the non-committed capacity.

$$flex_i(x,t) \leq rampc_i.E_i^{out}(x,t-1) + rampnc_i.[C_i(x) - E_i^{out}(x,t-1)] \quad (2.43)$$

The hourly variation of output power of each generation technology is then restricted in (2.44) and (2.45) according to the flexibility of the corresponding technology at the given hour.

$$E_i^{out}(x,t) \leq E_i^{out}(x,t-1) + flex_i(x,t) \quad (2.44)$$

$$E_i^{out}(x,t) \geq E_i^{out}(x,t-1) - flex_i(x,t) \quad (2.45)$$

2.5.3.1.2 Influence of ramping constraints on optimal capacity and production mix

At first, a sensitivity study is performed on the influence of technology ramp rates on the optimal power generation capacity mix. The ramp rate (technology-based) of the committed capacity is given in Table 2.4 for different power plants. The ramp rate of the non-committed capacity is

assumed at 60% of the ramp rate of the committed plant. For the gas turbine technology, the ramp rate of both committed and non-committed capacity is assumed at 1.

Table 2.4: Technology-based ramp rates of committed power plants (*rampc*)

Technology	rampc1	rampc2	rampc3	rampc4	rampc5	rampc6	rampc7	rampc8	rampc9	ramp10	rampc11
COAL-ST	0.12	0.12	0.12	0.12	0.24	0.33	0.42	0.51	0.63	0.75	1
GAS-CC	0.192	0.192	0.192	0.192	0.384	0.528	0.672	0.816	1	1	1
GAS-GT	1	1	1	1	1	1	1	1	1	1	1
URA-ST	0.01	0.03	0.05	0.08	0.16	0.22	0.28	0.34	0.42	0.5	1

The ramp rate of nuclear, coal, and gas-combine cycle technology is varied one by one within the range, given in Table 2.4, while the ramp rate of other technologies remains constant at the level of *rampc7*. Wind power capacity is fixed at 3400 MW.

Fig. 2.8 shows the installed capacity of thermal power plants as a function of ramp rate. According to Fig. 2.8.a, the ramp rate of base load technology, i.e. “URA-ST”, has a considerable impact when it varies in the range from 0.01 to 0.16. At a very low level of flexibility, it is mainly replaced by the mid-load technology (“COAL-ST”). According to Fig. 2.8.b, the ramp rate of mid-load technology has an influence when it varies in the range from 0.12 to 0.24. When a very low level of flexibility is assumed for this technology, it is mainly replaced by base- and peak- load technologies (“URA-ST” and “GAS-CC”). From Fig. 2.8.c it can be concluded that the installed capacity of “GAS-CC” is not sensitive to the ramp rate when it varies in the given range.

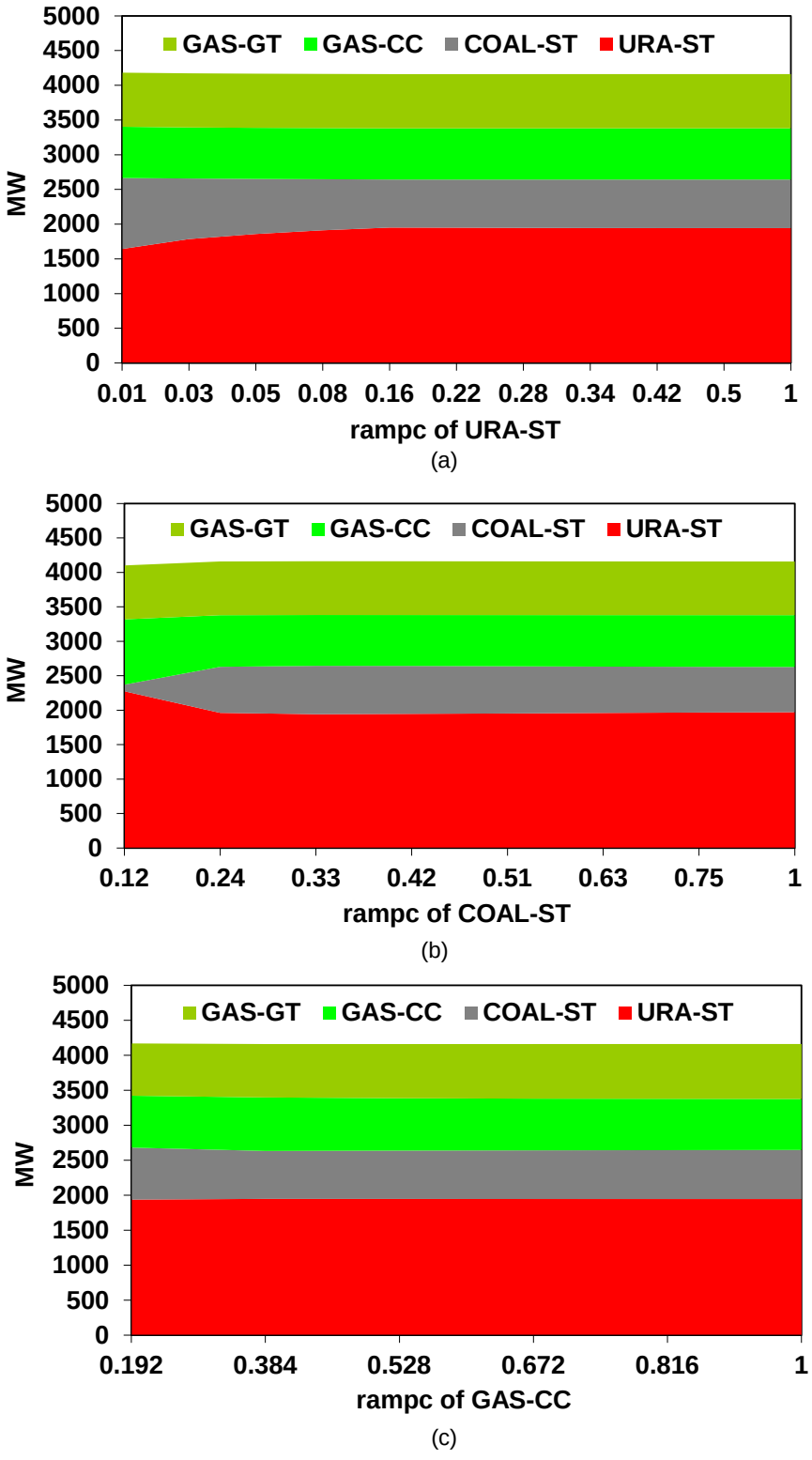

Fig. 2.8: Optimal capacity as a function of ramp rate of committed capacity (*rampc*) (a) URA-ST; (b) COAL-ST; (c) GAS-CC

As an example, output power of different power plant technologies is shown in Fig. 2.9 for a selected one-week period. Fig. 2.9.a shows the optimal dispatch when ramping constraints are not taken into account. Fig. 2.9.b demonstrates the optimal dispatch of power plants when ramping constraints are respected. The ramp rate (technology-based) of committed capacity of nuclear, coal-fired plant, and gas combined-cycle is assumed at 0.08, 0.33, and 0.53,

respectively. The ramp rate of non-committed capacity is assumed at 60% of the ramp rate of the committed capacity. For the gas turbine technology, ramp rate of both committed and non-committed capacity is assumed at 1. These have been determined through a sensitivity study to minimize deviation of LPIPOM solution in operational terms from the MILP results. A significant impact of ramp rates on the variation of output power of base- and mid- load technologies is noticed during hours 1-5, 23-31, 42-56, 116-127, 133-142, and 153-159. While excess production is zero during these hours when ramping constraints are not taken into account, restriction of the variation of output power leads to the curtailment of wind power at the specified time steps.

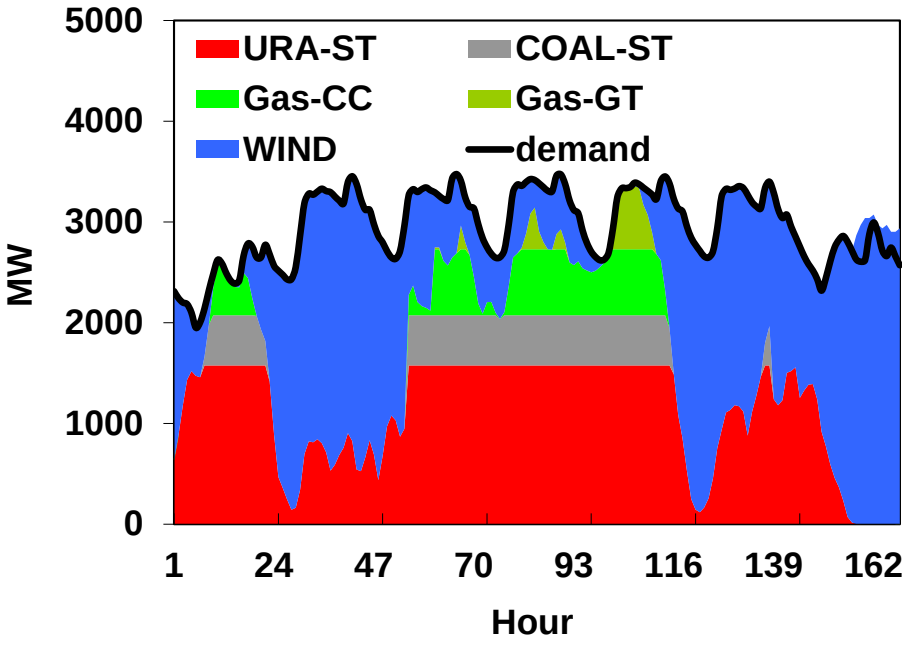

(a)

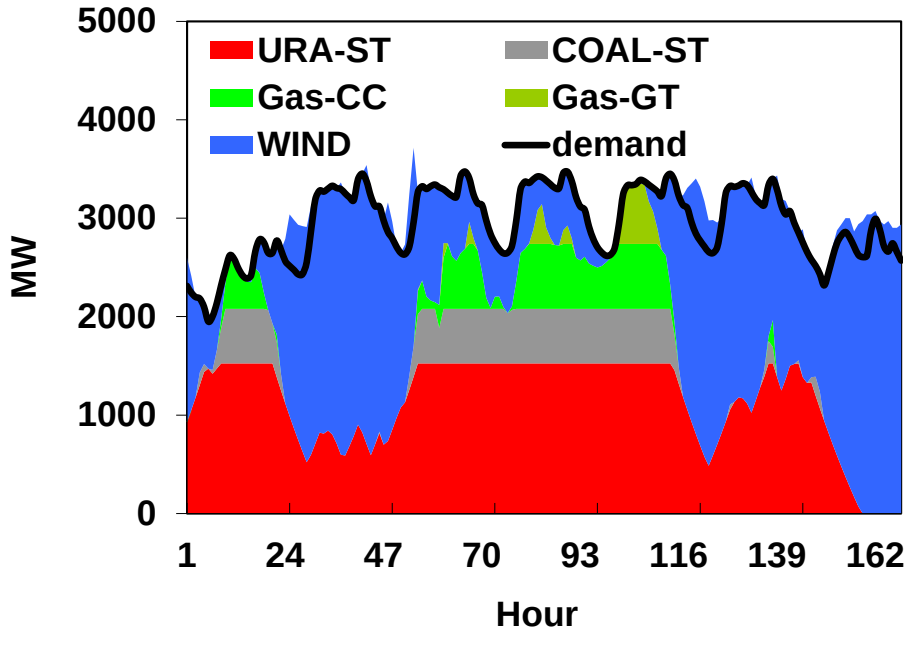

(b)

Fig. 2.9: Optimal dispatch over one week in Jan. (a) Without ramping constraints; (b) With ramping constraints

2.5.3.1.3 LPIPOM with ramping constraints vs. MILPOPM

The technical feasibility of the power generation system, optimized by LPIPOM, is now examined according to the operational restrictions of power plants. In this section, the influence of ramping constraints towards this aim is demonstrated by comparing the results obtained from LPIPOM with the results of MILPOPM in scenarios “RAMP” and “No RAMP”.

2.5.3.1.3.1 Data and assumptions

In scenario “No RAMP”, ramping constraints are not taken into account; in this scenario, 30% of the electricity demand is to be satisfied with wind energy that leads to the installation of 4718 MW wind power. In scenario “RAMP”, ramp rate (technology-based) of the committed capacity of nuclear, coal-fired plant, and gas combined-cycle is assumed at 0.08, 0.33, and 0.53, respectively. The ramp rate of non-committed capacity is assumed at 60% of the ramp rate of the committed capacity. For the gas turbine technology, ramp rate of both committed capacity and non-committed capacity is assumed at 1. Wind power capacity is fixed at 4718 MW to see the influence of ramping constraints on the optimal capacity of thermal power plants and discarded wind power while the wind power capacity remains unchanged as in scenario “No RAMP”. Other assumptions and data are described in section 2.5.2.2.

Scenario “RAMP” results in a different optimal generation capacity mix from the one, resulting in scenario “No RAMP”. The optimal capacity mix obtained from each scenario is downscaled according to the availability of power plants and is disaggregated based on the unit size levels, given in Table 2.3. These are then used as input to MILPOPM to represent the available capacity of each generation unit. The dispatch of generation units is then optimized by MILPOPM for each of these two power generation systems.

2.5.3.1.3.2 Results

The capacity of different power plant technologies is compared between scenarios “RAMP” and “No RAMP” in Fig. 2.10. It can be concluded that in scenario “RAMP”, less flexible generation plants are replaced by others, offering a higher degree of modulation. Hence, the installed capacity of URA-ST is reduced in “RAMP” scenario as compared to “No RAMP” while the capacity of COAL-ST and GAS-CC is increased.

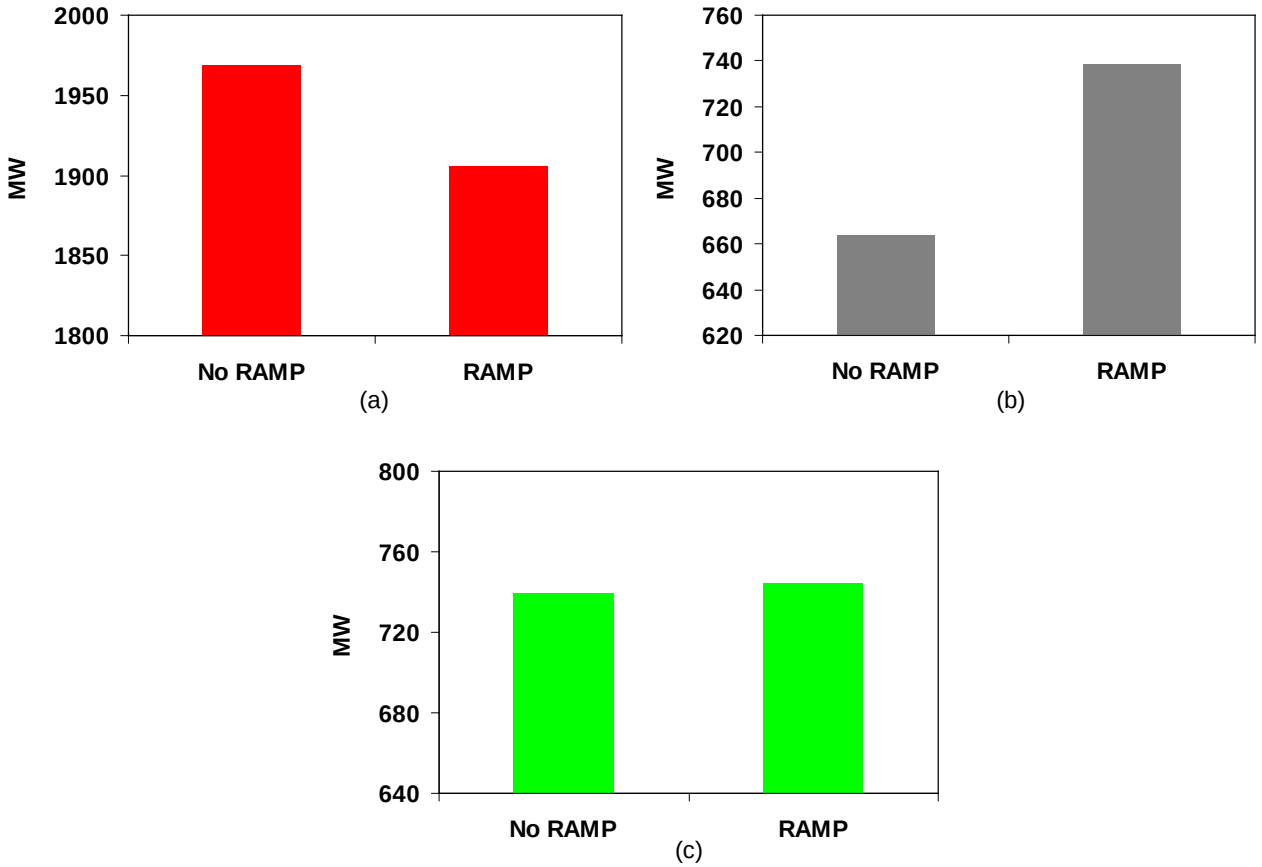

Fig. 2.10: Influence of ramping constraints on optimal thermal capacity mix (a) URA-ST; (b) COAL-ST; (c) GAS-CC

Total output power of each power plant technology is compared between the two scenarios in Table 2.5. When ramping constraints are respected, power production from nuclear power plants is reduced while output power of more flexible technologies such as the coal-fired and gas combined-cycle plant is increased. Total discarded wind power is nearly tripled when ramping constraints are taken into account. Moreover, in scenario “RAMP”, total operational cost is increased by 4% from the level in scenario “No RAMP”.

Table 2.5: Influence of ramping constraints on production mix and operation costs

Technology	Scenario No RAMP	Scenario RAMP
COAL-ST	2.45 TWh	2.81 TWh
GAS-CC	0.68 TWh	1.80 TWh
GAS-GT	0.25 TWh	0.35 TWh
URA-ST	12.63 TWh	11.38 TWh
WIND	7.04 TWh	7.04 TWh
demand	22.87 TWh	22.87 TWh
Wind curtailment	0.178 TWh	0.520 TWh
Operation costs	332 Mio.$	346 Mio.$

When ramping constraints are respected, sudden reduction of the output power of nuclear power plants during hours with a high amount of available wind energy is not allowed.

According to Fig. 2.11.a, during hours 10-13, nuclear power plants cannot be shut down because the hourly variation of output power is allowed only at a limited rate. However, nuclear power plants are off-line during these hours when ramping constraints are not respected (see Fig. 2.6.a). As a result, discarded wind power, determined by LPIPOM when ramping constraints are included, is closer to the wind power curtailment calculated by the MILP approach. This can be realized by comparing Fig. 2.6.c with Fig. 2.11.c.

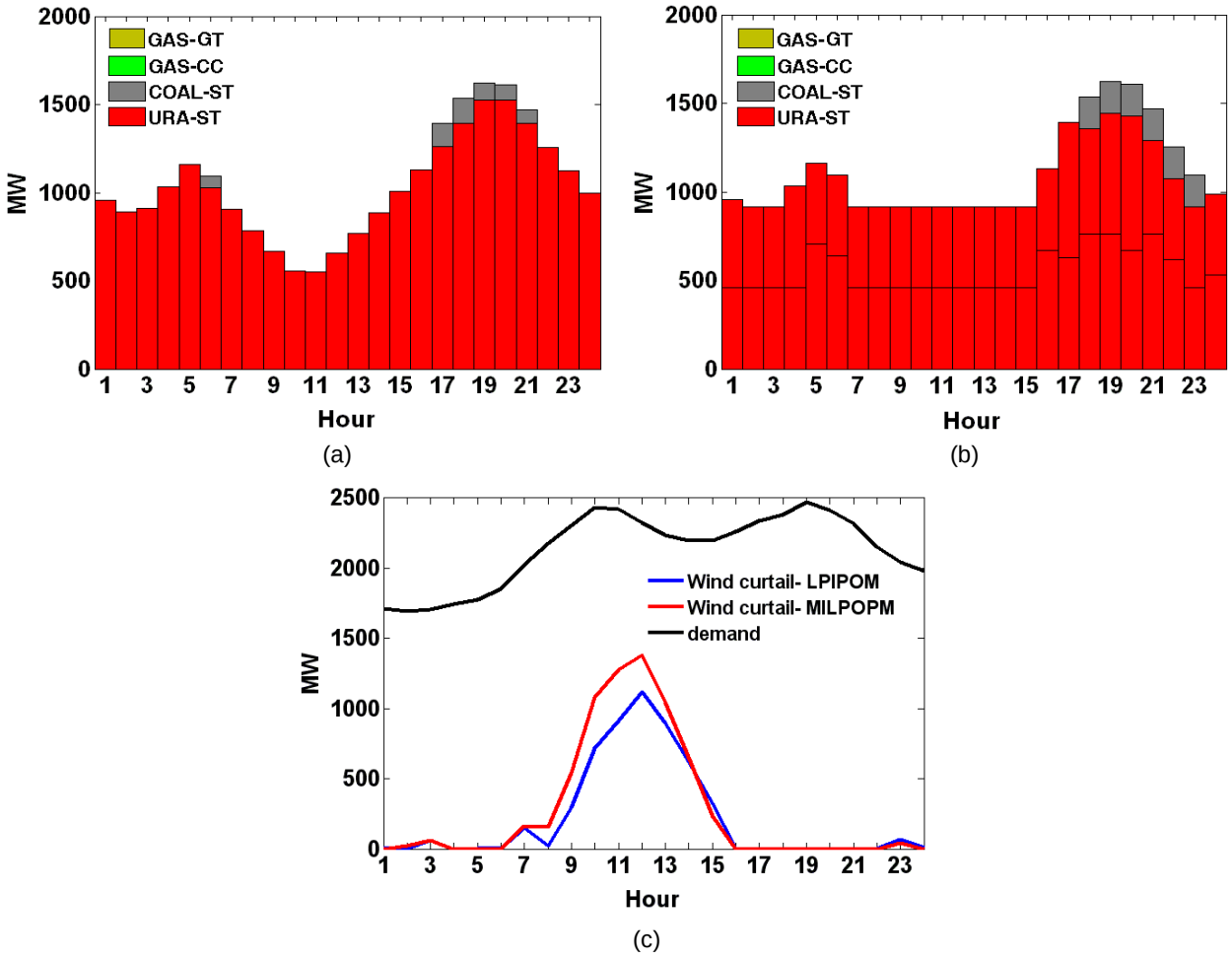

Fig. 2.11: Optimal dispatch of thermal power plants and wind power curtailment at a typical week-day in Sept. in scenario "RAMP" (a) Produced power from each technology by LPIPOM; (b) Produced power from each unit by MILPOPM; (c) Wind curtailment in LPIPOM vs. wind curtailment in MILPOPM

Improvement of the LPIPOM solution when ramping constraints are respected can also be realized by comparing Fig. 2.7 with Fig. 2.12. If ramp rates are respected, due to their low flexibility, nuclear power plants operate during hours 1-5 and can not be shut down as the wind power increases. Output power of nuclear power plants increases sequentially to reach the maximum output at the time of peak load (time step 10). As a result, the deviation of LPIPOM solution from the MILPOPM solution in terms of discarded wind power is reduced in comparison with the scenario "No RAMP".

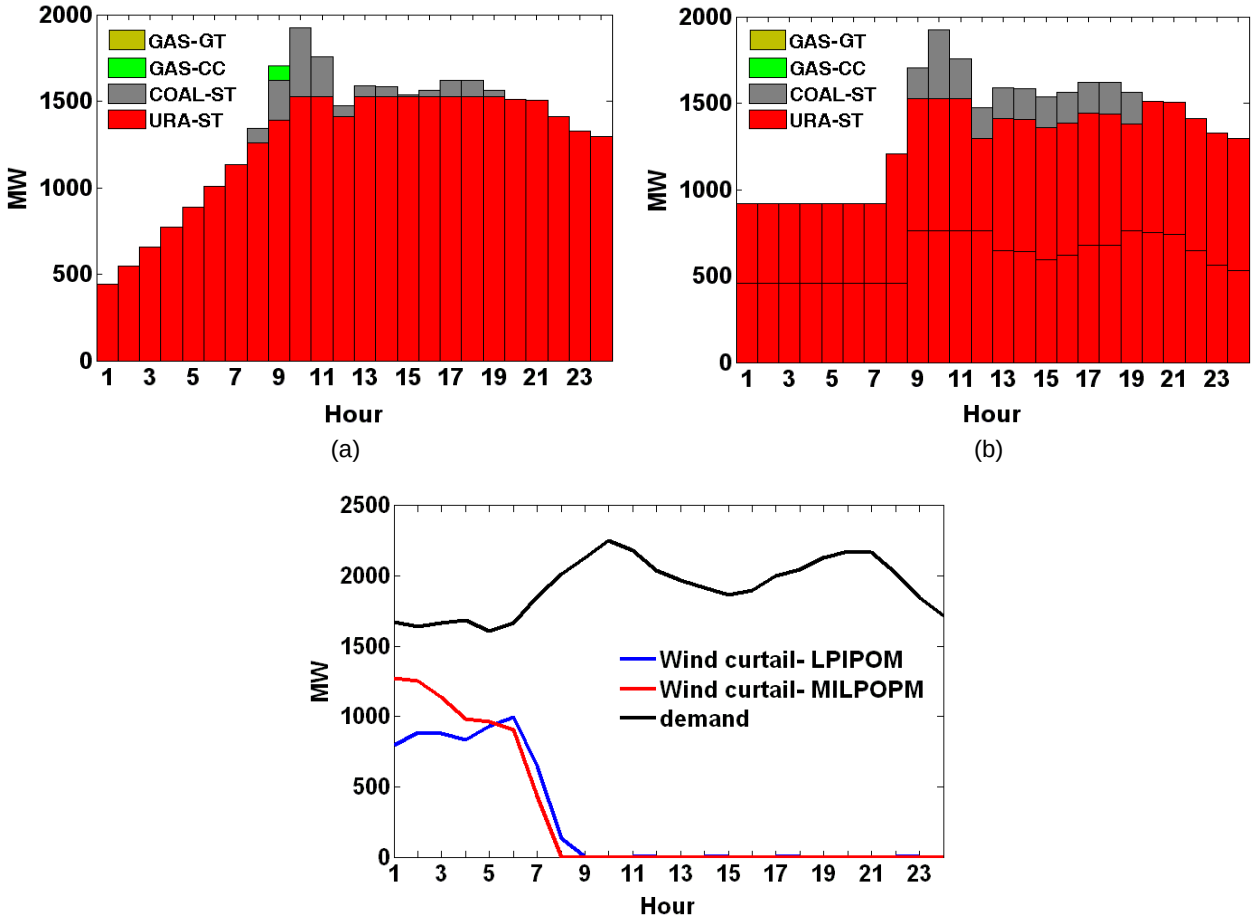

Fig. 2.12: Optimal dispatch of thermal power plants and wind power curtailment at a typical week-day in April in scenario “RAMP” (a) Produced power from each technology by LPIPOM; (b) Produced power from each unit by MILPOPM; (c) Wind curtailment in LPIPOM vs. wind curtailment in MILPOPM

The influence of ramp rates can also be demonstrated according to the total deviation of the LPIPOM solution from the results of MILPOPM in both scenarios “RAMP” and “No RAMP”. Fig. 2.13.a is obtained by subtracting total output power of each power plant technology, determined by LPIPOM, from total output power of the corresponding technology based on the MILPOPM solution. The deviation of total operational costs is visualized in Fig. 2.13.b. According to these, inclusion of ramping constraints leads to the reduction of the deviation of LPIPOM results from the technically feasible solution found by the MILP approach. In the “RAMP” scenario, the deviation of wind power curtailment is reduced by more than 85% as compared to the scenario “No RAMP”. Furthermore, when ramping constraints are taken into account, the deviation of total operational costs is reduced by 50% from its level in scenario “No RAMP”.

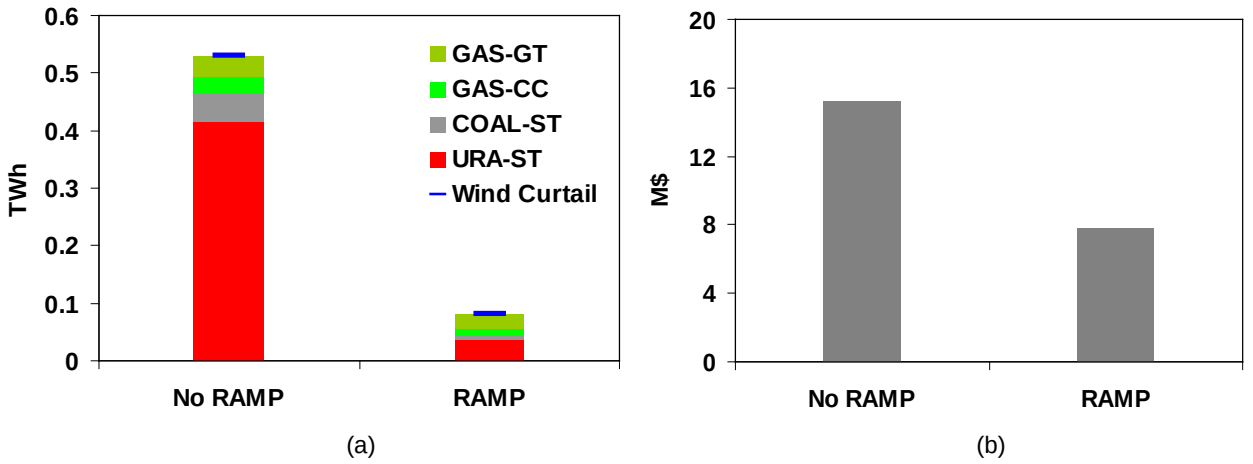

Fig. 2.13: LPIPOM with/without ramping constraints vs. MILPOPM (a) Power production per technology in LPIPOM subtracted from power production in MILPOPM; (b) Total operation costs in LPIPOM subtracted from total operation costs in MILPOPM

2.5.3.2 Technology start-up costs

Starting up a power plant causes additional costs. The power plant's boiler has to be preheated and the plant must be synchronized with the electricity network. Furthermore, attrition increases significantly due to the high variations in temperature during the start-up. Hence, start-up costs are an important factor in the optimization of power production schedule. Neglecting start-up costs, the technology with the lowest variable generation costs is chosen for production as long as the capacity of that technology is available. Inclusion of start-up costs results in a different optimal dispatch. As they are independent from the following length of production, they add a fixed cost component.

Start-up costs can suitably be formulated in a unit commitment problem with the help of binary variables as demonstrated in the MILPOPM formulation. In [57], different approaches are compared with respect to the implementation of unit commitment and start-up costs. Here, start-up costs are considered as a fixed block correlated to the minimum output capacity in the hour of start-up (see equation 2.40). This corresponds to the most efficient approach in order to obtain the cost-minimal dispatch under technical restrictions according to the study conducted in [57].

An attempt is made in this section to further improve the solution, found by LPIPOM, with respect to its technical feasibility in operational terms. This is realized through inclusion of additional constraints in LPIPOM to model start-up costs at a technology level. In addition to the technology ramping constraints, these restrictions help to represent technical limitations of thermal power plants in a linear investment planning model.

2.5.3.2.1 Inclusion of start-up costs in LPIPOM

The approach, used here to take account of start-up costs in a linear optimization model, has been inspired by the methodology proposed in [58]. The model distinguishes between three different group of variables related to the output power of a power plant technology. In the formulation of the base model (see section 2.4), the variable $E_i^{out}(t)$ is the output power of power plant technology i at time step t. To model start-up costs of dispatchable power plants, two other

additional variables are included: $E_i^{out\text{-}up}(t)$ is the capacity of technology *i* newly started at time step *t*, and $E_i^{out\text{-}d}(t)$ represents the capacity shut down at time step *t*. A new term (*sc*) is added to the objective function, given in equation (2.1), to take account of start-up costs. According to equation (2.46), an increase in power generation is associated with additional costs beyond pure fuel costs.

$$sc = \sum_{x} \sum_{i \in \Pr PG} \sum_{t} SC_i . E_i^{out-up}(x,t) \tag{2.46}$$

Moreover, the following constraints are to be respected for dispatchable power plants. Restriction (2.47) ensures that only the on-line capacity may produce power. The parameter (α) in restriction (2.48) reflects how the start-up costs are distributed over the optimization period. It allows differentiating between accounting only once for the start-up costs (start-up costs up to the highest generation level have to be paid only once if α is set to zero) and accounting for every MWh of increase in generation (when there is an increase of generation after a decrease, start-up costs have to be paid again if α is set to 1). Restriction (2.49) certifies that the total capacity started up and ready to produce (on-line capacity) can not exceed the total installed capacity.

$$E_i^{out}(x,t) - \sum_{tm=1}^{t} [E_i^{out-up}(x,tm) - E_i^{out-d}(x,tm)] \le 0 \tag{2.47}$$

$$\alpha_i . (\sum_{tm=1}^{t} [E_i^{out-up}(x,tm) - E_i^{out-d}(x,tm)]) - E_i^{out}(x,t) \le 0 \tag{2.48}$$

$$\sum_{tm=1}^{t} [E_i^{out-up}(x,tm) - E_i^{out-d}(x,tm)] \le C_i(x) \tag{2.49}$$

As the LP formulation does not allow an integer representation of plant conditions, each additional MWh of generation is accounted with both fuel costs and start-up costs whereas stable generation is accounted with fuel costs only. As a result, start-up costs are overestimated in situations where the load increases.

Different methodologies for modeling start-up costs have been compared in [57], concluding that the LP approach leads to the highest overall costs as each additional generation is accounted with both fuel costs and start-up costs, therefore, the weight of start-up costs is overestimated compared to other approaches. In comparison with the linear approach, in the MILP setup, the weight of start-up costs is significantly lower. Finally, it has been concluded that when the research focus is to obtain cost-minimal dispatch under technical restrictions, the MILP approach is preferable as it allows for the choice between keeping plants running or re-start them.

Again, the start-up costs implemented in the LPIPOM should be considered as restrictions on the technology level. Therefore, used parameters can not be directly compared with the input parameters representative for the power plant level in the MILP approach.

2.5.3.2.2 Data and assumptions

An optimization is performed by LPIPOM while start-up costs are included in the objective function as it is given in equation (2.46), and operational constraints (2.47)-(2.49) are taken into account. A one-year period with an hourly temporal resolution is considered. The wind power capacity is fixed at 4718 MW as before.

In scenario “RAMPSC”, start-up costs of nuclear power plants are included in LPIPOM as a technical restriction on base load power plants at a technology level to minimize the deviation of the LPIPOM solution from the results of MILPOPM. The start-up costs of nuclear power plants, implemented on a technology level in LPIPOM, are assumed at 5% of the used start-up costs on the power plant level in MILPOPM, given in Table 2.2. This lower number is due to the fact that start-up costs are accounted for too heavily in the LP approach; indeed, these start-up costs should be seen as a restriction on a technology level, rather than on a power plant level. The parameter (α) is assumed at 5%. These have been determined through a sensitivity study to minimize deviation of LPIPOM solution in operational terms from the MILP results. Ramping constraints are included as in the previous subsection. Other assumptions and data are described in section 2.5.2.2.

The optimal capacity mix, obtained from LPIPOM, is downscaled according to the availability of power plants and is disaggregated based on the unit size levels, given in Table 2.3. These are then used as input to MILPOPM to represent the available capacity of each generation unit. The dispatch of power generation units is then optimized by MILPOPM for subsequent 24-hour periods through a year.

2.5.3.2.3 LPIPOM with ramping constraints and start-up costs vs. MILPOPM

In this section, the influence of the inclusion of start-up costs of base load power plants in addition to technology ramping rates on the deviation of LPIPOM solution from the MILPOPM solution is demonstrated.

According to Fig. 2.14, inclusion of start-up costs of base load power plants in addition to technology ramping rates leads to a further improvement of the results, obtained from LPIPOM, due to its lower deviation from the MILPOPM solution in operational terms. As previously described, when only technology ramp rates are taken into account, the deviation of discarded wind power is reduced by more than 85% as compared to scenario “No RAMP”. Additional inclusion of start-up costs of base load power plants in scenario “RAMPSC” leads to the reduction of this deviation by 91% from the level in scenario “No RAMP”. Moreover, the deviation of total operational costs is reduced by another 4% from the level in scenario “RAMP”.

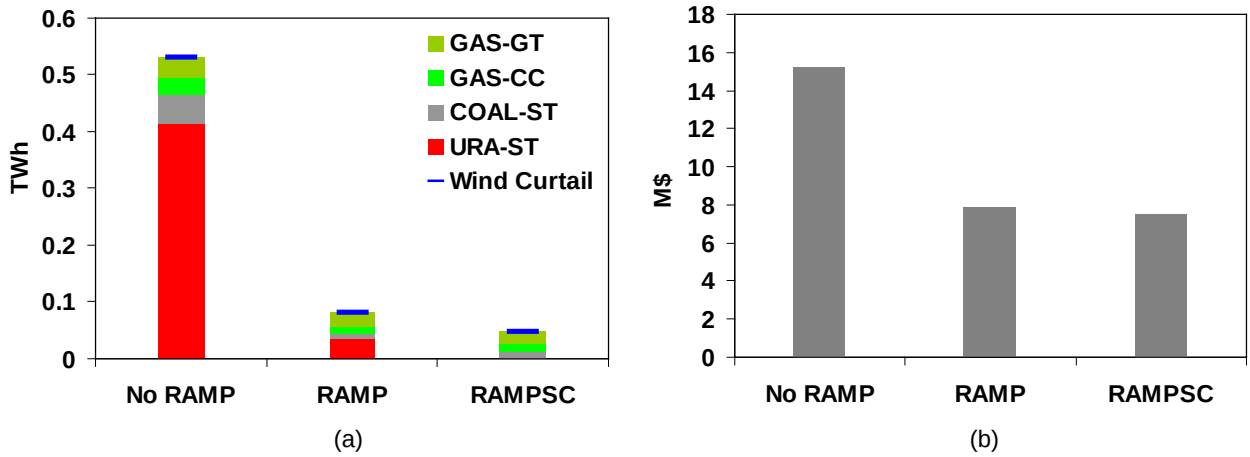

Fig. 2.14: LPIPOM with/without ramping constraints and start-up costs vs. MILPOPM (a) Production per technology in LPIPOM subtracted from production in MILPOPM; (b) Total operation costs in LPIPOM subtracted from total operation costs in MILPOPM

2.6 Conclusions

In order to analyze the impact of the variability of FRES on the structure and operation of the global electricity generation system, a global multi-regional electricity system optimization model has been developed based on the linear programming approach. The simulation methodology is a combination of a high temporal and geographical resolution. Capacities of power generation and storage systems as well as inter-zonal energy transport capacities are optimized by this model. Output power of power plant technologies, inter-zonal energy flows, CO_2 emissions, and marginal price of electricity are determined at every hour of the simulation period for each model region. The cost of avoiding one ton of CO_2, i.e. marginal price of CO_2 emissions, can also be concluded from this optimization model.

It has been demonstrated that the model in its simple form without inclusion of technical constraints is equivalent to the classical screening curve methodology. In such an investment planning model based on LP, investment decisions are optimized under different framework conditions while operational constraints of power plants are simplified. Consequently, the generation output can differ from the output power determined by a power system operation optimization model, taking into account technical restrictions of power plants at a detailed level. Specifically, regarding base load generation and wind power curtailment, the differences can be significant.

Therefore, as a reference model to evaluate the feasible solution according to operational restrictions of the power generation system, a power system operation optimization model has been developed based on the MILP approach. This methodology allows a detailed formulation of the technical restrictions of power plants.

To enhance the LP investment optimization model, additional linear constraints have been then proposed and incorporated in the LP investment and production optimization model. This is to bring its solution in terms of operation closer to the technically-feasible solution, determined by the power system operation optimization model based on the MILP approach. Technical restrictions are based on ramping constraints and start-up costs on a technology level.

It has been demonstrated that the inclusion of these constraints brings the output from the LP approach very close to the generation proposed by the MILP approach. Furthermore, with the inclusion of technical constraints, investment decisions move further towards flexible power generation technologies when increasing the share of FRES. Curtailment of wind power and total operational costs increase as a result. Ramping constraints have the highest influence on the results, and significant changes are noticed if a high share of wind power is integrated into a power generation system, which has a high capacity of non-flexible, base load power plants.

It is finally concluded that with the inclusion of a linear formulation of ramping constraints and start-up costs at a technology level in the LP investment and production optimization model, the deviation of the LP solution from the technically-feasible solution, determined by the MILP operation optimization model, is minimized. This leads to the improvement of the LP optimization model with respect to technical feasibility of its solution. For an illustrative case, the deviation of LP solution from the results of the MILP approach in terms of discarded wind power is reduced by 91% while the difference in operational costs is reduced by 51%.

3 Development of a global electricity system database

After having described the modeling approach, different data sources and approaches applied to determine the input parameters, which are required to perform an optimization of a future global electricity supply system, are described in this chapter.

3.1 Electricity production from renewable energy sources

Geographical dependencies of renewable energy sources and variable output power from intermittent renewable sources such as solar and wind energy are among the key input parameters of the electricity system optimization model. In the following, different data sources and approaches applied to determine the input parameters, which are related to the power system integration of renewable energy sources, are described.

3.1.1 Solar electricity production

In this part, data sources and approaches applied to calculate the time- and region- dependent capacity factor (*supim*) and upper capacity boundary (*cUp*) (see equations (2.4) and (2.7)) of solar electricity generation systems are described.

3.1.1.1 Processing of solar irradiation data

The satellite data of Surface Solar Irradiation Data Set (SSIDS) are used here to determine the geographic distribution of available solar energy at each time step. At a specific geographical position, the accuracy of measured solar irradiation on the ground is higher than the accuracy of evaluations based on satellite's data. However, measuring stations on the ground locate mostly far apart; values in between the stations are determined using an interpolation method as a function of longitude, latitude and elevation, which leads to a large inaccuracy. It has been shown in [59] that the accuracy of satellite's data for distances of higher than 50 km from the measuring location are higher than the accuracy of estimations based on the interpolation of measured values on the ground.

The SSIDS had been produced for SeaWiFS (Sea-viewing Wide Field-of-view Sensor), using data from the International Satellite Cloud Climatology Project (ISCCP). ISCCP DX data is on an equal grid with an effective 30x30 km pixel size. For SeaWiFS production, this data have been mapped on a 0.5˚x 0.5˚ rectangular grid [60]. This data includes three-hourly direct normal and global horizontal irradiance, diffuse fraction, and zenith angle for the time horizon from 1991 to 1993. Hourly values are approximated here using a linear interpolation method.

At first, a comparison is made between the SSI Data Set and ground-based measurements of the World Radiation Data Center (WRDC) [61], using the three-year average of global horizontal radiation for the time horizon from 1991 to 1993. This is shown in Fig. 3.1.a for the latitudes, varying in the range of 40°- 68°. The comparisons made for a few Asian countries, African regions, and Russia are visualized in Fig. 3.1.b, Fig. 3.1.c, and Fig. 3.1.d, respectively. A specific correlation between the extent of deviation and the geographical position can not be proposed. It is concluded that the values of SSIDS are in average 15% higher than the ground-based measurements of WRDC. In Europe, deviations are mostly lower than 20% with a mean level of 13%.

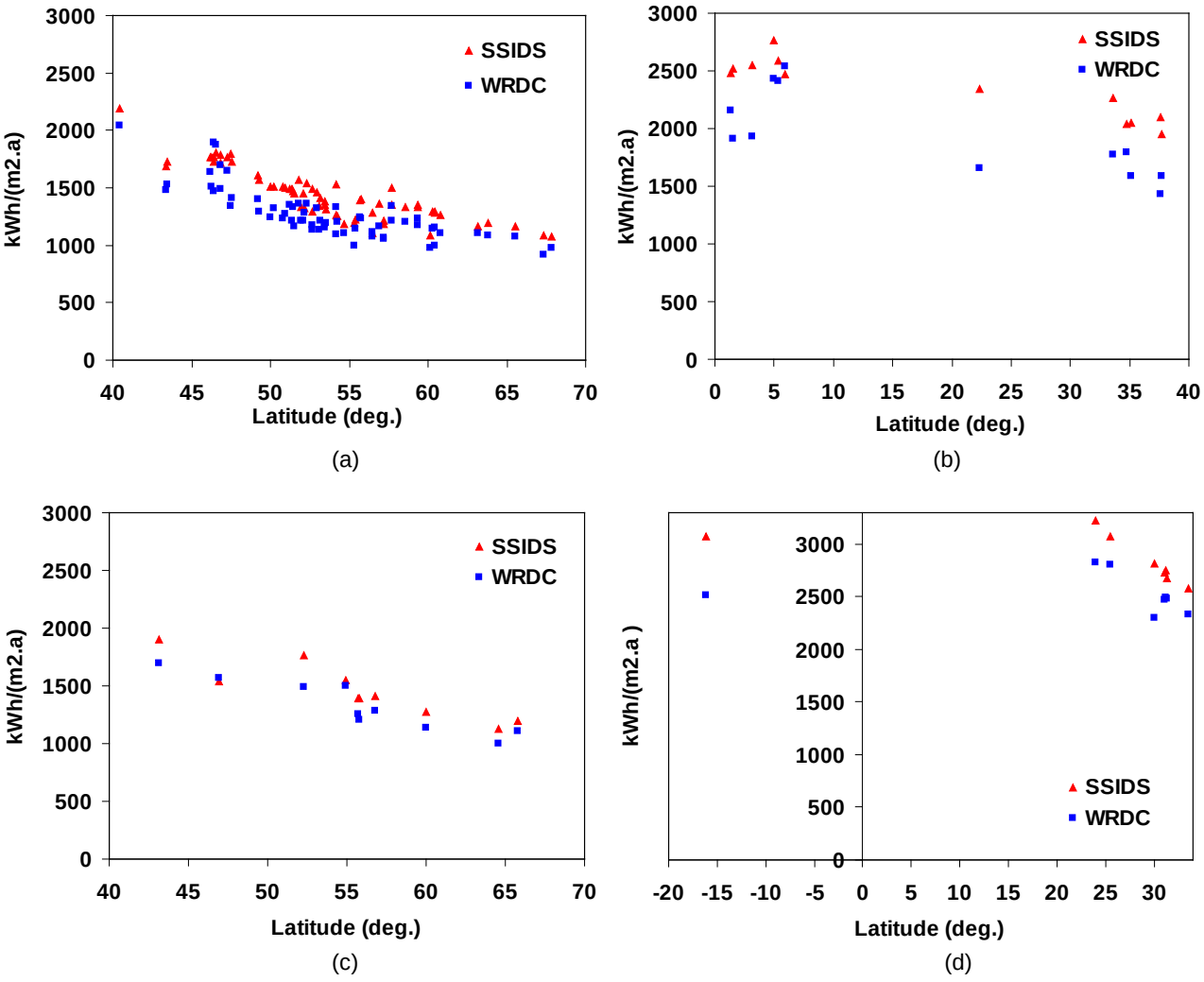

Fig. 3.1: Comparison of SSIDS and WRDC based on three-year average of global horizontal radiation over time horizon 1991-1993 (a) Europe; (b) South East Asia; (c) Russia; (d) Africa. Data source: [60, 61]

The intensity of extraterrestrial solar radiation when integrated over all wavelengths is called the solar constant and reaches to 1353 W/m^2 [62]. The irradiative flux is reduced upon traversing the earth's atmosphere due to reflection, scattering, and absorption. As a result, some portion of the solar power is lost while the remaining portion comprises directional and diffuse components. Thus, the global horizontal radiation comprises both the direct horizontal and diffuse horizontal radiation as it is represented in equation (3.1).

$$I_{GH} = I_{Diff-H} + I_{Dir-H} \tag{3.1}$$

The direct radiation incident on a terrestrial surface with an arbitrary inclination can be estimated from the equation (3.2); $I_{Dir,ts}$ represents the direct beam on a tilted surface; i_{inc} is the surface-solar incidence angle, and β_s is the solar altitude. For a surface that is perpendicular to the direct beam, i_{inc} becomes zero, and the incident radiation can be estimated from the equation (3.3).

$$I_{Dir,ts} = I_{Dir-H} \frac{\cos i_{inc}}{\sin \beta_s} \tag{3.2}$$

$$I_{Dir-N} = \frac{I_{Dir-H}}{\sin \beta_s} \tag{3.3}$$

While Concentrating Solar Power Systems (CSP) can only utilize the direct irradiance, Photovoltaic systems (PV) can convert the diffuse fraction as well. Thus, for PV systems, if modules are placed horizontally, electricity production can be determined, using the global horizontal radiation. For CSP systems, as a first approximation, it can be assumed that tracking of mirrors results in a mirror-plane perpendicular to the irradiation. Thus, direct normal irradiation can be used for the computation of electricity production by solar thermal power plants.

Fig. 3.2 shows the three-year average of annual global horizontal radiation on land sites. It has been produced using the SSI Data Set for a geographical grid with a spatial resolution of 2.5°x2.5°. The highest gain of irradiation is around 2500 kWh/(m^2.a). This is reached in western parts of South America near the Pacific Ocean around mean latitude of -20°, i.e in Chile, Bolivia, and northwestern Argentina. North Africa from latitude of around 8° to 32°, South Africa, Mexico, Middle East, South East Asia, and Australia are also considered as promising sites regarding the annual gain of irradiation. In Central and Western Europe, annual gain of radiation reaches to around 1000 kWh/(m^2.a), which corresponds to 40% of the maximum radiation on a terrestrial horizontal surface.

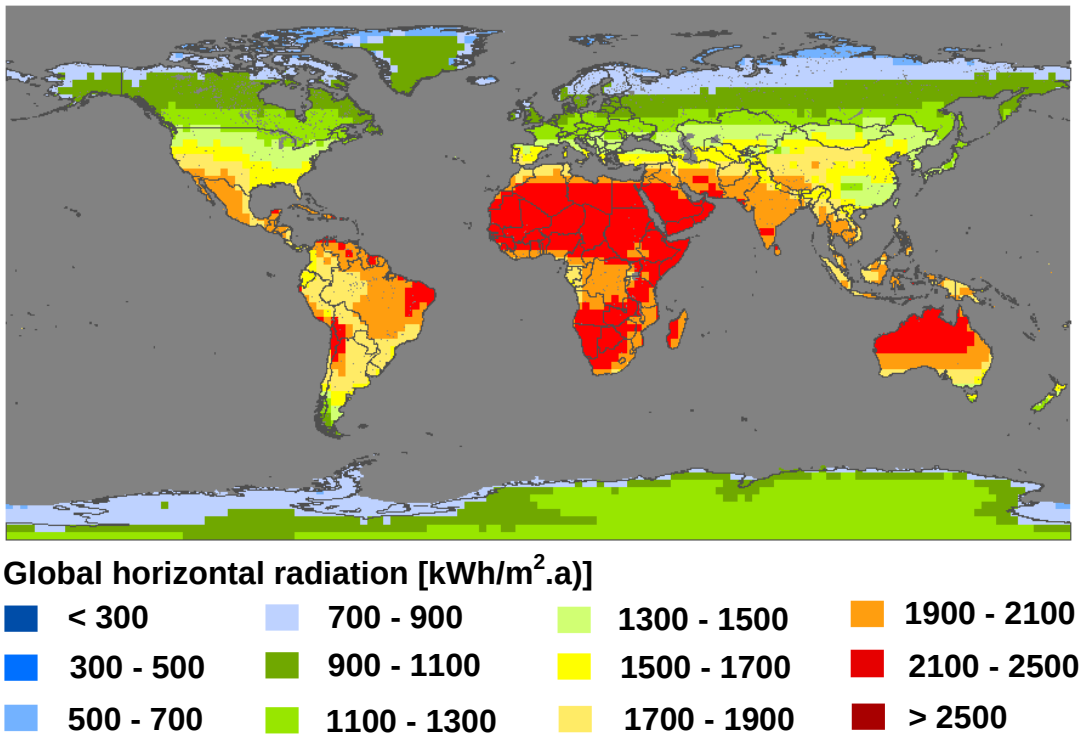

Fig. 3.2: Three-year average of annual global horizontal radiation on land sites over time horizon 1991-1993. Data source: [60]

Another advantage of PV electricity production in Sahara and sub-Saharan regions against production at higher latitudes is the lower seasonal variations, and, thus, a more balanced production through a year. For instance, proportion of global horizontal radiation in December to

global horizontal radiation of July is visualized in Fig. 3.3. In Sahara, this proportion reaches to 0.6; in sub-Saharan regions, PV electricity production in summer and winter is nearly equal. Promising sites of the Middle East, South East Asia, central and north-eastern Brazil, and Mexico also benefit from a balanced production through a year. Although Australia is considered as a promising site regarding the annual gain of global horizontal radiation, the production is characterized with extreme seasonal variations. According to Fig. 3.3, in Australia, the proportion of global horizontal radiation in December to global horizontal radiation of July is mainly greater than 2.

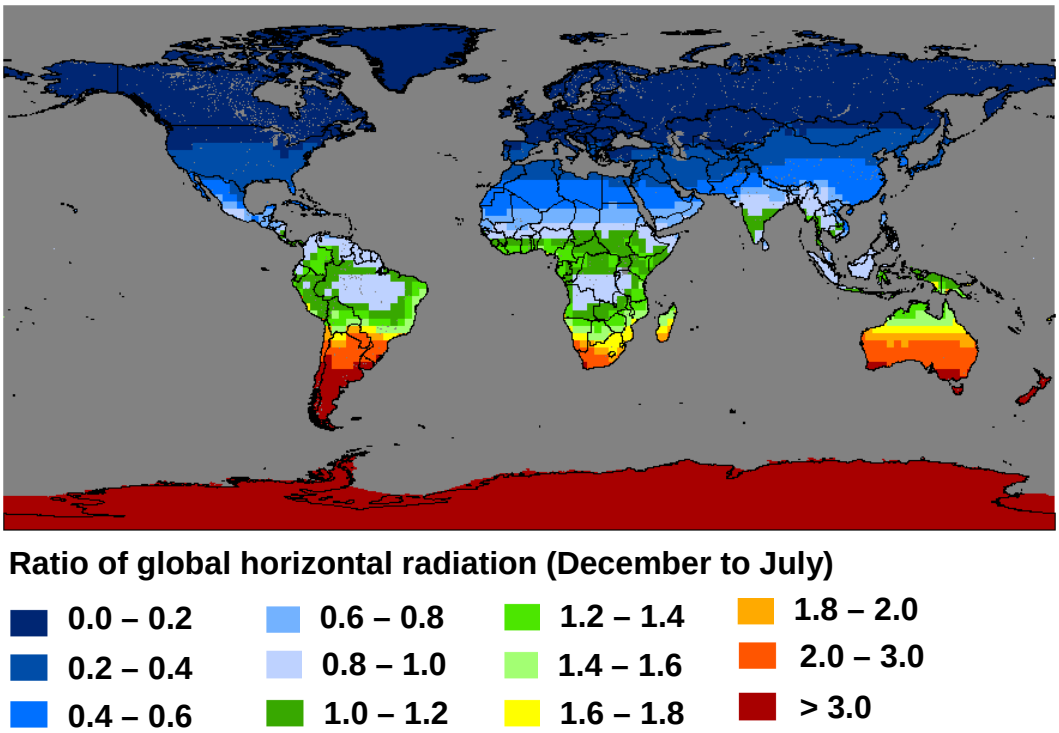

Fig. 3.3: Three-year average of ratio of global horizontal radiation in Dec. to global horizontal radiation of July over time horizon 1991-1993. Data source: [60]

3.1.1.2 Evaluation of geographical potential of solar electricity production

For centralized PV systems and solar thermal power plants, geographical potential is evaluated based on the elaborated analysis of global technical potential of solar thermal electricity production, conducted in [13]. There, land sites are categorized into suitable, limited suitable, and unsuitable regions according to natural conditions, land-use characteristics, and slope of the ground. On this basis, the maximum capacity that can be installed at each model region is determined.

Fig. 3.4 shows the categorization of global land sites for solar thermal electricity production based on the study conducted in [13]. It is concluded that suitable sites mostly locate in south of Sahara, Botswana, Namibia, Argentina, eastern Brazil, Bolivia, Mexico, Venezuela, central and western USA, and Kazakhstan.

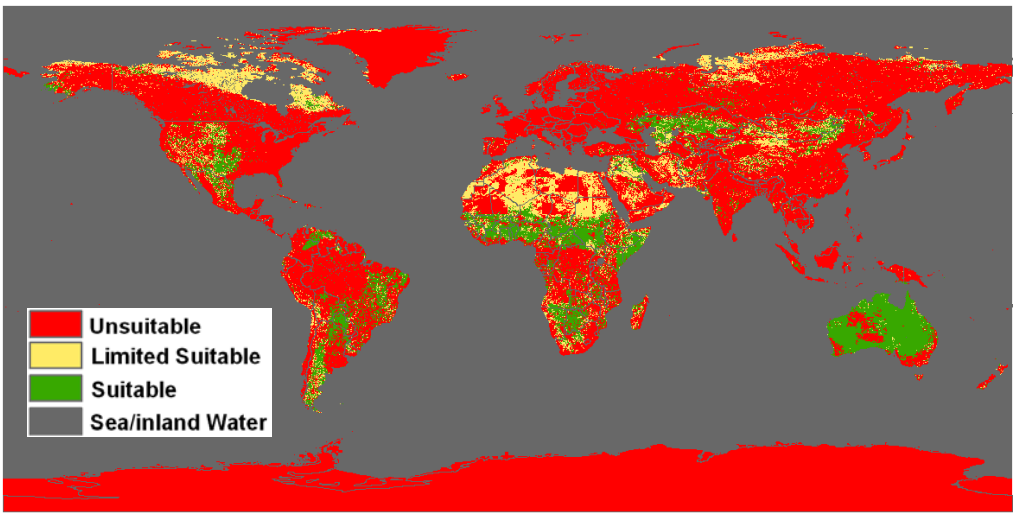

(a)

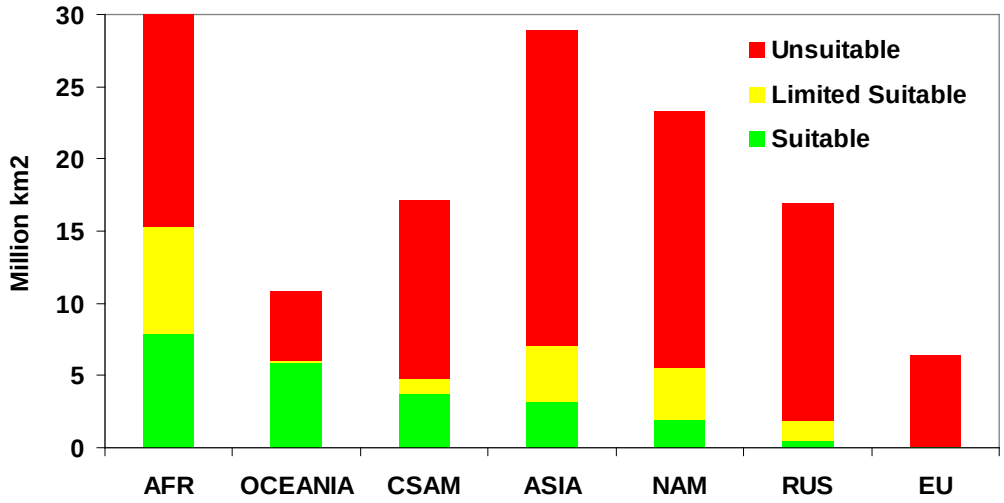

(b)

Fig. 3.4: Categorization of global land sites for solar thermal electricity production (a) Geographic distribution; (b) Absolute values for 7 world regions. Data Source: [13]

Since the available area is subject to different constraints for centralized and decentralized PV applications, the geographical potential is determined independently for these two application types.

In the study conducted in [63], the roof-top area per capita for the usage of PV applications has been assessed. However, this study is limited in the number of covered regions. In [14], based on the results obtained from [63], a correlation is proposed between the available roof- top area per capita and the GDP per capita. The available area for decentralized PV installations per grid-cell is then estimated, multiplying the available roof-top area per capita by the population of the corresponding grid-cell.

The orientation of PV modules and arrays towards the sun significantly influences the gain of output power. The optimal tilt and orientation of an array is a function of the latitude and the fraction of diffuse radiation. At optimal tilt, the amount of solar irradiation on the surface of arrays is maximized. However, when the arrays are not placed horizontally, the electricity output per unit area may suffer from shadowing effects of neighboring arrays, unless they are installed

at a proper distance from each other. The key factor in designing a utility scale PV plant is to gain the optimal ground area occupation ratio (GAOR) without significant reduction of the performance ratio. The GAOR is the ratio between the total surface of PV modules, used to realize the PV field, and the total ground area occupied by the PV field. Typical values of GAOR for a fixed PV installation in southern Italy is in the range of 0.3-0.6, which corresponds to a tilt angle in the range of 35°-25° while for the tracker systems, the GAOR is in the range of 0.2-0.3 [9].

The CSP plant's land occupation depends on the total installed collectors' surface and on the distance between the modules, which is required to minimize shadowing effects and to allow the maintenance of curved, reflecting mirrors. Additional surface is required for the power block and the heat storage system, which are usually located in the middle of the plant area and have a land occupation much smaller than the solar field.

In this study, the upper capacity boundary for CSP and centralized PV installations at each model region is the total available area, including both suitable and limited suitable sites, as it is evaluated in [13], reduced by the GAOR factor. The GAOR factor is assumed at 0.33 and 0.29 for PV and CSP power plants, respectively based on data from [9, 64].

3.1.2 Wind electricity production

The short-term variability of wind energy is a challenging issue for its integration into the power system. However, the advantage lies in the fact that wind speeds in distances corresponding to the scale of weather systems are not well correlated, in other words: wind is always blowing somewhere. A well interconnected network is thus a precondition to realize an optimal usage of spatial de-correlations of wind power production. Cross-border exchange of electricity enables capturing smoothening effects of geographical aggregation on the variations of wind power production. This improves the accuracy of wind power production forecasts and increases the capacity credit of wind power.

In the following, approaches applied to determine the capacity factor and upper capacity limit of wind energy converters, are described.

3.1.2.1 Processing of wind speed data

To evaluate the variable output power of wind turbines in on- and off- shore sites, the modeled wind speeds of World Wind Atlas (WWA) [65] are applied in this study. The WWA offers wind speeds for 4096 positions on the globe, located in onshore sites and near offshore coastal areas, based on the reanalysis data of National Center for Atmospheric Research and National Center for Environmental Prediction (NCAR/NCEP). This data includes wind speeds and moving direction at 50 m above the ground at six-hourly intervals for the time horizon from 1992 to 2001; it has been mapped on a geographical grid with a resolution of 2.5°x 2.5°.

The geographic distribution of a ten-year average of wind speed is shown in Fig. 3.5. High wind classes are seen, for instance, in Ireland, Scotland, and England as well as in Norway and other European coastal areas, northern African coastal area near the Atlantic Ocean, Greenland, Argentina, and Chile.

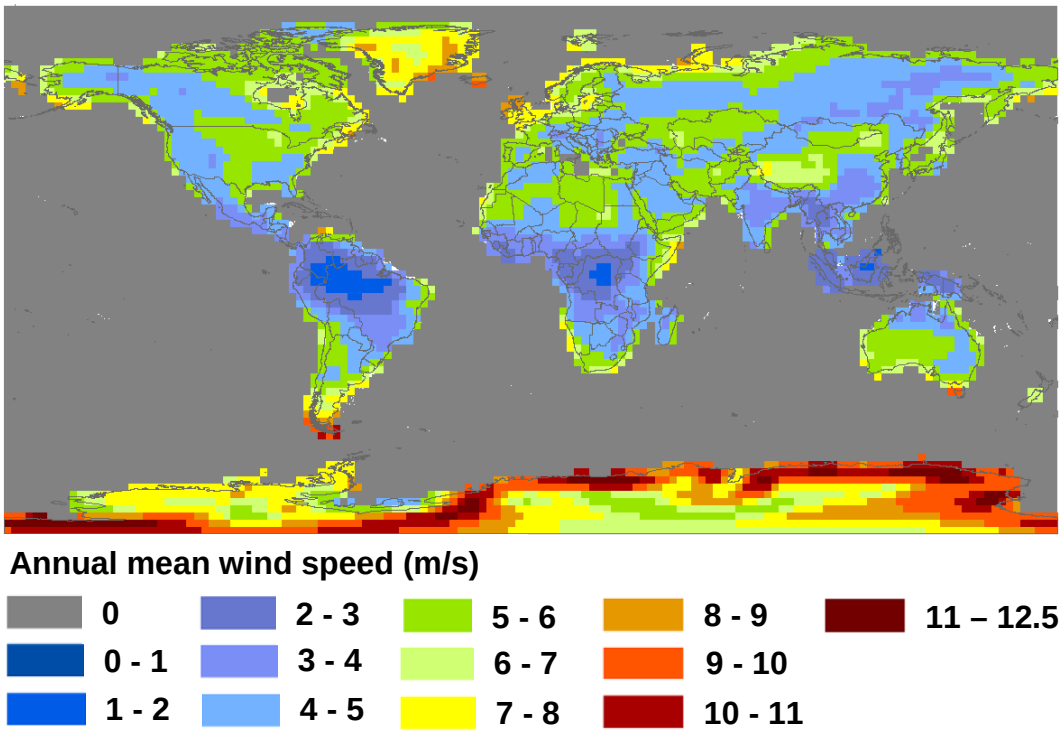

Fig. 3.5: Ten-year average of wind speed over time horizon 1992-2001. Data Source: [65]

The effect of six-hourly interval is that changes in wind speed, which occur at shorter time scales, are not captured. Consequently, very rapid changes of wind speed are not accurately represented; thus, intra-day variations are underestimated. For the purpose of modeling at a high temporal resolution, a suitable approach must be proposed to extend the available values for every six-hour to an hourly dataset while still retaining the variable characteristic of real wind speeds.

Here, hourly variations are approximated, using a statistical approach based on the Brownian Bridges method [66]. This is an improvement compared to a basic linear interpolation, which results in the underestimation of variations between six-hour intervals. To produce the statistically-interpolated database, the mean and variance are calculated using the time series of wind speed from WWA. This means that an individual normal distribution is required for each time step. A synthetic hourly time series of wind speed is then generated by sampling this particular normal distribution at random.

3.1.2.2 Normalized output power

Output power of a wind turbine depends on wind speed at the site and properties of the wind turbine, represented with a power curve. In the following, normalized output power also referred to as the wind power capacity factor is calculated from the meteorological data of WWA.

3.1.2.2.1 Relationship between wind speed and output power

Wind speed and energy content of the wind are governed by a third order relationship as it is expressed in equation (3.4); ρ_{air} is the density of air; *Area* represents the swept area of the turbine rotor blades, and *v* is the wind speed upstream the rotor. The electrical power of a wind

turbine depends on its technical properties and the wind speed as it is represented in equation (3.5). The power coefficient of wind turbine (c_p) is the proportion of electrical output to the energy content of wind. According to equation (3.6), when the wind speed at hub height exceeds the cut-in wind speed of wind turbine ($v_{cut\text{-}in}$), the power coefficient is at maximum ($c_{p,max}$); it starts to decline when the wind speed at hub height exceeds the rated wind speed (v_R) and reaches to zero when the wind speed at hub height is higher than the cut-out wind speed of turbine ($v_{cut\text{-}out}$). The maximum power coefficient of an ideal wind turbine is 16/27=0.593=$c_{p,Betz}$, which is known as the Lanchester-Betz-Joukowsky limit [67]. For a real wind turbine, the maximum power coefficient ($c_{p,max}$) is lowered by the conversion efficiency factor (η_T) as it is expressed in equation (3.7); P_R is the nominal power of wind turbine and is given in equation (3.8). In Fig. 3.6, the energy content of wind and the energy that can theoretically be harvested are visualized versus the electrical output of a real wind turbine.

$$P_{Wind} = \frac{1}{2}.\rho_{air}.Area.v^3 \tag{3.4}$$

$$P_{T,el} = c_p(v).P_{Wind} \tag{3.5}$$

$$c_p(v) = \begin{cases} 0 & v < v_{cut-in} \\ c_{p,\max} & v_{cut-in} \le v < v_R \\ \dfrac{2.P_R}{\rho_{air}.Area.v^3} & v_R \le v \le v_{cut-out} \\ 0 & v_{cut-out} < v \end{cases} \tag{3.6}$$

$$c_{p,\max} = c_{p,Betz}.\eta_T \tag{3.7}$$

$$P_R = c_{p,\max}.\frac{1}{2}.\rho_{air}.Area.v_R^3 \tag{3.8}$$

The wind speed varies with altitude due to frictional effects at the surface of the earth. The WWA data includes wind speeds at 50 m above the ground, which does not correspond to the hub height of modern wind turbines (80-130m). The wind speed at hub height can be approximated, for instance, based on the logarithmic approach [68]. According to equation (3.9), wind speed at hub height (v) can be determined from the given wind speed at reference height (v_{Ref}) and roughness length of the terrain (z_0). The roughness length varies from 0.0002 m at sea level to 1 m for cities and reaches to more than 2 m in densely occupied regions [69]. The assumed levels for the roughness length are given in (3.10), which is based on the classification made in [69].

$$v = \frac{\ln(\frac{H_x}{z_0})}{\ln(\frac{H_{Ref}}{z_0})}.v_{Ref} \tag{3.9}$$

$$z_0 = \begin{cases} 0.0002 & Roughness\ class\ 1\ ,\ Offshore \\ 0.03 & Roughness\ class\ 2\ ,\ Coast \\ 0.1 & Roughness\ class\ 4\ ,\ Onshore \end{cases} \tag{3.10}$$

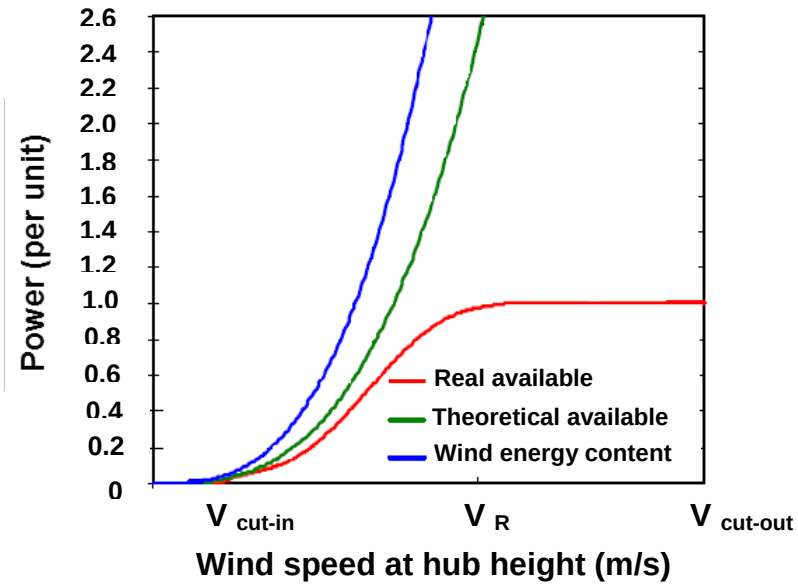

Fig. 3.6: Normalized output power of a real wind turbine vs. theoretical output and energy content of wind

3.1.2.2.2 Calculation of wind power capacity factor

Wind power capacity factor, also referred to as normalized output power, is given in equation (3.11). This is obtained by normalizing the electrical output by rated power of the wind turbine.

$$CF_{wind} = \begin{cases} 0 & v < v_{cut-in} \\ \left(\frac{v}{v_R}\right)^3 & v_{cut-in} \le v < v_R \\ 1 & v_R \le v < v_{cut-out} \\ 0 & v_{cut-out} < v \end{cases} \tag{3.11}$$

Short-term fluctuations of wind speed are in some degree smoothed out at the output power from a single wind turbine unit, both by the extent of the rotor and power control of the wind turbine. Aggregated power generation from more wind turbine units within an area will further smoothen out these short-term fluctuations as power generation from individual units is not completely correlated. The extent of the smoothening effect depends on the number of units, size of the area, and the time scale.

At present, no real time series of wind power production are available that allow a chronological simulation of worldwide wind power generation at on- and off- shore sites. Therefore, it is synthesized using the available information about wind speed.

Different methodologies exist to calculate wind power production or the capacity factor from the wind speed. This includes single-turbine power curve approach, aggregated wind power curves, and statistical modeling [70]. Using a single-turbine power curve, time series of aggregated power generation from a cluster of wind turbines is simulated using the time series of wind speed at a single point. Drawback of applying a single wind turbine power curve to estimate output power from an entire wind park is that it overestimates variations of wind power near cut-out wind speeds, especially at offshore sites, where distances between wind turbines are significant. However, an enhanced evaluation can be made based on the time series of wind

speed at a single point, using a standard power curve of a wind turbine, while smoothening effects in both time and space are taken into account. A methodology has been proposed in [71] to approximate an aggregated power curve of a wind park. Different methods applied to determine parameters of the Weibull distribution of wind speed are compared in [72]. In this study, a multi-turbine power curve approach is applied to simulate smoothening effects of geographical aggregation on variations of output power from a cluster of wind turbines. For instance, in Fig. 3.7, an adjusted multi-turbine power curve is compared with a single power curve, representative for a large-scale wind turbine.

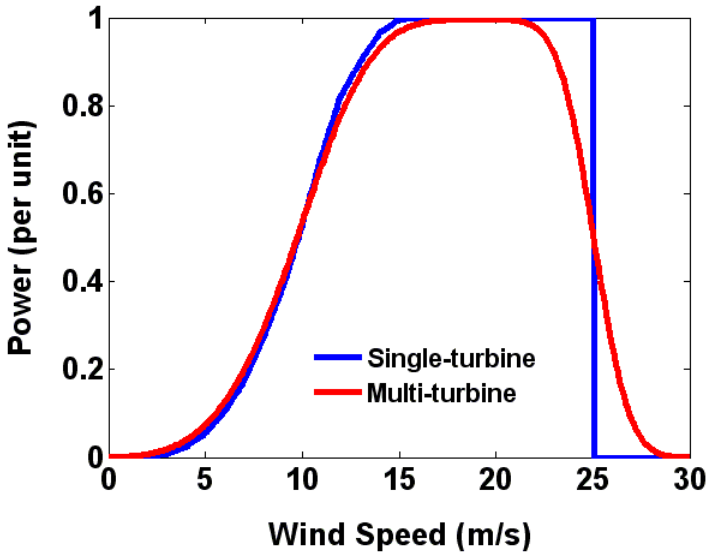

Fig. 3.7: A multiple-turbine power curve vs. a single-turbine power curve (E-70). Data Source: [65]

The wind power capacity factor has been approximated at each hour of the year for each cell of a geographical grid with a resolution of 2.5˚x2.5˚ using both a single-turbine and a multi-turbine power curve approach. Aggregated hourly variations of wind power capacity factor, approximated for a one-week period in winter, are shown in Fig. 3.8 for selected countries. It is concluded that the single-turbine power curve approach overestimates variations of output power from a wind park.

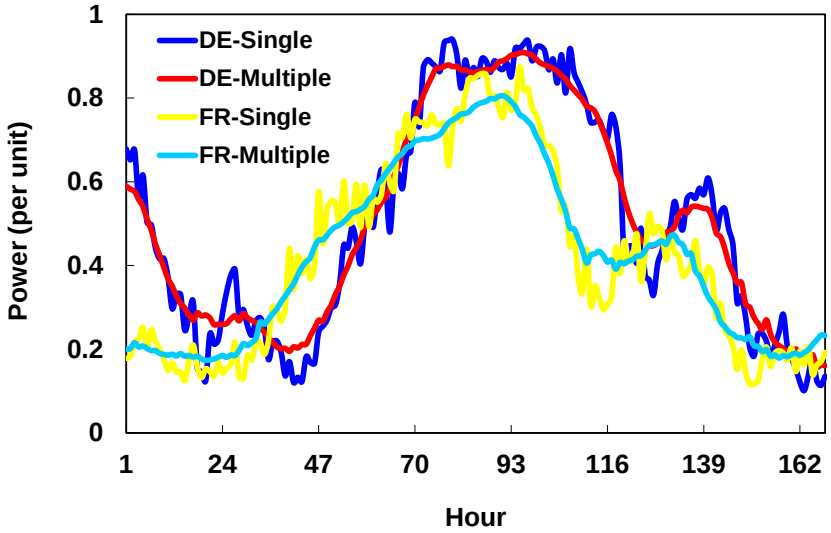

Fig. 3.8: Hourly variations of wind power capacity factor over one week in Feb. Data Source: [65]

The extent of the smoothening effect of geographical aggregation on variations of wind power can be demonstrated by comparing statistical parameters of the synthesized time series of normalized output power, using a single-turbine power curve, with statistical parameters of the generated time series based on the multi-turbine power curve approach. For instance, real produced wind power through the year 2009 in Germany is shown in Fig. 3.9. The relative standard deviation (standard deviation divided by mean) is 1.1 if the approximation is made, using a single-turbine power curve; it reduces to 0.9 if the multi-turbine power curve approach is applied. For comparison, the relative standard deviation of the real time series of wind power is 0.8.

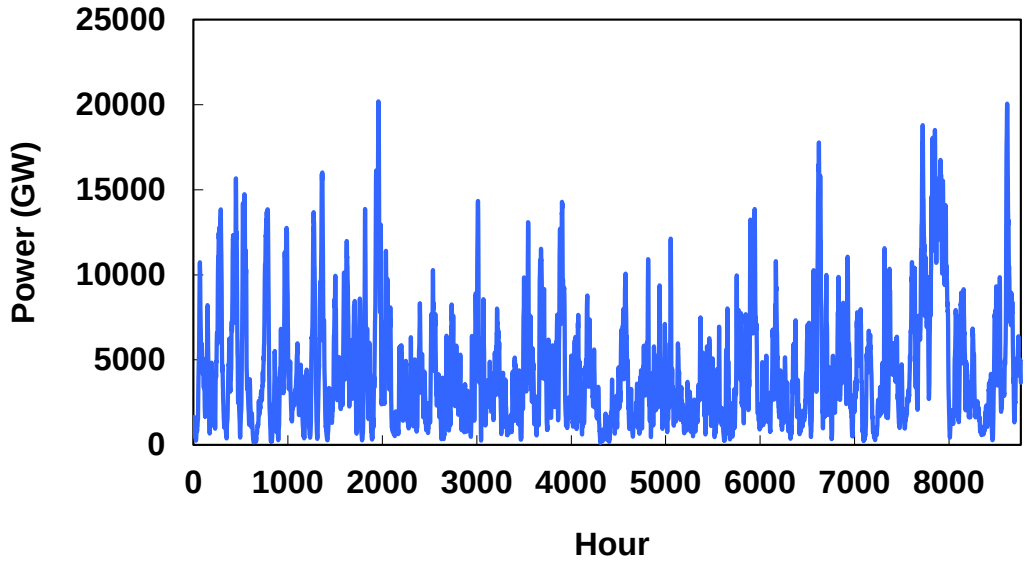

Fig. 3.9: Real total wind power production in Germany in year 2009. Data source: [73-76]

This influence is more evident when considering hourly variations of wind power production. If a single-turbine power curve is used, the standard deviation of variations is 0.29. Applying the multi-turbine power curve approach, this significantly reduces to 0.08. For the real time series of wind power normalized by the maximum production of the year, the standard deviation of variations is as low as 0.09.

In this study, hourly time series of normalized wind power are synthesized for each geographical grid-cell, using the wind speed data from WWA and applying the multi-turbine power curve approach proposed in [71]. For instance, Fig. 3.10 shows the geographic distribution of annual full load hours of wind power on suitable land sites, which has been approximated using the meteorological data of the year 2000. On this basis, the most promising sites locate in Somalia, Alaska, South America, western part of China, and England.

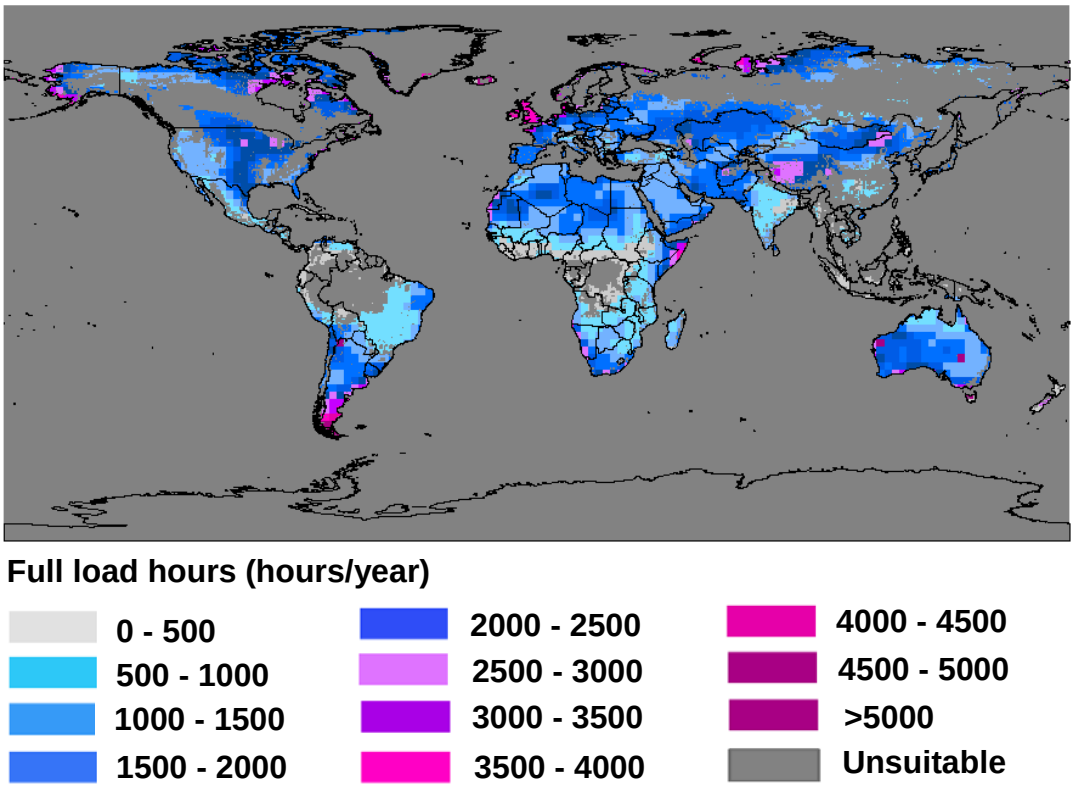

Fig. 3.10: Geographic distribution of wind onshore full load hours on suitable land sites in year 2000. Data source: [12, 65]

Seasonal variation of wind power is illustrated in Fig. 3.11, using the proportion of wind power production in July to the wind power production in February. It is seen that the European countries are characterized with a higher production in winter than in summer. In contrast, the northern African territories are characterized with a higher production in summer. Thus, we can benefit from different seasonal characteristics of wind power production when interconnecting these regions in order to reach a more balanced production through a year.

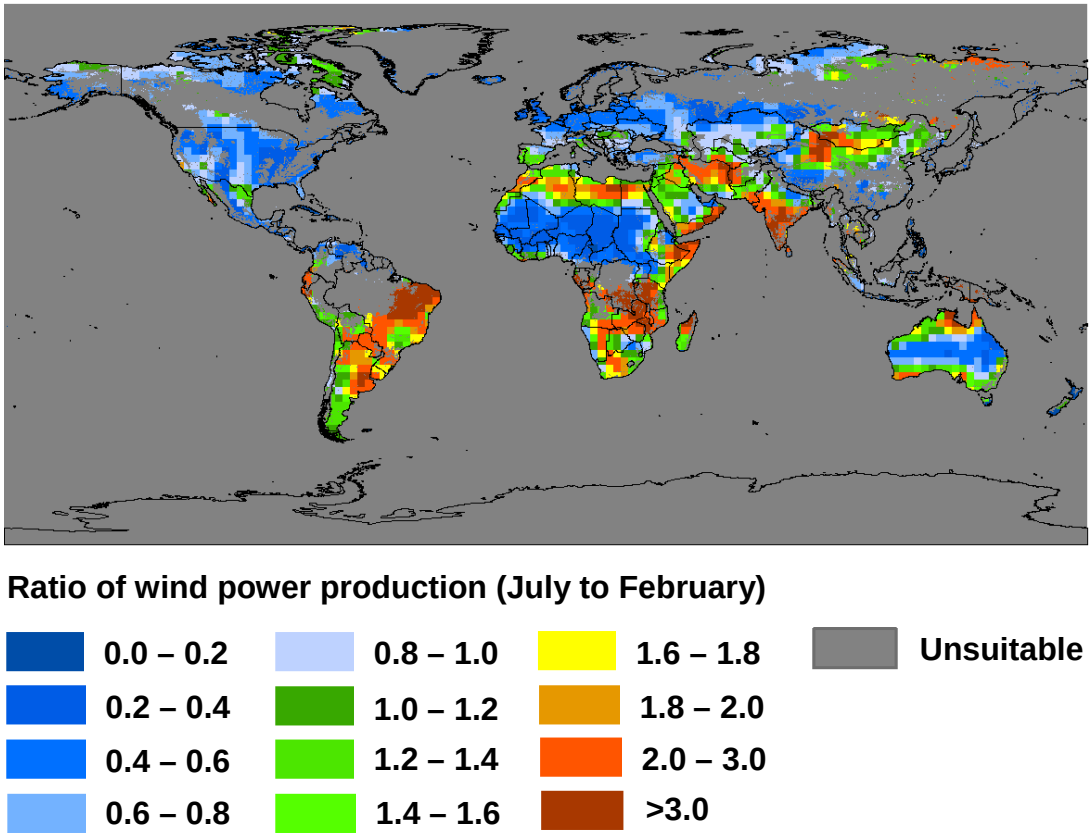

Fig. 3.11: Proportion of wind onshore power production in July to wind power production in Feb. on suitable land sites in year 2000. Data source: [12, 65]

Long-term variation of wind electricity production is visualized in Fig. 3.12. The figure shows the proportion of wind power production, which has been approximated using the meteorological data of the year 2000, to its ten-year average over the time horizon from 1992 to 2001.

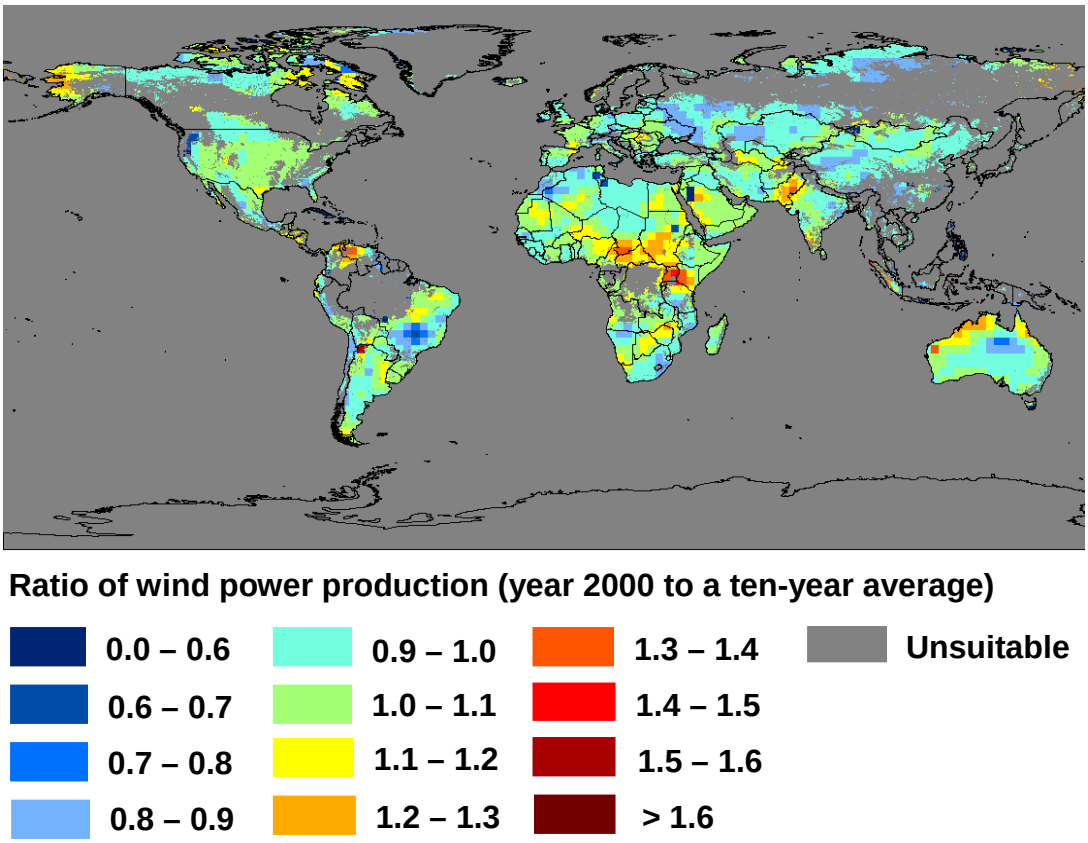

Fig. 3.12: Proportion of wind onshore power production in year 2000 to a ten-year average over time horizon 1992-2001 on suitable land sites. Data source: [12, 65]

3.1.2.3 Smoothening effects on wind power's variations

Time characteristics of wind power are highly dependent on the geographical position. Hence, geographical spreading of wind parks leads to a certain amount of smoothening and results in a less variable output power.

To demonstrate smoothening effects of geographical aggregation, normalized output power is illustrated in Fig. 3.13 for two specific grid-cells within a country; grid-cell *i* is centered at the latitude of 38.75° and the longitude of 3.75°, and grid-cell *j* is centered at the latitude of 41.25° and the longitude of 3.75°. Aggregated normalized output power, representative for the whole country, is also shown. To clarify smoothening effects, resulting from an enlargement of the production area, statistical properties of all time series are summarized in Table 3.1. These influences can specifically be understood when comparing the standard deviation of hourly variations of output power at different geographical scales. This factor significantly reduces when the dimension of the considered region is increased.

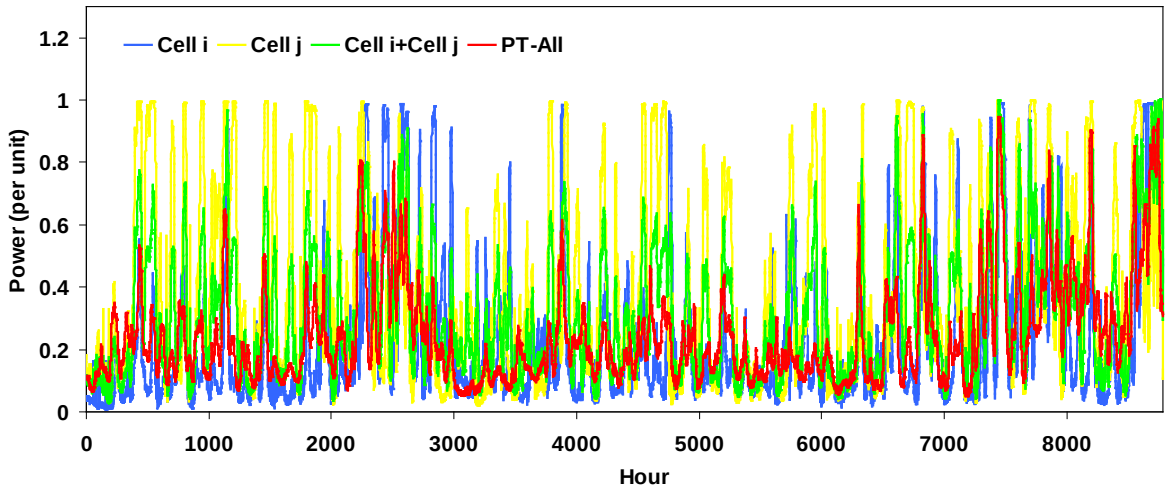

Fig. 3.13: Normalized wind power at selected positions. Data Source: [65]

Table 3.1: Statistical properties of time series of normalized wind power in Fig.3.13

Parameter	Cell i	Cell j	Cell i + Cell j	PT
Standard deviation	0.2393	0.3043	0.2141	0.1638
Standard deviation of hourly variations	0.4664	0.5076	0.2181	0.0501

Smoothening effects are stimulated if the time series of output power are aggregated over all grid-cells within one model region. Chronological order of hourly variations of output power over a one-month period in winter and in summer is visualized in Fig. 3.14 for selected model regions. Linear combination of all time series, representative for the total Europe, clarifies how smoothening effects become significant if wind parks are distributed over an extensive area. The explanation arises from the fact that variations of wind power in single regions are only slightly correlated or are totally de-correlated. As a result, aggregated time series is less variable than single-regional time series. Significant increase of produced power through periods of high wind speed and its sudden, significant reduction in periods of low wind speed, occurring within single isolated regions, is eliminated if the total area is interconnected.

This effect can also be realized when considering the annual duration curve of output power. This is visualized in Fig. 3.14.c for selected model regions and for the total Europe. Specific time characteristics can be noticed if wind turbines are installed at distant but interconnected regions with different meteorological conditions. The maximum achievable output reduces, and the rate of reduction is significantly decreased; thus, we achieve a balanced production through a year.

Statistical properties of the time series are represented in Table 3.2. Through enlargement of the production area, standard deviation, standard deviation of hourly variations, and the maximum production are considerably reduced while the minimum output power is increased.

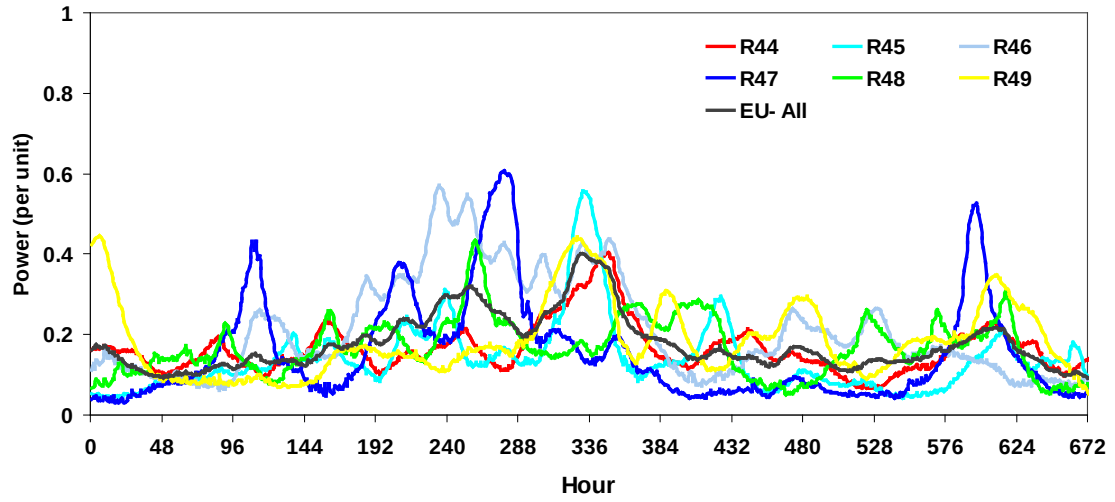

(a)

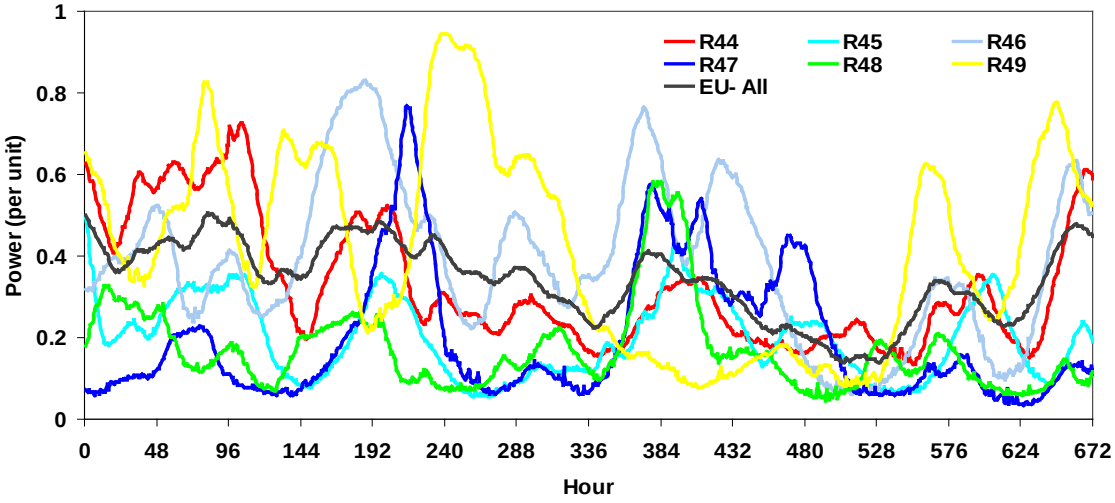

(b)

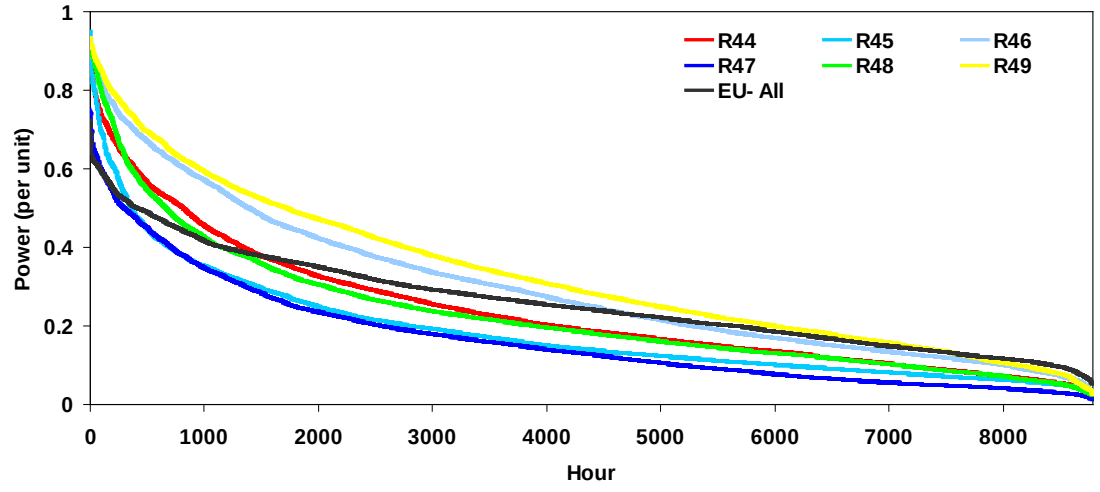

(c)

Fig. 3.14: Chronological order and duration curve of normalized wind power for selected model regions and total Europe (a) Chronological order in July; (b) Chronological order in Feb.; (c) Annual duration curve. Data Source: [65]

Table 3.2: Statistical properties of time series of normalized wind power in Fig. 3.14

Region	Maximum	Minimum	Standard deviation	Standard deviation of hourly variations
R 44	0.8941	0.0290	0.1621	0.0430
R 45	0.9524	0.0327	0.1386	0.0382
R 46	0.9123	0.0370	0.1880	0.0356
R 47	0.7571	0.0212	0.1346	0.0704
R 48	0.9152	0.0332	0.1622	0.0413
R 49	0.9437	0.0358	0.1939	0.0346
R 50	0.9459	0.0394	0.2734	0.0979
EU-All	0.7356	0.0651	0.1214	0.0130

These influences become even more evident when a global scale is taken into account. For instance, Fig. 3.15 shows the chronological order and duration curve of normalized wind power for selected model regions and on a continental basis. The figure additionally includes an aggregated curve, which is derived by summing the output power over all model regions.

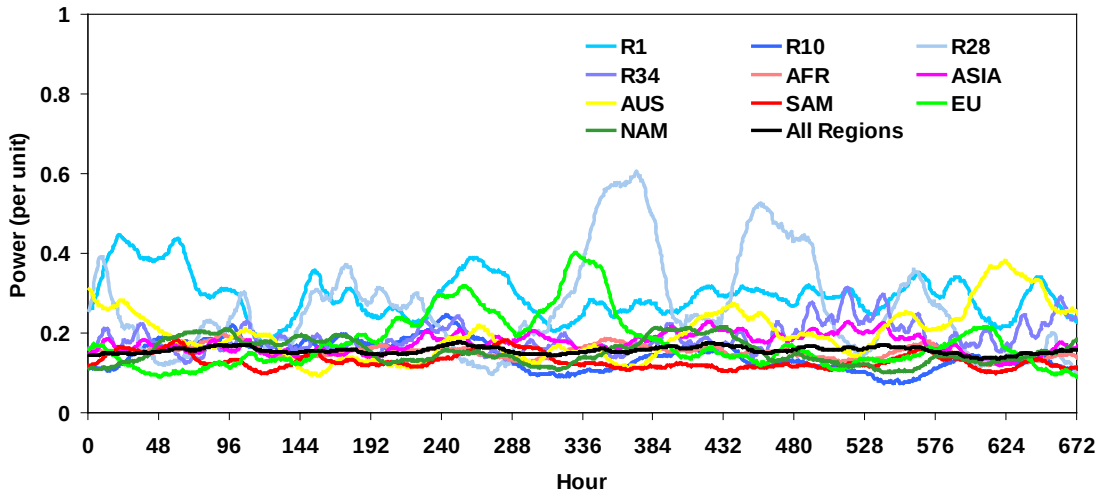

(a)

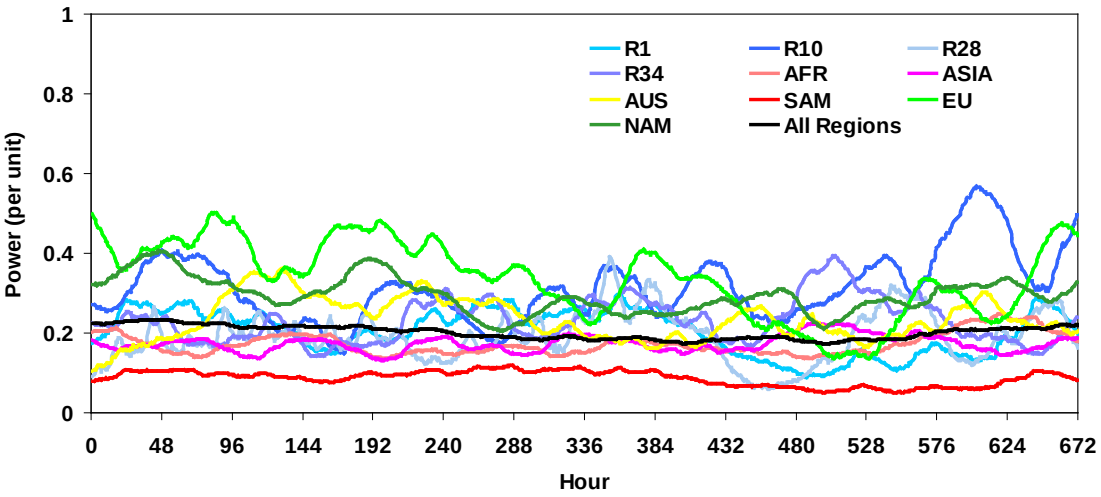

(b)

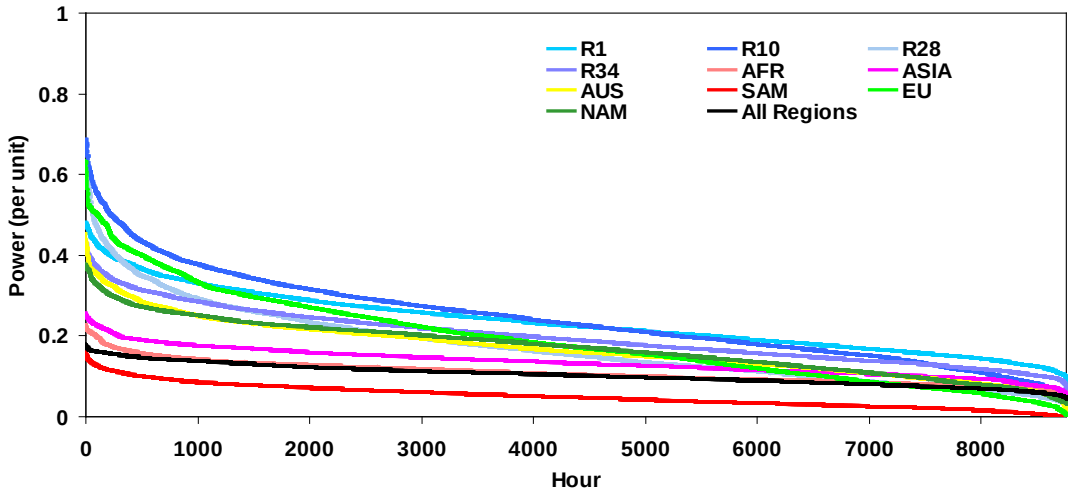

(c)

Fig. 3.15: Chronological order and duration curve of normalized wind power for selected model regions and total world (a) Chronological order in July; (b) Chronological order in Feb.; (c) Annual duration curve. Data Source: [65]

3.1.2.4 Evaluation of geographical potential of wind electricity production

In this study, the total on- and off- shore area that can be dedicated to electricity production from wind energy, is determined based on the elaborated analysis of the global technical potential of wind electricity production, conducted in [12]. There, geographical sites have been categorized into suitable and unsuitable regions according to natural conditions and land-use characteristics. Fig. 3.16 shows the geographic distribution and absolute levels of suitable areas for installation of wind turbines. According to this, suitable sites mainly locate in Sahara and sub-Saharan regions, Botswana, Namibia, Argentina, eastern and southern parts of Brazil, Bolivia, Mexico, middle and western parts of USA, western China, Middle East, Kazakhstan, Australia, and Europe.

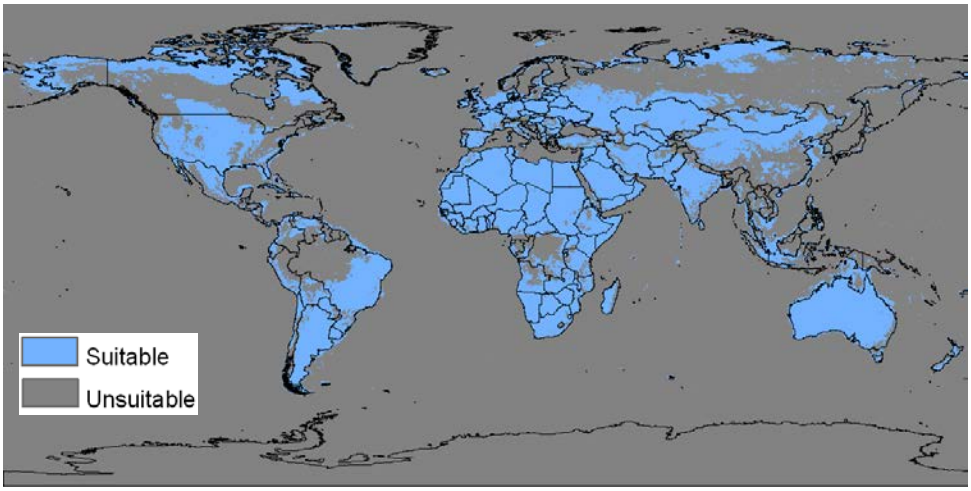

(a)

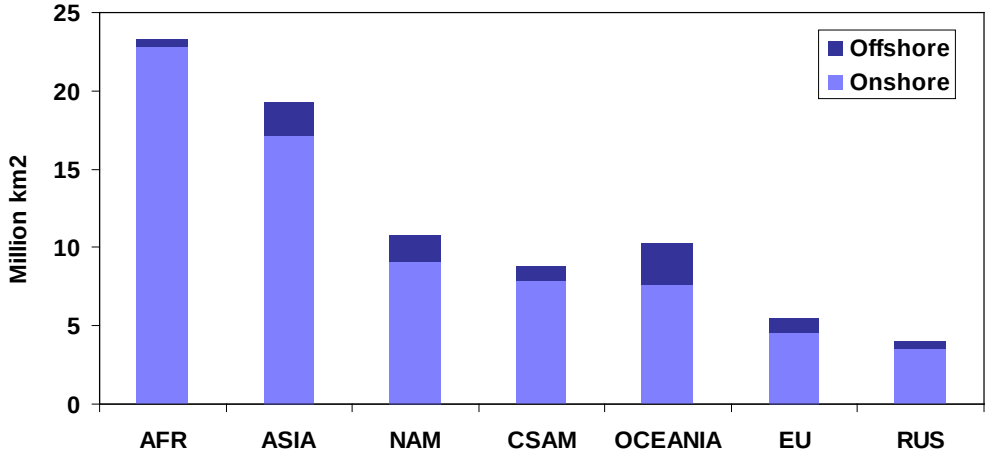

(b)

Fig. 3.16: Categorization of global sites for wind electricity production (a) Geographical distribution; (b) Absolute values for 7 world regions. Data Source: [12]

To evaluate the potential of wind electricity production in a prospective global electricity generation system, it is necessary to make projections with respect to possible technological and economical developments of wind turbines. These include factors such as rated power, hub height, and investment costs. The size of a wind turbine has increased significantly from an average rated power of less than 50 kW at the beginning of the 1980s to over 1 MW in 2005 [77]. Today, the commercial size of wind onshore turbines lies in the range of 750-2500 kW [78, 79]. For wind onshore, it is assumed here that the rated power will level off at 3 MW in a prospective electricity generation system [79]. For offshore sites, current average lies in the range of 2-6 MW [77]. Indeed, current and anticipated technology significantly limits the realizable potential for offshore wind electricity generation. Currently, wind farms are with a few exceptions, placed in shallow waters, with depths of up to around 25 meters [77]. In this study, it is assumed that the rated power will level off at 8 MW. These assumptions are in accordance with the findings and assumptions of other studies [77, 78, 80].

Related to the turbine size, the rotor diameter has also increased from around 15 m in the 1980s to 60-80 m for current turbines with an average size of 1-1.5 MW [79]. It has been proved

in [81] that a relationship exists between the rated power of a wind turbine and the rotor diameter; the historical development of these two parameters is given in [77]. The hub height is also partly related to the rated power. Indeed, there is a trade-off between increased power generation from wind reached at higher hub heights and the additional costs of larger wind turbines. In this study, it is assumed that the hub height in onshore sites equals to 99 m. The characteristics of wind turbine technology for onshore sites correspond to the technical data of ENERCON-101 [79]. The rotor diameter and hub height of the offshore technology is projected at 140 m and 120 m, respectively. These are comparable with assumptions made in other studies [12, 77].

To evaluate output power, the wind power density is a crucial variable. According to the literature, different values exist for the power density at a wind farm level, varying from around 17 MW/km^2 for dense arrays in California to 5-8 MW/km^2 for European wind farms [14]. In [82], an average power density of 14 MW/km^2 is assumed for European onshore sites while a wind power density of 8 MW/km^2 is used to estimate the Europe's onshore wind energy potential in [77]. In [77], a wind power density in the rage of 12-15 MW/km^2 is assumed for offshore sites. In [12], an average power density of 4 wind turbines per km^2 is assumed for onshore wind farms while the rated power of wind turbine is in the range of 1.8-3 MW. For offshore sites, an average power density of 0.25 and 1 wind turbine per km^2 is used while the rated power is assumed at 5 MW. Indeed, wind power density is determined as a compromise between minimization of shadowing effects and optimization of the usage of available area. Influential factors include meteorological conditions, dimension of the wind turbine, and the topography. In this study, an average power density of 8 MW/km^2 is assumed for suitable on- and off- shore sites. This includes a reduction of the power density due to installation of single turbines instead of wind farms; for instance, in year 2000, only 53% of the installed wind turbines were located in wind farms [14].

The availability factor is a fraction of the total amount of full operating hours through a year that a wind turbine is actually available and is set at 0.95 for wind onshore, allowing for repair, breakdowns, etc. [14, 77]. This is a low value in view of literature with values of up to 0.98. However, as a global average it is assumed to be realistic since regions with less experience at present are also covered in this study. For wind offshore, an average value of 0.9 is assumed according to the ranges, given in [77].

The array efficiency is the efficiency of a total wind farm, which decreases with closer spacing due to the interference of wind turbines. Its value is a function of the turbine spacing, configuration and the size of wind farms. Indicative empirically derived values in the literature vary between 0.49 and 0.96; 0.49 for high densities and 0.96 for low density wind farms [14]. In this study, a fixed array efficiency of 0.96 is assumed for onshore wind farms, and a value of 0.93 is used for offshore sites according to the levels, proposed in [14, 77].

3.1.3 Geothermal electricity production

Geothermal energy is the heat that originates within the earth. This heat is generated from a combination of two sources: the original heat produced from the formation of the earth by gravitational collapse and the heat produced by the decay of long-lived radioactive isotopes (U^{238}, U^{235}, Th^{232}, and K^{40}).

As the thermal conductivity of rock is very low, it will take billions of years for the earth to cool down. The total heat flow from the earth is estimated at 42 x 10^{12} W (conduction, convection, and radiation). Of this figure, 8 x 10^{12} W come from the crust, which represents only 2% of the total volume of the earth but is rich in radioactive isotopes; 32.3 x 10^{12} W come from the mantle, which represents 82% of the total volume of the earth, and 1.7 x 10^{12} W come from the core, which accounts for 16% of the total volume and contains no radioactive isotopes [83]. Based on more recent estimates, the total heat flow from the earth is about 6 percent higher than the level expressed in [83]. Even so, the cooling process is still very slow. The temperature of the mantle has decreased no more than 300 to 350 °C in three billion years, remaining at about 4000 °C at its base [84].

The difference in temperature between deep hotter zones and shallow colder zones generates a conductive heat flow from the former towards the latter. The mean terrestrial heat flow of continents and oceans is 65 and 101 mW/m^2, respectively, and if weighted corresponds to a global mean of 87 mW/m^2 [85]. With a total continental area of 147 Mio.km^2, the total annual energy reaches to 84000 TWh.

It has been estimated that the total heat content of the earth above an assumed average surface temperature of 15 °C is of the order of 12.6 x 10^{24} MJ and that of the crust is of the order of 5.4 x 10^{21} MJ [86]. Therefore, this is an inexhaustible energy source as the heat emanating from the interior of the earth is essentially enormous. However, the most critical factor for the classification of geothermal energy as a renewable source is the rate of energy recharge. In the exploitation of natural geothermal systems, energy recharge takes place by injection of thermal water on the same pace of the production from the resource. This justifies the classification of geothermal energy as a renewable source. However, in the case of Hot-Dry-Rock (HDR) systems and some of hot water aquifers in sedimentary basins, energy recharge takes place only by thermal conduction; due to the slow rate of this process, such reservoirs should be considered as finite energy sources [87].

While geothermal energy is an environmental-friendly source, it is not as renewable as solar and wind energy. Like the energy of the sun, the energy within the earth is immense and has a lifetime measured in billions of years. However, unlike the use of sunlight, utilization of geothermal energy can result in a temporary decrease of the available energy source. Re-injecting the geothermal fluid preserves the fluid volume of the reservoir. However, even with reinjection, the heat content of the reservoir gradually declines. The recovery period of a geothermal resource depends on its type and the level of exploitation. However, geothermal energy has a number of important advantages. Geothermal electric plants are not vulnerable to climatic conditions. The electricity production from these plants is strongly related to the capacity factor, which has continuously increased from an initial level of 64% [88]. The global average reached to 73% in 2005 [89]. The most advanced approaches for the resource development may increase the plant capacity factor even to a limit of 90%. This has already been reached in many geothermal fields, which are currently in operation. A capacity factor of 96% has been demonstrated in [84, 90]. According to [91], geothermal plants operate with high capacity (75-95%) and availability (92-99%) factors.

The worldwide installed capacity by the end of 2009 reached to 10.7 GW_{el} for geothermal electricity generation and 50.6 GW_{th} for direct heat usage. Approximately, 67 TWh of base load

electricity was produced with typical capacity factors of 75% [91]. The current status of geothermal electricity production is represented in Table 3.3.

The baseline scenario of IEA Energy Technology Perspectives (ETP) suggests that geothermal technology will provide 1% (approximately 300 TWh) of global electricity demand in 2050 [91]. Furthermore, the ETP BLUE Map scenario, which targets a 50% CO_2 reduction by 2050, suggests that geothermal electricity generation may increase up to 1060 TWh by 2050 [91]. Another forecast, presented in the world geothermal congress, indicates that the installed capacity for geothermal electricity production will go up to 160 GW_{el} by 2050 with an associated production of about 1261 TWh [91].

Table 3.3: Status of geothermal electricity production in year 2009. Data source: [91]

Country	**GWh_{el}/a**
United States	16603
Philippines	10311
Indonesia	9600
Mexico	7047
Italy	5520
Iceland	4597
New Zealand	4055
Japan	3064
Kenya	1430
El Salvador	1422
Costa Rica	1131
Turkey	490
Papua New Guinea	450
Russia	441
Nicaragua	310

3.1.3.1 Evaluation of geographical potential of geothermal electricity production

The geothermal heat flow significantly differs from one geographical position to another. The geographic distribution of vertical heat flow on land sites is shown in Fig. 3.17. This is based on an elaborated assessment of geothermal energy, conducted in [17]. The geothermal heat flow reaches to its maximum mainly on plate margins. A global average of geothermal heat flow on the continental area is 60 mW/m^2. Assuming that the thermal conductivity of rock is 2.5 W/(m.K), the temperature gradient becomes 24 K/km.

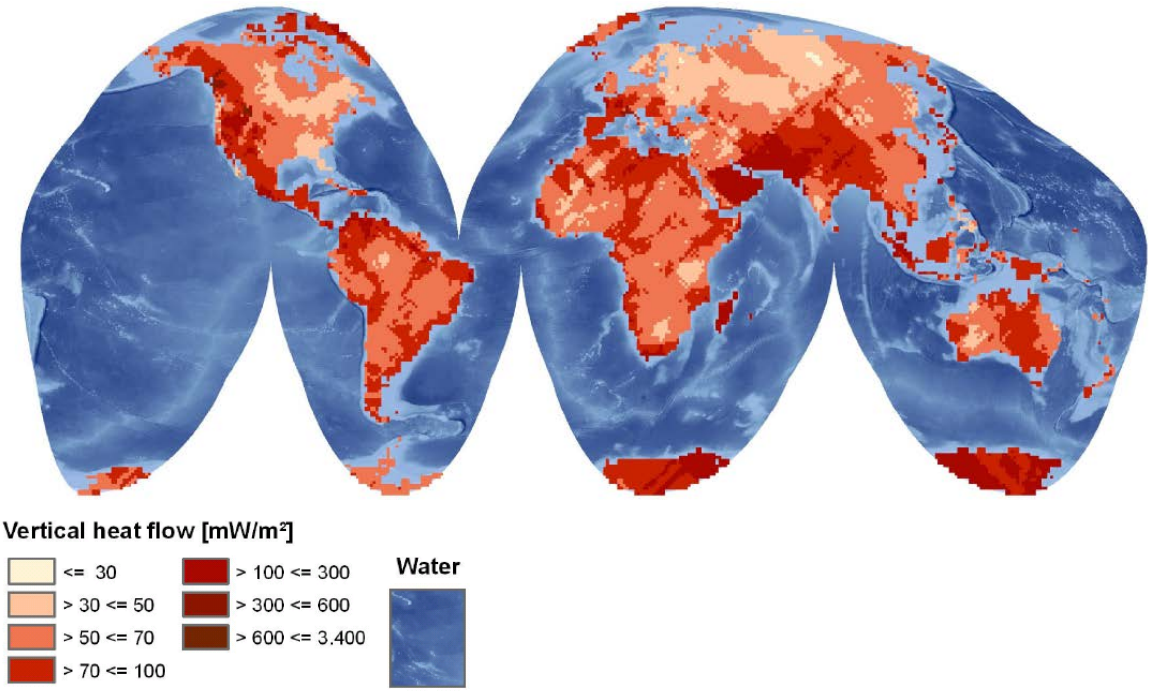

Fig. 3.17: Geographic distribution of geothermal heat flow on land sites. Source: [17]

For electricity generation from geothermal energy, high temperatures are relevant. The lower limit is highly dependent on economical conditions. For instance, for HDR technology, a lower limit of 180˚C is assumed in [27]. Assuming an ambient temperature of 10˚C, the temperature difference between the environment and the geothermal heat source becomes 170˚C. Assuming a mean temperature gradient of 24 K/km, this temperature can be reached at depths of around 7000 m.

With a total continental area of 147 Mio.km^2, the total heat flow rate from the earth reaches to 9.6 TW. A temperature difference of 200 K versus the earth's surface may be reached in average at a depth of around 8000 m. If only regions are taken into account, where a temperature difference of 200 K is reached at depths of lower than 4000 m, the heat flow reduces to 0.82 TW [30]. If this criterion is extended to include depths of lower than 5000 and 6000 m, the total heat flow rate is increased by 0.63 TW and 1.17 TW, respectively, compared to a lower depth of 4000 m.

Assuming an average conversion efficiency of 10%, potential for electricity production from geothermal energy corresponds to 3 to 8% of the global final electricity demand in year 2020 [92]. It is worth mentioning that potential of geothermal electricity is highly restricted due to available drilling technologies. With increasing the accessible depths, geothermal potential significantly increases, regarding the dependency of energy conversion efficiency on the temperature of a geothermal heat source.

In this study, regional potential for geothermal electricity production is approximated, using the geographic distribution of geothermal heat flow provided in [17]. A lower boundary of temperature difference between the geothermal heat source and the ambient temperature is assumed at 170 K while regions are categorized according to the required drilling depth. The first category includes sites, where the desired temperature difference is reached at depths of lower than 4000 m; therefore, ΔT (4000 m) ≥ 170 K. For the second category, the condition is

ΔT (4000 m≤ z≤6000 m) ≥ 170 K while for the third category ΔT (6000 m≤ z≤10000 m) ≥ 170 K. The results are represented in Table B3.1.

3.1.4 Biomass electricity production

Biomass is an attractive energy source from an energy security perspective. Resources are often locally available and conversion into secondary energy carriers is feasible without high investment costs. Moreover, it can have a positive impact on degraded land by adding organic matter to the soil. It can also play an important role in reducing GHG emissions since if it is produced and utilized in a sustainable way, the usage of biomass for energy purposes offsets fossil fuel GHG emissions.

Biomass co-firing in modern, large-scale coal power plants is efficient and cost-effective while it requires moderate additional investment costs. In general, combustion efficiency of biomass can be 10% lower than for coal at the same plant. Biomass can also be burned to produce electricity via a steam turbine in biomass-dedicated power plants. The typical size of these plants is smaller than coal-fired plants due to the scarce availability of local feed stocks and high transportation costs. The efficiency of co-firing in large-scale coal plants (35%-45%) is higher than the efficiency of biomass-dedicated plants (30%-35%). Additionally, biomass converted to biogas can be used in combustion engines with an efficiency factor in the range of 30%-35%, in gas turbines, or in highly efficient integrated gasification combined cycle (IGCC) plants with conversion efficiency in the range of 30%-40%. Biomass integrated gasification gas turbine (BIG/GT) is not yet in commercial usage; however, their economics is expected to improve [93].

In the short-term, co-firing remains the most cost-effective technology for electricity generation from biomass. In a mid- to long- term perspective, BIG/GT plants may expand significantly. IEA projections suggest that the share of biomass in electricity production may increase from the current level to 3%-5% by 2050, depending on underlying assumptions. This is a small contribution compared to the global potential of biomass energy (10%-20% of primary energy supply by 2050); however, biomass is also used for heat generation and to produce fuels for the automotive sector. Estimates of biomass potential at 100-200 EJ/year (roughly 10%-20% of primary energy supply in 2050) are based on the assumption of no water shortage and increasing agricultural yields in the coming decades. In this case, large amounts of arable land would be available for biomass production [93].

3.1.4.1 Evaluation of geographical potential for electricity production from biomass

The influence of major factors such as population growth and food production types and levels, which determine the land availability for biomass production, in addition to other social, environmental, ecological and economical boundary conditions, leads to the complexity of the estimation and projection of the global potential of biomass for application in the energy sector. Therefore, approximations vary significantly among studies because of different underlying assumptions and boundary conditions. A review has been made in [94] on a selection of 17 studies, discussing the future global usage of biomass for energy purposes. Land availability and yield levels in energy crop production are the most critical parameters with a high uncertainty that cause a substantial divergence among outcomes of different studies. For the time horizon from 2020 to 2030, the highest estimate is 300 EJ/year with a contribution of industrialized world regions at about 125 EJ/year; the lowest estimate is around 25 EJ/year with

a contribution of 8 EJ/year for industrialized countries. The lowest estimate for the year 2050 (47 EJ/year) is almost ten times lower than the highest estimate (450 EJ/y).

An elaborated analysis has been performed in [15] on the global potential for producing biomass fuels. According to this, theoretical potential of biomass energy reaches to around 2880 EJ/year; 42% comes from the forest area, 38% from oceans, 9% from grassland, and 5% from acre areas. The biomass potential is categorized into the primary biomass and secondary biomass. Primary biomass resources are produced directly by photosynthesis and are taken directly from the land. Energy crops are considered as primary biomass and are produced solely or primarily for usage as feed stocks in energy generation processes. However, priority of food production limits the total available land area that can be dedicated to the production of energy crops. By taking into account the vegetation types and land usage, worldwide available land area for producing energy crops has been approximated. Promising energy crops have been determined according to the climate conditions, land characteristics, and land availability. On this basis, regional potential for producing energy crops has been determined.

Sustainable production of forest biomass is also included in the category of primary biomass. Biomass is produced from conventional forestry systems, where biomass for energy is a by-product of timber production systems. Sustainability, which combines economical, environmental and social/cultural considerations in relation to the usage of forests, involves ensuring that the benefits from forests do not compromise opportunities of future generations. Based on the average specific growth rate of forests from historical data and the available forest area, which is restricted due to the environmental and topological restrictions, the total forest area has been estimated for each country. Potential of secondary biomass, i.e. waste streams including agricultural and forestry residues, animal residues and residues from processing organic materials, have been evaluated as well.

After all, global potential of biomass energy is evaluated at 751 EJ/year and is dominated by primary biomass while the share of secondary biomass is about 45 EJ/year. Potential of primary biomass is dominated by dedicated energy crops (623 EJ/year). Breakdown of potential of secondary biomass shows that it is dominated by wood residues (21 EJ/year) while the share of crop residues and biogas is estimated at 16 and 8 EJ/year, respectively. Fig. 3.18 shows the global potential of primary and secondary biomass disaggregated to 6 world regions. Non-industrialized regions of the southern hemisphere are of special interest as the biomass potential is adequate not only to satisfy the local energy needs but also to export the rest to the industrialized world regions.

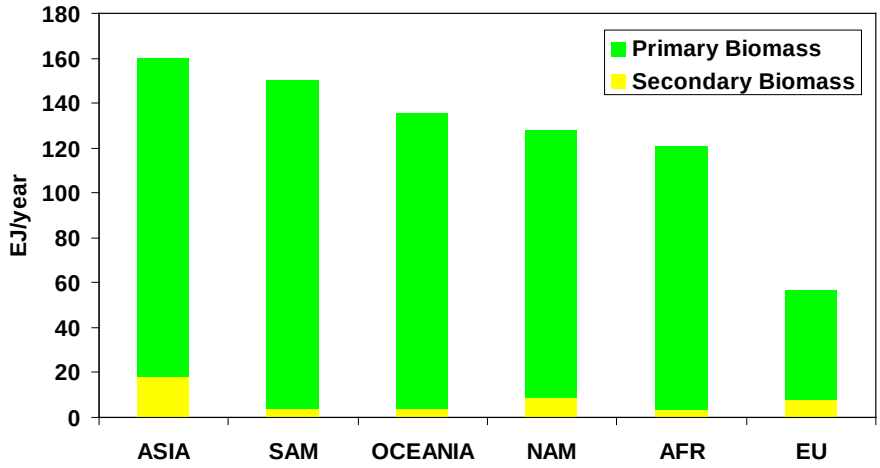

Fig. 3.18: Global potential of biomass energy disaggregated to 6 world regions. Data Source: [15]

Compared to other studies, this is a conservative evaluation of biomass potential. For instance, while total biomass potential in EU-15 is estimated at 7 EJ/year in [15], according to the study conducted in [95], biomass potential of this region reaches to 9 EJ/year by 2020. Furthermore, the former study does not include possible variations of biomass potential through a long-term horizon.

Potential of primary biomass is influenced by the demand for food as a function of population and diet, food production system, productivity of forest and energy crops, and increasing usage of bio-materials and other competing options for land usage. Because of the development of these influencing factors over time and the spatial distribution of resources, an assessment of the potential that integrates the food demand and supply at a detailed geographical level can provide new insights in the spatial distribution and time dynamics of the potential of biomass for energy purposes. In the study conducted in [14], geographical and technical potential of biomass energy has been assessed by applying the IMAGE 2.2. The geographical potential is the theoretical potential at land area available for production of biomass for energy purposes. The technical potential is the geographical potential reduced by energy losses, occurring through converting primary biomass to secondary energy carriers or to electricity. The global and regional potential of biomass energy has been assessed at a grid-cell level for a geographical grid with a spatial resolution of 0.5°x0.5° integrated with the spatial simulation of food and timber demand and supply over a long-term horizon. This assessment includes various interactions between population dynamics, technology change, and the land use pattern. The simulation is conducted over time, using a time frame to 2100. For the assessment of technical potential, regional assumptions are made regarding the conversion efficiency factor. For the future periods, the IGCC technology, which is expected to reach high efficiency levels and lower electricity production costs, is taken into account.

Finally, geographical and technical potential of energy crops has been determined over a time horizon to 2100 at three land-use categories: abandoned agricultural land, low-productive land, and rest land or remaining non-productive land. The future development paths have been envisaged using four scenarios, developed by the Intergovernmental Panel on Climate Change (IPCC) in its special report on emission scenarios (SRES): A1, A2, B1, and B2.

The A2 storyline and scenario family describes a very heterogeneous world. The underlying theme is self-reliance and preservation of local identities. Fertility patterns across regions converge very slowly, which results in continuously increasing global population. Economic development is primarily regionally oriented and per capita economic growth and technological changes are more fragmented and slower than in other storylines. The B1 storyline and scenario family describes a convergent world with the same global population that peaks in the mid-century and declines thereafter, as in the A1 storyline, but with rapid changes in economic structures towards a service and information economy, with reductions in material intensity and the introduction of clean and resource-efficient technologies. The emphasis is on global solutions to economic, social, and environmental sustainability, including improved equity, but without additional climate initiatives. The B2 storyline and scenario family describes a world, in which the emphasis is on local solutions to economic, social, and environmental sustainability. It is a world with continuously increasing global population at a rate lower than A2, intermediate level of economic development, and less rapid and more diverse technological change than in the B1 and A1 storylines [92].

According to the results of the study performed in [14], theoretical potential of biomass energy at the total terrestrial surface is about 3500 EJ/year. The geographical potential at abandoned agricultural land is the largest contributor. In year 2050, geographical potential at abandoned land ranges from about 130 to 410 EJ/year. For the year 2100, it ranges from 240 to 850 EJ/year. Available potential at low-productive land is negligible compared to other categories. The rest land area is assumed to be partly available, resulting in ranges of geographical potential from about 35 to 245 EJ/year for the year 2050 and from about 35 to 265 EJ/year in 2100. At a regional level, significant potential exists in Russia, East Asia, and South America.

Table 3.4 includes the geographical potential of energy crops at three land-use categories based on the B2 scenario. The regional potential does not exceed the projected primary energy demand in most world regions. Oceania has the highest relative geographical potential; in year 2050, biomass potential exceeds the local energy demand in all scenarios. In absolute terms, Russia has the highest potential, reaching a level of about 71 EJ/year for A2 scenario and 125 EJ/year for A1 scenario in year 2050.

Table 3.4: Geographical potential of energy crops at three land-use categories. Data source: [14]

Region	Abandoned agricultural land (EJ/year)		Low-productive land (EJ/year)		Rest land (EJ/year)	
	B2 2050	B2 2100	B2 2050	B2 2100	B2 2050	B2 2100
Canada	12	15	3	2	1	0
USA	46	55	1	0	3	3
Central America	4	10	0	0	1	1
South America	37	41	1	1	6	5
North Africa	1	2	0	0	0	0
West Africa	2	25	0	0	4	3
East Africa	2	5	0	0	3	2
South Africa	1	35	0	0	2	2
West Europe	15	17	0	0	1	1
East Europe	9	11	0	0	0	0
Russia	74	106	2	1	4	5
Middle East	1	2	0	0	2	1
South Asia	4	15	0	0	1	1
East Asia	43	61	1	1	3	4
South East Asia	2	10	0	0	1	1
Oceania	26	36	0	0	3	3
Japan	0	2	0	0	0	0
World	279	448	8	5	35	32

In a low-carbon electricity generation system of future with a high share of FRES, biomass power plants can play an important role as base load generators. Due to the application of biomass in the automotive sector and also for heat production, only a limited share of available potential can be dedicated to electricity production. In this study, biomass potential of model regions is determined according to the potential of biomass energy, evaluated in [14] based on the B2 scenario, as a conservative assumption. Thus, it is limited to the potential for biomass production from energy crops only.

3.1.5 Hydropower production

Hydropower has a substantial contribution to meeting today's electricity demand. Worldwide hydropower production has continuously increased with an annual growth rate of about 2.3% since 1980 [16]. The highest growth rates in the future coming years are expected to occur in developing regions or industrializing countries with high but not yet exploited hydropower potential, e.g. parts of Eastern Europe [16].

In the following, different assumptions and data sources used for the parameterization of hydroelectric power plants in the electricity system optimization model, including the technology type classification, seasonal variations of hydropower production, and the geographical potential are described.

3.1.5.1 Classification of hydroelectric power plants

Hydroelectric power stations can be classified according to the way they make usage of the inflow that they receive, depending on whether this cumulative flow must be used within a short period of time or whether it can be retained for a certain time period [16]. The classification applied in this study, distinguishes between run-of-river stations, reservoir stations, and pumped storage facilities. Run-of-river stations show fluctuations in energy production induced by low-flow or overflow periods due to their limited ability to retain water. The advantage of low investment costs is thus countered by fluctuations in electricity production. During low-flow periods, the stations cannot operate at their full installed capacity; flood flows, on the other hand, cause overflows, and the station is unexploited. In contrast, reservoir stations, depending on their storage capacity and operational management, can store water over long-term periods and provide a steady supply of electricity, relatively independent from variations of short-term inflows. In pumped-storage plants, water can be raised by means of pumps and stored in an upper reservoir to be used for producing power at peak load.

The UDI World Electric Power Plants database (UDI WEPP) [96] provides a comprehensive global data on all types of electric power plants, currently in operation or under construction. However, no distinction has been made between hydropower run-of-river plants and reservoir stations. In [97], the inventory of European hydropower stations above 1 MW is classified into different categories with respect to their installed capacity. However, no classification has been made regarding the type of operational mode. In this study, the share of reservoir hydroelectric power stations in Europe, in a few Asian countries, and in African regions is determined based on the studies conducted in [16, 27].

3.1.5.2 Seasonal variations of hydropower production

The capacity factor is one of the main input parameters to reflect the operational characteristics of hydroelectric power plants in the electricity system optimization model. In this study, mean monthly river discharge from the WaterGAP model [98] is used to evaluate seasonal variations of hydropower production. WaterGAP is a global model of water availability and water usage to assess the current status of water resources and to estimate the impact of climate change on the problem of water scarcity. Mapped on a geographical grid with a spatial resolution of 0.5°x0.5°, the WaterGAP simulates impacts of demographic, socio-economic and technological change on water consumption while it evaluates the influences of climate change on water availability and irrigation water usage.

Here, it is generally assumed that reservoir stations are able to store and to harness the total inflow volumes; thus, all the discharge is utilizable. However, a run-of-river station cannot utilize the portion of flood discharge that overflows the station, independent from the magnitude of excess discharge. Hence, a cut-off or a threshold level must be taken into account, above which the discharge cannot be harvested. The cut-off level is difficult to approximate as it depends on various factors such as technical characteristics and the maximum load of the run-of-river station. Due to insufficient data, it is not feasible to assign an individual cut-off level to each generation unit. Instead, a representative level must be taken into account. This is approximated here, using the seasonal regime of available discharge from the WaterGAP. The second highest mean monthly discharge is chosen as the cut-off level for the corresponding

grid-cell. It has been proven in [16] that the chosen cut-off value on this basis is adequate for Germany; however, in other countries, it may lead to deviations from actual conditions.

Fig.3.19 shows the approximated mean monthly capacity factors of hydropower reservoir stations for selected countries. It can be concluded that hydropower production is characterized with significant seasonal variations. For instance, in Estonia (EE), Germany (DE), and England (GB), the maximum hydropower production is reached in winter while it significantly declines through the summer period.

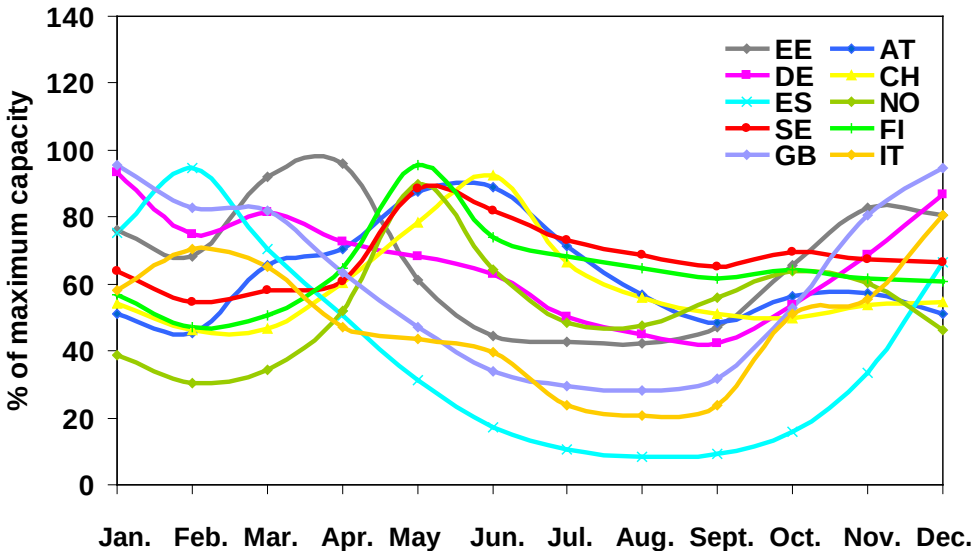

Fig. 3.19: Mean monthly capacity factors of hydro power reservoir stations. Data Source: [98]

3.1.5.3 Evaluation of geographical potential of hydropower production

The gross hydropower potential can be evaluated from the total mass of inflow to each grid-cell, taking into account its elevation. This is represented in equation (3.12); *m* is the mass of runoff at the corresponding grid-cell; *g* is the gravitational acceleration, and *h* is the height.

$$GP = m.g.h \tag{3.12}$$

The global theoretical hydropower potential can be determined, using run-off values at grid-cell level from the WaterGAP model in combination with a digital elevation map. In the studies conducted in [16, 27], for a geographical grid with a spatial resolution of 0.5°x0.5°, the cell internal potential has been calculated by assuming that the run-off generated within the cell falls from the mean elevation to its minimum elevation while the discharge from upstream cells is assumed to fall from the minimum elevation of the originating cell to the minimum elevation of the corresponding grid-cell. This approach is applied here to evaluate the available hydro energy in a prospective global electricity supply system. Based on this, total theoretical hydropower potential in Europe is 3300 TWh/a, and the worldwide potential reaches to 52500 TWh/a. This is in line with other findings in literature. For instance, in the study conducted in [99], the Europe's total theoretical hydropower potential is approximated at 3220 TWh/a.

3.2 Electricity demand

Another fundamental input to the electricity system optimization model is the final net electricity demand. The present value of global electricity demand as well as its development through a future time horizon and the chronological order of its short-term variations must be determined for each model region. In the following, different data sources and approaches applied to evaluate the final world electricity demand and adapt it to the geographical structure of the optimization model are described.

3.2.1 Final electricity demand

Spatially-explicit scenario interpretations of population for a geographical grid with a resolution of 0.5°x0.5° and the development of final electricity demand for 11 world regions are available at Greenhouse Gas Initiative (GGI) database of International Institute for Applied Systems Analysis (IIASA) from 1990 to 2100 in ten-year time intervals [92]. The database documents three baseline scenarios of different socio-economic and technological developments from IPCC scenarios: A2, B1 and B2. This database also covers climate stabilization scenarios, which have been imposed on the baselines. The development of final electricity demand based on different scenarios is visualized in Fig. 3.20. The reference scenario of International Energy Agency (IEA) [100] also provides a projection of final electricity demand from 2015 to 2030.

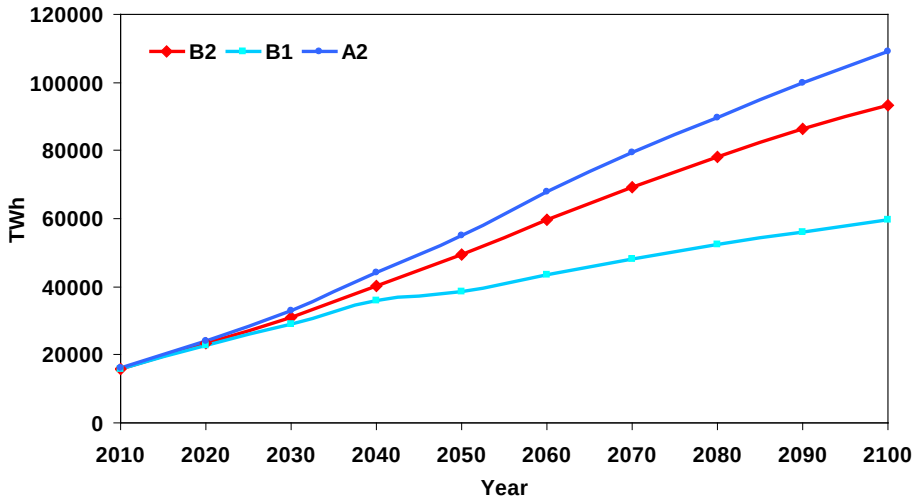

Fig. 3.20: Development of global final electricity demand. Data Source: [92]

In this thesis, the B2 scenario is selected as a basis to determine the development of electricity demand because of its moderate status compared to other scenario families. It also serves the purpose of long-term optimization regarding the covered time horizon; however, the projection made by IEA only considers a medium term. Fig. 3.21 shows the development of global final electricity demand based on B2 scenario, disaggregated to 11 world regions.

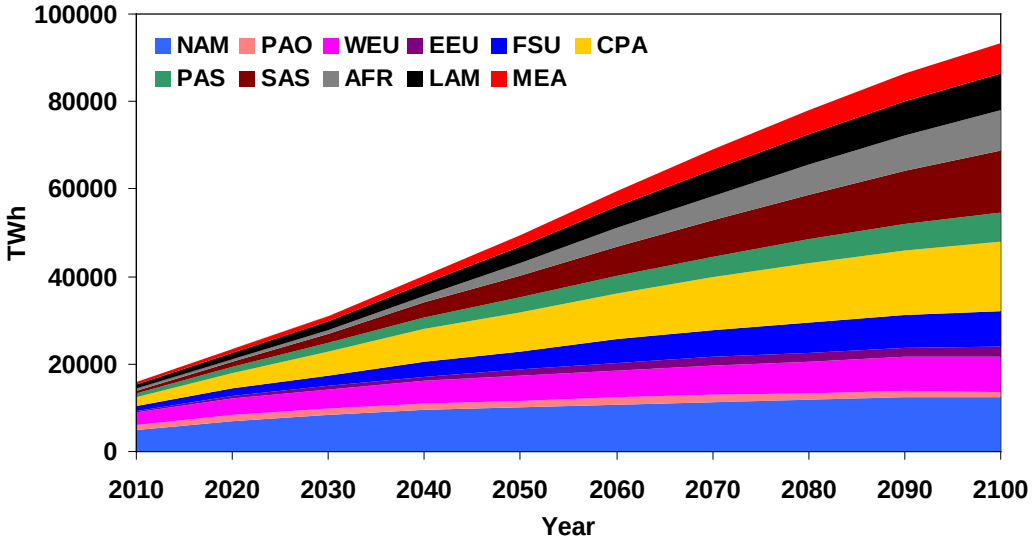

Fig. 3.21: Development of final electricity demand based on B2 scenario. Data Source: [92]

In this study, to derive unique values for each cell of a geographical grid with a spatial resolution of 2.5°x2.5°, electricity demand is spatially rescaled according to the geographic distribution of population. Fig. 3.22 shows the geographic distribution of expected final electricity demand in year 2050, using the B2 scenario of IPCC.

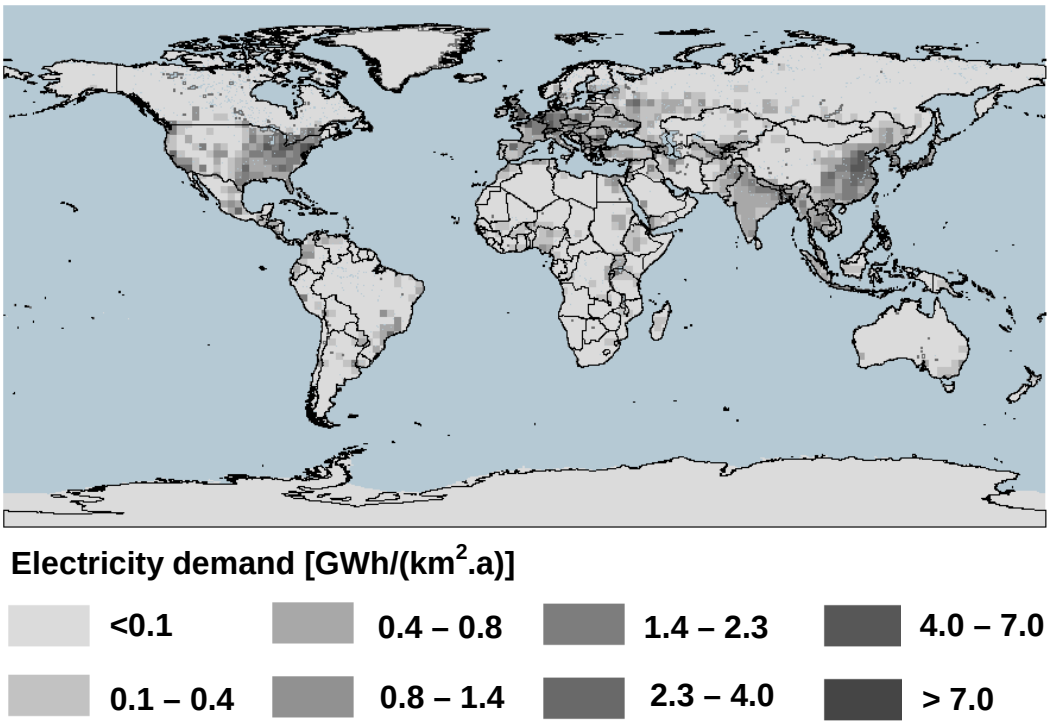

Fig. 3.22: Geographic distribution of final electricity demand in year 2050 based on B2 scenario of IPCC. Data source: [92]

3.2.2 Electrical load profiles

Using the GIS-based data of electricity load, developed in section 3.2.1, the annual level of final electricity demand can be determined for each model region. However, to represent the chronological order of hourly variations through a year, electrical load profiles (ELP) are required. Different factors influence the time characteristics of electricity load, including the industrialization level, climate characteristics, religion and traditions of the inhabitants. Hourly ELPs of European countries are available at [97, 101].

The hourly ELP of Norway, Sweden, Finland, and East Denmark is available at [102] only for the third Wednesday of January and July. Based on this, an hourly ELP for every Wednesday of the year can be synthesized, using the equation (3.13); the unknown hourly load *(P_{Wed})* lies in the time frame between (*Wed-i*) and (*Wed-j*) with known given load profiles ($P_{Wed\text{-}i}$ and $P_{Wed\text{-}j}$); *l* and *m* represent the time difference between *Wed* and *Wed-i* and between *Wed* and *Wed-j*, respectively.

$$P_{Wed}(t) = \frac{1}{l+m}(l * P_{Wed-i}(t) + m * P_{Wed-j}(t)) \qquad t \in \{1, 2, ..., 24\} \tag{3.13}$$

Using the ELP of West Denmark available at [97], hourly proportion of load on each week-day and weekend-day to the load on Wednesday of the corresponding week can be determined. This hourly time series of load proportion is then used to synthesize the electrical load pattern of Denmark, Norway, Sweden, and Finland on an annual basis.

The ELP of a number of countries including Columbia, Estonia, and South Africa has been provided by personal communication with local transmission system operators [103, 104]. For a number of countries such as Brunei, Malaysia, Uganda, Thailand, Mali, Niger, Jordan, Australia, Lebanon, Tunisia, Madagascar, Mauritius, and Grenada, it was possible to gain access only to average monthly profiles or typical daily load curves in winter and/or summer period [103]. Eventually, the hourly ELPs have been made available for 31 countries on an annual basis.

For Eastern Europe, South America, and African territories if no accurate information exists, the ELP is synthesized, using the ELP of the closest country with accessible data. This assumption has been made due to rather similar industrialization level and climate characteristics, taking into account the classification made in [103].

For Australia and North America, the normalized ELP of Western Europe is used as a basis to synthesize the electrical load pattern. This assumption can be made due to the nearly similar industrialization levels and living habits of inhabitants [103].

For Russia, Middle East, China, India, and other Asian countries hourly ELPs are not available on an annual basis. Furthermore, there exist large differences between the time characteristics of electricity load in these regions and the pattern of load in other countries with accessible information, located in Europe, South America, and Africa. This is mainly due to the different climate characteristics, industrialization levels, religion and traditional behaviors of inhabitants. Therefore, synthesizing the ELP from typical daily load profiles, using the time characteristics of electricity load in other countries with accessible information, leads again to a significant deviation from the actual behavior of electricity load. The normalized European ELP is then shifted to the Greenwich Mean Time (GMT) in order to provide a basis to synthesize the time

pattern of electricity load for countries without sufficient information; this is shifted afterwards to the corresponding time zones.

The normalized ELP of each model region is then approximated by linear combination (weighted by consumption) of electrical load patterns of comprising countries or time zones. Although this procedure does not lead to determination of the actual demand pattern, it serves the purpose to provide a rough estimation of the periodical behavior of electricity load in a prospective global electricity generation system and to deal with data inadequacy. Finally, the normalized ELP of each region is scaled, using the annual final electricity demand, evaluated in section 3.2.1.

3.2.3 Time characteristics of electricity load

As it was demonstrated, interconnection of regions with different climatic characteristics leads to smoothening effects on fluctuations of solar and wind power generation. Additional smoothening effects can be captured as a result of de-correlations of electricity load at distant locations.

Fig. 3.23.a shows the time characteristics of electricity load on selected days in South Africa. Compared to the load profiles of European countries (see Fig. 3.24), the demand pattern shows different time characteristics. The load decreases after a first peak around 8 a.m., represented in local time (GMT+2); there exists a second peak around 7 p.m., which is higher than the former. The maximum load increases from 1.06 to 1.16 of the average daily load while the minimum decreases from 0.88 to 0.85 of the mean daily load from January to July.

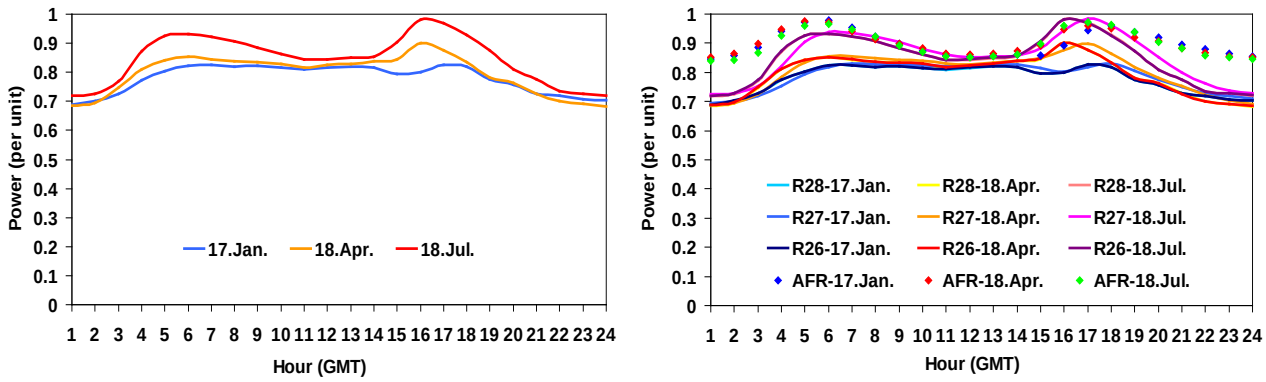

(a) (b)

Fig. 3.23: ELP on third Wednesday of Jan., April, and July normalized by annual peak (a) South Africa; (b) Model regions 26-28 and total Africa. Data Source: [103]

This ELP is then shifted to different time zones of African countries while the seasonal shift for the countries, located in the northern hemisphere, is taken into account. They are then aggregated to determine the ELP of each model region. Fig. 3.23.b shows the approximated load profiles of different model regions as well as an aggregated pattern, representative for all African countries. Through interconnection of regions from different time zones (GMT, GMT+1, GMT+2, and GMT+3) and from the two hemispheres, proportion of the minimum electricity load to the peak demand is increased by 28% as compared to the South African load pattern (see

Table B4.1). This clarifies the smoothed pattern of an aggregated ELP compared to the load profile of a single region.

Fig. 3.24 shows the electrical load profiles of European countries as well as aggregated patterns for model regions. The main common characteristic of all load patterns is a minimum around 4-5 a.m., followed by a gradual increase between 6 a.m. and 8 a.m., and a decline through night (after 9 p.m.). The major differences include the level of minimum load and peak load, the trend of load after 6 p.m., and the time of second peak. For instance, the maximum load varies in a range from 1.06 to 1.25 of average daily load while the minimum increases from 0.67 to 0.93 of mean daily load, according to the actual data of 17 Jan. 2007. As a seasonal average, the peak and the minimum vary in a range from 1.05 to 1.24 and from 0.69 to 0.92 of average daily load, respectively. In a few countries, a continuous decline of the load is noticed, which starts early in the afternoon and lasts till late in the evening. In other countries, the load pattern is nearly flat during working hours and has a continuous reduction in the evening. A number of regions are characterized with a distinct reduction of the load in the afternoon and a second peak in the evening. Furthermore, southern European countries (RO, GR, IT, and ES) are characterized with a higher electricity load in summer than in winter while in other European countries the load considerably reduces through the summer period. Finally, the figure clarifies the smoothed pattern of aggregated load profiles compared to the load patterns of single countries.

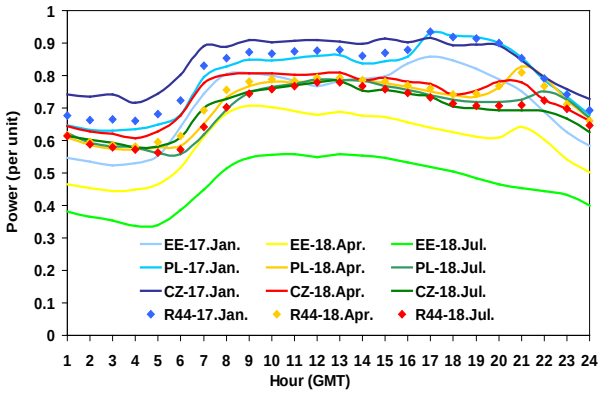

(a)

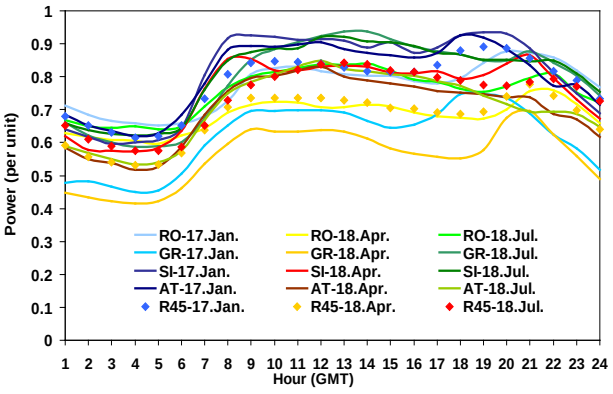

(b)

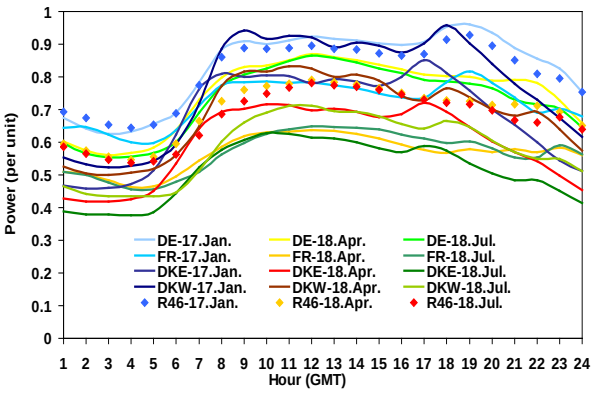

(c)

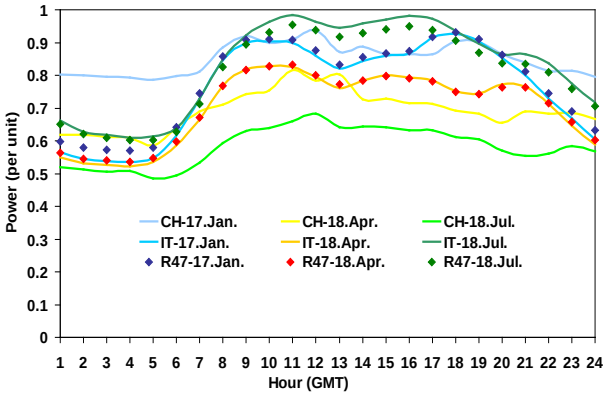

(d)

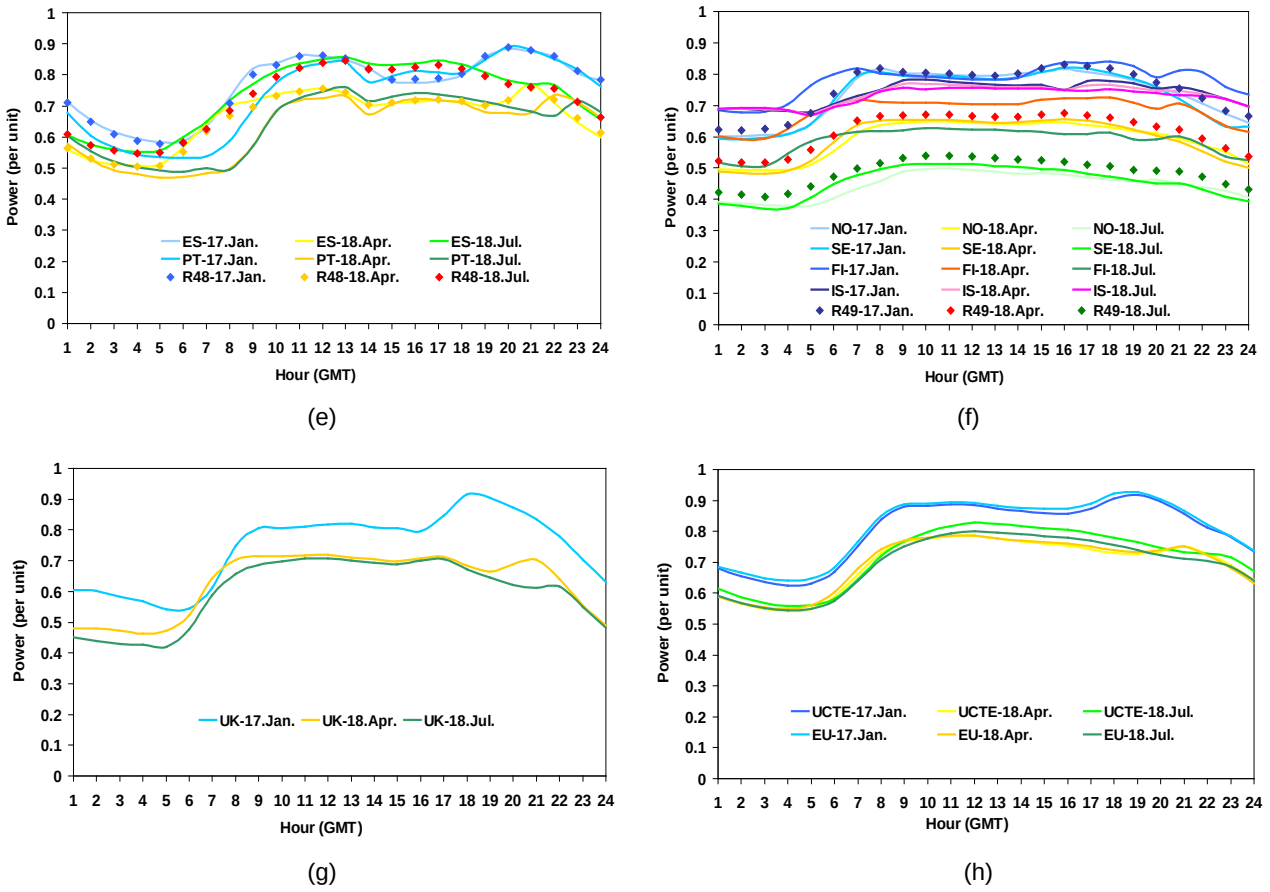

Fig. 3.24: ELP on third Wednesday of Jan., April, and July normalized by annual peak (a) Countries: EE, PL, CZ, and region 44; (b) Countries: RO, GR, SI, AT, and region 45; (c) Countries: DE, FR, DK, and region 46; (d) Countries: CH, IT, and region 47; (e) Countries: ES, PT, and region 48; (f) Countries: NO, SE, FI, IS, and region 49; (g) Countries: UK; (h) Aggregated load pattern for EU and UCTE. Data Source: [97, 101, 102, 104]

Fig. 3.25.a shows the time characteristics of electricity demand in Columbia. The load starts to increase around 5 a.m., represented in local time (GMT-6), till it reaches the first peak around noon. Afterwards, the load slightly decreases and is characterized with a second peak in the evening. The peak demand is around 1.4 while the minimum reaches to 0.67 of average daily load. As a tropical region, the load pattern does not significantly change through different seasons.

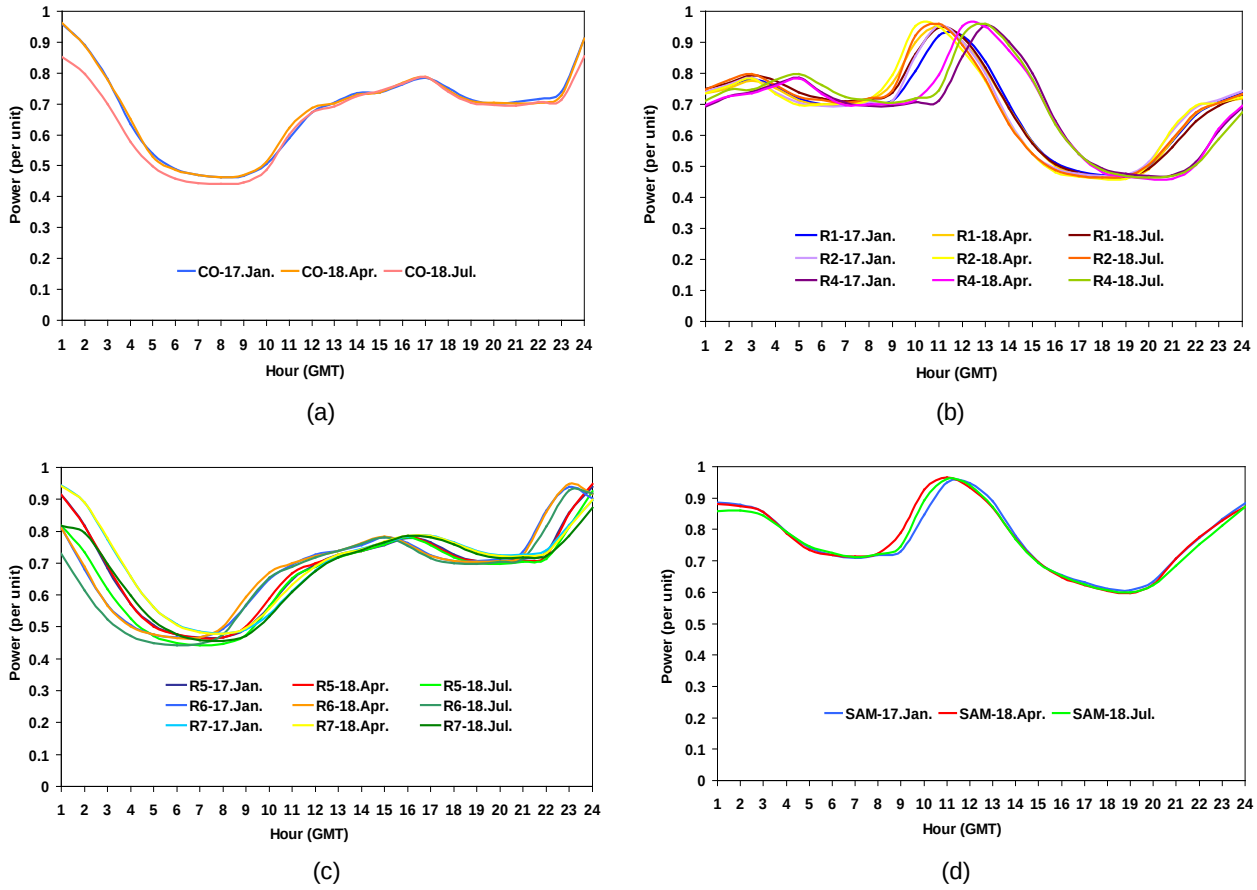

Fig. 3.25: ELP on third Wednesday of Jan., April, and July normalized by annual peak (a) Columbia; (b) Model regions 1, 2, and 4; (c) Model regions 5-7; (d) Total South America. Data source: [103]

Fig. 3.25.b, Fig. 3.25.c, and Fig. 3.25.d show the load profiles of other model regions and an aggregated profile, representative for South America. Through interconnection of regions from different time zones (GMT-3, GMT-4, GMT-5, and GMT-6) and from the two hemispheres, the proportion of minimum load to the peak demand increases by 25% compared to the Columbian load pattern. This again clarifies the smoothed pattern of an aggregated profile compared to the load pattern of a single region.

Finally, Fig. 3.26 shows the chronological order of hourly variations of electricity load over a year in selected model regions and also for the total world. The corresponding annual load duration curves are illustrated in Fig. 3.27. The normalized load profiles are scaled in this figure, using the projected final electricity demand in year 2050.

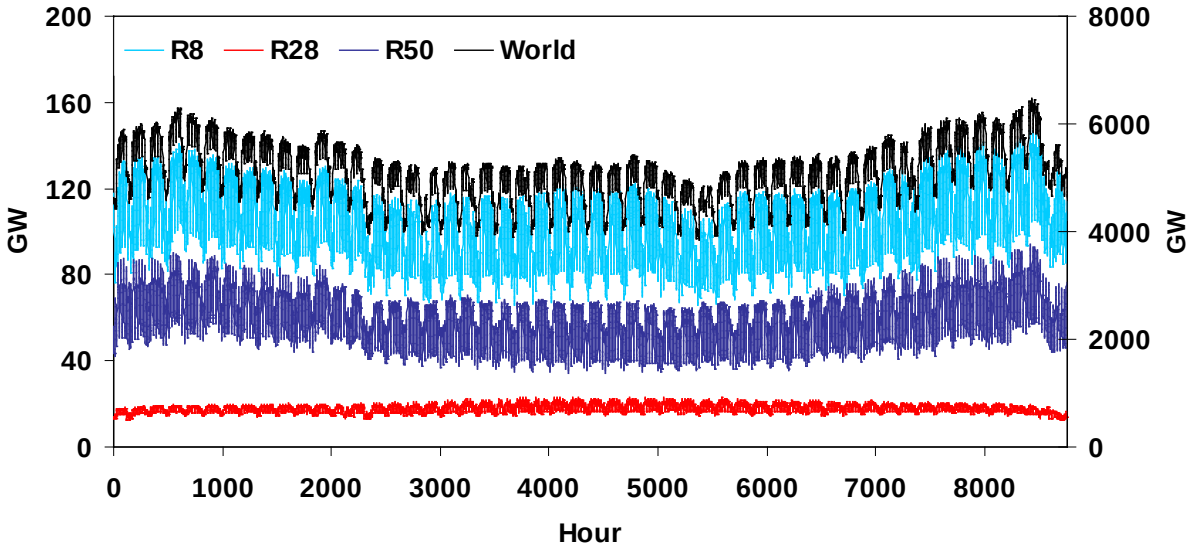

Fig. 3.26: Chronological order of hourly electricity load in year 2050 for selected model regions (left axis) and total world (right axis). Data Source: [92, 97], [101-104]

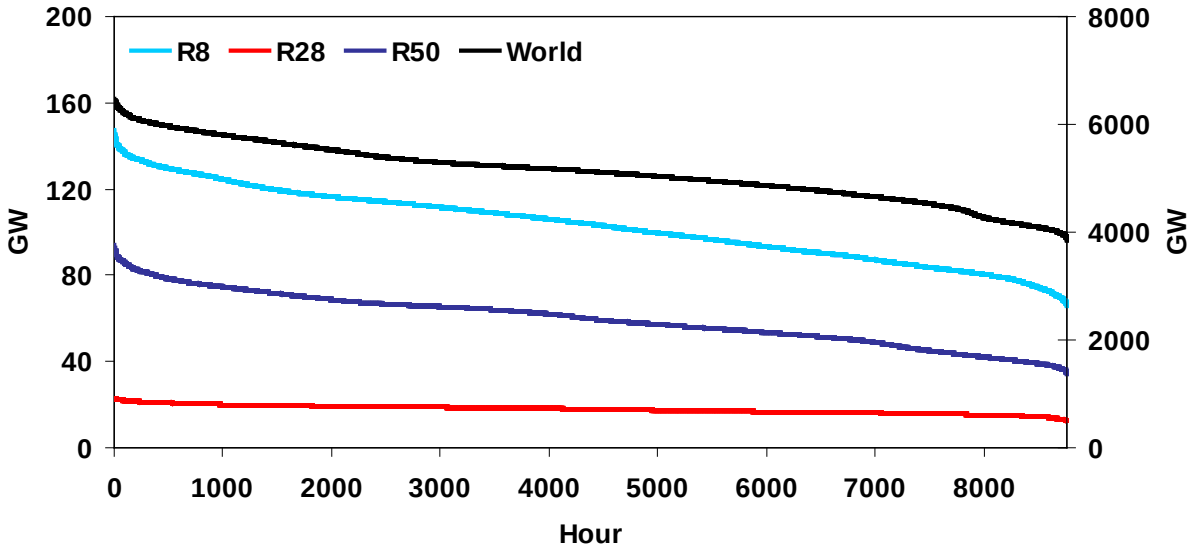

Fig. 3.27: Annual load duration curves for selected model regions (left axis) and total world (right axis) in year 2050. Data Source: [92, 97], [101-104]

3.3 Existing infrastructures

In order to represent existing infrastructures in the electricity system optimization model, currently operating power plants and already installed power transmission interconnections are now included in the model database.

3.3.1 Power plants database

The installed capacity of power plants is determined here, using the UDI world electric power plants database (UDI WEPP) [96]. This includes detailed information about each power plant of the world, including the name of the plant, company, installed and planned capacity, actual status (operating, under construction, decommissioned, retired, etc.), the year of commissioning, technology type, fuel type, and the location.

3.3.1.1 Classification of power plants

The UDI WEPP database provides detailed information about the technology and fuel type of each power generation unit. To reduce the complexity, power plants are aggregated according to the main fuel and technology type (see Table 3.5).

Table 3.5: Classification of power plant technologies

Name	Description
BIO-ST	**Fuel aggregation** All types of bio-fuels (bagasse, biogas, sewage digester gas, syngas from gasified wood or biomass, and bio-liquid fuels) or any waste (landfill gas, syngas from gasified refuse, waste gas from refinery or other industrial processes, waste heat, paper mill waste or sludges, and municipal solid waste) are aggregated to biomass (“BIO”). **Technology aggregation** Technologies used to generate electricity from “BIO” include: internal combustion engine, combined cycle, steam turbine, gas turbine, organic Rankine-cycle turbine, and reciprocating steam engine. These are aggregated and parameterized as steam turbine (“ST”).
COAL-ST	**Fuel aggregation** Coal, coke, and bitumen are aggregated to Coal (“COAL”). **Technology aggregation** Applied technology is the steam turbine (“ST”).
GAS-CC	**Fuel aggregation** Natural gas, blast-furnace gas, gasoil, coal syngas, coal steam gas, mine gas, gasified crude oil or refinery bottoms, LNG, LPG, and coke-oven gas are aggregated to natural gas (“GAS”). A few power plants in the database, having “unknown” fuel type, are considered in this category. **Technology aggregation** Conversion technologies include: steam turbine and combined cycle. These are aggregated and parameterized as combined cycle (“CC”).
GAS-GT	**Fuel aggregation** Natural gas, blast-furnace gas, flare gas or wellhead gas, syngas from gasified refuse, gasoil, coal syngas, coal steam gas, mine gas, gasified crude oil or refinery bottoms, LNG, LPG, and coke-oven gas are aggregated to natural gas (“GAS”). A few power plants in the database, having “unknown” fuel type, are also considered in this category. **Technology aggregation** Conversion technologies include: gas turbine, internal combustion engine, and fuel cell. These are aggregated and parameterized as gas turbine (“GT”).
GEO-ST	**Fuel aggregation** All types of resources (dry steam, binary, flash) are summed up in this category (“GEO”). **Technology aggregation** All types of conversion technologies (steam turbine and organic Rankine cylce) are aggregated and parameterized as steam turbine (“ST”).

LIG-ST	**Fuel aggregation** Lignite, lignite and bituminous coal, lignite and sub bituminous coal are aggregated to lignite (“LIG”). **Technology aggregation** Conversion technology is the steam turbine (“ST”).
OIL-CC	**Fuel aggregation** Oil and Oil shale are considered in this category (“OIL”). **Technology aggregation** Conversion technologies include: steam turbine and combined cycle. These are aggregated and parameterized as combined cycle (“CC”).
OIL-GT	**Fuel aggregation** Oil and Oil shale are considered in this category (“OIL”). **Technology aggregation** Conversion technologies include: gas turbine and internal combustion engine. These are aggregated and parameterized as gas turbine (“GT”).
HP-PS	Pumped storage hydroelectric power plants
HP-ROR	Conventional hydroelectric power plants i.e. run of river and hydro reservoir stations as well as wave and tidal energy converters are summed up in this category.
SOL-CSP	All types of solar thermal power plants are considered in this category
SOL-PV	Photovolatic
URA-ST	All types of nuclear fission power plants are summed up in this category.
WIND	Onshore wind energy converters
WIND-O	Offshore wind energy converters

3.3.1.2 Geographic distribution of power plants

In UDI WEPP database, the geographical position of each power plant is represented in terms of the continent, country, state, and the city, but not including the latitude and longitude of the location. However, this information is required for the purpose of modeling at a high geographical resolution.

The global energy production database, Carbon Monitoring for Action (CARMA) [4], is a global database, which is produced and financed by the Confronting Climate Change Initiative at the Center for Global Development. Starting from the capacity of each power plant based on the UDI WEPP database, energy production of each power plant has been approximated, using the North American technology-specific annual full operating hours. The following information is given for each power generation unit: plant name, power production through the years 2000 and 2007 and forecasted generation for the next decade, CO_2 emissions and CO_2 emissions intensity in 2000 and 2007 as well as forecasted emissions for the next decade, and the geographical position. The position of each power plant includes the continent, country, state, and the city of location as well as the latitude and longitude.

Here, through the linkage of the UDI WEPP to the CARMA database on a power plant basis, localization and mapping of existing power plants to model regions is realized. This is performed only when a country is spitted up into several regions.

3.3.1.3 Comparison of different data sources

A comparison is now made between the net installed capacity of electric power plants from the UDI WEPP database and the capacity of power plants based on other statistical data sources including the international electricity data of Energy Information Administration (EIA) [105] and United Nations (UN) energy statistics [106]. Fig. 3.28 shows regional differences of installed capacities of power plants according to different data sources. It can be concluded that the capacity of power plants, obtained from the UDI WEPP database, is roughly in the range of estimates given by other institutions.

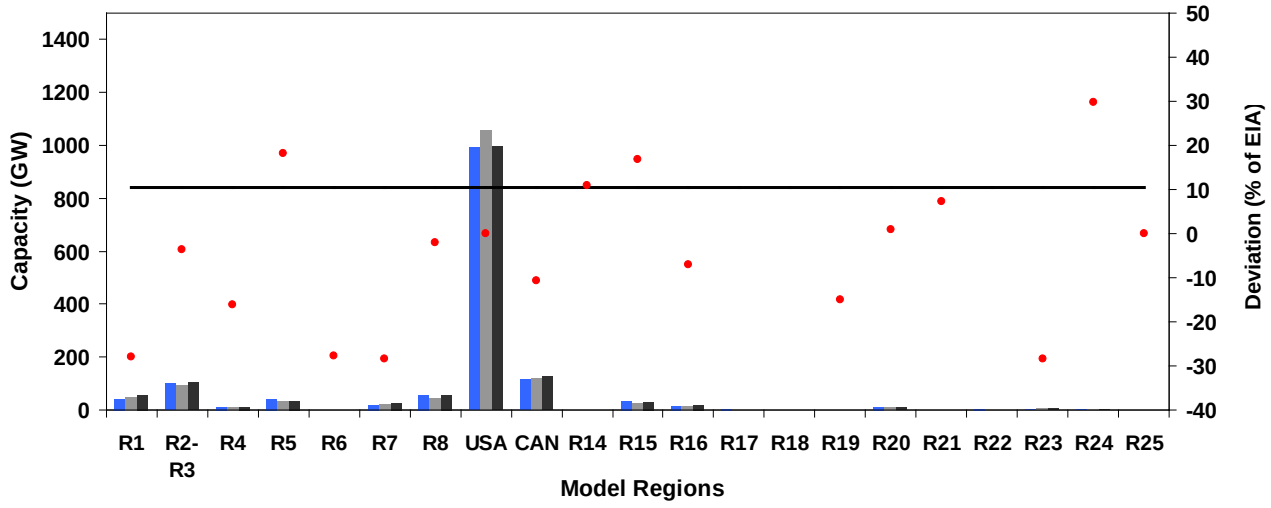

(a)

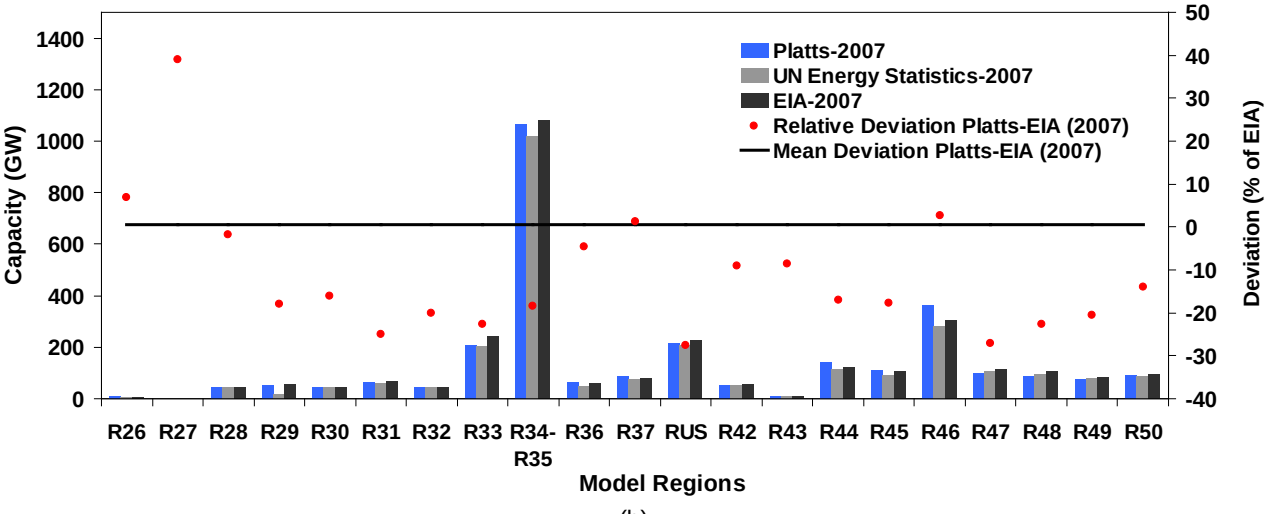

(b)

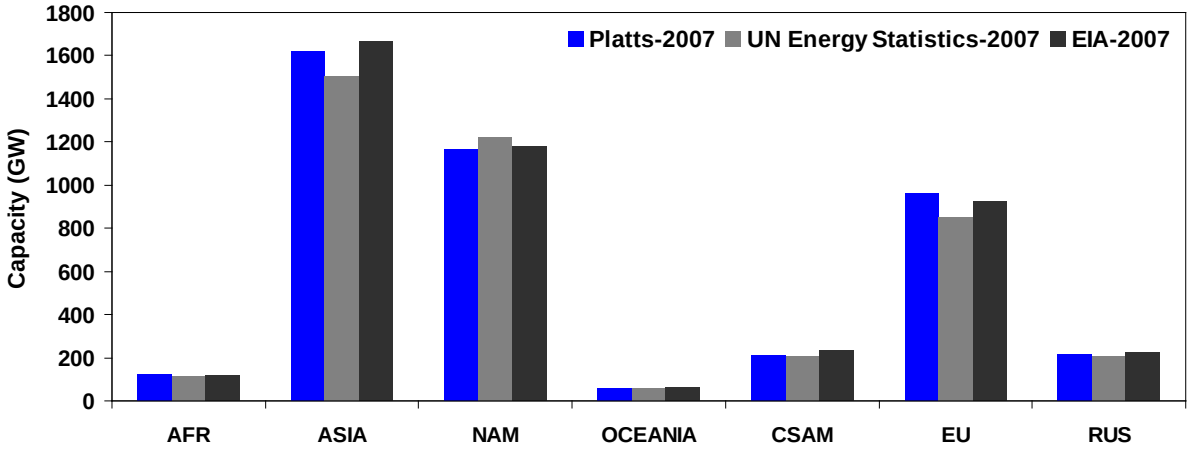

(c)

Fig. 3.28: Comparison of net installed capacity of power plants (a) Model regions 1-25; (b) Model regions 26-50; (c) Aggregated for 7 world regions. Data Source: [96, 105, 106]

3.3.1.4 Decommissioning of power plants

The remaining capacity of operating power plants through the future time periods is determined, using the year of commissioning as it is given in the UDI WEPP database and by assuming a technology-specific lifetime. For this purpose, the capacities of power plants with an actual status of operating or under construction are summed together. The technical lifetime of different power plants is given in Table 3.6.

Table 3.6: Technical lifetime of power plants. Data source: [52]

Technology	Minimum (a)	Mean (a)	Maximum (a)
BIO-ST	30	35	40
COAL-ST	30	45	60
GAS-CC	25	30	40
GAS-GT	30	40	50
GEO-ST	30	35	40
HP-PS	40	75	100
HP-ROR	40	75	100
LIG-ST	30	45	60
OIL-CC	25	30	40
OIL-GT	25	30	40
SOL-CSP	35	40	45
SOL-PV	25	30	35
URA-ST	40	50	60
WIND	20	30	35
WIND-O	20	30	35

The capacity of power plants, currently in operation or under construction, from 2007 to 2050 is shown in Fig. 3.29; the mean technical lifetime, given in Table 3.6, is used. These are then applied to represent the previously installed capacity of each power plant technology in model regions over the optimization horizon.

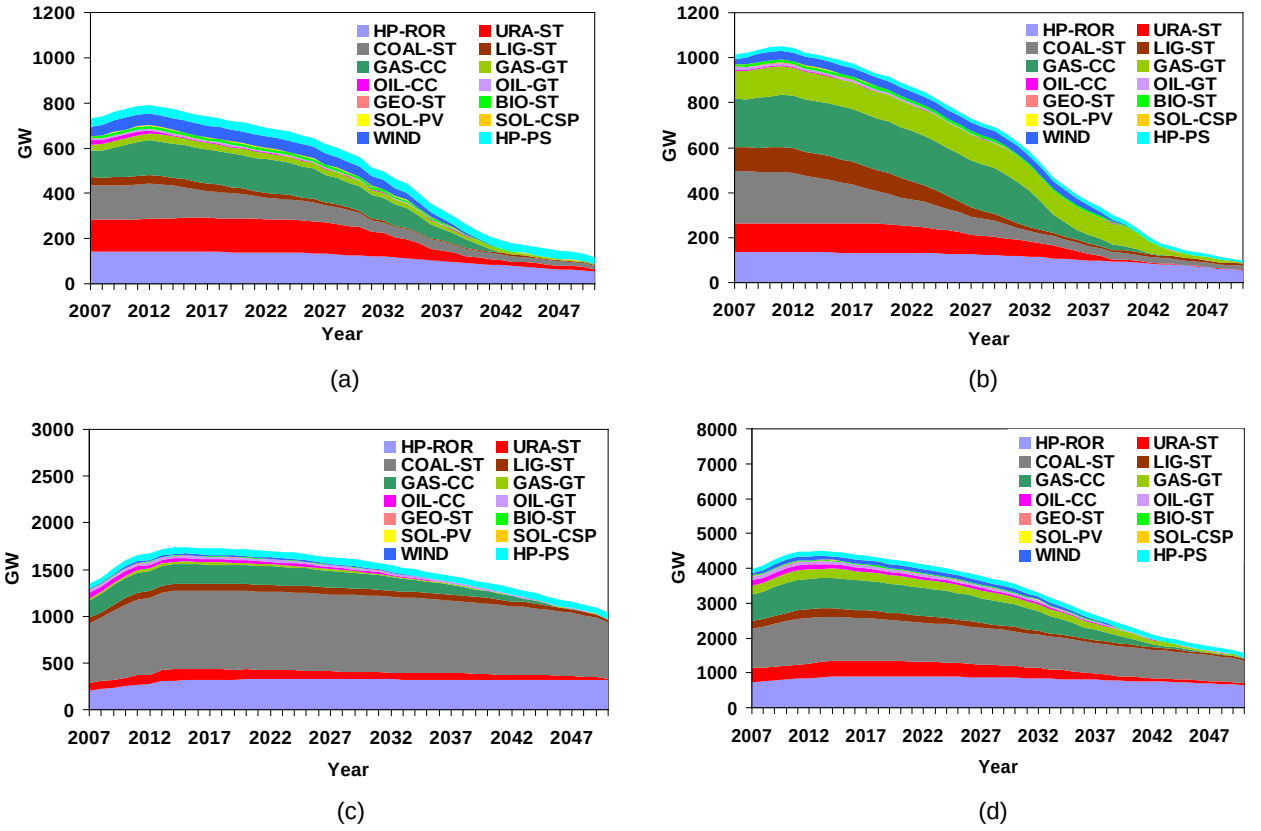

Fig. 3.29: Capacity of existing power plants over time horizon 2007-2050 (a) Europe; (b) North America; (c) Asia and Oceania; (d) Total world. Data Source: [96]

3.3.1.5 Future power plants

The UDI WEPP database also includes information about planned capacity expansions of power plants. This can be used as a basis to develop scenarios for growing capacity of renewable power plants in a prospective global electricity generation system. In Fig. 3.30, the planned capacity of different renewable technologies is illustrated over the time horizon from 2009 to 2025.

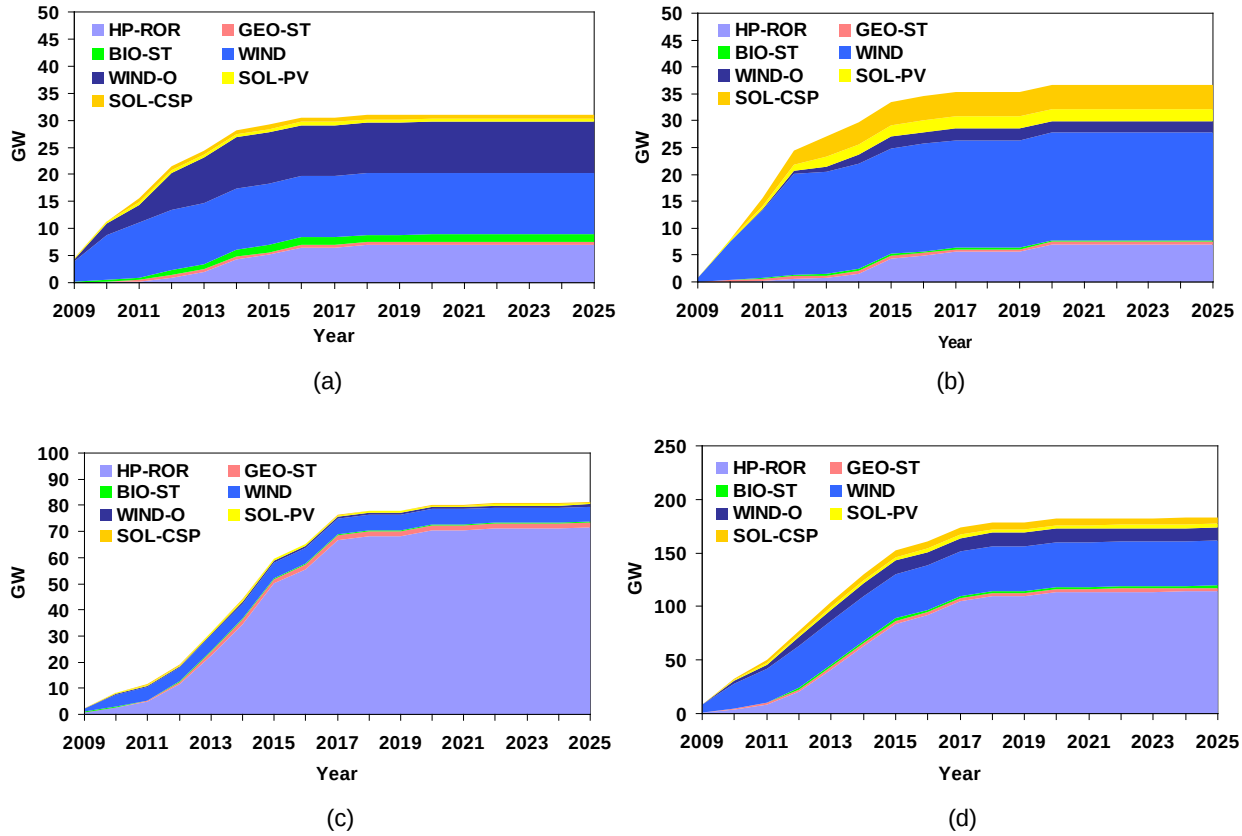

Fig. 3.30: Planned capacity of renewable power plants over time horizon 2009-2025 (a) Europe; (b) North America; (c) Asia and Oceania; (d) Total world. Data Source: [96]

3.3.1.6 Techno-economic parameters

3.3.1.6.1 Investment and operational costs

In this study, economical parameters of power plants are determined based on data from [24, 48, 49]. Table 3.7 provides a comparison between actual levels of investment and operation costs of power plants obtained from different data sources.

Table 3.7: Economical parameters of existing power plants. Data source: [24, 48, 49]

Technology	IfE 2010			IEA2010		ETM 2010		
	Investment $/kW$_{el}$	Fixed O&M $/kW$_{el}$/a	Variable O&M $/kWh$_{el}$	Investment $/kW$_{el}$	O&M $/kW$_{el}$/a	Investment $/kW$_{el}$	Fixed O&M $/kW$_{el}$/a	Variable O&M $/kWh$_{el}$
BIO-ST	-	-	-	2500-7431 Median:3281	33-289 Median:157	3777	158	0.0180
COAL-ST	1700	40	0.0058	602-2719 Median:2095	11-94 Median:42	1584	49	0.0013
GAS-CC	700	30	0.0029	538-1678 Median:1084	10-58 Median:32	914	12	0.0008
GAS-GT	550	17	0.0030	520	40	-	-	-
GEO-ST	-	-	-	1752-12887 Median:3901	40-140 Median:117	3168	122	0
HP-PS	1500	35	0.0009	2703	27	-	-	-
HP-ROR	-	-	-	757-19330 Median:2911	7-142 Median:29	2437	24	0
LIG-ST	2000	50	0.0058	1300—3485 Median:2347	40-105 Median:65	-	-	-
OIL-CC	-	-	-	-	-	938	15	0.0009
SOL-CSP	-	-	-	4347-5255 Median:5141	58-103 Median:58	4386	44	0
SOL-PV	-	-	-	2878-7381 Median:5153	11-177 Median:31	7310	40	0
URA-ST	2300	74	0.0008	1556-5863 Median:3740	52-222 Median:106	2071	73	0.0003
WIND	-	-	-	1223-3716 Median:1963	30-82 Median:48	1218	24	0
WIND-O	-	-	-	3464-6083 Median:4453	38-203 Median:128	2193	49	0

Notes:

- All costs are given in US$ (2008)
- Data from [24] is given in US$ (2000) and converted to US$ (2008) assuming an average inflation rate of 2.3% p.a
- Data from [49] is given in € (2005) and converted to € (2008) assuming an average inflation rate of 2.3% p.a and an average exchange rate of 1 US$=0.684 € as it is assumed in [48]

The levelised cost of electricity (LCOE) is a basis to compare the unit costs of different technologies over their economic lifetime. The LCOE is equal to the present value of the sum of discounted costs divided by the total produced power adjusted for its economic time value [48]. In order to compare all the cost components between different data sources, the LCOE is calculated, using the equation (3.14); *LCOE* is the levelised cost of electricity [$/kWh$_{el}$]; *INV* is the specific investment costs [$/kW$_{el}$]; *Af* is the annuity factor, given in equation (3.15); *FIXOM* is the specific fixed operation and maintenance costs [$/(kW$_{el}$.a)]; *FLH* represents the annual full operating hours [h/a]; *ef* is the emission factor [ton/kWh$_{th}$]; *CO2P* is the CO_2-price [$/ton]; *fP*

is the fuel price [\$/kWh$_{th}$]; η is the conversion efficiency; *VAROM* is the specific variable operation and maintenance costs [\$/kWh$_{el}$].

$$LCOE = \frac{INV.Af + FIXOM}{FLH} + \frac{ef.CO2P + fP}{\eta} + VAROM \quad (3.14)$$

$$Af = \frac{r.(1+r)^{ELIFE}}{(1+r)^{ELIFE} - 1} \quad (3.15)$$

The investment costs are annualized, assuming a discount rate *(r)* of 5% p.a and an expected economic lifetime *(ELIFE)* for each technology. The discount rate, used in LCOE calculations, reflects the return on capital for an investor in the absence of specific market or technology risks.

The emission factor, conversion efficiency, economic lifetime, and annual full load hours of different power plant technologies, used to calculate the LCOE, are given in Table 3.8. The same amount of full operating hours (own assumption) is used to estimate the LCOE from cost parameters, given in [24, 49]. The full operating hours are given in [48] for different technologies and are applied here to calculate the LCOE from the cost parameters, given in [48].

Table 3.8: Emission factor, efficiency, economic lifetime and FLH of power plants. Data source: [24, 48, 49]

Technology	Emission factor (ton/MWh$_{th}$)	Efficiency (%)	Economic lifetime (a)	FLH (h/a) Own assumption/IEA
BIO-ST	0	35	25	6000 / 7446
COAL-ST	0.3348	43	40	7000 / 7446
GAS-CC	0.2016	58	30	7000 / 7446
GAS-GT	0.2016	38	30	1500 / 7446
GEO-ST	0	20	25	6000 / 7066
HP-PS	0	80	80	4000 / 2540
HP-ROR	0	80	80	4000 / 4737
LIG-ST	0.396	38	40	7000 / 7446
OIL-CC	0.310	43	25	7000 / 7446
OIL-GT	0.310	35	25	2000 / 7446
SOL-CSP	0	15	25	2100 / 2628
SOL-PV	0	12	25	1700 / 1440
URA-ST	0	33	60	7500 / 7446
WIND	0	96	25	2300 / 2350
WIND-O	0	93	25	3400 / 3450

Fig. 3.31 shows the LCOE of power plant technologies based on different data sources. Fuel prices have been obtained from [48], and a CO_2-price of 30 US\$/ton has been used.

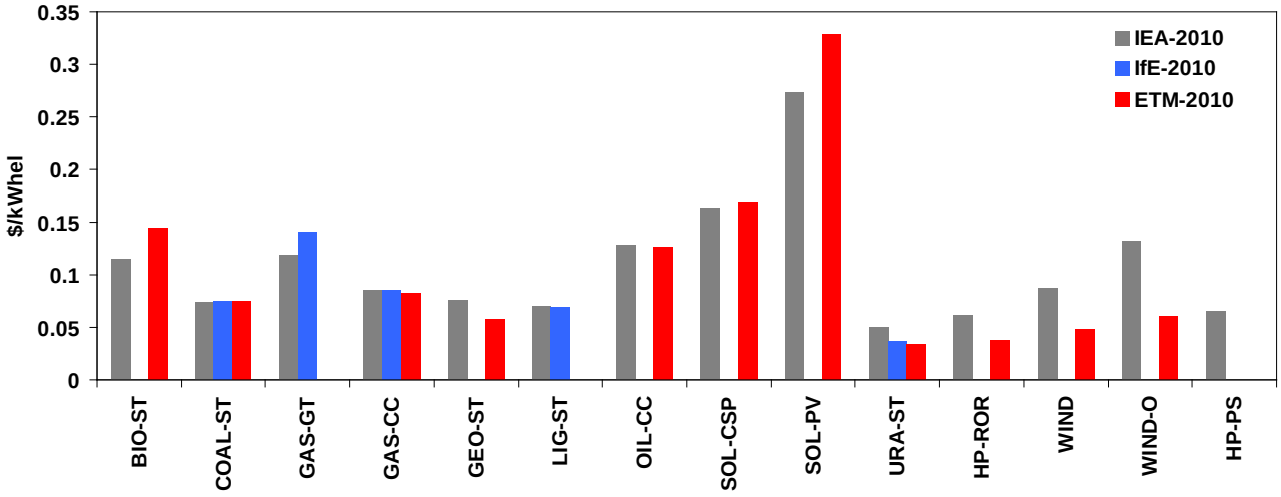

Fig. 3.31: Levelised cost of electricity. Data Source: [24, 48, 49]

Represented data sources also include information about future levels of techno-economic parameters of power plants. According to [48], actual data for wind onshore technology shows a very wide range, with overnight costs ranging from 1821 US$/kW to 3716 US$/kW. The reported capacities range from an individual unit of 2 MW to 200 MW; reported capacity factors range from 20% to 41%. Learning or experience curves reflect the reduction in the costs of electricity achieved with each doubling of the capacity, which is known as the progress ratio (PR). In [48], a leaning rate of 7% is assumed for wind onshore. Thus, the investment costs are expected to decrease to around 1400 US$/kW by 2020. The range of actual overnight costs for 8 reported offshore wind projects, documented in [48], vary from 2540 US$/kW to 5554 US$/kW; capacity factors range from 34% to 43%. Assuming a higher learning rate for offshore technology (9%), investment costs are expected to lie in the range of 2500-3000 US$/kW in 2020. In [48], capacities of PV power plants range from 0.002 MW to 20 MW; capacity factors range from 9.7% to 24.9%. Overnight costs exhibit a wide range from as low as 3067 US$/kW for a utility scale solar PV farm to 7381 US$/kW. Assuming a learning rate of 18% as suggested by the historical long-term trends in PV development, investment costs could drop by 70% from the current range of 4000-6000 US$/kW down to 1200-1800 US$/kW by 2030, with an important cost reduction of at least 40% already being achievable by 2015 and 50% by 2020 [48]. Table 3.9 provides a comparison between economical parameters of future power plants proposed by different institutions for the year 2020.

Table 3.9: Economical parameters of future power plants. Data source: [24, 48, 49] (All costs are in US$ (2008))

Technology	IfE 2020			IEA2020		ETM 2020		
	Investment $/kW$_{el}$	Fixed O&M $/kW$_{el}$/a	Variable O&M $/kWh$_{el}$	Investment $/kW$_{el}$	O&M $/kW$_{el}$/a	Investment $/kW$_{el}$	Fixed O&M $/kW$_{el}$/a	Variable O&M $/kWh$_{el}$
BIO-ST	-	-	-	-	-	2680	60	0.0167
COAL-ST	1600	40	0.0058	-	-	1523	49	0.0013
GAS-CC	630	30	0.0029	-	-	853	12	0.0008
GAS-GT	550	17	0.0030	-	-	-	-	-
LIG-ST	1830	50	0.0058	-	-	-	-	-
OIL-CC	-	-	-	-	-	877	15	0.0009
SOL-CSP	-	-	-	-	-	2802	28	0
SOL-PV	-	-	-	1534-3690	-	3655	21	0
URA-ST	2300	74	0.0008	-	-	1828	73	0.0003
WIND	-	-	-	1400	-	1036	24	0
WIND-O	-	-	-	2500-3000	-	1767	49	0

3.3.1.6.2 Technical parameters

Technical parameters of power plants, used as input to the electricity system optimization model, are described in this section. For instance, conversion efficiency of existing power plants is compared between different data sources in Table 3.10.

Table 3.10: Conversion efficiency of existing power plants. Data source: [24, 48, 49]

Technology	IfE (%)	IEA (%)	ETM (%)
BIO-ST	-	-	35
COAL-ST	33-47 (Median: 38)	39-47 (Median: 42)	38
GAS-CC	40-60 (Median: 53)	48-60 (Median: 57)	54
GAS-GT	29-39 (Median: 31)	38	-
HP-PS	80	-	-
HP-ROR	-	-	80
LIG-ST	30-43 (Median: 36)	30-45 (Median: 41)	-
OIL-CC	33- 38 (Median: 38)	-	53
OIL-GT	28-35 (Median: 32)	-	-
URA-ST	33	33	35

The efficiency of PV modules depends on the type of cells and the module's temperature. The efficiency of commercially available crystalline silicon modules has increased in the last decades from a few percentages in the early 1970's to 12-19% today [8, 14]. The most efficient crystalline silicon modules are expected to reach a target of 23% efficiency by 2020 [8]. The performance of a PV system suffers from the losses, occurring within the rest of the PV system,

e.g. inverter losses, mismatch losses, shading and cable losses, etc. These are taken into account in the performance ratio, which is expressed as the ratio between the actual performance of the system and the performance of the module under standard test conditions. The best systems have performance ratios between 0.66 and 0.85 [14].

In parabolic trough plants, the efficiency of the solar field reaches to around 50%; conversion efficiency of the steam cycle is around 30%; thus, the total net efficiency becomes 15% [64]. However, improvement of the efficiency of the solar field is highly expected in the future.

Other technical parameters including the availability factor (*AVF*) and technology ramp rates are given in Table 3.11. When in ramping constraints (see equations (2.43)-(2.45)) distinction is made between the committed capacity and the non-committed capacity, ramp rate of the committed capacity (*rampc*), given in Table 3.11, is used. Ramp rate of the non-committed capacity is then assumed at 60% of the ramp rate of the committed plant. Only for the high peak technology, i.e. gas turbine, both of the ramp rates are assumed at 100%. When no distinction is made between the on-line and off-line power plants to reduce the complexity of the problem, the same ramp rate (*ramp*) is used for both committed capacity and non-committed capacity. The technology ramp rates are determined mainly based on a methodological approach (see section 2.5) but have been inspired by literature review [22, 54, 56, 107]. Availability factors of power plants are based on an industry report [53].

Table 3.11: Other technical parameters of power plants. Data source: [22, 53, 54, 56, 91, 107]

Technology	Availability (% of maximum capacity)	rampc (% of maximum capacity/hour)	ramp (% of maximum capacity/hour)
BIO-ST	50*	33	25
COAL-ST	84	33	22
GAS-GT	95	100	100
GAS-CC	90	53	35
GEO-ST	70	33	25
HP-PS	95	-	-
HP-ROR	95	-	-
LIG-ST	85	21	14
OIL-CC	90	53	35
OIL-GT	95	100	100
SOL-CSP	99	-	-
SOL-PV	99	-	-
URA-ST	70-85	8	8
WIND	95	-	-
WIND-O	90	-	-

Notes:

*This low availability results from limited fuel availability

3.3.1.6.3 Fossil fuel prices and emissions costs

In this study, fuel prices are mainly determined based on data from [48]. In [100, 108] the development of fossil fuel prices is given over a time horizon from 2010 to 2030. Actual fuel prices and forecasted prices for the next 2 decades are given in Table 3.12. For biomass, an average price of 25.51 US$/MWh$_{th}$ is assumed based on the study conducted in [109].

Table 3.12: Actual and expected fossil fuel prices. Data source: [48, 100]

Fuel	2010 $/MWh$_{th}$	2015 $/MWh$_{th}$	2020 $/MWh$_{th}$	2025 $/MWh$_{th}$	2030 $/MWh$_{th}$
Hard Coal (OECD)	12.96	17.72	17.23	16.74	16.25
Natural Gas (OECD Asia)	39.92	46.02	50.77	53.43	56.12
Natural Gas (OECD EU)	35.14	40.21	44.44	47.03	49.62
Natural Gas (USA)	-	46.16	50.95	53.68	56.40
Uranium	3.08*	-	-	-	-

Notes:

- All costs are in US$ (2008)

- * Uranium price is 9.33 US$/MWh$_{el}$ and is converted to US$/MWh$_{th}$ by assuming a conversion efficiency of 33%.

However, if a country belongs to one of the main coal and gas producing regions, the domestic fuel price significantly differs from the world market price. For instance, Fig. 3.32 shows the deviation of domestic prices of natural gas and hard coal from world market prices in large coal and gas producing countries.

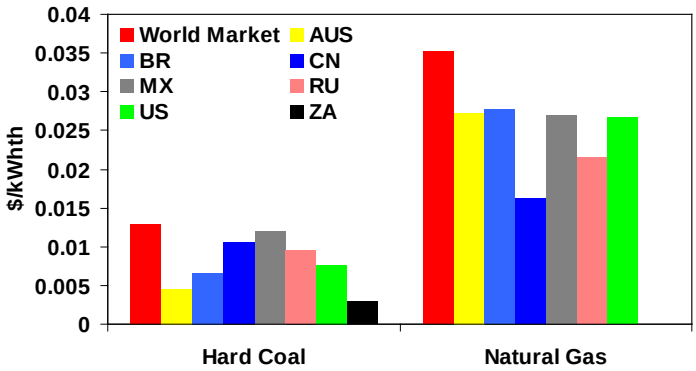

Fig. 3.32: Domestic prices of coal and gas vs. world market prices. Data source: [48]

3.3.2 Power transmission grid

The total transfer capacity (TTC) is the maximum feasible exchange between two interconnected areas compatible with operational security standards applicable at each system if future network conditions, generation and load patterns are perfectly known in advance. The net transfer capacity (NTC) is the maximum feasible exchange between two interconnected areas compatible with security standards applicable in both areas by taking into account technical uncertainties in future network conditions [110, 111]. The NTC is calculated from the TTC by subtracting a transmission reliability margin (TRM); TRM is a security margin that copes

with uncertainties on the computed TTC values, arising from unintended deviations of physical flows during operation due to the physical functioning of load-frequency regulation, emergency exchanges between transmission system operators (TSOs) to cope with unexpected unbalanced situations in real time, and inaccuracies in data collections and measurements. TRM is associated to the real-time operation, and its value is determined by each TSO in order to guarantee the operational security of its own power system. TRM may vary seasonally and may be up-dated according to possible modifications in the power system.

The European network of transmission system operators for electricity (ENTSO-E) [97] gathers and publishes the NTC values that have been determined by each TSO. These are used here to determine the existing capacities of power transmission interconnections between model regions in Europe. In [97] two NTC values are given for each transmission line, representative for winter and summer period. Furthermore, in the bilateral exchange matrix, the NTC from country A to B may differ from the estimated NTC from B to A. Here, as a conservative assumption, the lower NTC has been used to limit the power flow between model regions. For other model regions in Asia, Africa, and America no accurate information exists at the moment that allow representing the power transmission network structure. Hence, the existing power transmission interconnections between those regions are not included in the model database. As the focus of the present work is on the optimization of the structure of a prospective global electricity generation system that integrates a high share of FRES, this does not influence the scenario analyses and the obtained results in chapter 4. Indeed, the capacities of inter-regional power transmission lines are to be optimized under different framework conditions to facilitate integrating a high share of FRES into the power system; thus, huge capacities must be installed far beyond the existing levels (see chapter 4).

As a promising option for transmission of electricity over long distances, high voltage direct current (HVDC) technology is taken into account. The techno-economic parameters are given in Table 3.13. The investment costs are annualized assuming an economic lifetime of 30 years and a discount rate of 5% p.a.; annual fixed costs are assumed at 1.8% of the total investment costs. Transmission losses of a bipolar HVDC overhead line (OHL) vary in the range of 3.1-5 %/10^3km; transmission losses of bipolar HVDC sea cables vary in the range of 2.8-5.8 %/10^3km; the losses associated to transformer stations vary in the range of 0.5-1% per station [27, 112, 113]. Here, the energy losses of OHL transmission lines are assumed at 4%/10^3km while an average level of 3%/10^3km is used for sea cables. Two transformer stations are associated to each HVDC power transmission line, and the energy losses are assumed at 0.5% per station. Availability of transmission lines is assumed at 90%.

Table 3.13: Techno-economic parameters of HVDC power transmission lines. Data source: [27, 114]

Technology	Voltage (kV)	Capacity (MW_{el})	Length (km)	Line investment costs ($/$MW_{el}$/km)	Station costs (Mio.$/station)
HVDC-OHL [114]	500	6000	2000	83	875
HVDC-OHL [114]	765	6000	2000	125	700
HVDC-OHL [114]	800	6000	2000	63	875
HVDC-OHL [27]	600	4800	1000	102	350
HVDC Cable [27]	600	1000	1000	1023	350

3.4 Hydrogen as a secondary energy carrier

Application of hydrogen as an energy source for highly efficient fuel cells may offer a wide range of advantages in a prospective electricity generation system regarding the energy security and environmental issues. When a high share of FRES is integrated into the future power system, hydrogen that can be stored at high quantities and transported as an energy carrier over long distances can play an important role.

However, while hydrogen in many forms is the most abundant element in the universe, pure hydrogen does not exist in appreciable amounts. Hydrogen is always connected to other elements, like carbon in plants, petroleum or natural gas, or attached to oxygen. Therefore, to produce hydrogen, a primary energy source is required to break the chemical bond and separate the hydrogen from its partner.

3.4.1 Hydrogen production from renewable energy sources

To produce hydrogen, four major pathways exist: steam methane reforming (SMR), coal gasification, biomass gasification or pyrolysis, and electrolysis. However, in a sustainable energy system of future, the focus is laid on the production of hydrogen from renewable energy sources. Producing hydrogen through electrolysis is an energy-intensive process. However, in a sustainable energy system of future, this is a direct route from renewable electricity to a chemical energy carrier.

There are two main types of electrolyzers: conventional alkaline and proton exchange membrane (PEM), also known as solid polymer electrolyte (SPE). Alkaline units usually use a solution of potassium hydroxide as the electrolyte due to its high conductivity; these units can be either unipolar or bipolar. PEM electrolyzers use a solid polymer electrolyte and are essentially a PEM fuel cell that operates in reverse. Alkaline electrolyzers are a more mature technology than PEM electrolyzers and currently dominate the industrial market. However, PEM electrolyzers have a higher efficiency and are seen as a promising future option for electrolysis.

Conversion efficiency of electrolysis systems is high, ranging from 80 to 95% [115]. Table 3.14 gives the required energy, the electrolyzer's conversion efficiency, and the system efficiency for an alkaline electrolyzer and a PEM electrolyzer. To calculate the system efficiency, the energy requirement of the entire electrolysis system must be taken into account, not just the efficiency of the electrolyzer. Energy efficiency is defined as the higher heating value (HHV) of hydrogen (142 MJ/kg) divided by the energy consumed by the electrolysis system per kg of hydrogen produced. In a future scenario in [112], a high pressure alkaline electrolyzer with a hydrogen production rate of 515 Nm^3/h and a conversion efficiency of 77% is proposed for the year 2025.

Table 3.14: Technical parameters of electrolysis systems. Data source: [115]

Technology	Energy consumption (kWh_{el}/kg_{H2})	Electrolyzer efficiency (%)	System efficiency (%)
Alkaline bipolar	53.4	80	73
PEM	70.1	95	56

According to [112, 116], the investment costs of a high pressure alkaline electrolyzer with a capacity of 1.5 MW_{H2} is 1000 €/kW_{H2} (730 €/kW_{el}). In a future scenario, the investment costs reduce to 700 €/kW_{H2} (539 €/kW_{el}) by 2025.

Hydrogen can also be produced from biomass through gasification or pyrolysis. Hydrogen can also be obtained from reforming of alcohols or wood. Industrial natural gas reformers generate hydrogen with an energetic HHV efficiency of 90%; currently, this is the most economical method to produce hydrogen [117].

3.4.2 Hydrogen transport

Hydrogen can be transported as a compressed gas, as a liquid, or as a solid metal hydride. Two main factors, affecting the transportation costs of hydrogen, are the production rate and the delivery distance. At high distances and large quantities, transportation of gasified hydrogen through pipelines and transportation of liquefied hydrogen by ships are the most attractive options.

Distribution of hydrogen through pipelines has a high efficiency. The main disadvantage is the lower energy density of hydrogen as compared to that of natural gas. Indeed, the volumetric HHV energy content of hydrogen is about 3.5 times less than the energy content of natural gas. Thus, pipes with larger diameters are required to accommodate similar energy flow rates at identical pressures. Thus, at the same rate of energy flow, hydrogen requires about 3.85 times more energy than natural gas [118].

In [113], the efficiency of transporting hydrogen is compared with the efficiency of natural gas transfer through identical pipelines. However, in reality, the existing natural gas pipelines cannot be used for hydrogen transport because of diffusion losses, brittleness of materials and seals, incompatibility of compressors with hydrogen, and other technical issues. Also, hydrogen pipelines should have larger diameters to reduce the energy requirement for pumping. A pipeline with a diameter of 1 m and an internal pressure of 1 MPa (10 bar) is taken into account. Because of the equal energy flow requirement, hydrogen has to be moved at 31.4 m/s while natural gas is transported at a velocity of 10 m/s. Typically, a compressor is installed at every 150 km for transporting natural gas at a velocity of 10 m/s; each compressor consumes about 0.3% of the local energy flow. Applying this to the transport of hydrogen through an identical pipeline, each compressor would require 3.85 times the energy required for the transportation of natural gas, i.e. 1.16% of the local energy flow. The specific energy consumption to move hydrogen through this pipeline is then estimated at 10.9 kJ/(kg_{H2}.km). Thus, energy losses occur in transport reach to 7.8 %/10^3km based on the HHV of hydrogen. However, in the study conducted in [113], the fact that dedicated hydrogen pipelines should be designed with larger diameters as compared to natural gas pipelines is not taken into account. In [112], the losses occur in hydrogen transport are estimated at 4 %/10^3km for the state of the art technology; it reduces to 3.87 %/10^3km in 2025. Table 3.15 provides an overview on underlying assumptions and energy losses of hydrogen transport through pipelines based on different studies.

Table 3.15: Technical parameters of hydrogen pipelines. Data source: [112, 113]

Technology	Pipeline diameter (m)	Operating pressure (bar)	Flow velocity (m/s)	Transport losses (%HHV_{H2}/10^3km)
State of the art [113]	1	10	31	7.8
State of the art [112]	1.42	75	22.4	4.02
Scenario 2025 [112]	1.6	120	21.3	3.87

Total system costs include the capital costs of pipelines and compressors as well as the operation and maintenance costs including energy costs of the compressors. Capital costs are high and increase linearly with the distance. Thus, the economies of pipelines improve at higher capacities. Specific investment costs of hydrogen pipelines based on different data sources are given in Table 3.16. To derive the specific costs, the availability of pipeline is assumed at 90% as it is assumed in [112]. However, if this factor is reduced to 40%, the investment costs could increase to 190 US$/($MW_{H2}$.km), which is around two times of the investment costs of an HVDC overhead line. Here, annual fixed costs are assumed at 1.8% of total investment costs; investment costs are annualized assuming an economic lifetime of 30 years and a discount rate of 5% p.a.

Table 3.16: Economical parameters of hydrogen pipelines. Data source: [27, 112]

Technology	Capacity (GW_{H2})	Length (km)	Investment costs ($/$MW_{H2}$/km)	Variable O&M costs ($/$MWh_{H2}$)
State of the art [27]	38	5000	85	10.5
State of the art [112]	34	2500	70	2.9 (excl. fuel costs)
Scenario 2025 [112]	66	2500	40	1.8 (excl. fuel costs)

Alternatively, liquefied hydrogen (LH_2) can be transported by ship. However, liquefaction of hydrogen is an energy-intensive process. The medium size plant of Linde Gas AG in Germany has a production rate of 182 kg_{H2}/h, and the specific energy consumption is about 54 MJ/kg_{H2}; thus, its efficiency is 62% based on the HHV of hydrogen. Larger plants operate at higher efficiencies of up to 75%. A feasibility study has shown that a plant with a capacity of 12500 kg_{H2}/h consumes 30 MJ/kg_{H2} energy, i.e. 21% of the HHV energy content of the liquefied hydrogen; this corresponds to an overall efficiency of 79% [113].

Liquid hydrogen storage systems lose hydrogen by boil-off. To evaluate the transport efficiency of LH_2, this should be taken into account in addition to the energy required for the ship. For large vessels, boil-off rates might reach to 0.2-0.4 %/day [119]. At final stage, the liquefied hydrogen is compressed to transport the gasified hydrogen to the final destination to be used in fuel cells. The electrical energy required for the compression of hydrogen to 200-800 bar lies in the range of 15-20 MJ/kg_{H2} [113]. This corresponds to an efficiency of 86-90% based on the HHV of hydrogen. Technical data of LH_2-ships are given in Table 3.17.

Table 3.17: Technical parameters of LH_2-ships. Data source: [112]

Technology	Capacity (ton H_2)	Velocity (m/s)	Fuel consumption (GWh_{H2}/a)	Boil-off (%HHV_{H2}/day)	Transport losses (%HHV_{H2}/10^3km)
Barge Carrier	1036	9	154	0.4	3.1
SWATH Ship (Scenario 2025)	8150	9	596	0.2	1.8

Economical parameters of the liquefier and LH_2-ships are given in Table 3.18 and Table 3.19, respectively. Here, annual fixed costs are assumed at 1.8% of total investment costs; investment costs are annualized assuming an economic lifetime of 30 years and a discount rate of 5% p.a.

Table 3.18: Economical parameters of Liquefier. Data source: [112]

Technology	Hydrogen production rate (kg_{H2}/h)	Investment costs ($/$kW_{H2}$)
State of the art	2083	1579
Scenario 2025	14600	1287

Table 3.19: Economical parameters of LH_2-ships. Data source: [112]

Technology	Capacity (ton H_2)	Investment costs ($/$kW_{H2}$)
Barge Carrier	1036	6.15
SWATH Ship (scenario 2025)	8150	6.05

For instance, when liquefied hydrogen is transported by ship through a total delivery distance of 5400 km, if the electrolysis efficiency is assumed at 70% and the liquefaction process has an efficiency of 75%, the total net efficiency becomes as low as 44-47%. After the compression process, this could even further reduce to 38-42%. However, if the gasified hydrogen is transported through pipelines, the total net efficiency from electrolytic production of hydrogen up to the destination becomes 55% if transport losses are assumed at 4 %/10^3km. In Fig. 3.33, the efficiency of hydrogen transport technologies is compared with the efficiency of electricity transmission by HVDC over different transmission lengths.

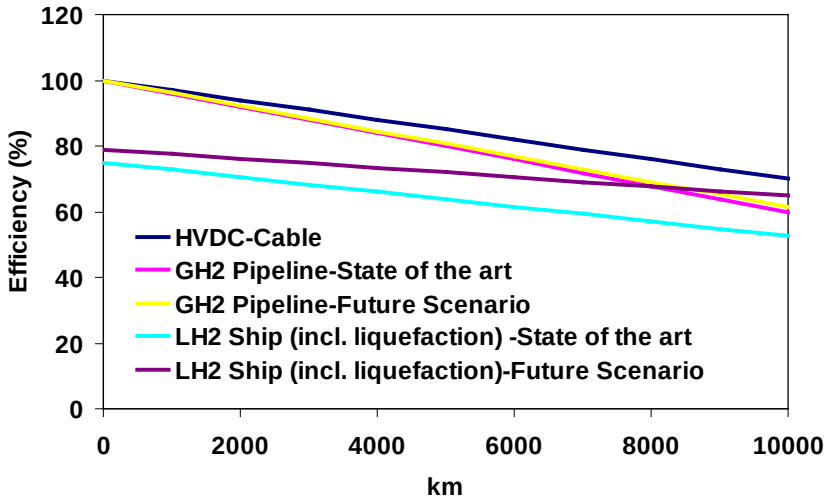

Fig. 3.33: Efficiency of hydrogen transport vs. efficiency of power transmission. Data Source: [27, 112, 113]

3.4.3 Electricity production from hydrogen

Most of the current focus of a possible shift towards hydrogen as an energy carrier is on its applications in the automotive sector. However, it can also be applied for power production in a sustainable energy system of future. Fuel cells are characterized with higher conversion efficiencies compared to other combustion technologies. In the category of low temperature fuel cells, phosphoric acid fuel cells (PAFC) are the most mature technology with least room for further improvement or cost reduction. The alkaline fuel cells (AFC) are not either likely to benefit from large-scale investment and deployment and resulting technical developments. The proton exchange membrane fuel cells (PEMFC) have better prospects for cost reduction in the future; this is likely to become the long-term option for power generation from sources of pure hydrogen such as hydrogen produced via electrolysis. The molten carbonate fuel cells (MCFC) and solid oxide fuel cells (SOFC) are in the category of high temperature fuel cells. Table 3.20 provides an overview on techno-economic parameters of different fuel cell technologies. In this study, the investment costs of fuel cells are annualized assuming an economic lifetime of 25 years and a discount rate of 5% p.a.

Table 3.20: Techno-economic parameters of fuel cells - actual. Data source: [27, 120]

Technology	Capacity (kW_{el})	Investment costs ($/$kW_{el}$)	Efficiency (%)
PAFC	200	5600	40
PEMFC	200	4092	35
MCFC	2000	3500	46
SOFC	100	3898	45

Table 3.21 shows the projected costs and expected efficiencies for the year 2020, which are proposed by the National Renewable Energy Laboratory (NREL).

Table 3.21: Techno-economic parameters of fuel cells - 2020 targets. Data source: [120]

Technology	Capacity (kW_{el})	Investment costs ($/$kW_{el}$)	Efficiency (%)
PEMFC	200	1830	38
MCFC	2000	1508	50
SOFC	100	1938	51

3.4.4 Hydrogen storage

Hydrogen can be stored as a compressed gas, as a liquid, or combined with a metal hybrid. Liquid hydrogen is produced through the energy-intensive process of liquefaction and requires an insulated storage container. As liquid hydrogen is stored as a cryogenic liquid at its boiling point, any heat transfer to the liquid causes some hydrogen to evaporate. Thus, a major concern is to minimize hydrogen losses caused by the liquid boil-off. Compressed gas storage is the simplest form of storage; the only required equipment is the compressor and the pressure vessel [121]. However, the main problem is the low storage density, which depends on the storage pressure. Higher storage pressures, however, result in higher capital and operational costs.

Above-ground storage of hydrogen employs high-pressure spherical or cylindrical tanks with pressures as high as 30 MPa while low-pressure spherical tanks with large diameters can also be used [121]. Capital costs of pressure vessels are in the range of 625- 2080 US$/kg$H_2$[1] [121]. Large alternating, double-action compressors may have efficiencies in the range of 65-70% [121].

Underground storage is the most economical way to store hydrogen in large quantities and for long-term periods. According to [121], costs are in the range of 2.50-18.90 US$/kg$H_2$[1]. This is obviously less than the costs of liquid hydrogen storage and of the above-ground compressed gas storage. The operational costs of underground storage are limited to the energy costs and maintenance costs required for compressing the gas into underground storage and boosting the pressure coming back out. One estimate for the operational costs of underground storage is 0.1-3.9 US$/kg$H_2$[1] [121].

[1] Costs are represented In US$ (1995)

4 Model applications and results

In this chapter, the developed methodology is applied to investigate optimal configuration of a renewable-based global electricity supply system under different framework conditions.

4.1 Geographical structure

The model, developed and applied in this thesis, covers a worldwide scale. The spatial resolution of the model is at first limited according to the geographical detail of the used meteorological data. Additionally, temporal resolution and geographical accuracy are limited according to the accessible computation power and due to the long calculation time.

Global macroeconomic energy models are mostly characterized with a coarse spatial resolution; the regions are mainly differentiated based on the political borders [24, 25]. Here, the central objective for developing a global, multi-regional electricity system optimization model is to represent the global grid structure and required capacities for energy transport. Thus, the geographical structure of this global model is determined according to the geographic distribution of electricity demand and renewable energy supply.

The global model, developed and applied in this thesis, has 50 regions. A number of neighboring countries, having the same level of technical potential of renewable electricity production, are aggregated to one region. In other cases, a large country is disaggregated to a number of sub-regions to represent an inhomogeneous distribution of renewable energy sources and/or electricity demand. The zonal configuration of the model is represented in Table A.1.

4.2 Scenario-based analysis

In the following, scenario analysis is performed. The starting point to analyze the system's behavior and to quantify the influences of an ideal global grid and energy storage systems is the so-called "full renewable supply" scenario. Considering a long-term perspective, the model is applied to optimize the structure of a global electricity supply system, which relies on the maximum feasible share of FRES. The target is to propose an ideal configuration for a prospective, low-carbon electricity generation system of the world in order to have an optimal usage of spatial de-correlations of wind and solar energy. This is to specifically quantify the influences of an ideal global grid to mitigate negative consequences of integrating a high share of FRES into the global electricity generation system.

Deployment of emission-free energy sources such as wind and solar in the electricity sector can play an important role in the reduction of GHG emissions. Therefore, in the next step, taking into account a time frame from 2020 to 2040 in five-year time steps, a detailed analysis is performed on driving and hindering forces of CO_2 emissions of the world electricity supply sector. By considering a realistic development of the used economical parameters and technical restrictions of power plants on a technology level, the model is applied to study possible influences on CO_2 emissions abatement and the CO_2-price. Influences caused by the power system integration of solar and wind energy and benefits of an ideal global grid are investigated.

Due to the geographical dispersion and fluctuations of the primary energy source, large-scale integration of solar and wind power into the electricity system requires extensive adaptations.

Thus, a parametrical study is then performed by varying the integration share of FRES and the renewable energy mix. The is to determine the required structural adaptations in order to mitigate negative consequences caused by the power system integration of various shares and combinations of solar and wind energy into a medium-term global electricity supply system. What is an optimal energy mix under different framework conditions and how much energy storage and/or inter-zonal power transmission capacity is required to facilitate integrating different shares and combinations of FRES into the global power system are the questions that are covered in this part.

4.2.1 Full renewable supply in 2050

As a starting point, the model is applied to analyze a highly renewable case for a prospective global electricity generation system. The central question of the analysis is: how should a renewable-based electricity supply system of the world be designed and operated to realize an optimal usage of spatial de-correlations of FRES and of the electricity demand?

The global model is applied to demonstrate in a prospective global electricity supply system, transmission of electricity and hydrogen over long distances allows gaining profit from spatial de-correlations of short-term and seasonal variations of FRES and to reduce the required backup capacities. Starting from an end point of a full renewable supply, the maximum feasible share of solar and wind power and their optimal combination, optimal geographic distribution of solar and wind power plants, inter-zonal capacities for energy transport, inter-zonal energy flows, and capacities of energy storage systems are determined based on an ideal globally-interconnected structure of a future electricity generation system.

4.2.1.1 Scenario setup

Dispatchable power plants of each region are aggregated to one backup technology, named “BP”. As promising options for renewable electricity production, wind energy converters for on- and off- shore sites, PV, and CSP are taken into account. Renewable technologies can be installed at each region, taking into account the geographical potential (see sections 3.1.1 and 3.1.2). Annual gain of energy, temporal fluctuations, availability of suitable sites for wind and solar electricity production, and proximity to the load centers, are the factors, which are considered through the optimization, to select the promising generation sites.

Boundary conditions such as energy transport possibilities, availability of energy storage systems, fossil fuel prices, and climate policies have significant impact on the optimal configuration of a future electricity generation system. As a starting point for analyzing the behavior of a renewable-based electricity generation system, the first two options - energy transport and storage - are crucial. Thus, the scenarios, presented here, allow quantifying benefits of a global grid and analyzing influences of energy storage systems in a prospective electricity generation system, which integrates the maximum feasible share of solar and wind energy. Scenarios are described in Table 4.1.

Table 4.1: Scenarios and underlying assumptions

Scenario	Underlying assumptions
No Link	- Inter-regional energy transport is not allowed. - Energy storage is not allowed.
Link	- Inter-regional transmission of electricity is allowed. - Energy storage is not allowed.
LinkPSto	- Inter-regional transmission of electricity is allowed. - Energy storage by HP-PS is allowed.
LinkH2Sto	- Inter-regional transmission of electricity is allowed. - Energy storage by H2-Sto is allowed.
Link-H	- Inter-regional transmission of electricity is allowed. - Energy storage is not allowed. - All cost components of HVDC are reduced by 50%.
LinkPSto-H	- Inter-regional transmission of electricity is allowed. - Energy storage by HP-PS is allowed. - All cost components of HP-PS are reduced by 50%.
LinkH2Sto-H	- Inter-regional transmission of electricity is allowed. - Energy storage by H2-Sto is allowed. - All cost components of ELCLYS and FUCELL are reduced by 50%.

In all scenarios, the costs of renewable technologies are projected to be low while the backup technology is an expensive option; the latter is characterized with high variable operation costs and a high level of operational flexibility. This approach allows determining an ideal configuration of a renewable-based electricity supply system of the world not based on an actual level or a realistic development of technology costs and existing technical restrictions but mainly according to the geographical and temporal dependencies of FRES.

Techno-economic parameters used as input to the electricity system optimization model are given in Table 4.2. For “BP” technology, techno-economic parameters of the gas turbine technology, given in [49], are used. Fuel costs are based on the projected price of natural gas, as it is given in [100]. A global carbon price of 50 US$/ton is used according to the projection made in [52]. For “WIND” technology, projected costs of the year 2050 are taken from [24]. To make the “WIND-O” technology competitive, projected costs for the year 2050, given in [24], are reduced by 8%; the costs of “SOL-PV” and “SOL-CSP” power plants are also reduced by 50% from the levels proposed in [24]. For electrolysis systems (“ELCYS”), the costs and efficiency are determined based on the study conducted in [112]. Techno-economic parameters of fuel cells (“FCELL”) are based on the future levels, proposed in [120].

Table 4.2: Techno-economic parameters. Data source: [24, 49, 100, 112, 120] (All costs are in US$ (2008).)

Technology	Lifetime (a)	Efficiency (%)	Fuel price ($/MWh$_{th}$)	Investment ($/kW$_{el}$)	Fixed O&M ($/kW$_{el}$/a)	Variable O&M ($/kWh$_{el}$)
BP	25	35	49.62	550	11	0.0039
ELCLYS	30	77	-	1102	11	0.002
FCELL	30	60	-	1148	11	0.002
SOL-CSP	25	25	-	713	7	0
SOL-PV	25	20	-	1097	11	0
WIND	25	100	-	1036	24	0
WIND-O	25	100	-	1462	24	0

Techno-economic parameters of energy storage systems are given in Table 4.3. As a promising option for storing hydrogen, underground compressed gas storage is taken into account. Availability of “HP-PS” and “H2-Sto” is assumed at 95% and 90%, respectively.

Table 4.3: Techno-economic parameters of energy storage systems. Data source: [24, 48, 49, 121] (All costs are in US$ (2008).)

Technology	Lifetime (a)	Efficiency (%)	Investment ($/kW$_{el}$)	Investment ($/kWh$_{el}$)	Fixed O&M ($/kW$_{el}$/a)	Variable O&M ($/kWh$_{el}$)
HP-PS	80	80	1420	10	18	0.001
H2-Sto	30	100	-	0.1433	-	0.000

For inter-regional transmission of electricity, costs of the 600kV HVDC technology, given in Table 3.13, are used. Indeed, hydrogen transport by pipelines and LH_2-ships has to compete with power transmission. Mainly due to the energy-intensive liquefaction process, the efficiency of transporting hydrogen as a liquid is significantly lower than the efficiency of transportation of gasified hydrogen through pipelines (see section 3.4.2). Assuming that the efficiency of the compression process lies in the range of 86-90% [113], energy losses, occurring through transportation of liquefied hydrogen by ships and compression at the site, is far beyond the losses, occurring in electricity transmission via HVDC (see Fig. 3.33). On the other hand, the efficiency of transporting hydrogen through pipelines is nearly identical to the efficiency of electricity transmission via HVDC. Thus, to reduce the complexity of the problem, hydrogen is mainly used for stationary power production while inter-zonal energy transport in “Link-” scenarios is at first limited to power transmission.

In order to determine the electricity demand of model regions in year 2050, the final electricity demand projected based on the B2 scenario of IPCC, which is available for 11 world regions, was spatially rescaled according to the geographic distribution of population (see section 3.2). Hourly time series of wind power capacity factor and solar irradiation have been determined, using the meteorological data of the year 1993, given in [60, 65]. This has been chosen as it is the latest period that both the time series of wind speed and of solar irradiation were available at global scale at the time of writing. The approach applied to calculate these input parameters is described in sections 3.1.1 and 3.1.2.

An optimization is performed over one year. Temporal resolution is limited according to the accessible computation power and due to the long calculation time. Between six and thirteen weeks are simulated in all scenarios to represent the total year. The selected weeks are equally distributed over the whole year to capture short-term variations as well as seasonal characteristics of renewable power production and of the electricity demand. At the highest temporal resolution, every fourth week of the year, i.e. 2184 hours, are chronologically simulated. Moreover, to select the modeled time steps, it is taken into account that the summed levels over all time steps, hourly variations, and statistical properties of the time series of renewable supply and of the electricity demand is close to the levels, derived from complete annual profiles. Statistical properties of different time series of wind power capacity factor and solar irradiation and electrical load profiles, which are summed over all regions, are compared in Table 4.4; “tsH” and “tsL” represents the highest and the lowest temporal resolution; “ts-all” is used to represent complete annual profiles.

In Fig. 4.1 and Fig. 4.2, duration curves of electricity load, of wind power capacity factor, and of normalized solar irradiation based on the modeled time steps are compared with the complete annual duration curves.

Table 4.4: Statistical properties of time series of renewable supply and electricity demand

	Max./Max. (ts-all)	Min./Min.(ts-all)	Mean/Mean (ts-all)	std/std(ts-all)	std-var/std-var (ts-all)
Demand-tsH	0.97	1.00	1.00	0.97	1.03
Demand-tsL	0.96	1.00	0.99	1.01	1.04
Wind-tsH	0.92	1.01	1.02	1.04	1.32
Wind-tsL	0.87	1.01	1.03	1.12	1.09
WindO-tsH	0.92	1.13	1.03	0.98	1.41
WindO-tsL	0.92	1.15	1.05	1.13	1.42
PV-tsH	0.99	1.03	1.00	0.99	0.99
PV-tsL	0.98	1.03	1.00	0.99	0.99
CSP-tsH	0.95	1.00	0.99	0.98	0.98
CSP-tsL	0.92	1.80	0.99	0.96	0.96

Notes:

- Demand is the electrical load profile summed over all regions

- Wind is time series of wind onshore capacity factor summed over all regions; WindO is time series of wind offshore capacity factor summed over all regions; PV is time series of global horizontal irradiation summed over all regions; CSP is time series of direct normal irradiation summed over all regions

- tsH includes the modeled time steps at the highest temporal resolution, i.e. 2184 h; tsL includes the modeled time steps at the lowest temporal resolution, i.e. 1008 h; ts-all includes all time steps of a year, i.e. 8760 h

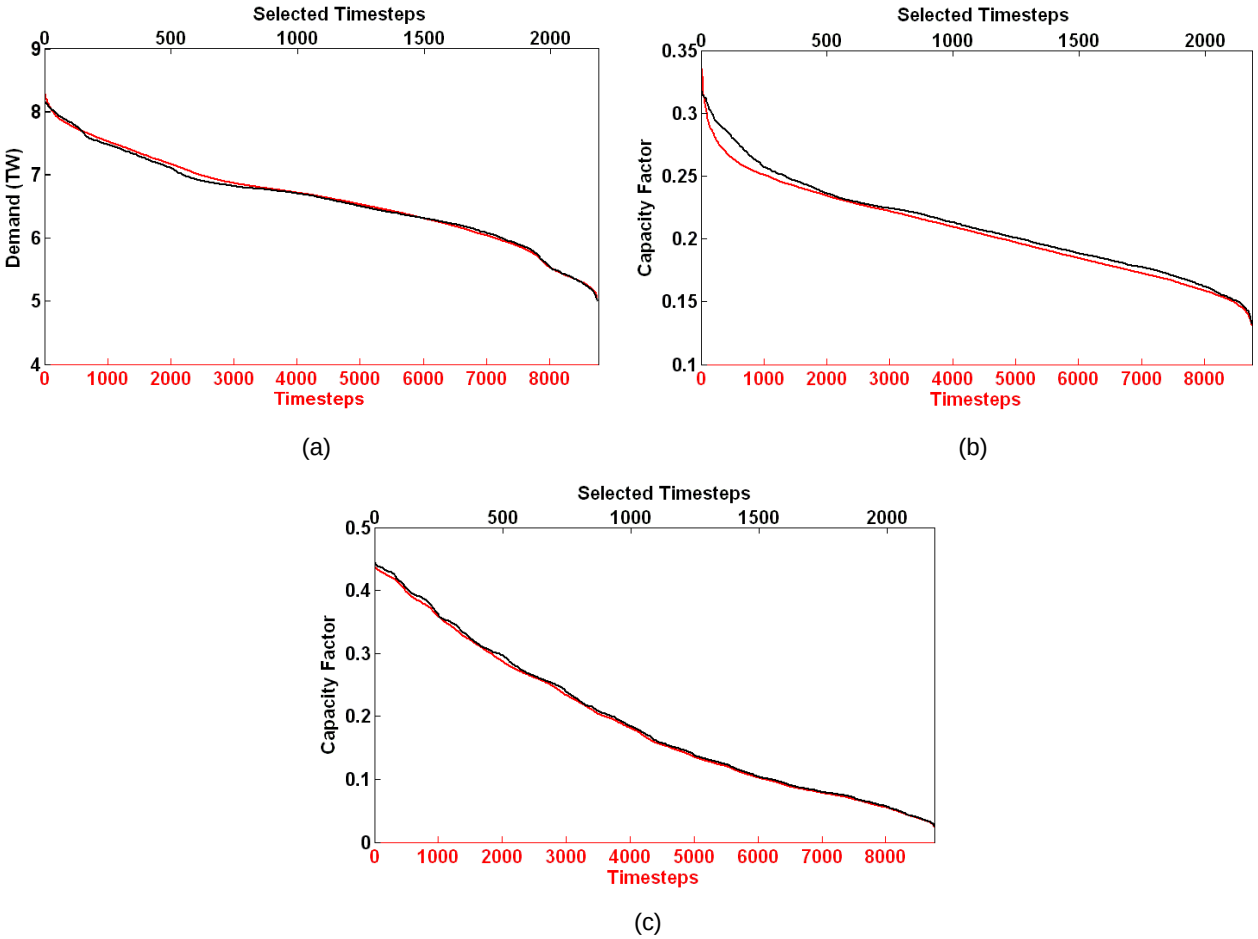

Fig. 4.1: Duration curves based on modeled time steps at the highest temporal resolution (black) vs. complete annual duration curves (red) (a) Electricity load summed over all regions; (b) Wind onshore power production summed over all regions and normalized; (c) PV electricity production summed over all regions and normalized

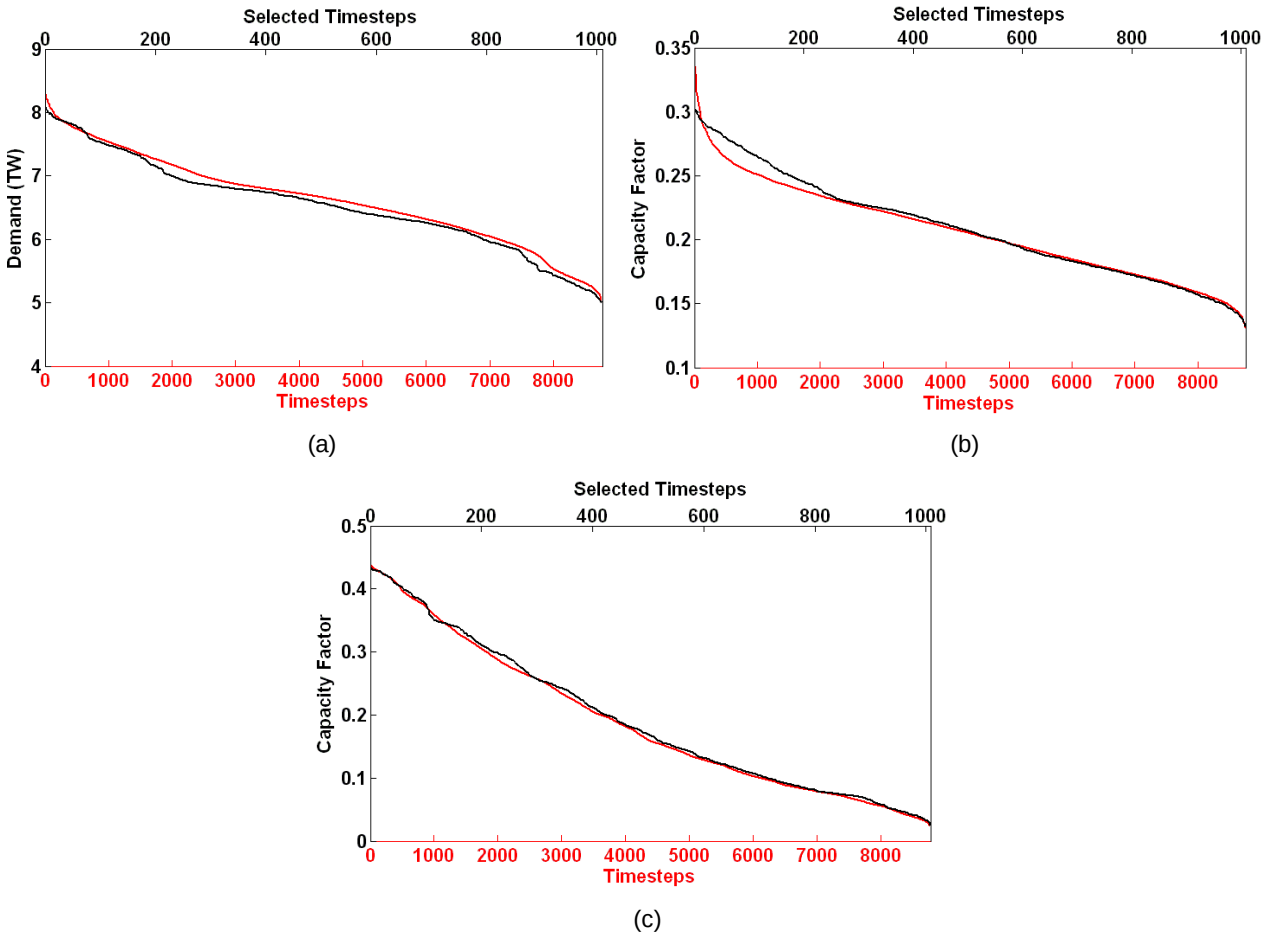

Fig. 4.2: Duration curves based on modeled time steps at the lowest temporal resolution (black) vs. complete annual duration curves (red) (a) Electricity load summed over all regions; (b) Wind onshore power production summed over all regions and normalized; (c) PV electricity production summed over all regions and normalized

4.2.1.2 Results

4.2.1.2.1 Optimal power generation capacities and energy mix

Total installed capacities for power generation and storage is visualized in Fig. 4.3.a for the first four scenarios, represented in Table 4.1; Fig. 4.3.b shows the electricity produced by each technology and the resulting excess production. As described before, all dispatchable power plants at each region are aggregated and parameterized as one backup technology, which is assumed to have a high operational flexibility. Thus, technical restrictions of power plants such as minimum operating level, ramp rates, and start-up costs are not taken into account. Therefore, the required backup capacity and the discarded energy, presented here, must be considered as lower limits.

At first, comparing the electricity generation system of today with the scenario results clarifies that if integrating a high share of solar and wind energy into the power system, the system may not be designed and operated as the centralized, fossil-fuel based electricity generation system of today. In scenario “No Link”, around five times the peak demand power generation capacity is required to satisfy 80% of the global electricity demand with renewable energies. This is more

than two times of the proportion of the total installed capacity to the peak demand in the present electricity generation system.

Comparing the results of scenarios “Link” and “No Link” clarifies how in an ideal globally-interconnected structure smoothening effects on variations of output power from weather dependent renewable power generation units can be captured. The most promising sites for renewable power production are made accessible for wide area usage, and, as a result, the necessary backup power reduces by a factor of 3 as compared to the scenario “No Link”. When storage is also included, even less backup capacity is needed; it reduces by a factor of 7 in scenario “LinkH2Sto” and by a factor of 15 in scenario “LinkPSto”.

Furthermore, the possibility for international electricity exchange in scenario “Link” results in the reduction of excess production by 11% as compared to the “No Link” scenario. Inclusion of the possibility for energy storage in addition to the inter-regional transmission of electricity in scenarios “LinkH2Sto” and “LinkPSto” leads to the reduction of discarded energy by 18% and 46%, respectively. This is a share of produced electricity that can neither be consumed at the time of production, nor can be economically stored for later usage.

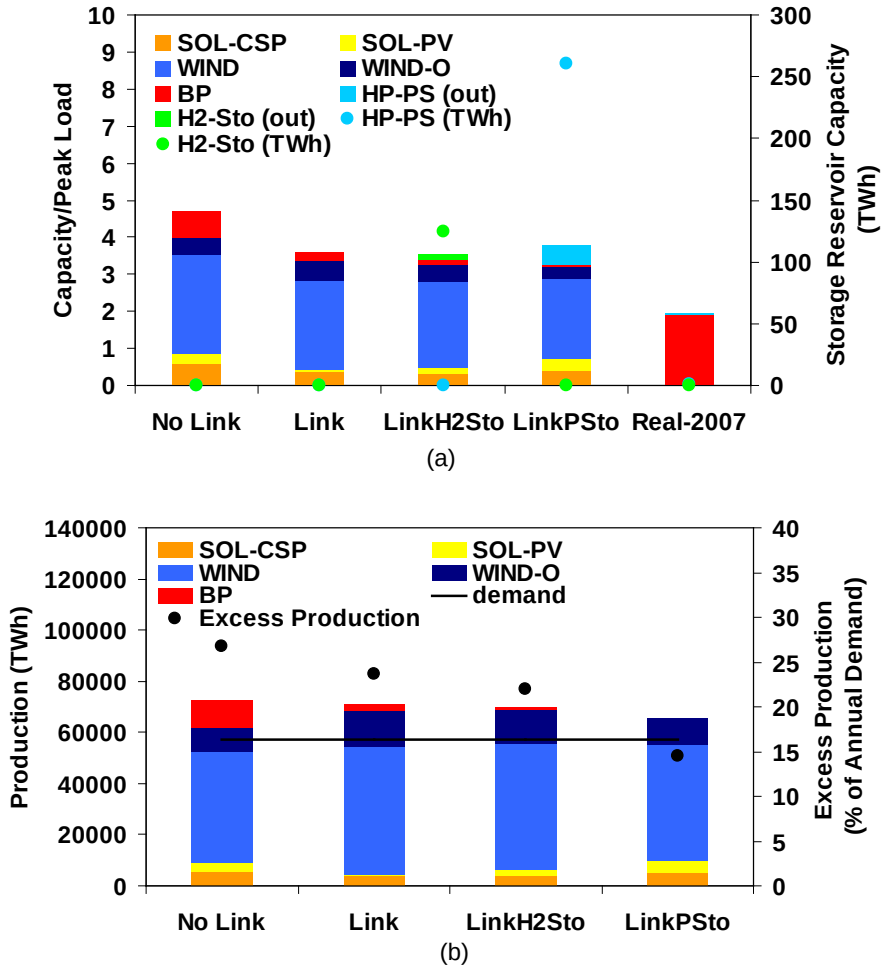

Fig. 4.3: Scenarios “No Link”, “Link”, “LinkH2Sto”, and “LinkPSto” vs. electricity generation system of today (13 weeks are simulated.) (a) Total power generation capacity mix normalized by annual peak demand; (b) Total power production mix and excess production

Due to the less power production from backup technology in scenario “Link”, CO_2 emissions are reduced by 78% from the level in scenario “No Link”. If storage is also included, this reduces by 91% and 99% in scenarios “LinkH2Sto” and “LinkPSto”, respectively.

Fig. 4.4 compares global power generation capacities and energy mix, obtained from the last three scenarios in Table 4.1, with the results of scenario “No Link”. When the costs of power transmission systems are reduced by 50% in scenario “Link-H”, the total required backup capacity reduces by a factor of 4 from its level in scenario “No Link”. In “LinkH2Sto-H” scenario, the required backup capacity reduces by a higher factor of 15 compared to the factor of 7 obtained from the scenario “LinkH2Sto” (see Fig. 4.3 and Fig. 4.4).

Excess electricity production, occurring in scenario “Link-H”, is nearly equal to the excess production of scenario “Link”. In scenarios “LinkH2Sto-H” and “LinkPSto-H”, the discarded energy is reduced by 28% and 50% from the level in scenario “No Link”, respectively.

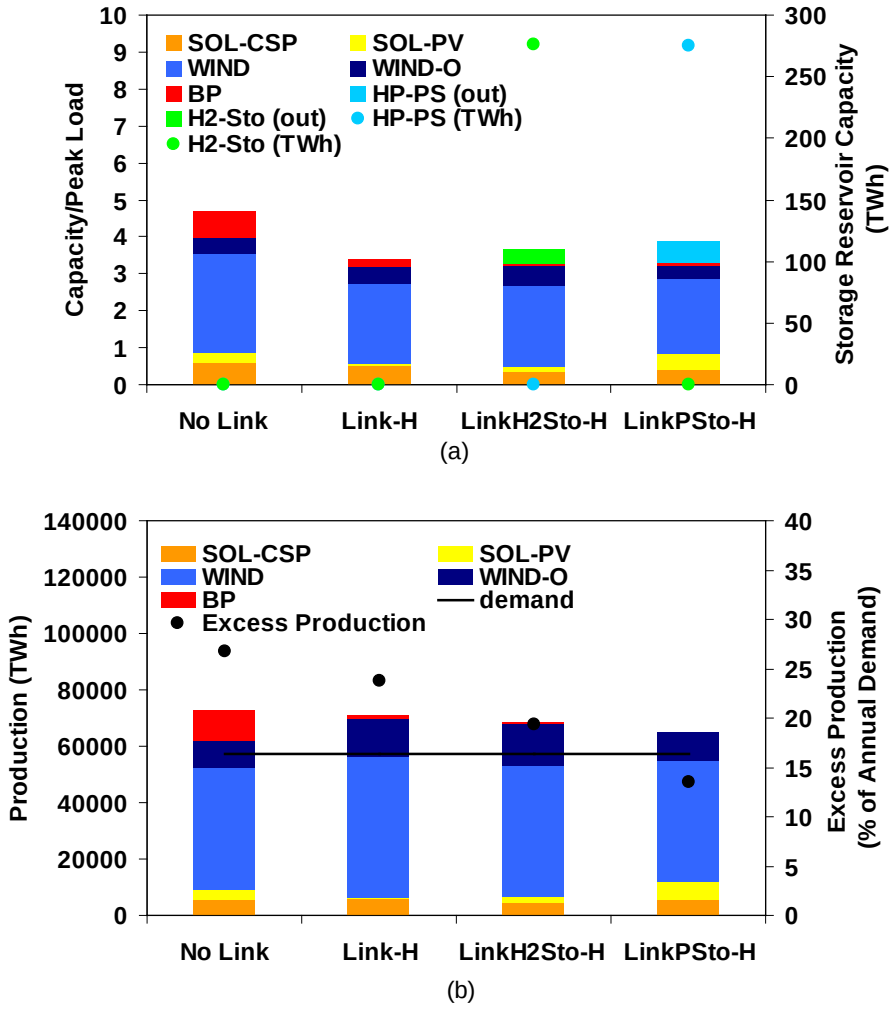

Fig. 4.4: Scenarios “Link-H”, “LinkH2Sto-H”, and “LinkPSto-H” vs. “No Link” (13 weeks are simulated.) (a) Total power generation capacity mix normalized by annual peak demand; (b) Total power production mix and excess production

The applied simulation methodology also allows representing hourly variations of output power from different technologies through a year. For instance, Fig. 4.5 shows the chronological order of total produced power by different technologies in scenario “Link”, which is obtained by

summing the output power over all regions at modeled time steps. In this scenario, energy storage systems are not available to compensate for temporal mismatch between the demand and supply. However, the globally-interconnected structure realizes an optimal usage of spatial de-correlations of FRES and of the electricity load to facilitate integrating the maximum feasible share of solar and wind power into the electricity system.

The intra-diurnal variations of solar energy positively correlate with the daily pattern of electricity load. However, solar energy is characterized with extreme seasonal variations, and there exists an anti-correlation between the inter-seasonal variations of solar electricity production and that of the electricity load. Thus, in winter period and during hours with no gain of irradiation, the electricity demand must be satisfied with the backup technology. However, wind power production is more evenly distributed between the hours of day and night and through different seasons. As a result, when increasing the power production from wind energy, the required backup capacity reduces. This makes the solar energy in total less attractive as compared to wind energy. Therefore, in scenario Link, 90% of the total produced power stem from wind energy, 7% from solar, and 3% from the backup technology. In summer, the share of wind reduces while the share of solar energy increases as compared to the winter period. The system thus benefits from different seasonal characteristics of solar and wind energy. The excess production at each time step can be determined by subtracting the load from the total produced power at the corresponding hour.

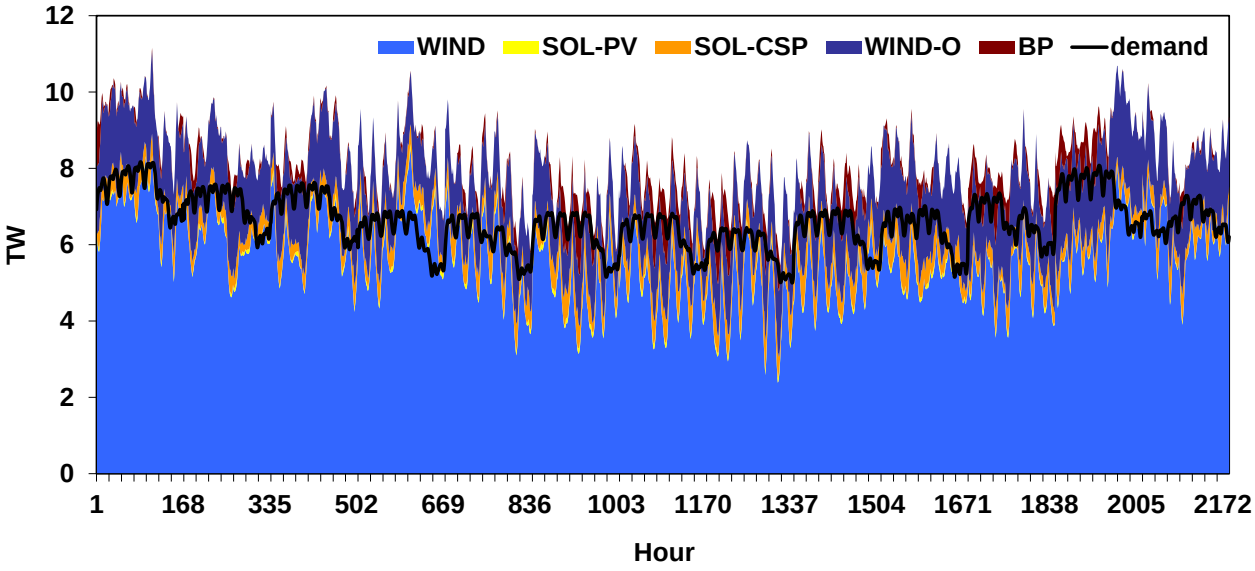

Fig. 4.5: Chronological order of hourly variations of output power in scenario “Link” (13 weeks are simulated.)

4.2.1.2.2 Optimal generation sites and inter-zonal energy flows

The geographical structure of the model allows identifying the promising sites for renewable power production and quantifying energy transport capacities and inter-zonal energy flows.

The geographic distribution of the optimal energy mix, obtained from the “Link” scenario, is demonstrated in Fig. 4.6. This corresponds to the spatial distribution of technical potential of solar and wind electricity production (see section 3.1). Solar thermal power plants are distributed over the most promising sites, having a high annual gain of irradiation and low

seasonal variations (see Fig. 3.2, Fig. 3.3, and Fig. 3.4). These include North Africa, Central and North America, Middle East, South East Asia, eastern part of China, and South Europe. The promising on- and off- shore sites for wind power production are also determined by the optimization model. The high potential of wind energy on the northern European coasts in Scandinavia and England results in a high share of wind energy in the overall supply. A high share of wind energy is also seen in Argentina and Somalia due to the high level of technical potential. Backup power is mainly installed in regions, having a low potential for wind electricity production or a high level of electricity demand.

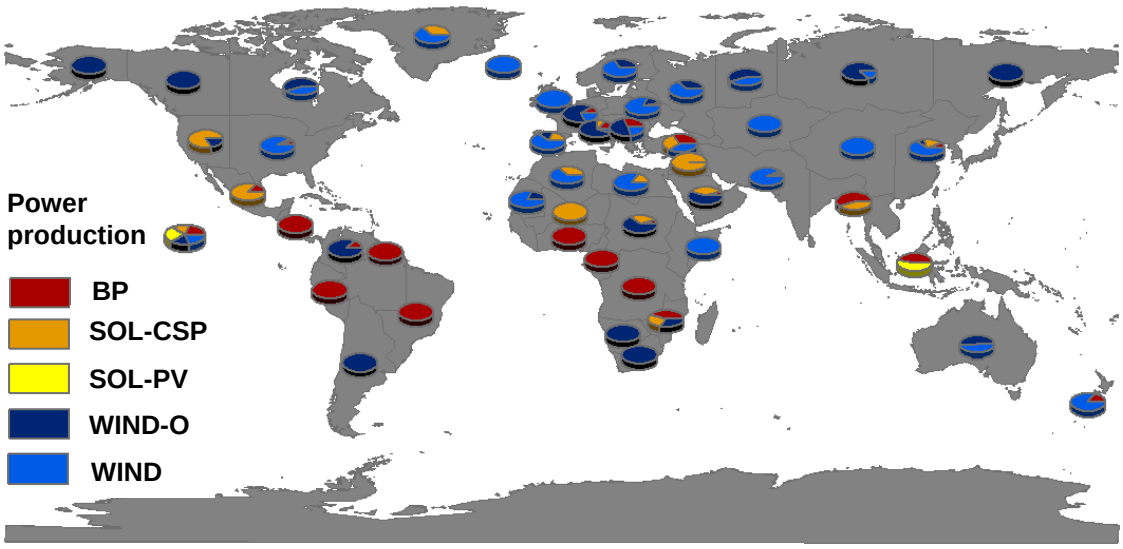

Fig. 4.6: Geographic distribution of optimal energy mix in scenario “Link” (13 weeks are simulated.)

For comparison, Fig. 4.7 shows the geographic distribution of optimal energy mix in scenario “LinkPSto”. When energy can be stored to compensate for temporal mismatch between the demand and supply, solar energy becomes more competitive. The share of solar energy increases in the most promising generation sites such as North Africa, Central America, Middle East, and South East Asia.

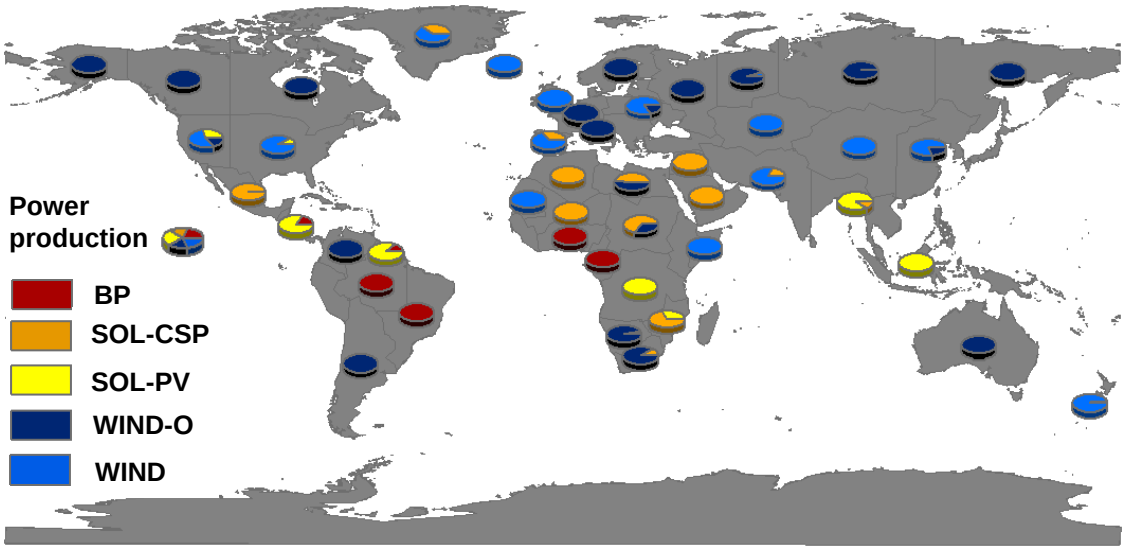

Fig. 4.7: Geographic distribution of optimal energy mix in scenario “LinkPSto” (13 weeks are simulated.)

Scenarios “Link”, “LinkH2Sto”, and “LinkPSto” are characterized with significant inter-zonal energy flows. In these scenarios, about 60% of total produced electricity is transported between the regions. This share increases to more than 80% in scenario “Link-H”.

In scenarios “Link” and “Link-H”, energy supply must be just-in-time with respect to consumption patterns. This forces to transmit electricity from the regions, having a high technical potential of renewable electricity production or available backup capacity, to the distant consuming regions. The power transmission grid is thus used to make an optimal usage of spatial de-correlations of renewable supply. Consequently, short-term fluctuations of regional consumption or renewable power production have a significant impact on the structure of power transmission grid. This is evident in the fact that the grid becomes massively oversized. High capacities are installed in “Link” and “Link-H” scenarios to transmit wind and solar electricity from optimal generation sites or the produced backup power to the consuming regions, located far apart. In scenario “Link”, inter-regional power transmission lines with a maximum capacity of 1000 GW are installed to transmit this vast amount of renewable electricity; the total inter-regional power transmission capacity reaches to around 10 TW. However, when energy storage is included, for instance, in scenario “LinkPSto”, the total inter-zonal power transmission capacity reduces to around 7 TW while the maximum capacity reaches to 1200 GW. The explanation arises from the fact that with the inclusion of storage, it is possible to produce the required energy nearby its point of consumption and apply storage to buffer any temporal mismatch between the demand and supply. Transmission lines are then mainly used to compensate for geographical discrepancies in renewable energy supply.

Optimal power transmission grid structure in scenario “Link” is shown in Fig. 4.8. One noticeable feature is the major energy flows to the projected high load centers of South East Asia, China, and India. Highly concentrated potential of wind electricity in Australia results in its contribution as an exporting country next to the utilized potential nearby the consuming regions. The import of wind electricity from Alaska offshore sites through Far East to eastern part of China is also concluded from the optimization. In the European interconnected area, major energy flows take place from England to Western Europe. High capacities are installed to transmit wind and solar

electricity from North Africa through Southern Europe to the consuming regions of Central and Western Europe. This area is additionally supplied with wind energy imported from Scandinavia. Huge capacities are also installed to transmit wind electricity from Argentina with a significant potential to the northern territories. The full operating hours of inter-regional power transmission lines lies in the range of 1000-7800 hours per year. The maximum is limited according to the assumed availability factor (see section 3.3.2).

For comparison, Fig. 4.9 shows the optimal global grid structure in scenario “LinkPSto”. It is realized that the capacity of power transmission lines over long distances is reduced from the “Link” scenario. For instance, the capacity of inter-continental transmission lines including the link between South America and North America, the link between Alaska and China through Far East, and the interconnection between Oceania and South East Asia is lower than the “Link” scenario.

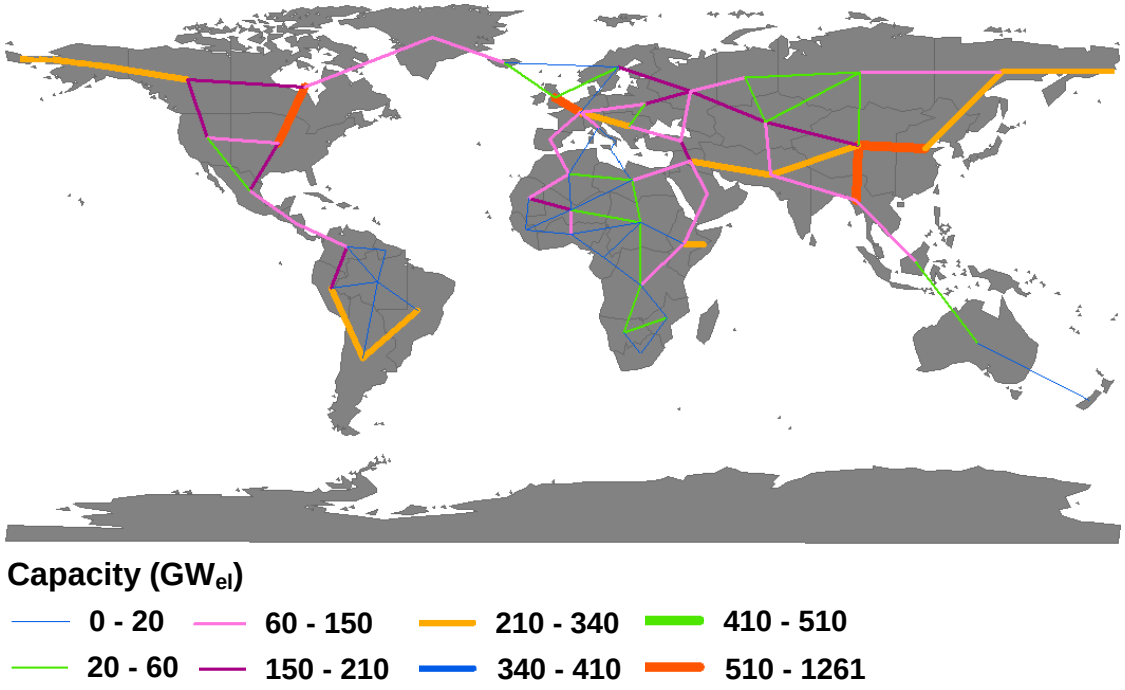

Fig. 4.8: Optimal power transmission grid structure in scenario “Link” (13 weeks are simulated.)

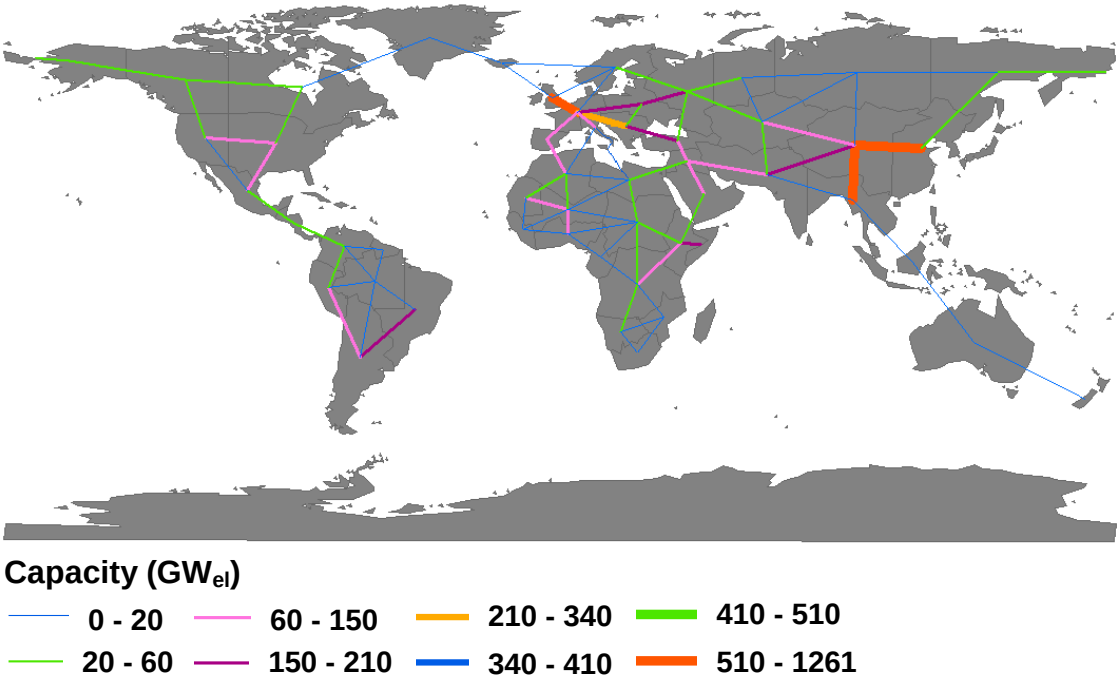

Fig. 4.9: Optimal power transmission grid structure in scenario “LinkPSto” (13 weeks are simulated.)

4.2.1.2.3 Influence of selected time steps on optimization results

To show the dependency of results on modeled time steps, a sensitivity study is now performed on the influence of selected time steps on the optimization results.

A possible influence on power generation capacities and the production mix is shown in Fig. 4.10. The figure compares optimal power generation capacities and the energy mix, obtained from the scenarios “Link” and “Link-H” at the highest temporal resolution (“ts-H”), with the results of scenarios “Link” and “Link-H” at the lowest temporal resolution (“ts-L”). The global power generation capacity reduces by less than 1% in scenarios “Link-tsL” and “Link-H-tsL” compared to scenarios “Link-tsH” and “Link-H-tsH”. In proportional terms, if the simulation time steps are reduced from thirteen weeks to six weeks, the backup capacity reduces by 4% and 16% in scenarios “Link-tsL” and “Link-H-tsL”, respectively. Table 4.5 provides an overview on variations of the total installed capacity of each power plant technology when the modeled time steps are reduced from thirteen weeks to six weeks.

Furthermore, in scenario “Link-tsL”, total excess production increases by 2.6% from its level in scenario “Link-tsH”; excess production increases by 3.7% in scenario “Link-H-tsL” as compared to the scenario “Link-H-tsH”.

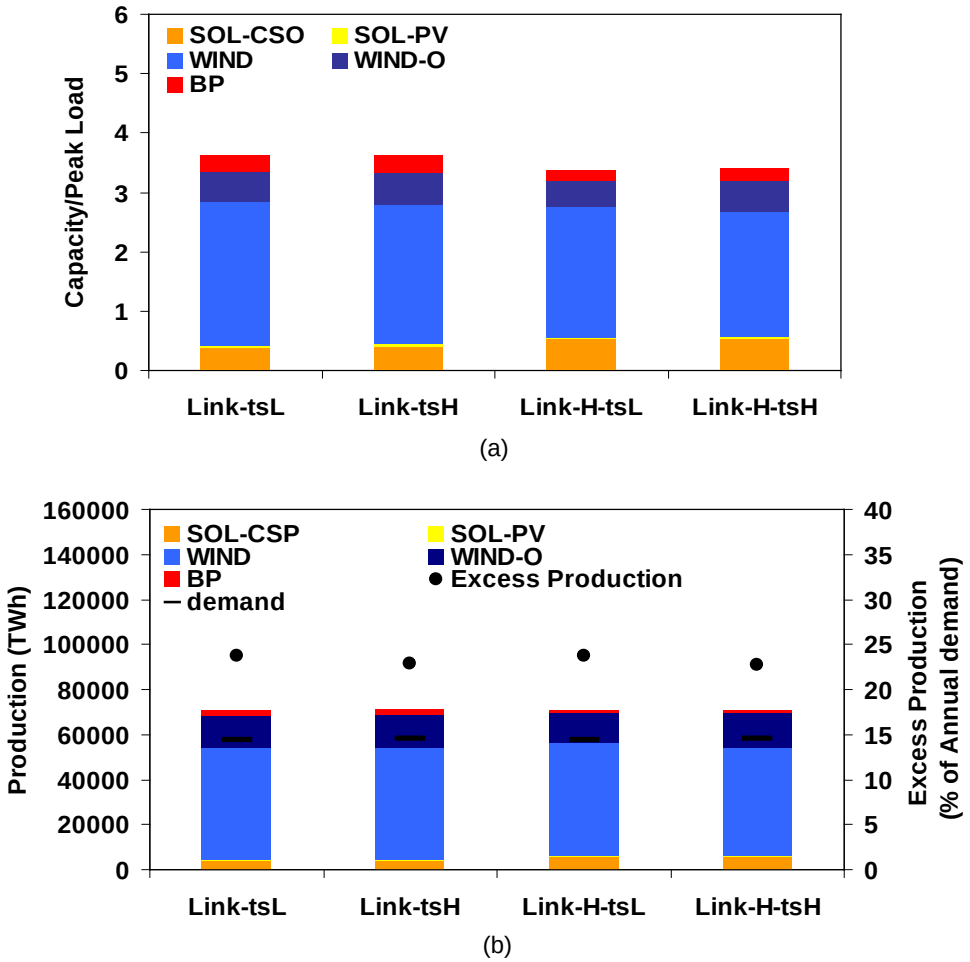

Fig. 4.10: Influence of modeled time steps on total power generation capacity and power production mix (a) Total power generation capacity normalized by annual peak demand; (b) Total power production mix and excess production

Table 4.5: Influence of modeled time steps on total installed capacity of power plants

Technology	Link-tsL (% of capacity in Link-tsH)	Link-H-tsL (% of capacity in Link-H-tsH)
BP	- 4%	- 16%
SOL-CSP	- 5%	+ 0.1%
SOL-PV	- 9%	- 35%
WIND	- 4%	- 15%
WIND-O	+ 2%	+ 5%

Fig. 4.11 shows the geographic distribution of optimal energy mix in scenario “Link-tsL”. This is nearly identical to the results obtained from the scenario “Link” when the temporal resolution is at the highest level (see Fig. 4.6). However, in specific regions, large deviations from the most realistic solution achieved at the highest temporal resolution can be noticed. When in scenario “Link” the modeled time steps are reduced from thirteen weeks to six weeks, as a regional average, the installed capacity of “BP”, “SOL-CSP”, “SOL-PV”, “WIND”, and “WIND-O” varies by + 11%, - 6%, - 2%, - 0.5%, and - 5%, respectively.

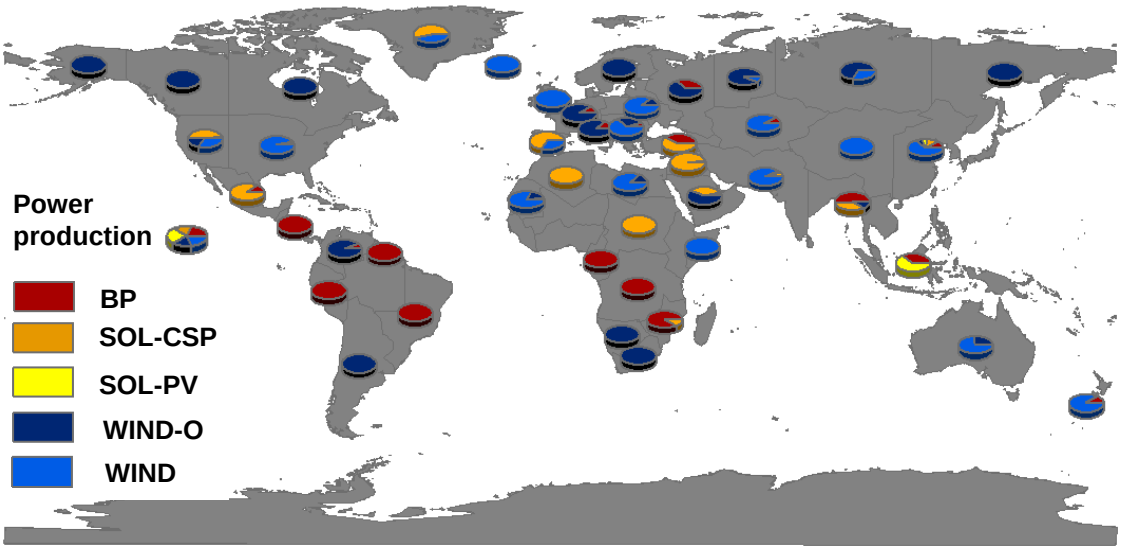

Fig. 4.11: Geographic distribution of optimal energy mix in scenario “Link” (6 weeks are simulated.)

The optimal structure of the power transmission grid and inter-zonal energy flows are also influenced by the modeled time steps. For instance, in scenario “Link-tsL”, both the total inter-zonal power transmission capacity and the total inter-regional energy flows reduce by 8% as compared to the scenario “Link-tsH”. This is visualized in Fig.4.12.

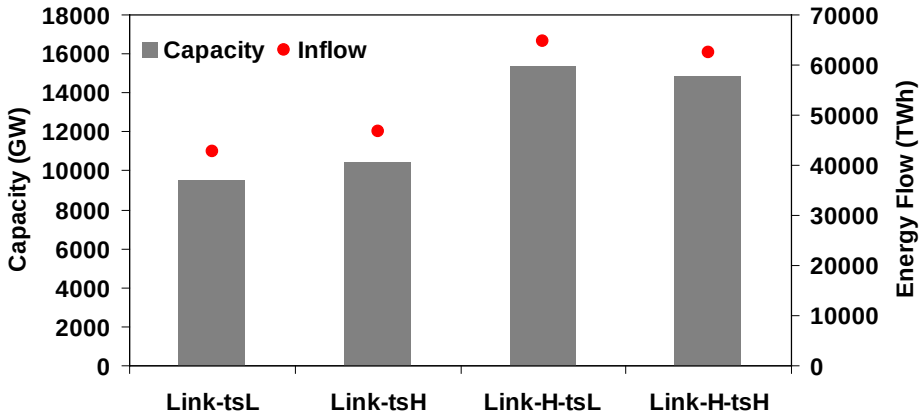

Fig. 4.12: Influence of modeled time steps on total inter-zonal power transmission capacity and electricity flows

It is concluded that the optimization results are influenced by the modeled time steps due to the different short-term fluctuations and seasonal variations of input time series such as wind power capacity factor, solar irradiation, and electricity demand. Higher renewable power and backup capacities are installed in some regions while fewer capacities are installed at others. However, comparison of the aggregated results based on the simulation of six weeks and the results obtained at the highest temporal resolution (thirteen weeks) shows that the optimization results do not significantly change if the temporal resolution is reduced by 50%.

The design of a future global electricity generation system is a complex optimization problem. The temporal resolution of the model is limited according to the accessible computation power

and regarding the long calculation time. Thus, reduction of the modeled time steps and the geographical disaggregation cannot be avoided.

In this thesis, the focus is mainly laid on the developed methodology and providing insight in underlying principles rather than the projection of a future electricity generation system and proposing fixed and absolute numbers. The behavior of a future, renewable-based, global electricity supply system is to be analyzed under different framework conditions. The influences of an ideal global grid and energy storage systems to mitigate negative consequences of integrating a high share of solar and wind power on the operation of the electricity generation system are investigated. This is performed through sensitivity analysis and by comparing the results of different scenarios at the highest feasible temporal and geographical resolution. The absolute levels are, however, subject to inaccuracy and uncertainty.

4.2.1.2.4 Scenarios with international transport of hydrogen

In this part, influences of the possibility for international transport of hydrogen are studied. In all scenarios, hydrogen can be used as an energy storage medium while it can also be transported between the regions. As a starting point of the analysis, the scenario “NoLink” (see Table 4.1) is extended to include the possibility for inter-continental transport of hydrogen. In this scenario, named “LinkGH2”, it is assumed that hydrogen can be transported through pipelines from regions, having a high potential of solar and wind energy, to the distant consuming regions.

North Africa is characterized with a significant technical potential of solar and wind electricity production while it is far apart from highly consuming regions of Western and Central Europe. Here, it is assumed that hydrogen can be produced by renewable electrolysis in North-western Africa and transported to the consuming European regions. Australia is also characterized with a significant potential of wind and solar energy; however, it is subject to rather high fluctuations. Thus, availability of energy storage systems and energy transport technologies may provide a competitive framework for the contribution of Australia in exporting renewable electricity to the load centers of South East Asia and China. Thus, it is assumed that hydrogen can be produced through renewable electrolysis in Australia and transported to the consuming regions of South East Asia. Furthermore, hydrogen, produced by wind electrolysis in Argentina, can be transported to the highly consuming regions of North America. In the specified consuming regions, hydrogen can be used either to satisfy the electricity demand at the time of generation or being stored for later usage.

In scenario “LinkGH2”, the techno-economic parameters, given in Table 4.2 and Table 4.3, are used. The costs and energy losses of GH_2 pipelines are based on a future scenario, proposed in [112] (see Table 3.15 and Table 3.16). A lower diameter of 1 m is assumed for offshore pipelines. In scenario “LinkGH2-H”, the costs of fuel cell and electrolyzer are reduced by 50% from the levels, given in Table 4.2, while other underlying assumptions remain unchanged as in scenario “LinkGH2”.

In scenarios “LinkGH2” and “LinkGH2-H”, hydrogen is transported between the regions to produce electricity at the specified load centers. Hence, power production from the backup technology and total CO_2 emissions are lower than the scenario “NoLink” (see Fig. 4.13). In Fig. 4.13.b, total CO_2 emissions, resulting in scenarios “LinkGH2” and “LinkGH2-H”, are

subtracted from total CO_2 emissions in scenario “No Link” and are represented as a percentage of total emissions in the latter scenario.

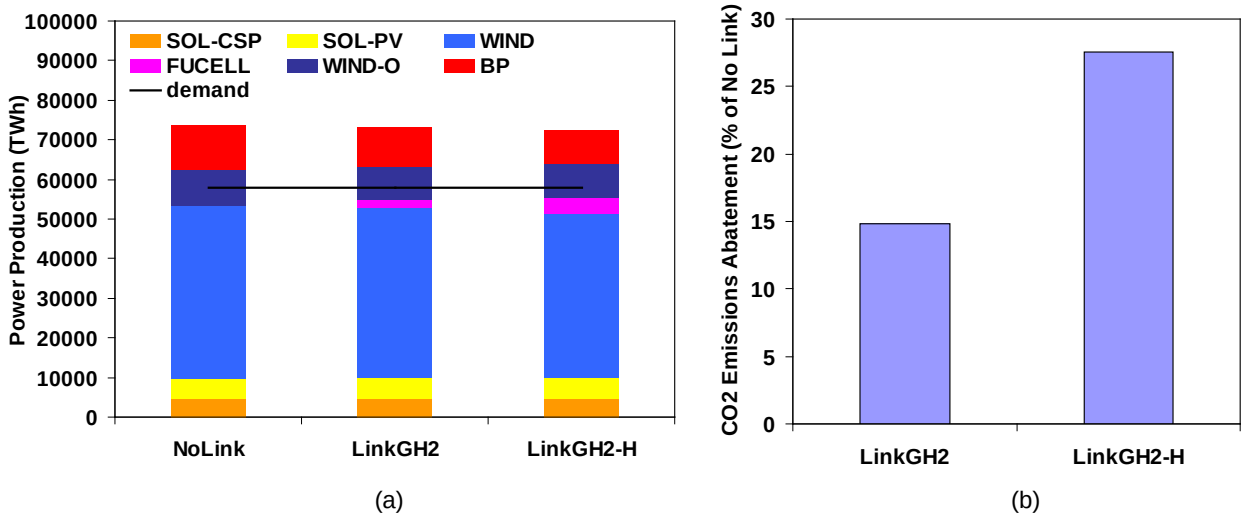

Fig. 4.13: Scenarios “LinkGH2” and “LinkGH2-H” vs. scenario “No Link” (13 weeks are simulated.) (a) Total power production mix (b) Total CO_2 emissions abatement

Installed capacities for power generation and energy storage at hydrogen consuming regions are shown in Fig. 4.14. In scenario “LinkGH2-H”, fuel cells are used in consuming regions of South East Asia (“R36”) and China (“R35”) to generate electricity from hydrogen, produced by electrolysis using electricity from “SOL-CSP”, “WIND-O”, and “WIND” power plants in Australia. Cost reduction has a lower impact on the application of hydrogen for electricity production at European consuming regions as compared to the load centers of South East Asia.

According to Fig. 4.14.b, in Europe, fuel cells are installed in both scenarios “LinkGH2” and “LinkGH2-H” in all consuming regions (“R44”, “R45”, and “R46”) to generate electricity from hydrogen. Hydrogen is produced by electrolysis using electricity from “SOL-CSP” and “WIND” power plants in North Africa. The installed capacities for electricity production from hydrogen (“FUCELL”) and hydrogen storage (“H2-Sto”) are the highest at region “R46”, the main load center of Western Europe. In scenario “LinkGH2-H”, the capacity of “FUCELL” and “H2-Sto” is considerably higher to apply hydrogen in order to satisfy the significant electricity demand in USA (“R10”). For this purpose, hydrogen is produced through electrolysis using electricity from “WIND-O” power plants in South America.

The inter-regional capacities, dedicated to the transportation of hydrogen, are visualized in Fig. 4.15. In scenario “LinkGH2-H”, the capacity of the link between Australia and South East Asia is significantly higher than in scenario “LinkGH2”. In both scenarios, high capacities are installed to transmit hydrogen from North Africa through South Europe to the consuming regions of Western and Central Europe. The capacity installed in scenario “LinkGH2-H” to transport hydrogen from South America to the load center of North America is more than two times of the corresponding capacity in scenario “LinkGH2”.

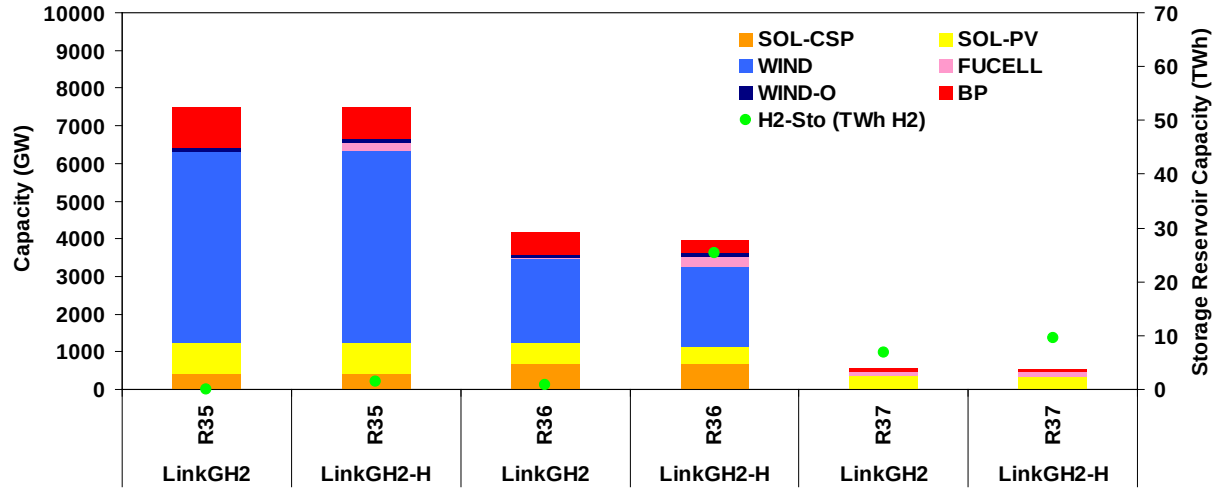

(a)

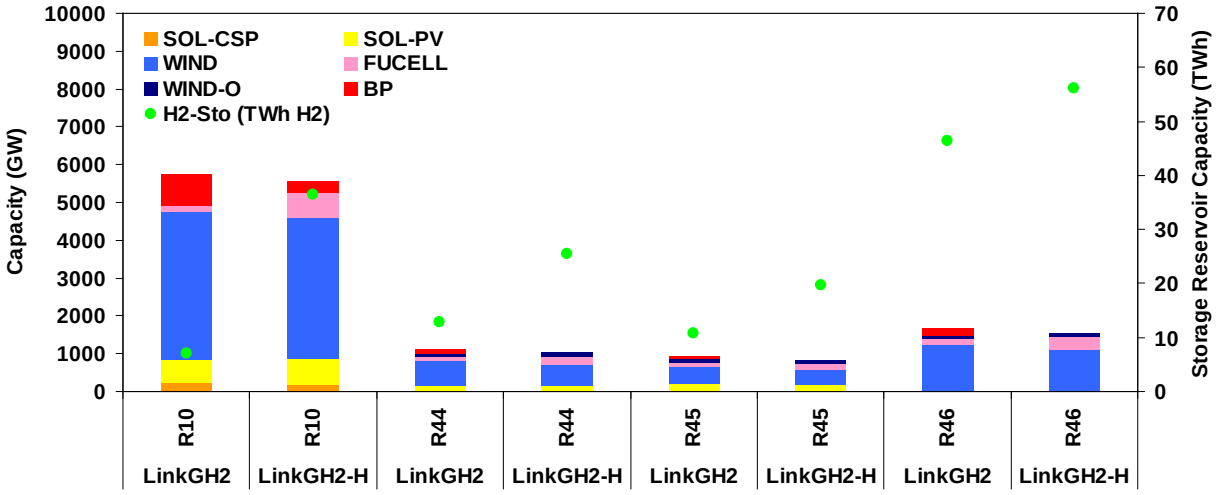

(b)

Fig. 4.14: Power generation and hydrogen storage capacity in scenarios “LinkGH2” and “LinkGH2-H” (13 weeks are simulated.) (a) South East Asia and China (model regions 35,36,37); (b) North America and Europe (model regions 10,44,45,46)

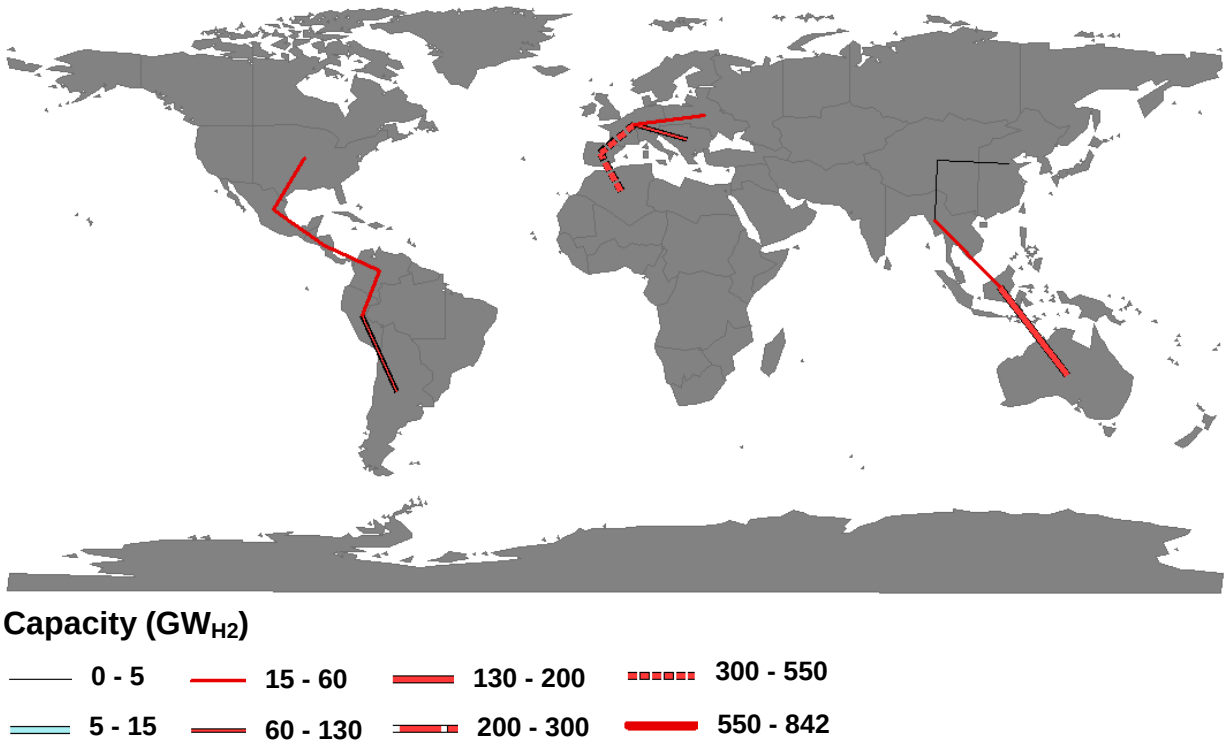

(a)

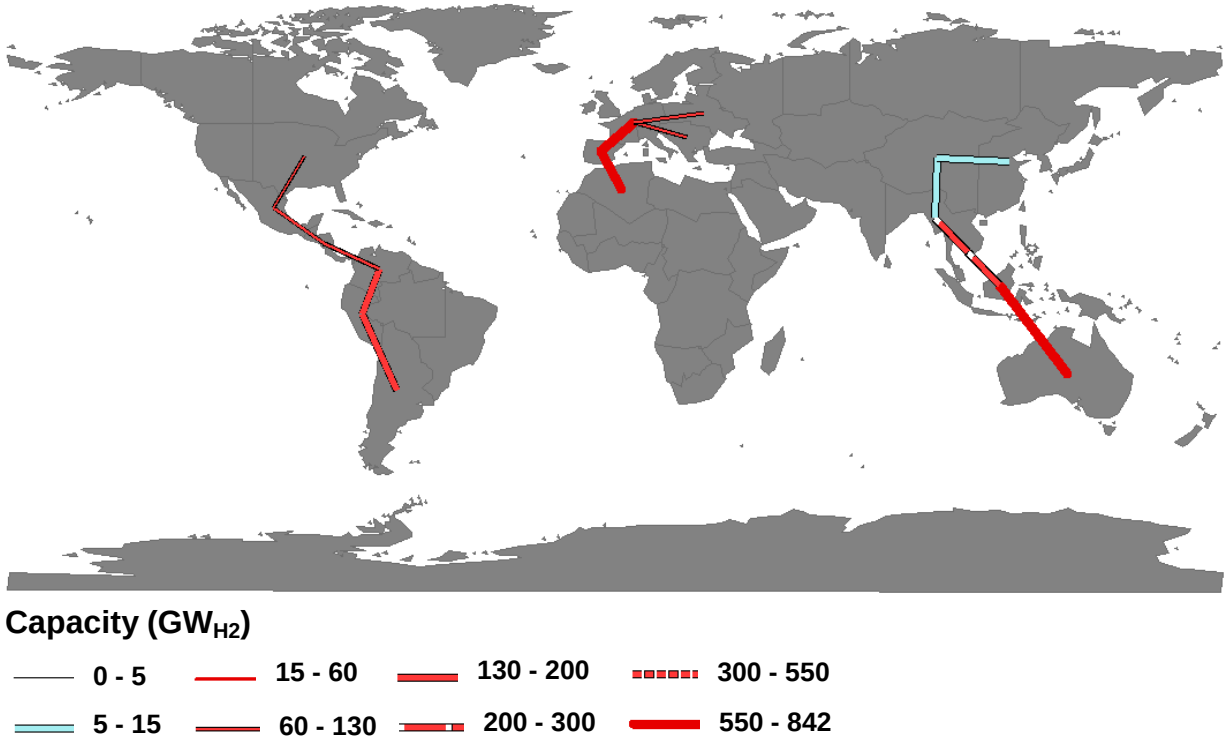

(b)

Fig. 4.15: Inter-regional hydrogen transport capacities (13 weeks are simulated.) (a) Scenario “LinkGH2” (b) Scenario “LinkGH2-H”

In the next step, the “Link” scenario (see Table 4.1) is extended to include the possibility for international exchange of hydrogen. In this scenario, named “LinkHVDC-GH2”, inter-continental energy transport between the regions with a highly concentrated potential of renewable energies and the main load centers is possible only through the transportation of hydrogen. These include the link between North Africa and Central Europe through Southern Europe, the interconnection between Australia and South East Asia, and the link between South America and North America. Thus, in scenario “LinkHVDC-GH2”, hydrogen is produced by renewable electrolysis at the most promising generation sites, where the technical potential of solar and wind electricity production is very high, in order to be transported to the distant consuming regions. There, it can be used either to produce electricity at the time of demand or being stored for later usage. The rest of supply area in interconnected via HVDC power transmission lines.

In scenario “LinkHVDC-GH2”, the techno-economic parameters, given in Table 4.2 and Table 4.3, are used while the costs of electrolyzer and fuel cell are reduced by 50% from the levels, given in Table 4.2. The costs and efficiency of GH_2 pipelines are based on a future scenario, proposed in [112] (see Table 3.15 and Table 3.16).

Installed capacities for power generation and hydrogen storage at hydrogen producing and hydrogen consuming regions are shown in Fig. 4.16. Hydrogen is mostly used in Western Europe (“R46”) followed by USA (“R10”) and South East Asia (“R36” and “R37”) to generate electricity. Hydrogen is stored to buffer any temporal mismatch between the demand and supply, and it is mainly applied to provide intra-diurnal balancing needs rather than inter-seasonal storage.

According to Fig. 4.16.b, hydrogen is produced, using electricity from “WIND-O” power plants of South America (“R1”). This region is characterized with a significant potential of wind electricity production (see Fig. 3.10), but it is subject to rather high seasonal variations (see Fig.3.11). Besides, the local electricity demand is far below the levels seen at the load centers of North America (see Fig. 3.22). Thus, the possibility to transport and store hydrogen as a secondary energy carrier provides the balancing needs required to apply this huge potential for satisfaction of the electricity demand in North America. Hydrogen is also produced by electrolysis using electricity from “SOL-CSP” and “WIND” power plants of North Africa (“R16”). Furthermore, hydrogen is produced using electricity from “SOL-CSP”, “WIND”, and “WIND-O” power plants in Australia (“R42”) while it is dominated by wind onshore. However, in scenario “Link”, only “WIND” and “WIND-O” power plants are installed in Australia (see Fig. 4.6). The explanation arises from the fact that a huge potential of solar energy is localized in Australia, but it is subject to high fluctuations that requires huge storage to compensate (see Fig. 3.3). Thus, when the possibility for energy storage is included in scenario “LinkHVDC-GH2”, application of solar energy becomes competitive. Furthermore, in scenario “LinkHVDC-GH2”, energy transport from Australia through South East Asia to China is only through GH_2 pipelines; therefore, South East Asia can not be additionally supplied with the imported electricity from western China as it occurs in the “Link-” scenarios with no possibility for hydrogen transport. These circumstances provide a competitive framework to apply the electricity produced by “SOL-CSP” power plants in Australia in order to produce hydrogen that can be used at the load centers of South East Asia.

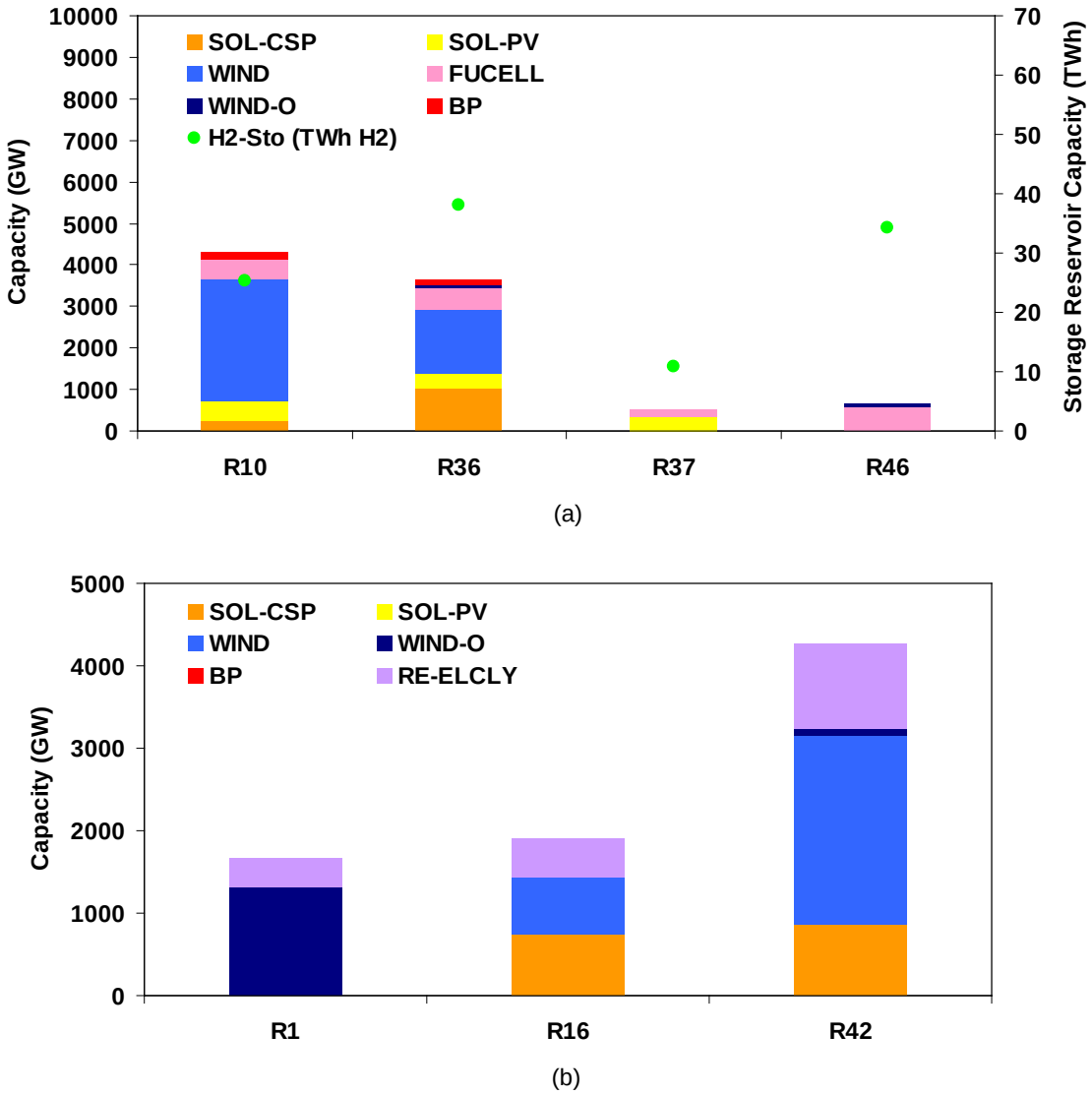

Fig. 4.16: Power generation, hydrogen production and storage capacity in scenario “LinkHVDC-GH2” (13 weeks are simulated.) (a) Hydrogen consuming regions (model regions 10,36,37,46); (b) Hydrogen producing regions (model regions 1,16,42)

Inter-regional energy transport capacities, obtained from the scenario “LinkHVDC-GH2”, are visualized in Fig. 4.17. The link between Australia and South East Asia has the highest hydrogen transport capacity followed by the transmission line between North-western Africa and Europe.

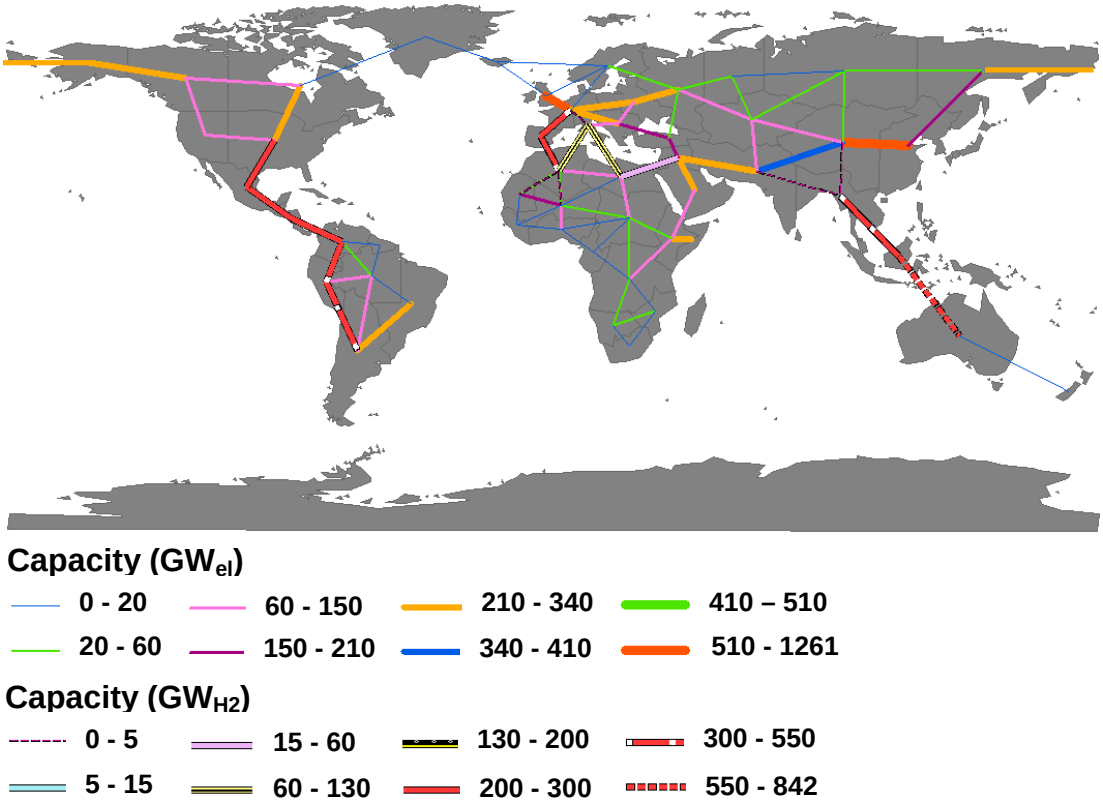

Fig. 4.17: Inter-regional energy transport capacities in scenario “LinkHVDC-GH2” (13 weeks are simulated.)

Finally, Fig.4.18 shows a comparison between the scenarios “Link” and “LinkHVDC-GH2”. In scenario “LinkHVDC-GH2”, 7% of the global electricity demand is satisfied with hydrogen, which is applied as an energy source for fuel cells. Due to the possibility for energy storage in scenario “LinkHVDC-GH2”, excess production reduces from the total discarded energy in scenario “Link”. Power production from the backup technology and total CO_2 emissions are lower in scenario “LinkHVDC-GH2” while the total system costs increase by 7% in comparison with the scenario “Link”.

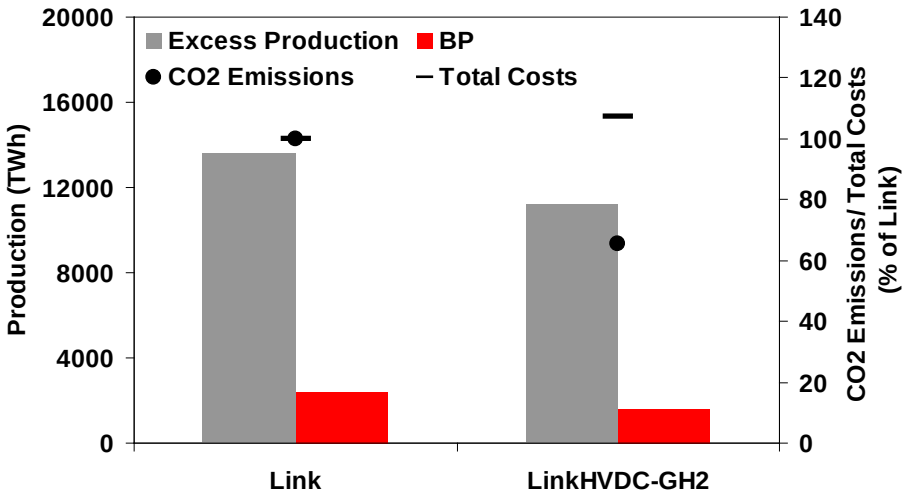

Fig. 4.18: Scenario “Link” vs. scenario “LinkHVDC-GH2” (13 weeks are simulated.)

4.2.1.3 Conclusions

The developed optimization model in its basic form has been applied to specifically investigate the benefits of dispersed generation from FRES in a globally-interconnected structure of a future electricity supply system. The role of an ideal global grid, the influence of international transport of hydrogen, and the impact of energy storage systems has been analysed.

Comparing the electricity generation system of today with the scenario results shows that a power system that integrates a high share of FRES cannot be designed and operated as a centralized, fossil-fuel based electricity generation system. Thus, extensive adaptations are required to mitigate negative consequences caused by the power system integration of FRES.

A globally-interconnected structure is an ideal configuration to make an optimal usage of spatial de-correlations of output power from weather dependent renewable energy sources. The scenario analysis shows that if the supply area consists of isolated regions, around five times the peak demand (38 TW) power generation capacity is needed to satisfy 80% of the global electricity demand in 2050 with FRES. However, in an ideal globally-interconnected structure, the most promising sites for renewable power production are made accessible for wide area usage, and the necessary backup power can be reduced by a factor of 4. If energy storage is also included, even less backup capacity is needed. Moreover, inclusion of both energy storage and international exchange of electricity leads to the reduction of excess production. Inter-regional transmission of electricity results in the reduction of excess production by about 11% compared to a baseline scenario with no possibility for energy transport or storage. When energy storage is additionally included, this can be reduced by 18-46%.

The geographical structure of the model also allows identifying promising sites for renewable power production as well as energy transport capacities and inter-zonal energy flows. The geographic distribution of optimal energy mix corresponds to the geographic distribution of renewable energy supply. Solar thermal power plants are distributed over the most promising sites, including North Africa, Central and North America, Middle East, South East Asia, China, and South Europe. Wind energy is distributed more evenly. The significant potential of wind energy on the northern European coasts in Scandinavia and England results in a high share of wind energy in the overall supply. When energy storage is included, solar electricity becomes more competitive. The share of solar energy increases in regions with a highly concentrated potential such as North Africa, Central America, Middle East, and South East Asia.

Scenarios, having the possibility for electricity exchange, are characterized with significant inter-zonal energy flows. Inter-regional power transmission lines with a maximum capacity of 1000 GW_{el} are installed, and 60-80% of the total produced electricity is transported between the regions. When energy storage is included, the total inter-regional power transmission capacity reduces by about 30%. Transmission lines are then mainly used to compensate for geographical discrepancies in renewable supply.

Finally, a comparison was made between a scenario, where the total area is interconnected only through HVDC power transmission lines, and a scenario, where the inter-continental energy exchange between North Africa and Europe, South- and North- America, Australia and South East Asia is realized with hydrogen transport while the rest of area is interconnected via HVDC power transmission lines. In the latter scenario, hydrogen can be used either to produce

electricity at the time of demand or being stored for later usage while in the former scenario energy storage is not included. In the latter scenario, around 7% of the global electricity demand is satisfied with hydrogen, which is applied as an energy source for fuel cells. The maximum inter-regional capacity reaches to 850 GW_{H2} to transport the hydrogen produced from solar and wind energy in Australia to satisfy the electricity demand at distant load centers of South East Asia. In the latter scenario, excess electricity production reduces by 18% compared to the former. Correspondingly, power production from the backup technology and total CO_2 emissions reduce by 34% while the total system costs increase by 7%.

4.2.2 CO_2 emissions abatement in world electricity sector

In this section, the model is applied to perform a detailed analysis of CO_2 emissions abatement in the global electricity supply sector.

The potential for reducing CO_2 emissions in the long-term has been evaluated in various studies by focusing on national electricity generation systems [122, 123]. While the issue of long-term technological change has a high priority, short-term effects, caused by the internalization of emissions costs in an existing fleet of generation plants, may not be ignored. This concerns the influences on CO_2 emissions before an optimal mix of low emitting power generation technologies could be brought online. In the short run, the demand for electricity would be met at the lowest cost by re-dispatching the existing generation units according to their marginal costs, which has risen by the CO_2-price. Short-term effects of imposing prices on CO_2 emissions have been studied, for instance, in [21, 124].

In this study, the focus is laid on both of the specified time horizons relevant for studying the systematic influences on CO_2 emissions of the global electricity generation system. Possible influences on the CO_2 emissions abatement and the CO_2-price are studied using the methodology described in chapter 2. While the potential for reducing CO_2 emissions in the short-term is evaluated, long-term abatement in the global electricity supply sector and required structural changes are studied while a special focus is laid on the influences caused by the integration of solar and wind power and the role of an ideal global grid.

At first, the focus is laid on short-term effects of imposing prices on CO_2 emissions of an existing fleet of generation plants. The total abatement that would be achieved in year 2006 if there was an internalization of emissions costs in all parts of the world is quantified. Afterwards, the interaction of different influencing factors of CO_2 emissions such as load, fuel prices, and the share of FRES are investigated in detail; as results, the topology of abatement is presented as a function of influencing parameters. In the third step, taking into account a long-term horizon from 2020 to 2040, new investments in the electricity supply sector, required to satisfy the proposed global CO_2 emissions reduction targets, are identified. Furthermore, the influence of an increasing power generation from solar and wind energy on the CO_2-price and the role of an ideal global grid is investigated.

4.2.2.1 Model validation

In its standard form, the model is based on a number of assumptions that may be regarded as unrealistic according to the real power generation systems. For instance, it is assumed that the prices paid for fossil fuels and used for dispatch decisions are uniform, i.e. equal through all

model regions. These are annual average prices in international markets. However, in reality, they vary considerably through the year and different countries. Furthermore, techno-economic parameters of each power plant technology are assumed to be uniform through all regions. The maximum production from conventional power plants is restricted by the standard availability factor (see equation 2.6) while contract considerations are not taken into account in dispatch decisions of power generation units. Moreover, it is assumed that wholesale markets are completely liberalized.

While these deviations from real conditions are typical for modeling purposes, the question, whether the model can properly mimic the behavior of an actual electricity generation system, has to be addressed. Question remains also concerning the consequent effect of the deviation from an actual condition on the estimation of CO_2 emissions abatement in response to a CO_2-price. For this purpose, simulation results are compared with a real power generation mix.

4.2.2.1.1 Non-calibrated model vs. actual generation

The objective here is to examine if the applied simulation methodology and the used database are capable of representing an actual mix of produced power. The year 2000 has been chosen for calibration as it is the latest period, for which all the required datasets were available at the time of writing. It also represents the time point, when the carbon price did not exist in any part of the world.

At first, the non-calibrated model is run using the power plant stock as it existed in year 2000 based on data from [96] along with the electricity demand, given in [105]. Thirteen weeks are simulated to represent the whole year.

The net transfer capacities from [97] are applied here to represent existing power transmission interconnections between the model regions, locating in Europe. However, no accurate and consistent information exists about the capacity of power transmission lines in other parts of the world. Furthermore, the international electricity exchange database of Energy Information Administration (EIA) [105] provides information about the total imported and exported electricity per country while it does not include the information of a bi-lateral exchange matrix. This inhibits determining the historic value of electricity exchange between the model regions. Moreover, these vary considerably through the year; however, the historic data only includes annual levels. Thus, due to the lack of sufficient information for model regions outside Europe, inter-zonal exchange of electricity is not included in the calibration or restricted by implementing a low upper capacity boundary.

Ramping constraints are respected on a technology level to represent technical restrictions on the operation of power plants (see section 2.5). The ramp rate (*ramp*) of different power plant technologies is given in Table 3.11. Techno-economic parameters of power plants and fuel prices are represented in Table 4.6. Annual average fuel prices in international markets are obtained from [125].

Table 4.6: Techno-economic parameters of power plants. Data source: [14, 24, 49, 64, 77, 91], [125-128] (All costs are in US$ (2008).)

Technology	Efficiency (%)	Fuel price ($/MWh$_{th}$)	Variable O&M ($/kWh$_{el}$)	Availability (% of maximum capacity)	Emission factor (ton/MWh$_{th}$)
BIO-ST	38	11.4	0.0058	50	0
COAL-ST	38	7.1	0.0058	84	0.440
GAS-GT	34	16	0.0030	95	0.308
GAS-CC	52	16	0.0030	89	0.308
GEO-ST	20	0	0.0001	69	0
HP-ROR	80	0	0.0001	95	0
HP-PS	86	0	0.0001	95	0
LIG-ST	34	3.5	0.0058	85	0.520
OIL-CC	46	19.8	0.0030	89	0.473
OIL-GT	31	19.8	0.0028	95	0.473
SOL-CSP	15	0	0	99	0
SOL-PV	12	0	0	99	0
URA-ST	34	0.94	0.0008	70-85	0
WIND	96	0	0	95	0
WIND-O	93	0	0	90	0

The non-calibrated model's output is compared with the real power production mix of year 2000 in Fig. 4.19. Comparison of the aggregated power production in Fig. 4.19.a shows that the simulation results are very close to the real estimates. However, the total power production from the optimization model is 2% lower than the real produced power. The deviation is nearly zero for Europe; however, it reaches to -4% for Asia.

In the used historical data, the total net electricity consumption[1] is lower than the total net electricity generation[2]. The explanation arises from the fact that energy losses, occurring due to reserve power production, as well as power transmission and distribution losses are not included in the net electricity consumption. The cost minimization model, thus, matches the total produced power to the net electricity demand while it only considers the inter-regional power transmission losses. Therefore, in addition to energy losses, resulting from reserve power production, the energy losses, occurring through intra-regional transmission and distribution of electricity, are not taken into account due to the coarse geographical resolution of the optimization model. Furthermore, the deviation is higher in regions outside Europe due to the lack of accurate historical data about the bilateral electricity exchange and the capacity of power transmission interconnections between those regions.

By comparing the electricity generation obtained from the optimization model, which is categorized into power plant technology types, with the actual power production mix of year 2000, higher deviations can be noticed (see Fig. 4.19.b). These are mainly caused by the differences between the domestic fuel prices and the prices paid for fossil fuels in international

[1] Net electricity consumption is computed as generation, plus imports, minus exports, minus transmission and distribution losses.
[2] Net electricity generation is the amount of gross generation less the electrical energy consumed at the generating station(s) for station service or auxiliaries.

markets. Finally, it is concluded that there exists a general tendency: the model decides to use more coal and lignite than was actually utilized while it underestimates the usage of natural gas and oil. This tendency exists for all continents; however, the deviation is very low in Europe followed by America.

One influential factor is the ratio of the domestic price of natural gas and coal to the world market price of crude oil. The domestic prices that differ from uniform values, used in the simulation, may lead to such deviations. Another influential factor is the actual lower availability of coal- and lignite- fired power plants than standard availability factors, used as input to the electricity system optimization model. Lower availability can be caused by technical restrictions and/or lack of fuel supply.

Furthermore, according to the applied deterministic approach, forecasting errors of electricity load and unforeseen fluctuations of wind power plants are not taken into account. Moreover, the model respects ramp rates of power plants at a technology level. However, detailed technical restrictions of power generation units such as minimum operating point, minimum up and down time requirements, and start-up conditions cannot be directly formulated within a non-mixed integer problem. Thus, base- and mid- load technologies are considered to be more flexible than real generation plants. As a result, the model uses the cheapest available technology in dispatch decisions, and the contribution of flexible, peak and high peak generators is underestimated.

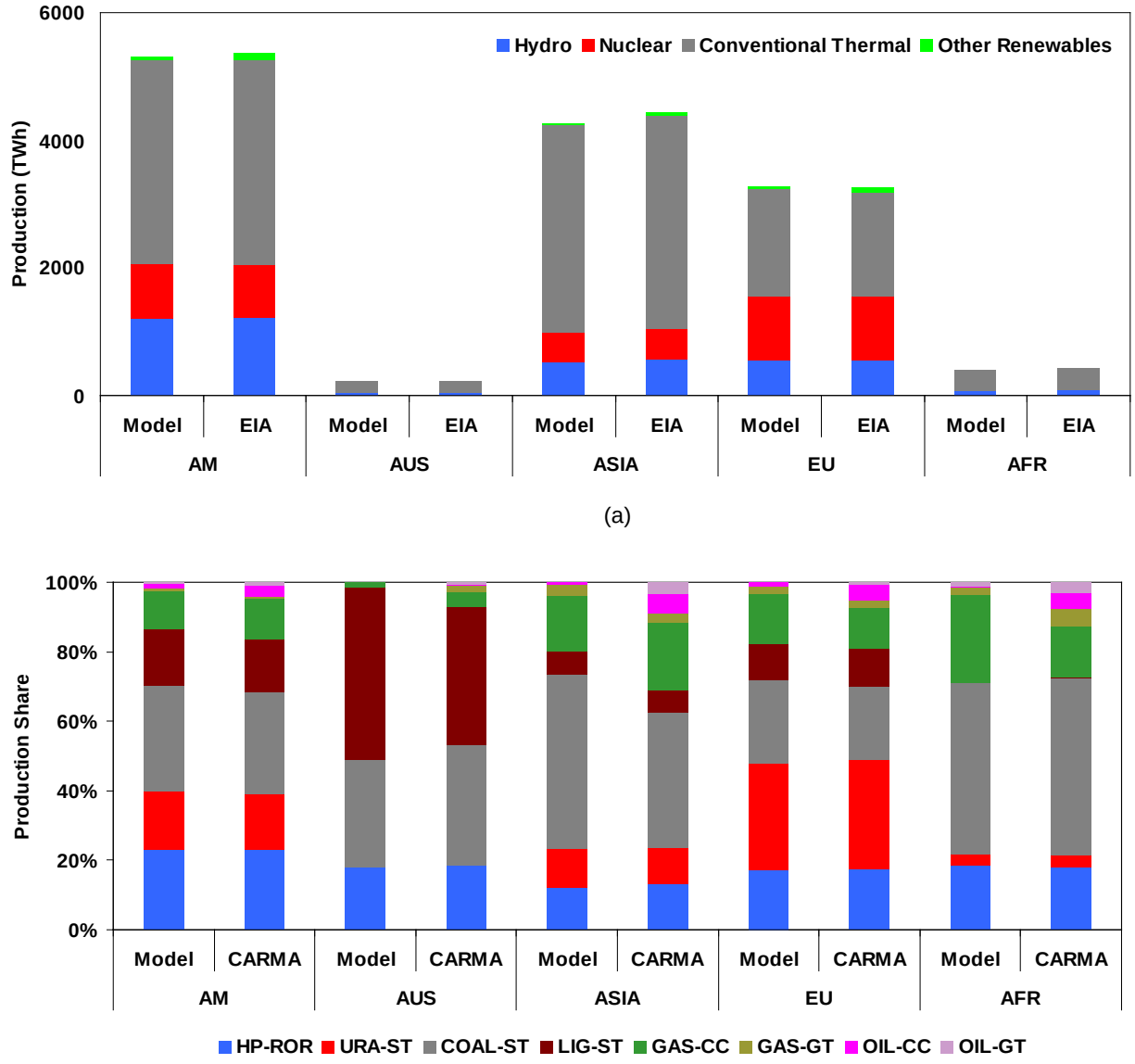

Fig. 4.19: Model results vs. real net electricity generation of year 2000 (a) Comparison with EIA; (b) Comparison with CARMA

4.2.2.1.2 Model calibration

To minimize the deviation of model's results from the real power production mix of year 2000, a sensitivity study is performed by varying the availabilities of power plants and fuel prices. In order to focus on the generation from fossil fuels, which are the sources of emissions, the power produced from biomass, hydro, solar, and wind are matched to real values as closely as possible. A calibrated model is then developed through stages, which yields the least deviation from the real estimates. One main correction in developing a calibrated model is to introduce region-specific availability factors for nuclear power plants to match their electricity generation to the real power production of nuclear power plants based on data from [105]. Moreover, availability factors of coal- and lignite- fired power plants are reduced, and factors are introduced to change fuel price ratios in specific regions. Furthermore, in specific regions, total annual electricity demand is scaled to compensate for power transmission and distribution

losses and match the total power production to the actual net electricity generation, as it is given in [105]. The main assumptions, made through the calibration, are summarized in Table C.1.

As a measure of overall improvement, root mean square (RMS) of absolute differences between the results, obtained from the optimization model, and the real values in terms of power generation per fuel per zone is minimized through steps. Fig. 4.20 clarifies the minimized deviation from the real power production mix, achieved through the calibration. Lower availability of coal- and lignite- fired power plants in the calibrated model compared to the base model leads to their replacement with gas combine-cycle and oil-fired plants. Reduction of RMS clarifies improvement of the results after calibration; at global scale, this factor is finally reduced by 54% from the level in the non-calibrated model.

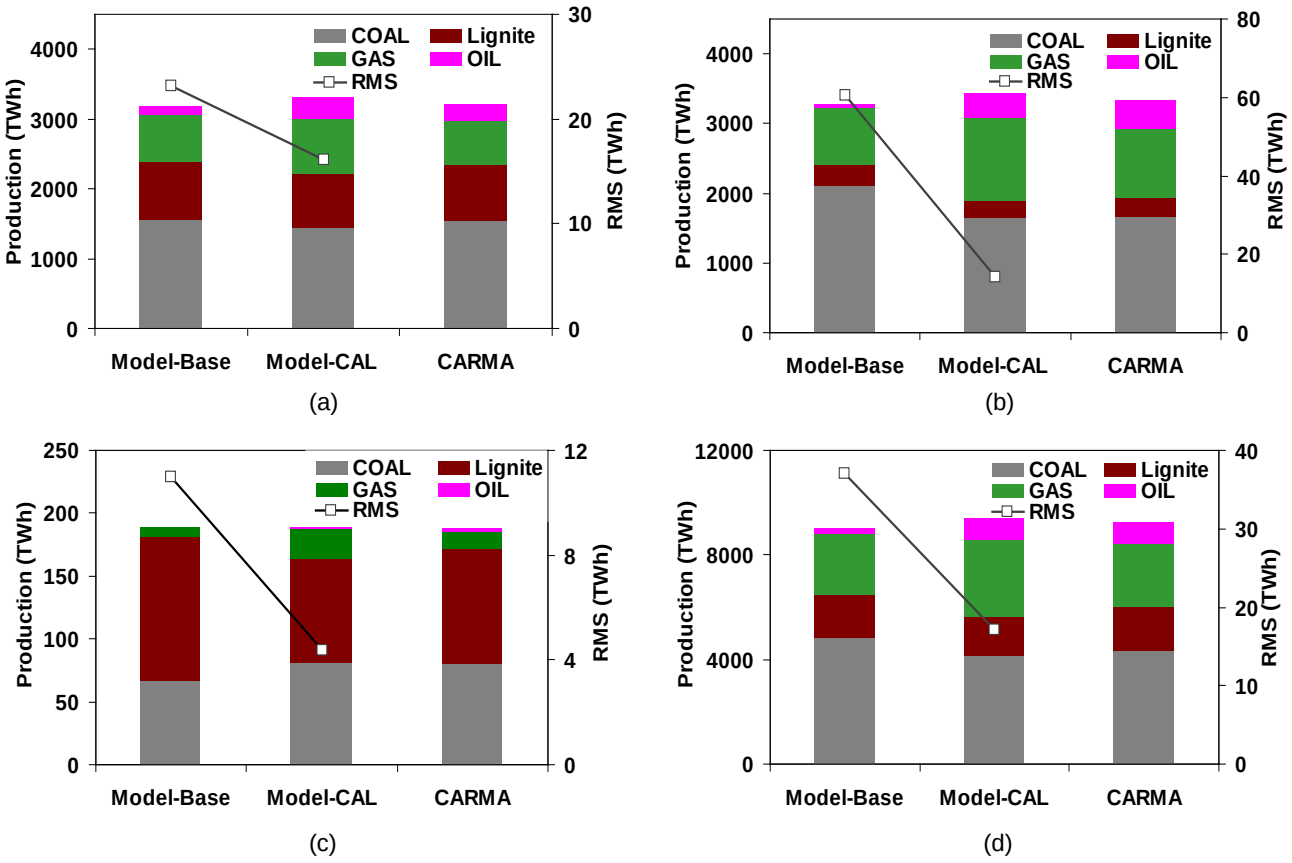

Fig. 4.20: Power generation per fuel type in non-calibrated model (Model-Base) and calibrated model (Model-CAL) vs. real net generation of year 2000 (a) America; (b) Asia; (c) Australia and New Zealand; (d) World

Total CO_2 emissions, obtained from the optimization model, are also in good accordance with the data. According to an approximation performed in [4], CO_2 emissions from the power sector were 9395 million tons through the year 2000. Applying the calibrated model, total CO_2 emissions of year 2000 would reach to 9750 million tons, which is only 3.7% higher than the real estimate given in [4]. The non-calibrated model approximates total CO_2 emissions at 5% above the referenced value.

4.2.2.2 Short-term potential for CO_2 emissions abatement

Possible influences on CO_2 emissions of the global electricity supply sector in a short-term perspective and the influence of model calibration on estimation of CO_2 emissions abatement are studied in this subsection. The model is applied to estimate the total abatement that would be achieved if a global carbon price existed in year 2006. This year has been chosen as it is the most recent year after internalization of emissions costs in the European countries, for which all the required data were available at global scale at the time of writing.

The model based on its standard assumptions and the calibrated version are run using the power generation capacity of year 2006, as it is given in [96], along with the electricity demand and fuel prices based on data from [105, 129]. For this purpose, in the calibrated version, only the adjusted availability factors are taken into account while the fuel costs are assumed at annual average prices of the world market, and are uniform through all regions. This can be explained according to the fact that the deviation of domestic fuel prices from international market prices, which has been estimated for the year 2000, cannot be assumed to remain valid in year 2006.

At first, the CO_2-price is assumed at zero in all model regions to estimate CO_2 emissions that would occur without its existence. This is used as a basis to approximate the possible reduction of CO_2 emissions in response to a global carbon price. In other simulation runs, the aim is to estimate the emissions that would occur if a uniform CO_2-price existed in all countries through the year 2006. The average CO_2-price of the European power sector through the year 2006 (18 €/ton) is used as a global carbon price. Both the calibrated model and the non-calibrated version are applied for this purpose. The emissions abatement is determined by taking the difference between the runs that incorporate the carbon price and the base case with a zero CO_2-price.

The consequent effect of calibrating the model to actual data and the influence of implementing a CO_2-price can be at first realized by considering the share of coal-fired generation in total produced power from fossil fuels. This is visualized in Fig. 4.21.a. The CO_2-price leads to the substitution of coal with natural gas and oil; the extent of this influence depends on the available unused capacity of these lower emitting power plants. According to Fig.4.21.a, this is more evident in summer period as most of the regions are characterized with a lower electricity demand and, thus, more available unused gas-fired capacity in summer than in winter period. Moreover, as expected, the production share of coal in the calibrated version is lower than the coal share in the non-calibrated model. Indeed, a higher utilization of lower emitting natural gas- and oil- fired plants compensates for the reduced usage of coal in the calibrated model. Therefore, less natural gas- and oil- fired capacity is available in the calibrated model for fuel switching in response to the CO_2-price; As a result, less potential exists to reduce the emissions as compared to the non-calibrated model.

If a zero CO_2-price existed in all countries, total CO_2 emissions of year 2006 would reach to 12445 million tons according to the results obtained from the calibrated model. According to the results of the non-calibrated model and the potential for emissions reduction, estimated by the calibrated version, an upper and a lower bound of 1165 and 625 million tons can be proposed for the abatement that would be achieved through fuel switching in response to a global carbon price of 18 €/ton in year 2006. The non-calibrated model overestimates the CO_2 emissions and

the achievable abatement due to the higher utilization of existing coal- and lignite- fired power plants than in reality (see section 4.2.2.1.1). However, the calibrated model approximates a minimum level for the short-term potential of CO_2 emissions abatement. Indeed, downward adjustment of the availability of coal- and lignite- fired power plants in the calibrated version (see section 4.2.2.1.2) leads to the reduction of CO_2 emissions and achievable abatement. Total CO_2 emissions, estimated by the calibrated and the non-calibrated model at a zero CO_2-price, and the potential of CO_2 abatement through fuel switching are visualized in Fig. 4.21.b.

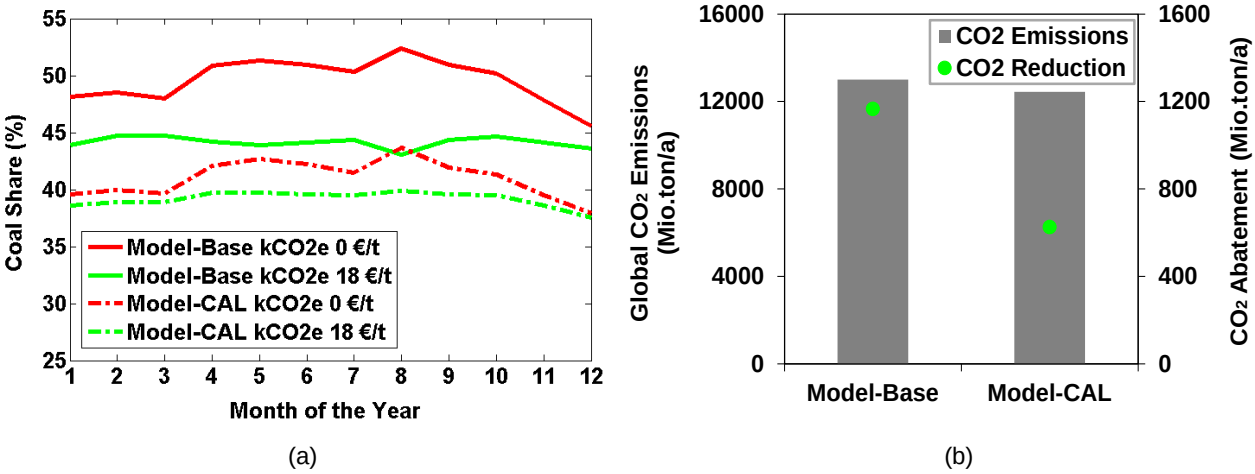

Fig. 4.21: Influence of a global carbon price of 18 €/ton on CO_2 emissions of year 2006 (a) Mean monthly share of coal-fired generation in total fossil-fired power production (COAL-ST, LIG-ST, GAS-CC, GAS-GT, OIL-CC, and Oil-GT); (b) Total CO_2 emissions at a zero CO_2-price and abatement potential

To analyze influences on CO_2 emissions of a global electricity generation system in a mid- to long- term horizon, in the next subsections, the investment and production optimization model is applied, using the previously installed capacity of power plants along with the electricity demand and fuel prices of the corresponding time period. Estimated regional availability factors are obtained from the calibrated model and applied for existing power plants; however, for the new vintages standard availability factors are used. Fuel costs are assumed at annual average prices of the world market, and are considered to be uniform through all regions. This can be explained according to the fact that the deviation of domestic fuel prices from international market prices, which has been applied to minimize the difference between the simulation results and the real power production mix of year 2000, cannot be assumed to remain valid in the future coming periods.

4.2.2.3 Topology of abatement - complex interaction of influential factors

So far, the potential of CO_2 abatement in the world electricity supply sector on a short-term perspective, caused by fuel switching in response to a global carbon price, has been evaluated. In this part, interaction of different influential factors of CO_2 emissions is studied in detail. These include the system load, fuel prices, and the share of renewable energies in addition to the CO_2-price. A specific share of FRES is taken into account in accordance with medium-term prognoses, using the scenarios developed in the following subsection.

4.2.2.3.1 Scenario setup

An optimization is performed for a medium-term horizon, the year 2025. Thirteen weeks are simulated to represent the total year. To determine the electricity demand, the B2 scenario, developed by IPCC in its special report on emission scenarios (SRES), is used. Time series of wind power capacity factor and solar irradiation are determined based on the meteorological data of the year 1993, given in [60, 65]. The approach applied to estimate these parameters is described in sections 3.1.1, 3.1.2, and 3.2.

While in the baseline scenario extension of renewable power plants is not allowed, in scenarios "WND-OPT" and "WND-OPT-CFH", extension of wind power at each region up to the technical potential is possible. The model chooses the most promising sites to install new wind power plants according to the wind power's investment costs, annual full load hours, temporal fluctuations and correlation with regional electrical load profiles as well as proximity to densely populated areas. The "WND-" scenarios differ in the applied time series of wind power capacity factor. The average wind power capacity factor is 20% and 25% in scenarios "WND-OPT" and "WND-OPT-CFH", respectively. This is due to the lower assumed cut-in wind speed and rated wind speed to transform the wind velocity to active power output in preparation of the time series of wind power capacity factor for scenario "WND-OPT-CFH".

It is assumed that the nuclear power's operation time is restricted to 34 years for all regions, and new investments are not allowed. Moreover, it is assumed that hydro power plants are not expandable beyond operating capacities. New investments in geothermal power plants are restricted according to the planned capacities, given in [96]. Already installed capacities for power transmission and storage up to the year 2009 are set as upper capacity boundaries. A rather low CO_2-price of 24 €/ton is used. Fuel prices are projected based on the development pathways proposed in [49, 100]; these are represented in Table D.3 from 2020 to 2040. Techno-economic parameters of power plants are based on data from [24, 48, 49]. These parameters are given in Table 4.7 for operating power plants; investment costs and energy efficiency of new vintages are given in Table D.1 and Table D.2 over the time horizon 2020-2040. The investment costs are annualized using the technology-specific economic lifetimes, given in Table 3.8, and by assuming a discount rate of 5% p.a. The standard availability factors, given in Table 3.11, are used to downscale the capacity of new power plants due to periodic maintenance and forced outages. The technology-based ramp rates of power plants are given in Table 3.11.

Table 4.7: Techno-economic parameters of existing power plants. Data source: [24, 48, 49, 100, 127] (All costs are in US$ (2008).)

Technology	Efficiency (%)	Fixed O&M ($/kW$_{el}$/a)	Variable O&M ($/kWh$_{el}$)	Emission factor (ton/MWh$_{th}$)
BIO-ST	38	80	0.0058	0
COAL-ST	38	40	0.0058	0.335
GAS-GT	34	17	0.0030	0.202
GAS-CC	52	30	0.0030	0.202
GEO-ST	20	150	0.0001	0
HP-ROR	80	20	0.0001	0
HP-PS	86	35	0.0009	0
LIG-ST	34	50	0.0058	0.396
OIL-CC	46	28	0.0030	0.310
OIL-GT	31	19	0.0028	0.310
SOL-CSP	15	44	0	0
SOL-PV	12	40	0	0
URA-ST	34	74	0.0008	0
WIND	96	24	0	0
WIND-O	93	49	0	0

Fig. 4.22 shows the total power generation capacity mix in a prospective global electricity generation system, which is obtained from the optimization model for year 2025, using the three described scenarios. The base case represents a coal-based system with nearly zero penetration share of wind power while this share reaches to 17% and 34% of the global electricity demand in scenarios “WND-OPT” and “WND-OPT-CFH”, respectively.

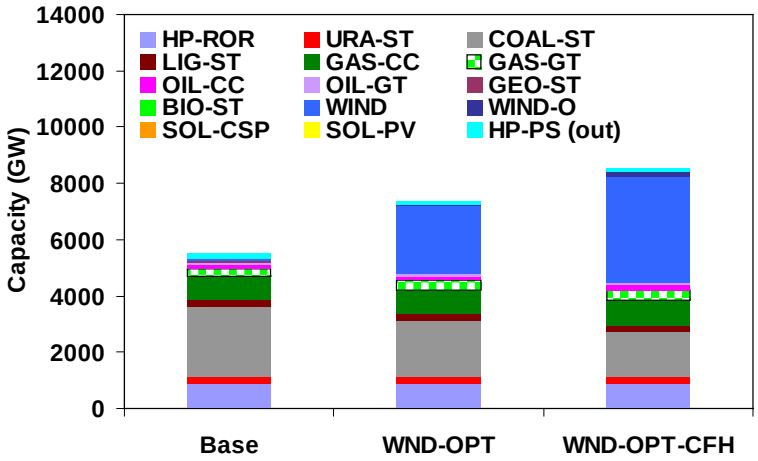

Fig. 4.22: Optimal power generation capacity mix in scenarios “Base”, “WND-OPT”, and “WND-OPT-CFH”

Fig. 4.23 compares the total installed capacity for wind power production in scenarios “WND-OPT” and “WND-OPT-CFH” with the scenarios of the Global Wind Energy Council (GWEC)

[78]. The scenario “Advanced 2030” with 20% penetration share of wind power is the closest to the optimization results, obtained from the scenario “WND-OPT”.

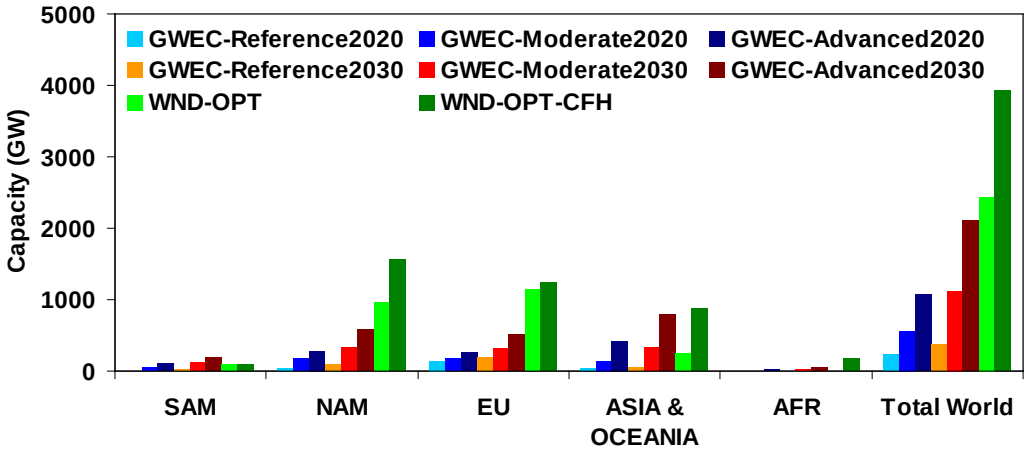

Fig. 4.23: Total wind power capacity in scenarios “WNDOPT” and “WNDOPT-CFH” vs. Global Wind Energy Council scenarios

The optimal capacity of power plants, obtained from the scenarios “Base” and “WND-OPT”, is then used as a basis to represent two possible configurations of a medium-term global electricity generation system, differing in the integration share of FRES.

4.2.2.3.2 Influence of load and CO_2-price

The capacity of power plants are now fixed at the optimal levels, obtained from the scenarios “Base” and “WND-OPT”; a sensitivity study is then performed, using the variation of CO_2-price and fuel price ratios. In all cases, the CO_2-price is increased from zero to 100 €/ton at intervals of 20 €/ton. Another influential factor is the ratio of the natural gas price to the price of hard coal. However, at first, the focus is laid on the influence of hourly electricity load and the CO_2-price; thus, constant fuel prices are used.

The residual load is identified as a main influencing factor of CO_2 emissions. Higher load implies more energy production. The residual load – a part of load, not being covered by wind energy – must be satisfied with fossil energy, and, thus, correlates with hourly emissions. Fig. 4.24.a and Fig. 4.25.a show the dependency of hourly global emissions on hourly load at different CO_2 prices for the power generation system of “Base” and for the “WND-OPT” scenario, respectively.

The achieved abatement is determined by subtracting the CO_2 emissions at each hour at a positive CO_2-price from the CO_2 emissions, occurring at the corresponding hour at a zero carbon price. According to Fig. 4.24.b and Fig. 4.25.b, hourly CO_2 emissions abatement decrease with the residual load regardless of the CO_2-price and the share of wind energy. In response to a CO_2-price fuel switching occurs; the possibility for fuel switching with constant fossil fuel prices depends on the available capacity of low emitting generation plants. At lower levels of electricity load, in the coal-based system of baseline scenario and in an electricity generation system with a moderate share of wind energy, obtained from the “WND-OPT” scenario, coal-fired power plants operate at base load; thus, gas-fired plants are available for

substitution at higher CO_2 prices. However, at peak load, power plants mostly operate at their full installed capacity; thus, the potential for fuel switching diminishes. Due to the lower utilization of coal-fired power plants in scenario "WND-OPT" as compared to their utilization in the base case, the potential for fuel switching is reduced at any given CO_2-price. This effect is more evident at lower levels of electricity load.

Furthermore, it can be concluded that a CO_2-price of 20-40 €/ton is not adequately high to encourage a significant abatement in the considered electricity generation systems. Limited fuel switching occurs only at lower levels of electricity load. At a higher CO_2-price of 60 €/ton, a significant level of abatement is achieved. However, saturation effects occur afterwards, and further changes at higher CO_2 prices (80-100 €/ton) are insignificant.

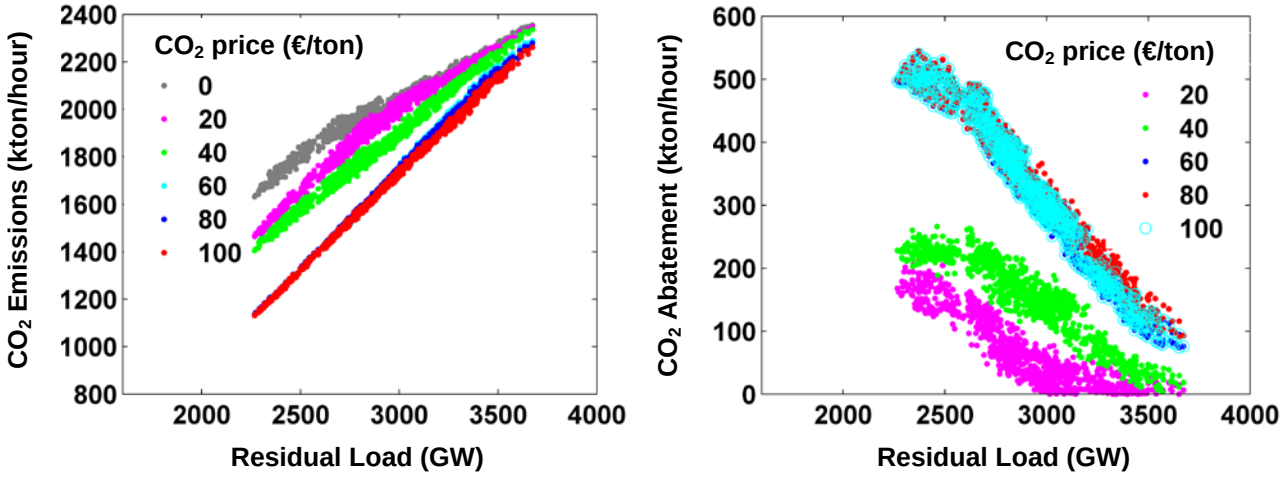

(a) (b)

Fig. 4.24: Influence of load and CO_2-price on CO_2 emissions in scenario "Base" (a) Sorted hourly CO_2 emissions summed over all regions; (b) Corresponding abatement

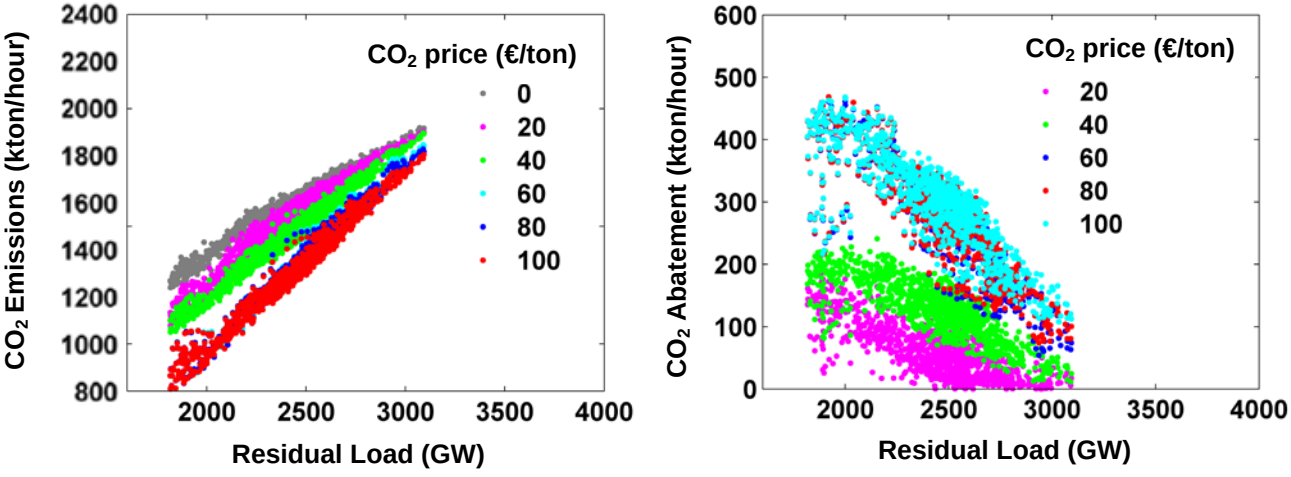

(a) (b)

Fig. 4.25: Influence of load and CO_2-price on CO_2 emissions in scenario "WND-OPT" (a) Sorted hourly CO_2 emissions summed over all regions; (b) Corresponding abatement

4.2.2.3.3 Fuel price effects

Fuel prices have a substantial impact on the utilization of power plants and resulting emissions. Achieved abatement in response to a CO_2-price at any given fuel prices is also influenced by system load and the available capacity of low emitting generation plants. However, in order to clarify the absolute impact of fuel prices, variations of electricity load through the year are initially excluded from the results.

Fig. 4.26 and Fig. 4.27 show the CO_2 emissions and the corresponding abatement at a typical winter peak hour over a range of fuel price ratios in scenarios “Base” and “WND-OPT”, respectively. At a zero CO_2-price, when the gas price is reduced to zero, total CO_2 emissions at this hour reach to around 2000 and 1500 ktons in scenarios “Base” and “WND-OPT”, respectively (see Fig. 4.26.a and Fig. 4.27.a). If the gas price rises, the power produced from coal substitutes the power generation from natural gas. Correspondingly, the CO_2 emissions rise and at a gas to coal price ratio of 2 reach to a peak of around 2150 and 1600 ktons in scenarios “Base” and “WND-OPT”, respectively. According to Fig. 4.26.a and Fig. 4.27.a, when increasing the CO_2-price, lines are pushed down, and the peak of abatement is shifted to the right. Indeed, at any given CO_2-price, when increasing the gas price, less efficient gas-fired units are initially replaced by the most efficient coal-fired power plants. At higher gas prices, it is economic to replace even the most efficient combined-cycle power plants with lignite-fired units. At higher CO_2 prices, the capacity utilization of coal-fired units is reduced due to the higher emissions costs, and gas combined-cycle plants mainly operate at base load. Hence, switching opportunities are exhausted at higher gas prices.

The abatement, achieved in response to a CO_2-price, is calculated by taking the difference between the emissions at the corresponding CO_2-price and the emissions, occurring at a zero CO_2-price. Fig. 4.26.b and Fig. 4.27.b show the corresponding abatement in scenarios “Base” and “WND-OPT”, respectively. At a low gas price, there are very few switching opportunities because gas-fired power plants have been already committed as base load generators. Thus, increasing the CO_2-price cannot lead to a significant increase of their utilization level. Thus, all the abatement lines reach their minimum at zero gas price. When increasing the price of natural gas, more coal-fired capacity is committed at the expense of natural gas until the technical limits of the system are reached. This creates opportunities for fuel switching, which can be utilized with increasing the CO_2-price. Hence, the abatement rises when increasing the gas price. However, at any given CO_2-price, there is a gas to coal price ratio, which is adequately high to make further switching in favor of natural gas economically unattractive. From this point onward, more switching opportunities are continuously created by increasing the gas price until the technical limits are reached. However, at the given CO_2-price, further commissioning of low emitting gas-fired units at the expense of coal-fired plants is economically unattractive. Therefore, all the abatement lines reach a peak and fall afterwards. At higher CO_2 prices, the peak of abatement is higher and occurs mainly at a gas to coal price ratio of 2.

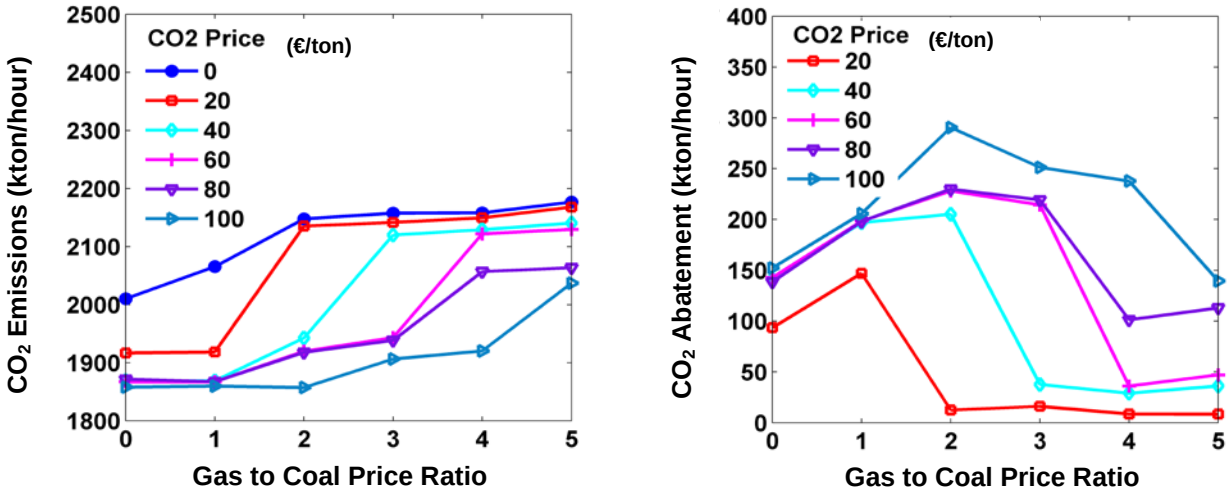

(a) (b)

Fig. 4.26: Influence of CO_2-price and fuel price on CO_2 emissions at a typical winter peak hour in scenario "Base" (a) CO_2 emissions summed over all regions; (b) Corresponding abatement

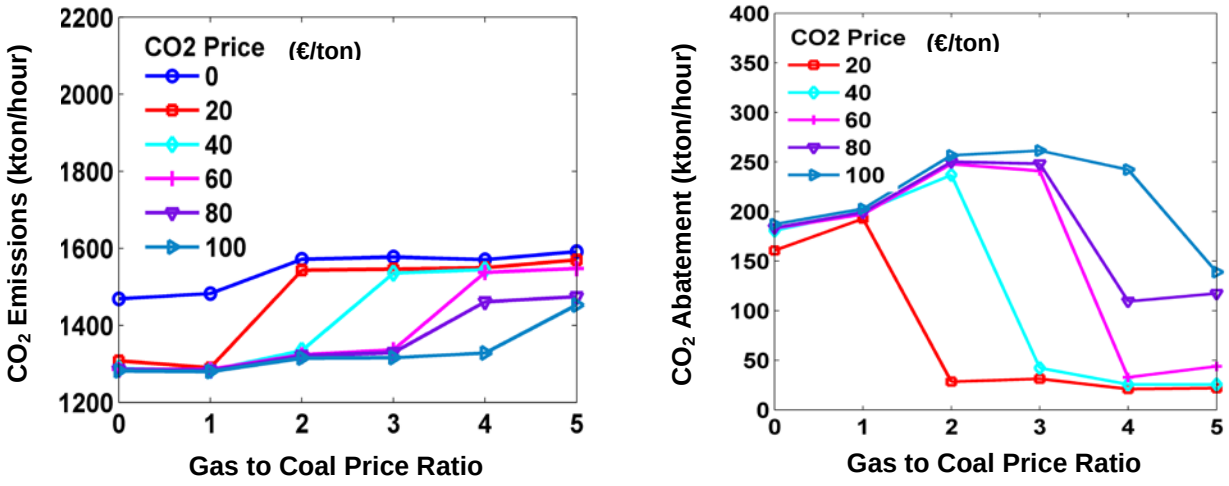

(a) (b)

Fig. 4.27: Influence of CO_2-price and fuel price on CO_2 emissions at a typical winter peak hour in scenario "WND-OPT" (a) CO_2 emissions summed over all regions; (b) Corresponding abatement

CO_2 emissions of the power system are changed due to the variation of capacity utilization of fossil-fired power plants. This is caused by the variation of the CO_2-price and the fuel costs. In order to clarify the underlying effects, imposed by price variations, and making a comparison between the base case and the "WND-OPT" scenario, capacity utilization of fossil-fired power plants is illustrated in Fig. 4.28 and Fig. 4.429 at a typical winter peak hour as in Fig. 4.26 and Fig. 4.27.

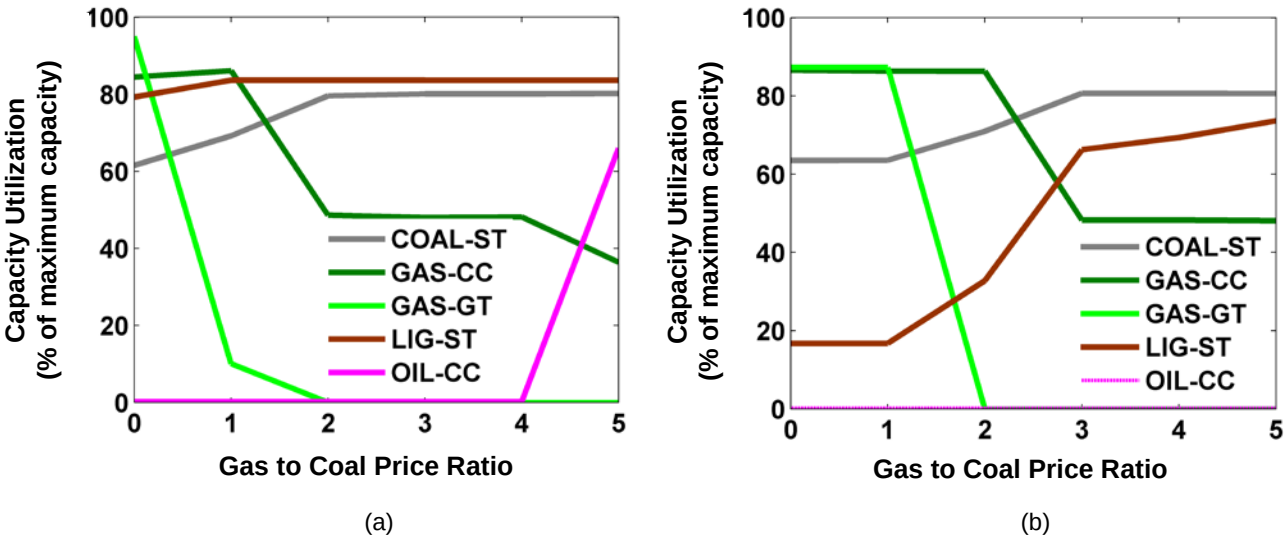

Fig. 4.28: Capacity utilization of thermal power plants at a typical winter peak hour in scenario "Base" (a) CO_2-price is 0 €/ton; (b) CO_2-price is 40 €/ton

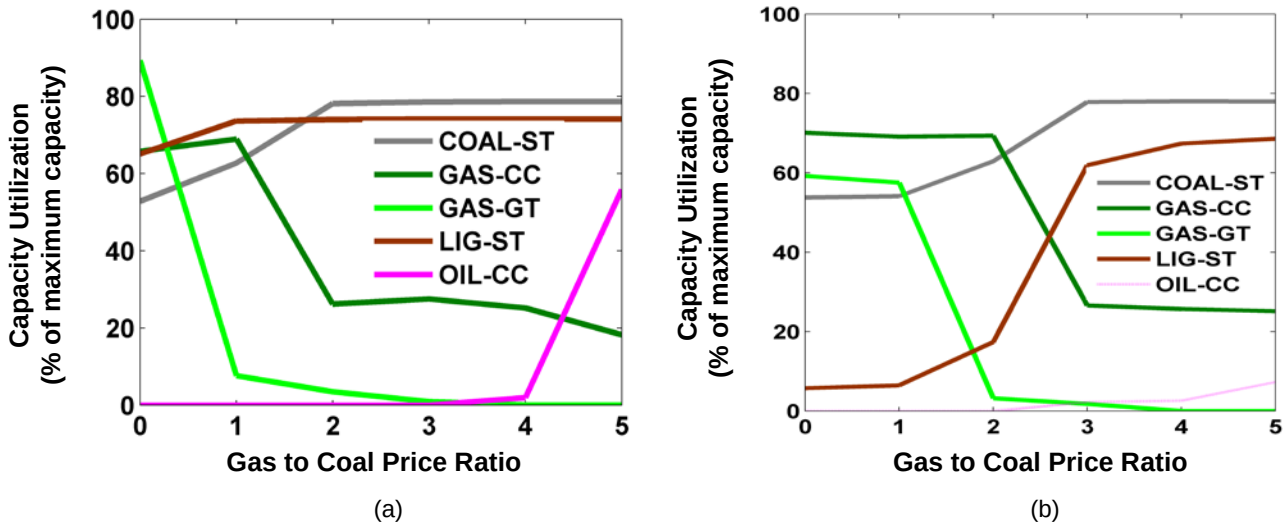

Fig. 4.29: Capacity utilization of thermal power plants at a typical winter peak hour in scenario "WND-OPT" (a) CO_2-price is 0 €/ton; (b) CO_2-price is 40 €/ton

According to Fig. 4.28 or Fig. 4.29, when increasing the CO_2-price, the point, where the capacity utilization of gas combined-cycle plants starts to decrease, moves towards a higher gas price. At a positive CO_2-price, the capacity utilization of gas turbine significantly reduces at a gas to coal price ratio of 2. By comparing the capacity utilization of gas turbine between Fig. 4.29.a and Fig. 4.29.b, a significant reduction is noticed at a gas price of zero when increasing the CO_2-price. However, according to Fig. 4.28, this effect is negligible in the baseline scenario. Indeed, additional reduction of the power produced by fossil-fired power plants in scenario "WND-OPT" is balanced through a higher usage of energy storage to reduce the discarded wind power.

The storage output at this winter peak hour is shown in Fig. 4.30 as a function of the gas to coal price ratio for various levels of the CO_2-price. According to Fig. 4.30.b, at a zero gas price, the storage output significantly rises in response to an additional increase of the CO_2-price. This

occurs because the system has the potential to reduce the discarded wind power through a higher application of energy storage. As a result, discarded wind power reduces at maximum by 5% (240 TWh) when the CO_2-price is increased from 0 to 60 €/ton. This effect additionally contributes in the reduction of CO_2 emissions, achieved through fuel switching. Thus, the CO_2 emissions abatement, achieved at this winter peak hour in scenario "WIND-OPT", is higher than the base case (see Fig. 4.26.b and Fig. 4.27.b).

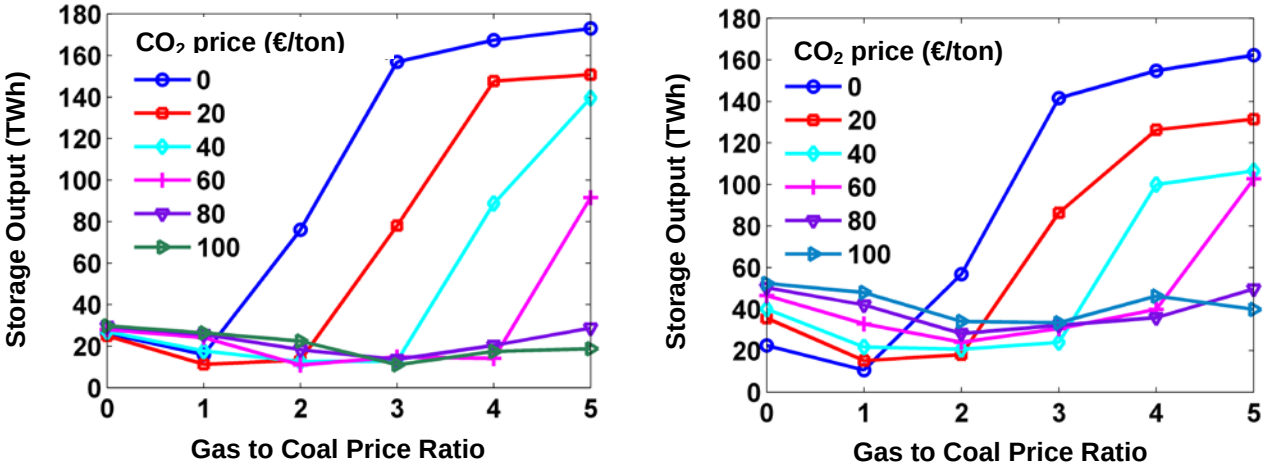

Fig. 4.30: Storage output power at a typical winter peak hour (a) Scenario "Base"; (b) Scenario "WND-OPT"

According to Fig. 4.30, in both scenarios, when increasing the gas price, the storage output reduces until it reaches a minimum, where gas and coal are economically balanced at the given CO_2-price. It starts to rise when the gas price is adequately high to make the application of coal-fired plants as base load generators economically attractive at the given CO_2-price. As the gas price is further increased, application of energy storage becomes more and more economical to store the power produced by coal-fired power plants for peak shaving purposes. It follows a similar trend in both scenarios.

Finally, Fig. 4.31 shows the combined effect of load and fuel price on CO_2 emissions abatement in baseline scenario at the CO_2-price of 60 €/ton. At higher ranges of load and extreme levels of the gas price, CO_2 emissions are not influenced by the carbon price. The maximum level of abatement occurs at lower levels of electricity load and at a gas to coal price ratio of 2.

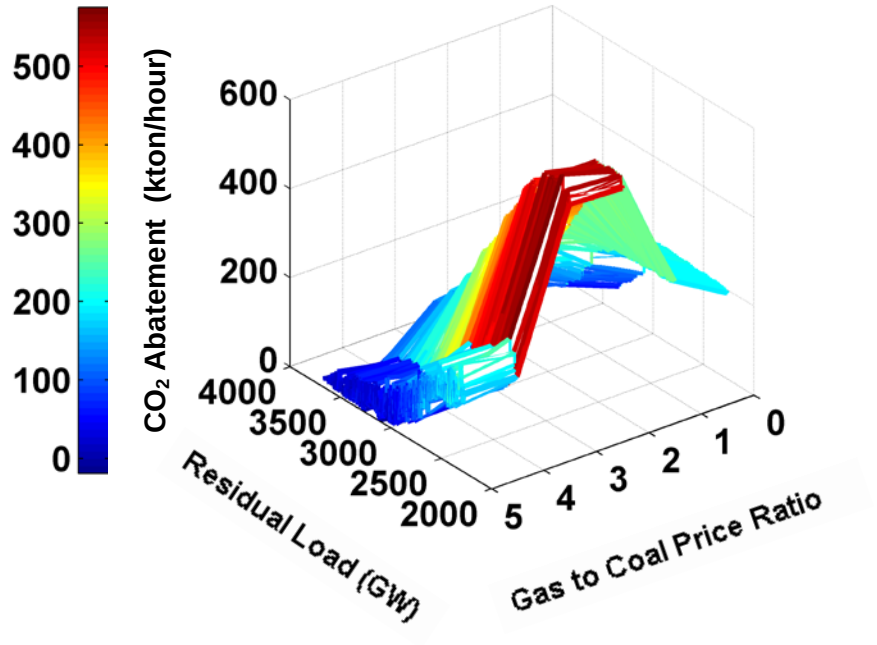

Fig. 4.31: Three-dimensional representation of a combined influence of load and fuel price on CO_2 emissions abatement in scenario "Base" at a CO_2-price of 60 €/ton

4.2.2.4 Long-term CO_2 emissions abatement

So far, it has been demonstrated that the CO_2 emissions can be reduced by switching from high carbon fuels such as coal to low carbon fuels such as natural gas. However, for many world regions, this option has consequences on the security of supply, as they would then become dependent on the imported natural gas. Moreover, the potential is relatively limited. Ambitious emissions reduction targets cannot be achieved without deployment of zero carbon energy sources such as wind and solar.

Thus, in this part, the focus is laid on the new investments in the world electricity supply sector, required to achieve long-term CO_2 emissions reduction targets. The optimal configuration of a prospective global electricity supply system is investigated when global emissions caps are binding. Thus, in the following scenarios, production is constrained by regulated CO_2 emissions. The CO_2-limit is implemented as a global system constraint; therefore, through the optimization process it is assumed that reductions take place where it is cheapest to do so regardless of the geographical position.

As described in section 2.4, in a CO_2-regulated scenario, the dual variable of the CO_2 emissions constraint, given in (2.29), represents the financial value added to the system if CO_2 emissions might be increased by one unit. This determines the global carbon price correspondent to the proposed level of abatement.

4.2.2.4.1 Influence of FRES on marginal price of CO_2 emissions

At first, the effect of an ambitious global emissions reduction target of 38% below the level of emissions in year 2000 is studied. Optimal structure of a global electricity generation system in year 2025 is studied based on different scenarios. In the base case, existing capacities of solar and wind power are set as upper capacity boundaries. In scenario "REOPT", the penetration

share of solar and wind power is optimized. In scenarios “RE50-WP0”, “RE50-WP50”, and “RE50-WP100”, solar and wind power production are constrained to satisfy 50% of the global electricity demand. The share of wind energy is increased from zero to 50% and 100% of total solar and wind power production in scenarios “RE50-WP0”, “RE50-WP50”, and “RE50-WP100”, respectively. In all scenarios, it is assumed that nuclear and hydro power plants are not expandable beyond operating capacities. New investments of geothermal power plants are restricted according to the planned capacities, given in [96]. Available capacities for power transmission and storage are fixed at the total installed capacities of year 2009. Techno-economic parameters of existing power plants are given in Table 4.7. Investment costs and conversion efficiency of new power plants and projected fuel prices are given in Table D.1, Table D.2, and Table D.3, respectively. Scenarios and their underlying assumptions are summarized in Table 4.8.

Table 4.8: Scenarios and underlying assumptions

Scenario	Underlying assumptions
Base	- Total CO_2 emissions are limited to 5745 million tons. - Extension of solar and wind power beyond today is not allowed.
REOPT	- Total CO_2 emissions are limited to 5745 million tons. - Upper capacity boundary of solar and wind power at each region is the technical potential.
RE50-WP0	- Total CO_2 emissions are limited to 5745 million tons. - Upper capacity boundary of solar and wind power at each region is the technical potential. - Solar and wind power are forced to satisfy 50% of global electricity demand. - Wind share is 0% of total solar and wind power production.
RE50-WP50	- Total CO_2 emissions are limited to 5745 million tons. - Upper capacity boundary of solar and wind power at each region is the technical potential. - Solar and wind power are forced to satisfy 50% of global electricity demand. - Wind share is 50% of total solar and wind power production.
RE50-WP100	- Total CO_2 emissions are limited to 5745 million tons. - Upper capacity boundary of solar and wind power at each region is the technical potential. - Solar and wind power are forced to satisfy 50% of global electricity demand. - Wind share is 100% of total solar and wind power production.

The global power production mix in different scenarios is shown in Fig. 4.32. When implementing a CO_2-limit while no possibility exists for extension of solar and wind power plants in baseline scenario, the production is characterized with an extensive application of gas combined-cycle and biomass power plants. As a result, the CO_2-price in baseline scenario is higher than the CO_2-price, obtained from other scenarios.

Application of solar energy in scenario “RE50-WP0” allows increasing the utilization of coal-fired plants while power production from gas combined-cycle plants is lower than the base case. Contribution of biomass power plants is insignificant, and less power is produced from hydro and nuclear power plants in comparison with the base case. Increasing the share of wind energy in scenarios “RE50-WP50” and “RE50-WP100” allows even a higher application of coal-

fired plants while power production from gas combined-cycle plants is further reduced as compared to “RE50-WP0”. However, operation time of hydro and nuclear power plants is higher than the solar-only case.

The explanation arises from the fact that the daily pattern of solar energy positively correlates with the diurnal behavior of electricity load. Thus, in scenario “RE50-WP0”, in summer period, during hours with a high gain of irradiation, there is a full integration of solar energy at specific sites, having high installed capacities for solar electricity generation. This leads to the reduction of operation time of hydro and nuclear power plants as compared to other scenarios. However, in winter period and during hours with no gain of irradiation, the electricity demand is mainly satisfied with additional gas-fired capacities. However, wind power production has a timely pattern, which is more evenly distributed between the hours of day and night and through different seasons. Thus, when increasing the share of wind power, total power production from emission-free hydro and nuclear power plants increases from its level in the solar-only case. This allows a higher utilization of coal-fired plants; thus, power production from gas-fired units can be reduced while the same level of abatement is achieved as in the solar-only case.

According to Fig. 4.32, marginal price of CO_2 emissions decreases while increasing the share of wind energy; it reaches to its lowest level in scenario “REOPT”. Based on the obtained results from this scenario, the optimal share of wind power reaches to 52% of the global electricity demand.

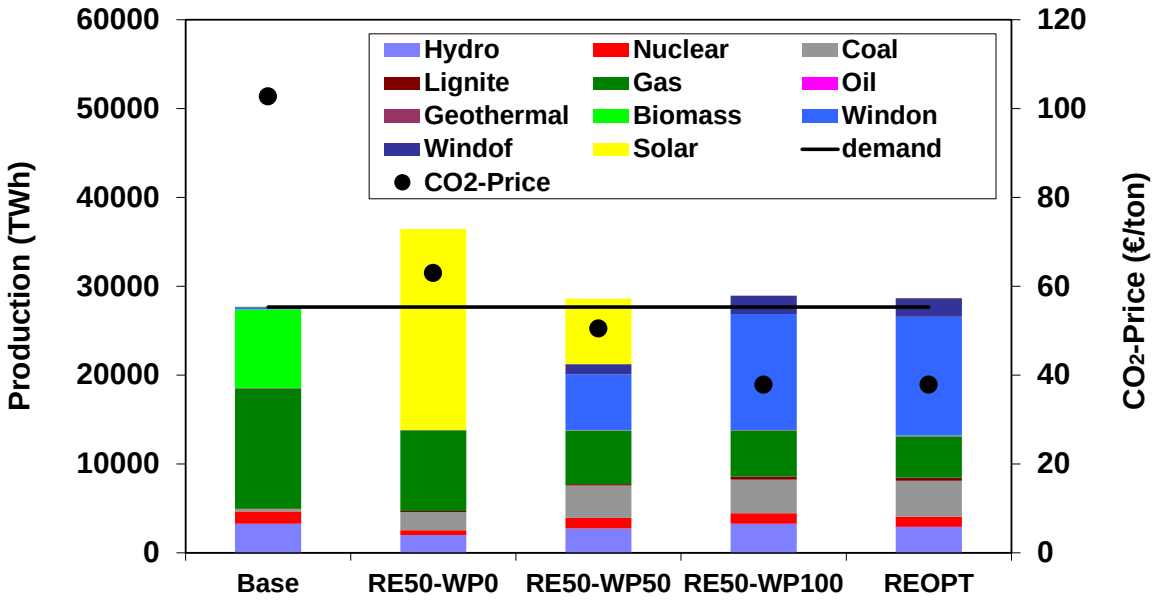

Fig. 4.32: Total power production mix and marginal price of CO_2 emissions

4.2.2.4.2 Influence of international electricity exchange in a prospective low-carbon electricity generation system

Challenges arise when integrating a high share of solar and wind power into an electricity generation system mainly due to their short-term fluctuations. Smoothening effects, captured in a dispersed generation structure, can alleviate the problem. Not only statistical smoothening effects of geographical aggregation but also inter-continental, seasonal anti-correlations may provide a competitive framework for the deployment of solar and wind energy. Therefore, the focus of this subsection is laid on the influence of international electricity exchange in an ideal, globally-interconnected electricity supply structure.

Here, a long-term horizon from 2020 to 2040 in five-year time steps is taken into account; the focus is laid on the role of an ideal global grid as a solution option for large-scale integration of FRES. In scenario “Link”, the new capacity of inter-regional power transmission lines is optimized. To evaluate the absolute impact of a global grid, the scenario “No Link” is also considered, having no possibility for extension of the power transmission grid while other underlying assumptions are similar to the scenario “Link”. As before, it is assumed that nuclear and hydro power plants are not expandable beyond the existing capacities. New installations of geothermal power plants are restricted according to the planned capacities, given in [96]. The capacities of energy storage systems are fixed at the total installed capacity of year 2009. Projected fuel prices are given in Table D.3. Techno-economic parameters of each power plant technology are assumed to be uniform through all regions. These parameters are given in Table 4.7 for operating power plants. For the new vintages, the conversion efficiency increases while the investment costs of renewable technologies reduce over the future time periods. Techno-economic parameters of new power plants are given in Table D.1 and Table D.2. For inter-regional transmission of electricity, costs of to the 500kV HVDC technology, given in Table 3.13, are used. Scenarios are described in Table 4.9.

The IPCC working group one (WG1) proposed an early action scenario for 550 ppmv concentration level [2,5]. In this study, in scenarios with the postfix of “-CO2H”, total CO_2 emissions from the power sector at each time period are limited according to the IPCC WG1 CO_2 stabilization scenario. Stabilization at lower concentration levels advances the date, when emissions need to peak, and results in a higher cumulative abatement by the end of the century. Here, in a more stringent scenario, represented with a postfix of “-CO2L”, the CO_2 emissions limits are tightened according to the first category of stabilization scenarios in IPCC fourth Assessment Report (AR4) [1, 3]. The CO_2 emissions path is set to the minimum path, proposed in [1], which leads to the stabilization of CO_2 only concentrations at the level of 350 ppmv by 2100. The contribution share of the power sector in total abatement is estimated from the historical data. According to CARMA [4], CO_2 emissions from the power sector in year 2000 reaches to 9395 million tons. This corresponds to 42% of total CO_2 emissions through this year based on data from [5]. The implemented CO_2 limits are represented in Table 4.10.

Table 4.9: Scenarios and underlying assumptions

Scenario	Underlying assumptions
Link-CO2L	- CO_2-limit is based on 350 ppmv concentration level. - Inter-regional power transmission capacities are optimized.
Link-CO2H	- CO_2-limit is based on 550 ppmv concentration level. - Inter-regional power transmission capacities are optimized.
No Link-CO2L	- CO_2-limit is based on 350 ppmv concentration level. - Inter-regional power transmission capacities are fixed as today.
No Link-CO2H	- CO_2-limit is based on 550 ppmv concentration level. - Inter-regional power transmission capacities are fixed as today.
Link-CO2L-SOL	- CO_2-limit is based on 350 ppmv concentration level. - Inter-regional power transmission capacities are optimized. - Costs of solar power plants are reduced by 50%.
No Link-CO2L-SOL	- CO_2-limit is based on 350 ppmv concentration level. - Inter-regional power transmission capacities are fixed as today. - Costs of solar power plants are reduced by 50%.

Table 4.10: Implemented CO_2 limits in million metric tons

Scenario	Year 2020	Year 2025	Year 2030	Year 2035	Year 2040
CO2H	10059	10335	10611	10777	10943
CO2L	6107	4698	3758	2819	2067

The optimal power generation capacity mix, summed over all regions, is illustrated in Fig. 4.33 for the first four scenarios over the considered time horizon. In scenario “Link-CO2H”, the total wind power capacity is 2822 GW in 2020 and rises to 10000 GW by 2040. The average wind power capacity factor is 27%, and its penetration share reaches to 58% of the global electricity demand by 2040. In the more stringent scenario, named “Link-CO2L”, the installed capacity for wind power production rises from 4570 to 15285 GW through the considered time horizon. Implementing a tighter CO_2-limit, the coal-fired capacity is reduced while the capacity of gas-fired plants is higher as compared to the “Link-CO2H” scenario. With the assumed costs and conversion efficiency, solar power plants are not selected for large-scale penetration when the power transmission grid structure is optimized. However, in scenario “No Link-CO2L”, the total installed capacity for solar electricity generation significantly increases in the final periods; it rises to 5 GW in 2035 and reaches to 18 GW by 2040.

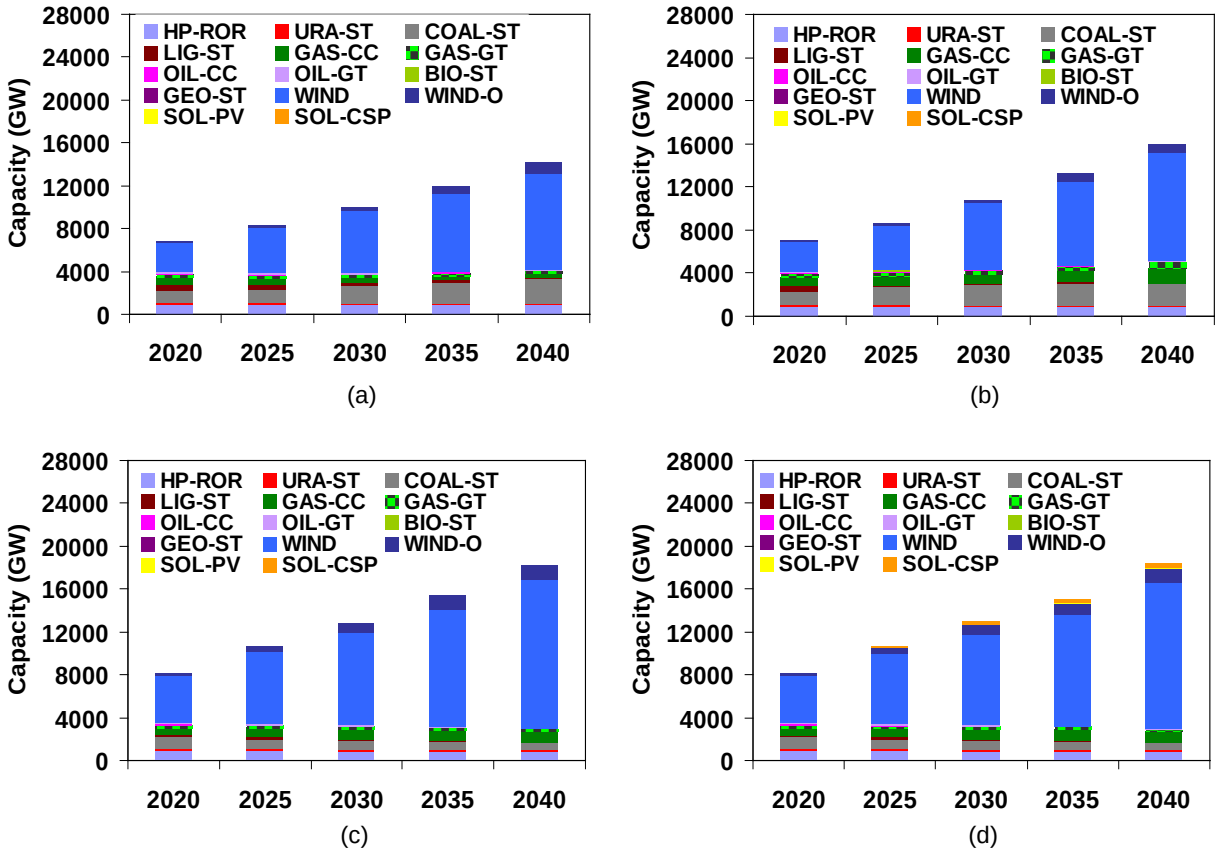

Fig. 4.33: Global power generation capacity mix over time horizon 2020-2040 (a) Scenario "Link-CO2H"; (b) Scenario "No Link-CO2H"; (c) Scenario "Link-CO2L"; (d) Scenario "No Link-CO2L"

A sensitivity study is now performed on the influence of the costs of solar power plants. In scenarios "Link-CO2L-SOL" and "No Link-CO2L-SOL", the costs of solar power plants are reduced by 50% from the level used in previous scenarios. The optimal capacity of solar electricity generation systems, obtained from different scenarios, is visualized in Fig. 4.34 over the considered time horizon.

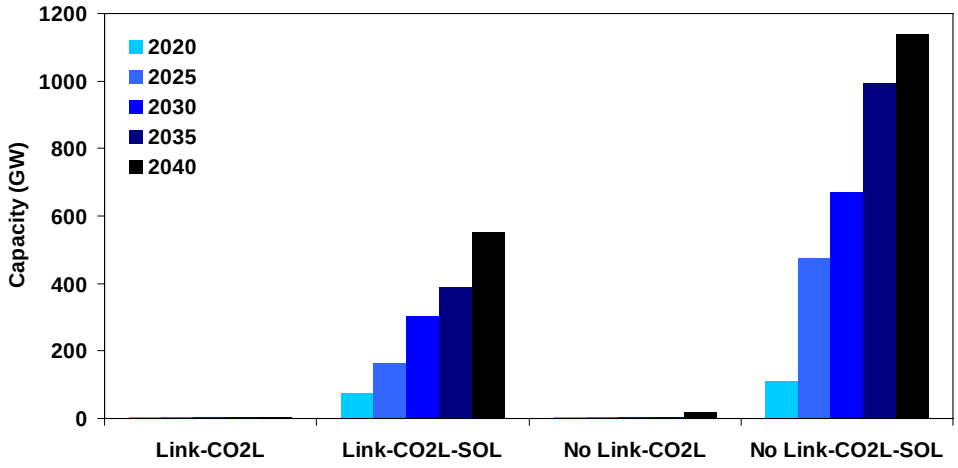

Fig. 4.34: Total capacity of "SOL-PV" and "SOL-CSP" over time horizon 2020-2040

The optimal structure of a global power transmission network is shown in Fig. 4.35. Inter-regional power transmission lines with a maximum capacity of 230 GW and 460 GW are installed in scenarios “Link-CO2H” and “Link-CO2L”, respectively to transmit wind electricity from regions, having a highly concentrated potential, to the distant load centers.

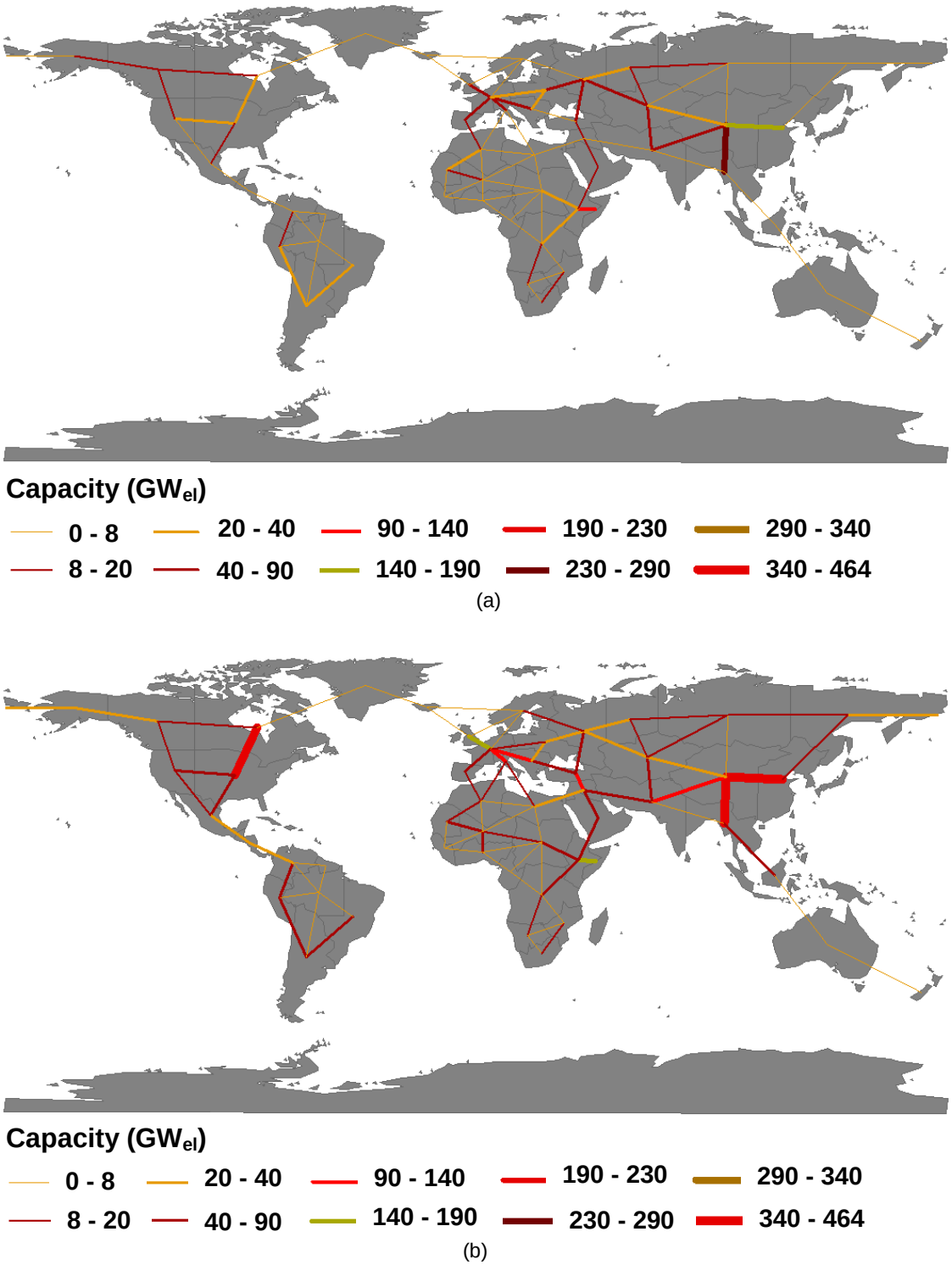

Fig. 4.35: Optimal power transmission grid structure in year 2040 (a) Scenario “Link-CO2H”; (b) Scenario “Link-CO2L”

The influence of a global grid can be realized by comparing “No Link-” scenarios with “Link-” scenarios. Fig. 4.33 clarifies the over-installation of power generation capacities, occurring in scenarios “No Link-CO2L” and “No Link-CO2H”; higher capacities for gas-fired generation and wind power production are required to achieve the same level of CO_2 abatement as it is achieved in scenarios “Link-CO2L” and “Link-CO2H”, respectively.

In scenario “Link-CO2H”, the CO_2-price does not significantly increase through the considered time horizon and remains near 16 €/ton (see Fig. 4.36). However, in scenario “No Link-CO2H”, it rises to 35 €/ton by 2040. This effect becomes even more evident when tightening the CO_2-limit. In scenario “No Link-CO2L”, the global carbon price rises to 147 €/ton by 2040 compared to the carbon price of 61 €/ton in scenario “Link-CO2L”.

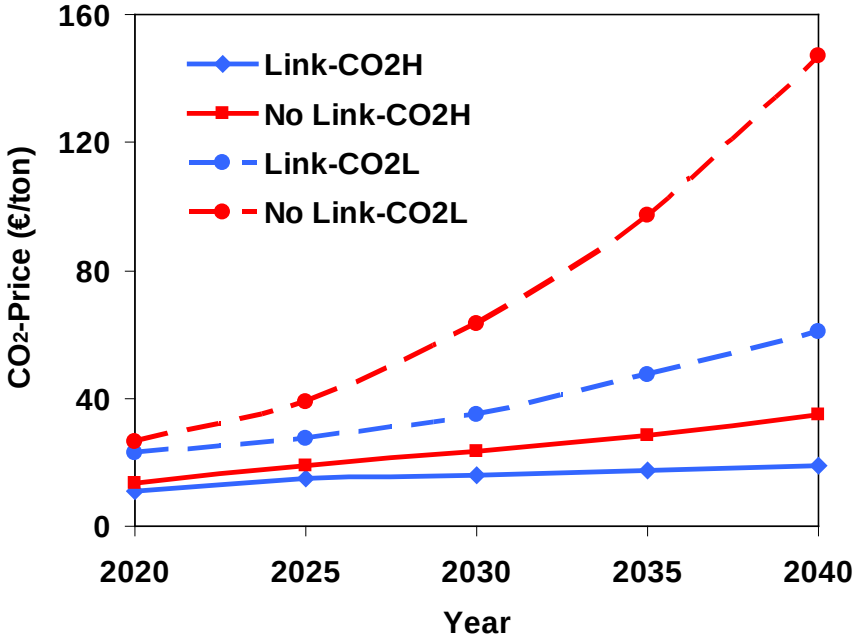

Fig. 4.36: Development of global carbon price over time horizon 2020-2040

4.2.2.5 Conclusions

The developed methodology in chapter 2 has been applied to study complex interactions of different factors, influencing CO_2 emissions of the power system. While the potential for reducing CO_2 emissions in the short-term with an existing fleet of generation plants was evaluated, long-term abatement in the power sector and required structural adaptations with a special focus on the influence of solar and wind energy was studied.

At first, the global model was examined versus a real power production mix to validate its appropriateness for modeling electricity generation systems. Overall, it is concluded that the model overestimates the usage of coal and lignite while it underpredicts the produced power from gas and oil. This might be caused by the lower availability of coal- and lignite- fired power plants in reality due to the technical restrictions and/or lack of fuel supply, regulatory constraints, and also different domestic fuel prices. Mainly by adjusting the availabilities of coal- and lignite-fired plants, simulation results correspond to the actual generation. Indeed, this calibration has a

significant impact on the estimation of CO_2 emissions abatement as the usage of coal and lignite has a direct impact on the possible amount of fuel switching. The calibrated model was then applied to quantify the potential for reducing emissions in response to a global carbon price with an existing fleet of generation plants, i.e. by means of fuel switching. It has been concluded that the total emissions would be reduced by 5% (several hundreds of million tons) if a CO_2-price of 18 €/ton existed in all countries through the year 2006.

Through sensitivity study using the input parameters, projected for a medium time horizon, it was shown that the achievable abatement in response to a CO_2-price is significantly influenced by the structure of the electricity generation system as well as load and fuel price relationships. It is concluded that a complex relationship exists between CO_2 abatement and influencing factors such as CO_2-price, fuel prices, and electricity load. Indeed, all these factors must lie within a specific range at the same time that fuel switching can occur.

Another general conclusion concerns the influence of large-scale integration of FRES on the global carbon price. Implementing a CO_2-limit induces long-term technological change. The possibility for extension of solar and wind power has a high impact on the CO_2-price. It has been shown that the reduction of the carbon price strongly correlates with the contribution of wind power. For instance, through supplying 50% of the global electricity demand in year 2025 with solar energy, CO_2 emissions can be reduced by 38% from the CO_2 emissions of year 2000 while the certificate price is 39% lower in comparison with an electricity generation system with a zero share of solar and wind energy but with a similar level of CO_2 emissions. If this share of electricity is satisfied with wind energy, the certificate price reduces by 63% while the same level of abatement is achieved.

When a time horizon from 2020 to 2040 is taken into account, optimization results show that wind energy is extensively employed to meet ambitious emissions reduction targets. In year 2020, total wind power capacity reaches to 4570 GW and rises to 15285 GW by 2040. Extension of wind power at this level allows limiting CO_2 emissions from the global electricity supply sector to 6107 million tons in 2020, i.e. 35% reduction from the emissions of year 2000; this reduces to 2067 million tons by 2040 while the CO_2-price rises to 61 €/ton. However, this can only be achieved if power transmission interconnections are extended far beyond the existing capacities. If the power transmission grid structure is not optimized, over-installation of capacities up to 18% is unavoidable to satisfy the proposed CO_2-limit in 2040. In this case, the CO_2-price significantly rises to 147 €/ton by the end of the time horizon.

It is worth mentioning that in the applied methodology, technical restrictions of power plants are not taken into account at a detailed level as in a short-term operation optimization model, e.g. based on the MILP approach. Therefore, the model optimizes the power transmission grid structure, capacity of power plants, and power production mix while technical restrictions of power plants are respected at a technology level rather than on a power plant basis as in a unit commitment problem. Thus, required investments in flexible generation plants and the marginal price of CO_2 emissions are underpredicted while the feasible share of FRES that can be integrated into the power system is overestimated. However, regarding the scale of the problem, these influences are very low in proportional terms (see section 2.5).

4.2.3 Integration of FRES into the global power system

Due to geographical dispersion and fluctuations of the primary energy source, large-scale integration of solar and wind power requires extensive adaptations. A parametrical study is performed in this part by varying the integration share of FRES and the renewable energy mix. The aim of this study is thus to determine the system adaptation needs in order to mitigate negative consequences caused by the power system integration of various shares of solar and wind energy and to achieve a specific level of CO_2 abatement. How much storage and/or power transmission capacity is needed and what would be the optimal energy mix and optimal geographic distribution of solar and wind power plants different boundary conditions are the questions that are covered in this part.

4.2.3.1 Scenario setup

To determine the feasible share and optimal combination of solar and wind power in a future global electricity system and to represent the required structural adaptation, a medium time horizon, the year 2025, is taken into account. Six to thirteen weeks are simulated to represent the whole year. Assumed techno-economic parameters and projected fuel prices are given in Table 4.7, Table D.1, Table D.2, and Table D.3. The ramp rate (technology-based) of power plants is given in Table 3.11. The availability factors, given in Table 3.11, are used to downscale the capacity of existing power plants due to periodic maintenance and forced outages. For inter-regional transmission of electricity, the costs of the 500kV HVDC technology, given in Table 3.13, are used.

To analyze worldwide influences of integrating different shares and combinations of FRES into the future electricity generation system and to investigate system adaptation needs, a two-dimensional parametrical study is performed, applying the methodology developed in chapter 2. The penetration share of FRES (*a*), given in equation (4.1), is a fraction of the global electricity demand, which is satisfied with FRES. This is calculated by obtaining the electricity produced from wind onshore, wind offshore, PV, and CSP minus the excess solar and wind power production; *b* is the share of wind energy in total power production from FRES, and it is given in equation (4.2). Total wasted energy (*EL*) is calculated in equation (4.3). This includes the excess electricity production as a fraction of the electricity produced from FRES that can neither be utilized at the time of generation, nor can be economically stored for later usage. It also includes the losses, occurring through energy storage and power transmission.

$$a = 1 - \frac{\sum_x \sum_{i \notin \mathrm{Pr}\, FRES} \sum_t E_i^{out}(x,t)}{\sum_x \sum_t dem(x,t)} \tag{4.1}$$

$$b = \frac{\sum_x \sum_t [E_{WIND}^{out}(x,t) + E_{WIND-O}^{out}(x,t)]}{\sum_x \sum_t [E_{WIND}^{out}(x,t) + E_{WIND-O}^{out}(x,t) + E_{SOL-PV}^{out}(x,t) + E_{SOL-CSP}^{out}(x,t)]} \tag{4.2}$$

$$EL = \sum_x \sum_{i \in \mathrm{Pr}\, PG} \sum_t E_i^{out}(x,t) - \sum_x \sum_t dem(x,t) \tag{4.3}$$

The penetration share of FRES (*a*) is varied from 0 to 90% of the global electricity demand in 10% intervals. For each case, the share of wind energy *(b)* is increased from 0 to 100% of total solar and wind power production. The share of electricity generation from FRES in total produced electricity and the renewable energy mix is forced through implementing a global system constraint (equations (2.30) and (2.31)).

Capacity expansion of solar and wind power plants at each region is limited to the corresponding geographical potential; thus, the geographic distribution of new capacities for solar and wind power production is optimized by the model. The model chooses the most promising sites to install solar and wind power plants according to the annual gain of energy, temporal fluctuations and correlation with regional electrical load profiles as well as proximity to the load centers. New investments of conventional power plants are also quantified through the optimization. Furthermore, it is assumed that nuclear and hydro power plants are not expandable beyond the operating capacities. New investments of geothermal power plants are restricted according to the planned capacities, given in [96].

In the baseline scenario, capacity expansion of power transmission lines and energy storage systems is not allowed; existing capacities are used as upper capacity boundaries. In a second set of scenarios, named “Link”, the capacity of energy storage systems is fixed as today; the focus is laid on the influence of a global grid to overcome challenges, arising due to the short-term variability of FRES, and to alleviate the problem of geographical dispersion. In a third set of scenarios, named “Storage”, the role of energy storage to provide inter-diurnal and inter-seasonal balancing needs is studied; in this scenario, extension of the power transmission network beyond the existing capacities is not allowed. In a fourth set of scenarios, named “Link-Storage”, the influence of capacity expansion of both power transmission lines and energy storage systems is studied. These are summarized in Table 4.11.

Table 4.11: Scenarios and underlying assumptions

Scenario	Optimization of power transmission capacities	Optimization of energy storage capacities
Base	No	No
Link	Yes	No
Storage	No	Yes
Link-Storage	Yes	Yes

4.2.3.2 Results

4.2.3.2.1 Wasted energy

At first, the influence of energy storage and an ideal global-link concept on the maximum feasible share of solar and wind power and wasted energy is studied. Fig. 4.37 shows the variation of total wasted energy in the parameter space for different scenarios. In all scenarios, total wasted energy is allowed up to 100% of the global electricity demand.

Fig. 4.37.a shows the results of the baseline scenario; the white area represents infeasible cases with a total wasted energy of higher than 100% of the global electricity demand. For instance, if limiting the maximum wasted energy to 100% of the global electricity demand, more

than 60% of the demand cannot be satisfied with FRES if the share of solar energy is higher than 90% of total solar and wind power production. This can be described according to the fact that an anti-correlation exists between the seasonal pattern of electricity load and the seasonal pattern of solar electricity production. Most of the consuming regions are characterized with a higher load in winter than in summer (see section 3.2). Furthermore, solar irradiation is only available during the day time. Thus, in the baseline scenario, assuming that no possibility exists for capacity expansion of energy storage systems or the power transmission interconnections to provide the required balancing needs, a high share of solar energy is not feasible.

With inclusion of the possibility for extension of energy storage capacities or the power transmission interconnections, higher shares of FRES become feasible and wasted energy is significantly reduced. For instance, in scenario “Storage”, 90% of the global electricity demand can be satisfied with solar electricity while wasted energy reaches to 60% of the global electricity demand (see Fig. 4.37.c). If power transmission capacities are optimized (Fig. 4.37.b), total wasted energy reduces even further mainly at FRES shares of higher than 70% and when the renewable energy mix is dominated by wind energy (*b>70%*). However, in the baseline scenario, the maximum wasted energy reaches to 100% of the global electricity demand when the parameters (*a)* and (*b)* reach to 90% and 50%, respectively. This is significantly higher than the wasted energy, occurring in scenarios “Link” and “Storage” at the same penetration share of solar and wind power. It can also be concluded that when power transmission capacities are optimized while energy storage capacities are fixed as today, at FRES shares of mainly higher than 60% of the demand, higher shares of wind power are favourable due to the lower amount of wasted energy.

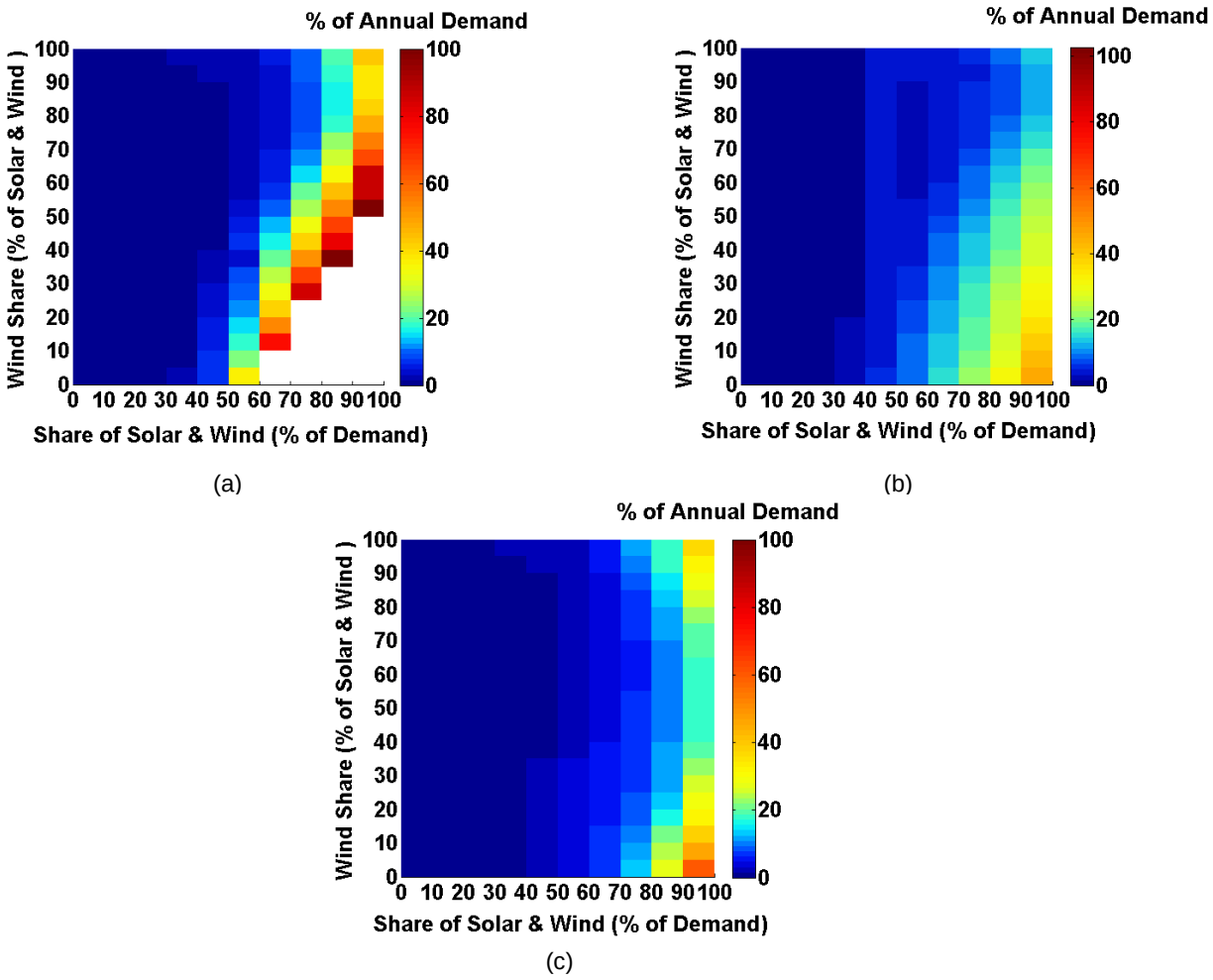

Fig. 4.37: Two-dimensional representation of total wasted energy (a) Scenario “Base”; (b) Scenario “Link”; (c) Scenario “Storage”

To make a comparison between scenarios “Link” and “Storage”, the three-dimensional representation of total wasted energy is visualized in Fig. 4.38. The total wasted energy rises rather exponentially when increasing the share of FRES while its steepness is influenced by the renewable energy mix and available regulating systems. It is seen that at any given share of FRES, wasted energy decreases when increasing the share of wind energy till it reaches a minimum; it remains nearly constant within a range and rises afterwards. This effect is more pronounced and the extent of variation around the minimum is higher at FRES shares of higher than 50%. Finally, it can be concluded that at any given share of FRES, wasted energy is minimized at a specific combination of solar and wind power, which is highly dependent on available regulating systems. In scenario “Storage”, optimal combination of solar and wind power in terms of avoiding wasted energy is generated when the share of wind varies between 45% and 85% of total solar and wind power production. For instance, when 90% of the global electricity demand is satisfied with FRES, the minimum occurs at 50% contribution share of wind power. In scenario “Link”, the minimum is shifted towards higher shares of wind power. This clarifies how we can benefit from different fluctuating patterns of solar and wind energy in combination with an optimal geographic distribution of renewable power plants adapted to available regulating systems.

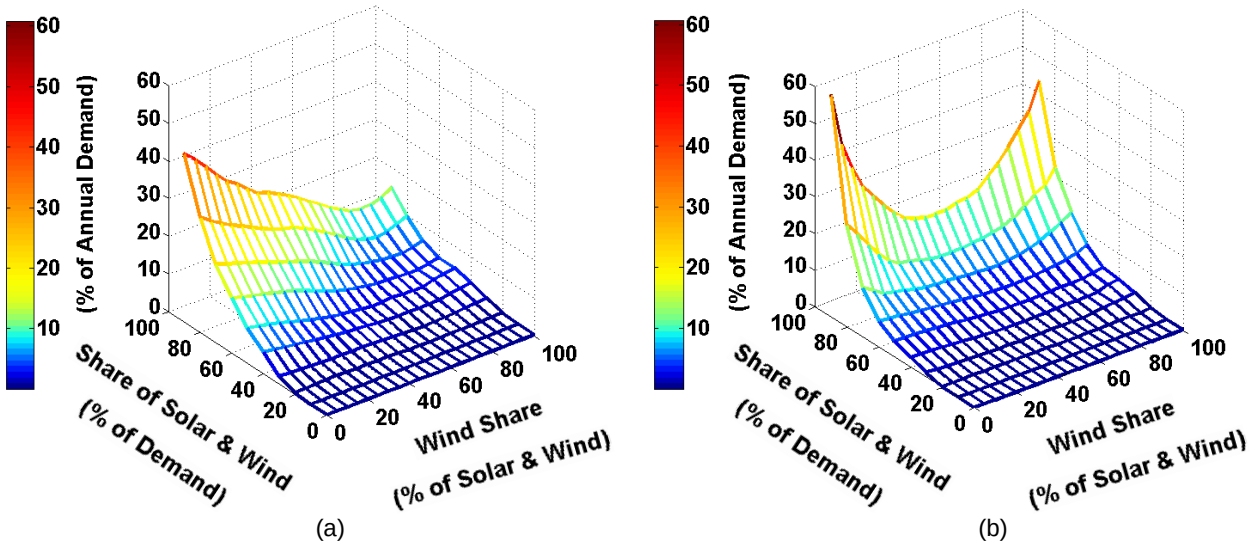

Fig. 4.38: Three-dimensional representation of total wasted energy (a) Scenario "Link"; (b) Scenario "Storage"

It is concluded that the optimal mix of solar and wind power that leads to the minimum wasted energy highly depends on available capacities for energy storage and the possibility for inter-regional power transmission. When the total area is interconnected in scenario "Link", the optimal renewable energy mix is characterized with a higher share of wind power as compared to the base case. If energy storage capacities are optimized while power transmission capacities are fixed as today as in scenario "Storage", wasted energy is minimized at even lower contribution shares of wind energy as compared to the reference scenario. Table 4.12 represents the optimal renewable energy mix in terms of minimal wasted energy at FRES shares of higher than 50% of the global electricity demand for different scenarios.

Table 4.12: Optimal renewable energy mix in terms of minimal wasted energy (b_{MinEP})

a (% of demand)	b (% of solar and wind) Scenario Base	b (% of solar and wind) Scenario Link	b (% of solar and wind) Scenario Storage
50	70	80	60
60	75	85	60
70	80	90	60
80	80	85	50
90	85	85	50

Wind energy is more abundant than solar energy, but it is characterized with a highly variable pattern. In scenario "Link", assuming that energy storage capacities cannot be expanded beyond today, the power transmission grid is mainly used to make an optimal usage of de-correlations between short-term variations of wind power at distant locations. However, higher shares of solar energy become favorable when the possibility for electricity exchange between the regions is restricted as in the base case or in scenario "Storage". This is mainly due to the less stochastic nature of solar energy as compared to wind energy and the positive correlation between the daily pattern of electricity load and that of solar irradiation. When the capacity of energy storage facilities is optimized to compensate for temporal mismatch between the

demand and supply, solar electricity becomes even more competitive. In scenario “Storage”, electricity is produced in proximity to the load centers, and energy storage is applied to buffer any temporal mismatch between production and consumption.

4.2.3.2.2 Power transmission grid structure

Fig. 4.39 shows the optimal geographic distribution of solar and wind power plants in scenario “Link”. In this case, 60% of the world electricity demand is satisfied with FRES while the share of wind reaches to 85% of total solar and wind power production. This is an optimal renewable energy mix in terms of minimal wasted energy (see Table 4.12). Solar thermal power plants are mainly installed in North Africa due to the high gain of irradiation and possibility for power transmission to the load centers of Europe. High capacities for wind electricity production are installed at the main load centers of China, Europe, and USA as well as in Argentina, where the technical potential of wind electricity production is very high and exceeds the local electricity demand.

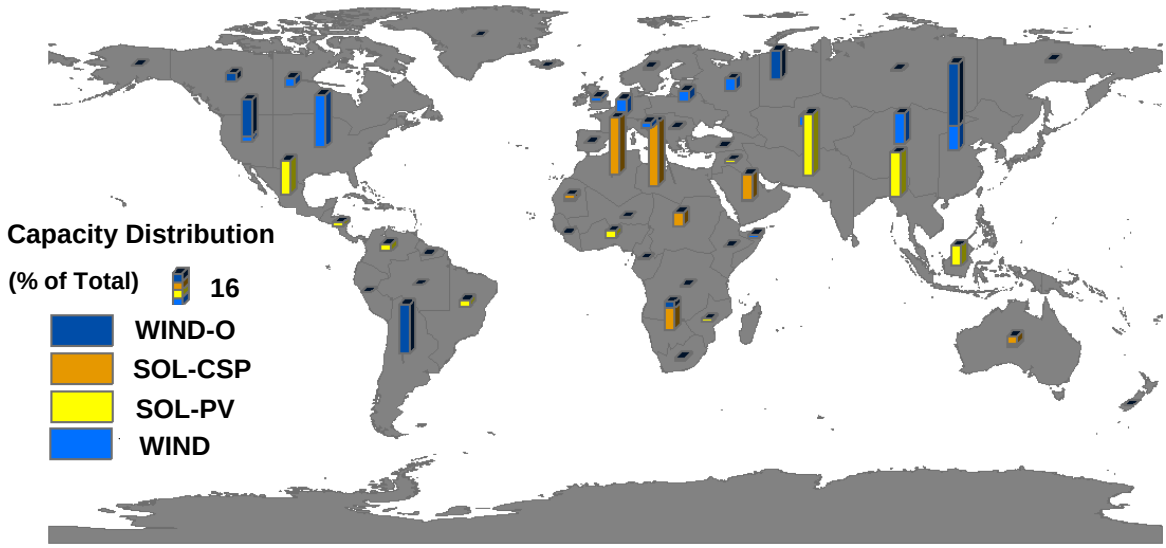

Fig. 4.39: Optimal geographic distribution of solar and wind power plants in scenario “Link” (a=60%, b=85%)

Power transmission capacities, installed between the regions, are visualized in Fig. 4.40 and Fig. 4.41. Correspondingly, inter-regional power transmission lines with a maximum capacity of 168 GW are installed to transmit wind and solar electricity from generation sites to the distant consuming regions (see Fig. 4.40.a). However, at a low share of FRES, power production is mainly centralized; as a result, the capacity of power transmission lines significantly reduces, and the grid becomes more homogenous (Fig. 4.40.b).

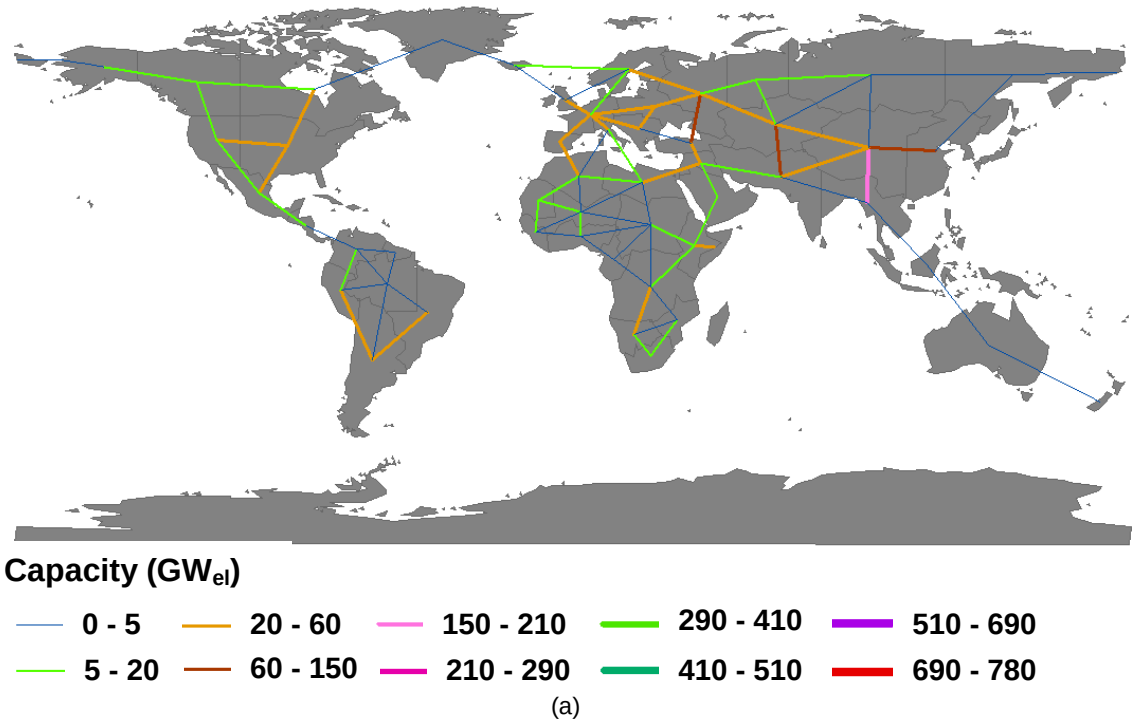

Capacity (GW_{el})

0 - 5 | 5 - 20 | 20 - 60 | 60 - 150 | 150 - 210 | 210 - 290 | 290 - 410 | 410 - 510 | 510 - 690 | 690 - 780

(a)

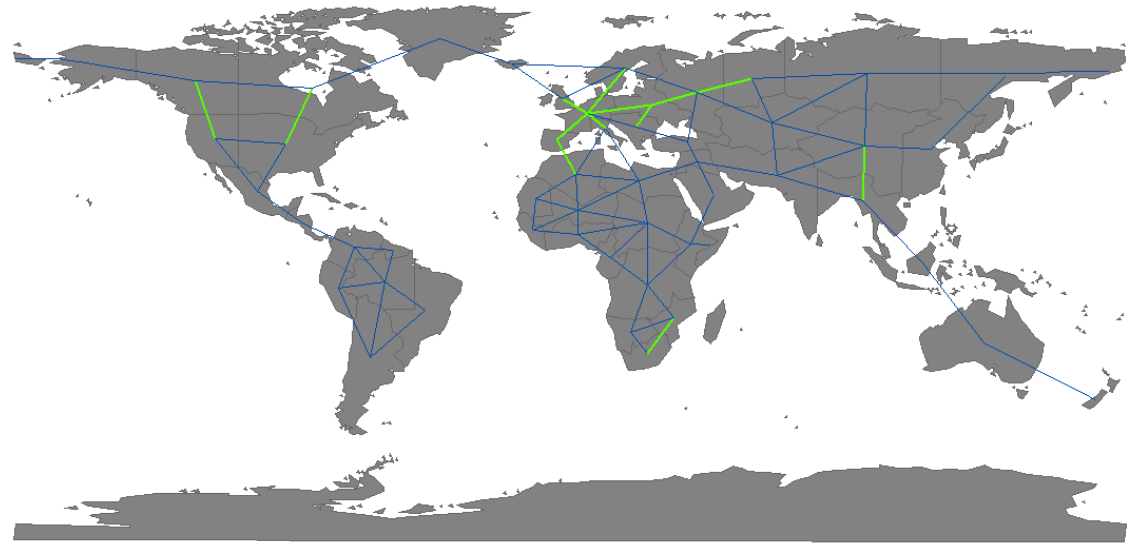

Capacity (GW_{el})

0 - 5 | 5 - 20 | 20 - 60 | 60 - 150 | 150 - 210 | 210 - 290 | 290 - 410 | 410 - 510 | 510 - 690 | 690 - 780

(b)

Fig. 4.40: Optimal power transmission grid structure in scenario “Link” (a) a=60%, b=85%; (b) a=20%, b=85%

When the share of solar energy is increased, one interesting feature is the high capacities installed to transmit wind electricity from Alaska offshore sites through Far East to the main load center of eastern China. Furthermore, the electricity produced from “SOL-PV” and “SOL-CSP” power plants cannot be stored; therefore, high capacities are required to transmit the power at peak-load time steps to interconnected regions with a high level of demand but low gain of irradiation. As a result, significantly high capacities are installed to transmit solar electricity from North Africa through Southern Europe to Western and Central Europe. The same situation

exists to transmit solar electricity from Central America to the U.S. as well as the link between Australia and South East Asia (Fig. 4.41).

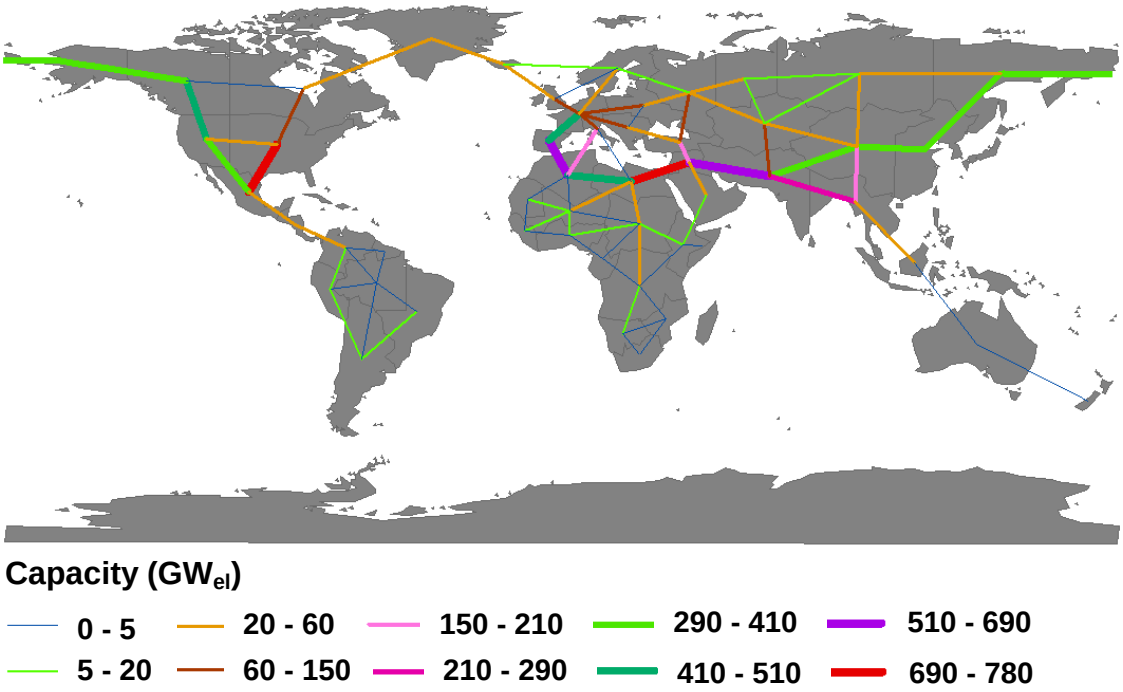

Fig. 4.41: Optimal power transmission grid structure in scenario “Link” (a=60%, b=10%)

Aggregated inter-zonal power transmission capacities are shown in Fig. 4.42.a. As expected, when increasing the share of FRES, the total power transmission capacity increases. For instance, if the penetration share of FRES is 50% of the global electricity demand, the total inter-zonal power transmission capacity reaches to 6884 GW and 1219 GW when the share of wind is 0% and 100% of total solar and wind power production, respectively. Proportion of the total investment and fixed costs of inter-zonal power transmission lines to the total investment and fixed costs of power generation and energy storage systems is shown in Fig. 4.42.b. This proportion is the highest when the share of FRES varies in the range of 50%-100% of global electricity demand and the share of solar energy varies from 60% to 100% of total solar and wind power production. Overall, it remains below 8% for a dominant share of the parameter space.

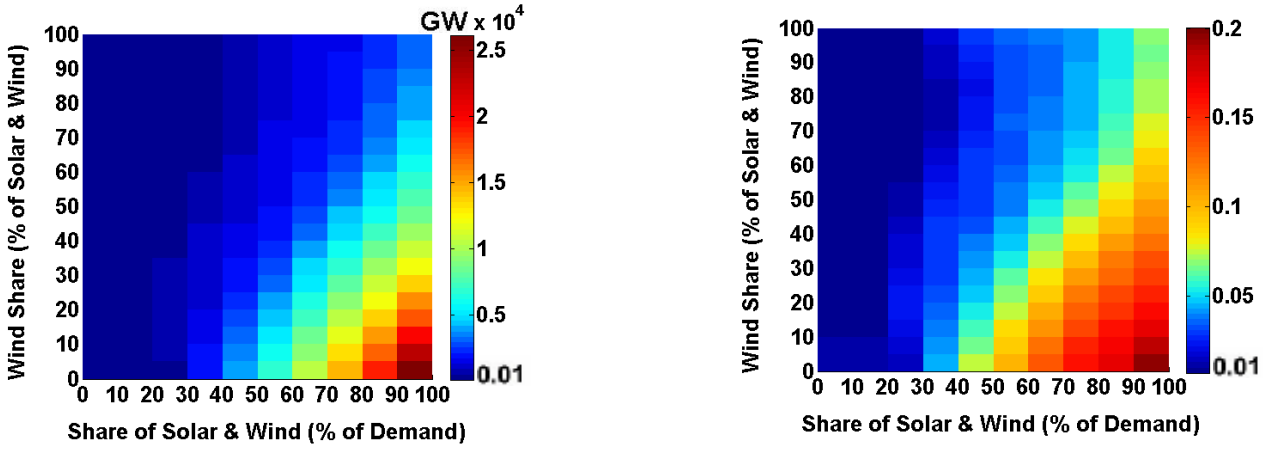

Fig. 4.42: Scenario "Link" (a) Total inter-zonal power transmission capacity; (b) Proportion of total investment and fixed costs of power transmission to investment and fixed costs of power generation and storage

4.2.3.2.3 Required backup and renewable power generation capacity

Another key factor is the backup capacity required to allow integrating a specific share of FRES into the power system. Fig. 4.43 shows the total new backup capacity as a function of the penetration share of solar and wind power in scenarios "Base" and "Link".

The total backup capacity, newly installed in baseline scenario, is shown in Fig. 4.43.a. Again, the white area represents infeasible cases with a total wasted energy of higher than 100% of the global electricity demand as in Fig. 4.37.a. The maximum and minimum required backup capacity is 50% and 10% of the global peak demand, respectively. It remains mainly higher than 30% in the feasible area of the parameter space. According to Fig. 4.43.b, in scenario "Link", the new backup capacity varies from 0% to 43% of the maximum global electricity demand. It remains below 30% for a dominant share of the parameter space. It can be concluded that in all scenarios, at any given share of FRES, the required backup capacity reduces when increasing the share of wind power. This effect becomes even more evident if the share of FRES is higher than 40% of the global electricity demand.

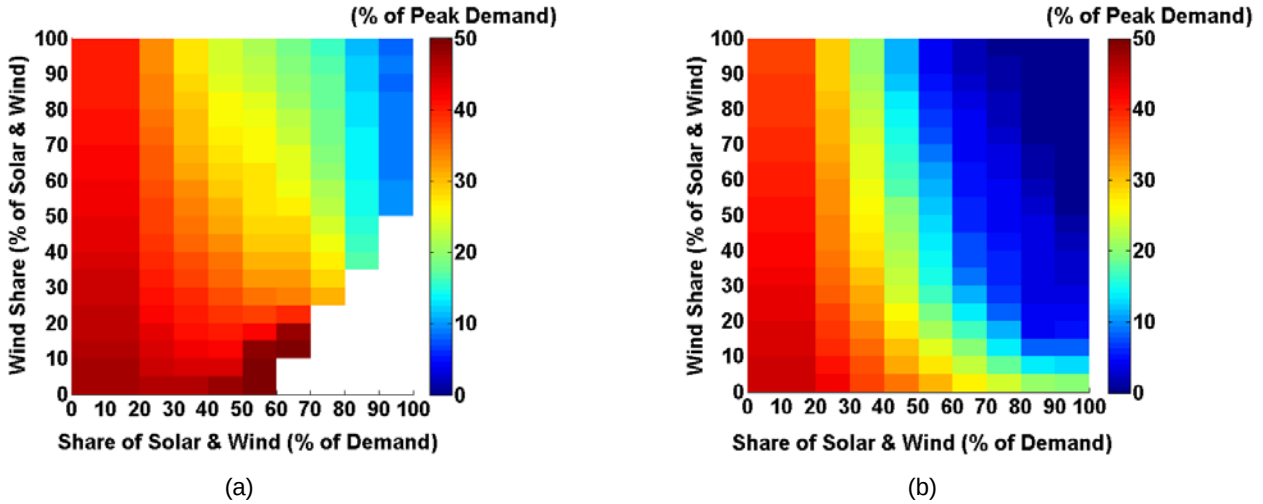

Fig. 4.43: Total new backup capacity as a percentage of global peak demand (a) Scenario "Base"; (b) Scenario "Link"

The share of coal and gas combined-cycle in total new backup capacity is shown in Fig. 4.44. When increasing the power production from FRES, utilization of thermal power plants is reduced. As a result, investment decisions in electricity generation systems are more and more affected by the investment and fixed costs of power plants rather than their variable operation costs. Thus, the capacity share of coal-fired power plants continuously reduces, and gas combined-cycle power plants are installed instead.

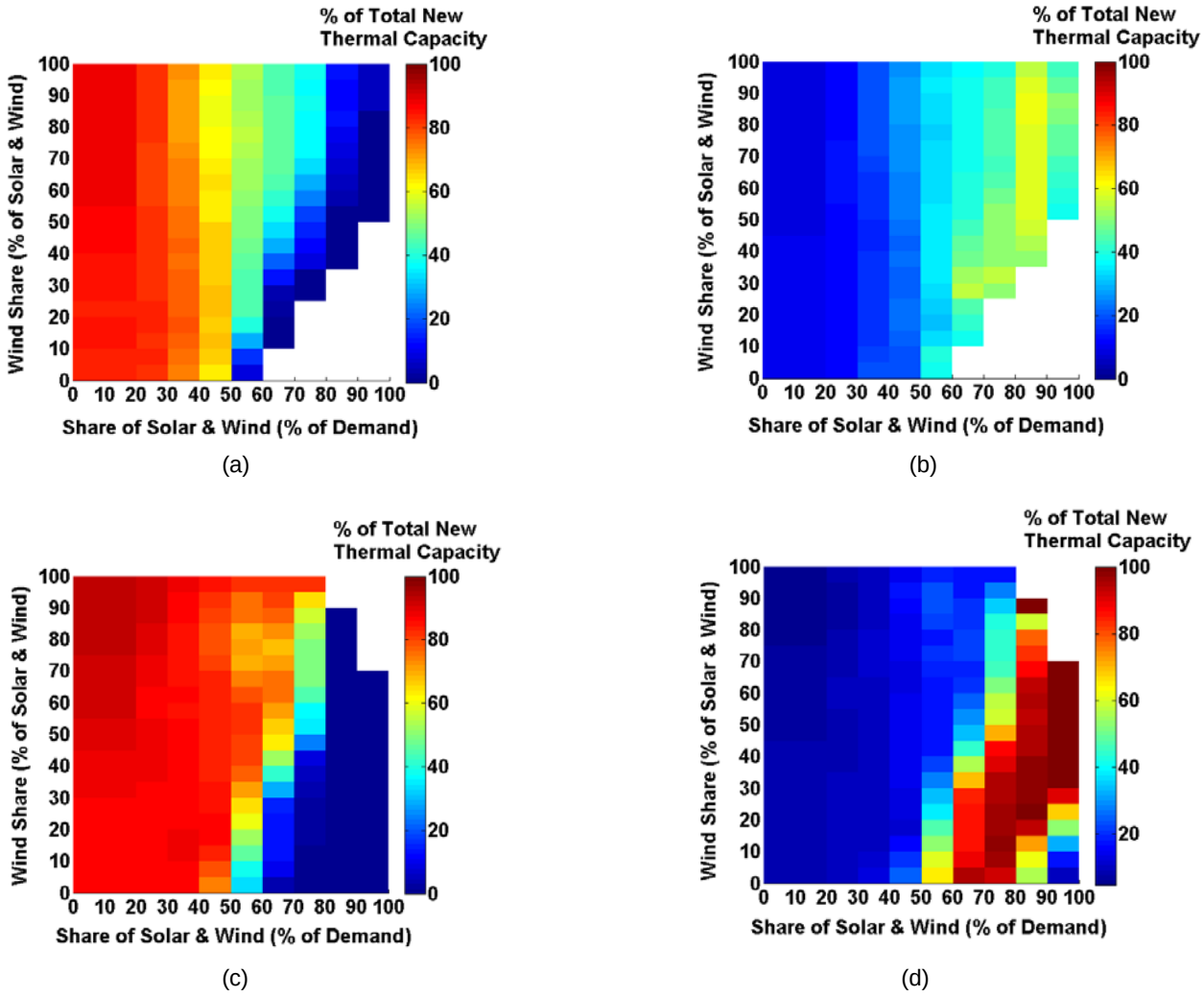

Fig. 4.44: Capacity share of “COAL-ST” and “GAS-CC” in total new backup capacity (a) “COAL-ST” share in baseline scenario; (b) “GAS-CC” share in baseline scenario; (c) “COAL-ST” share in scenario “Link”; (d) “GAS-CC” share in scenario “Link”

Total solar and wind power generation capacity in scenarios “Base” and “Link” is shown in Fig. 4.45. This is identical to the pattern of total wasted energy, visualized in Fig. 4.37. Total renewable power and new backup capacities must be installed according to Fig. 4.43 and Fig. 4.45 to allow integrating the corresponding share of solar and wind power.

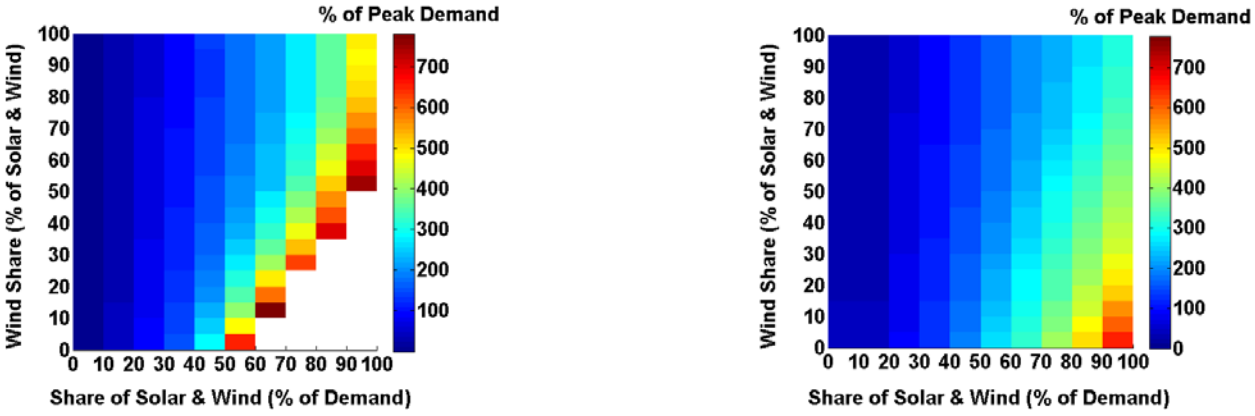

Fig. 4.45: Total solar and wind power generation capacity as a percentage of global peak demand (a) Scenario "Base"; (b) Scenario "Link"

4.2.3.2.4 CO_2 emissions

According to Fig. 4.46, the share of fossil fuel power generation in total produced electricity reduces in general when increasing power production from solar and wind energy. For instance, in Fig. 4.46.a, power production from coal continuously reduces in pace with an increasing generation from FRES.

According to Fig. 4.46.b and Fig. 4.46.c, at any given share of FRES, when increasing the power production share of solar energy, utilization of nuclear and lignite-fired power plants continuously decreases. This mainly occurs when the share of FRES exceeds 50% and 20% of the global electricity demand, respectively. Increasing the share of wind energy allows a lower utilization of gas-fired power plants, and the power production from base load power plants such as nuclear and hydro is increased as compared to a renewable energy mix, which has a higher share of solar energy. Indeed, due to the positive correlation between the diurnal pattern of electricity load and the daily pattern of solar irradiation, there is a full integration of solar energy during hours of peak load when a high share of solar energy is integrated into the power system. This leads to the reduction of operation time of base load power plants. However, in winter period and during hours with no gain of irradiation, the electricity demand must be satisfied with additional capacities of peak-load generators such as gas-fired power plants. Wind power production has a timely pattern, which is more evenly distributed between the hours of day and night and through different seasons. Hence, when increasing the share of wind energy, total power production from gas-fired plants can be reduced from its contribution at higher shares of solar energy.

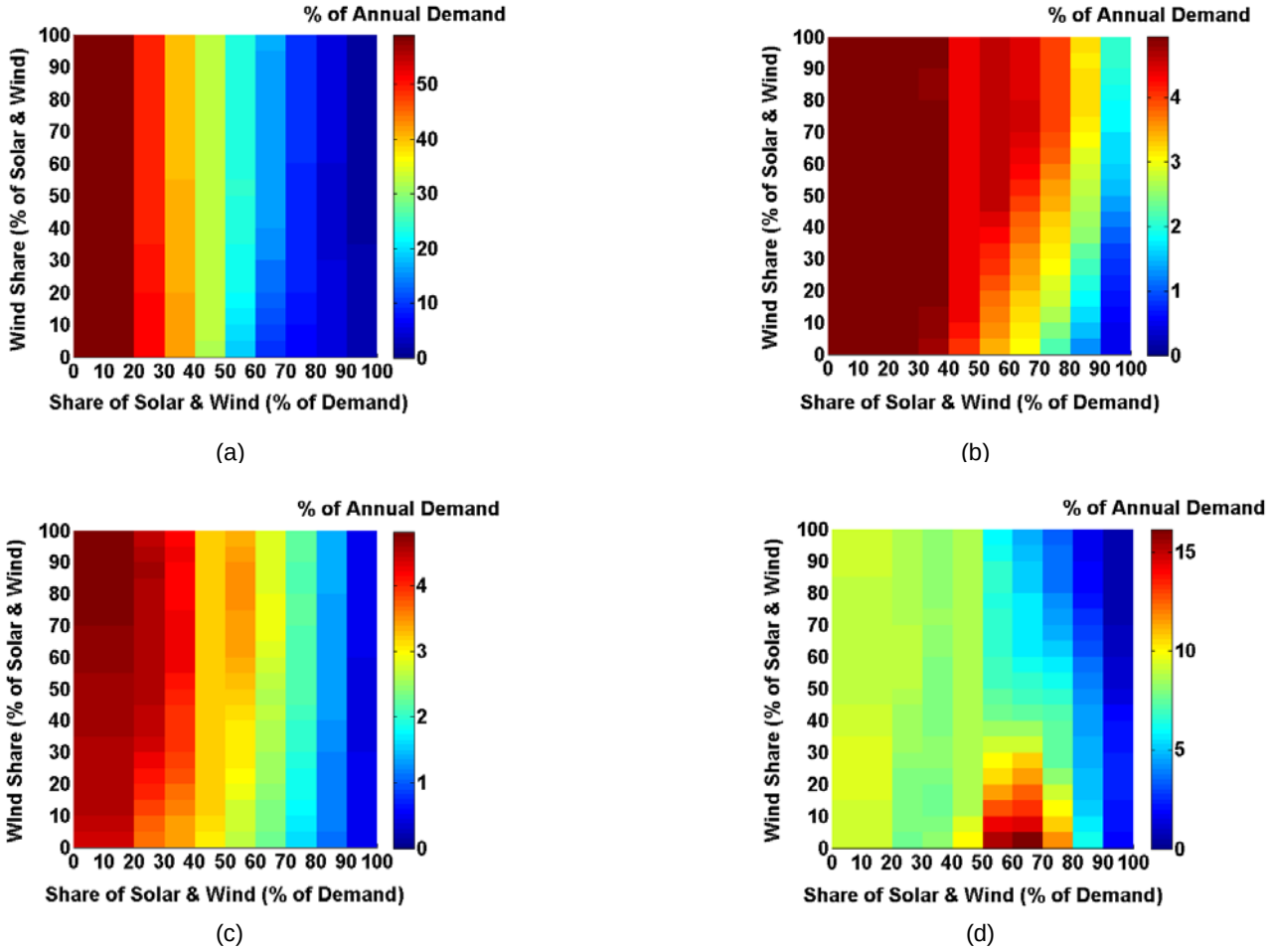

Fig. 4.46: Power production share of fossil-fired power plants in scenario “Link” (a) “COAL-ST”; (b) “URA-ST”; (c) “LIG-ST”; (d) “GAS-CC”

The electricity produced from FRES substitutes the fossil fuel power generation and leads to the reduction of total CO_2 emissions. For instance, total annual CO_2 emissions in scenario “Link” are shown in Fig. 4.47. The CO_2 abatement is mainly caused by the reduced utilization of coal-fired power plants, which mainly starts from a FRES share of 20%. It is seen that a significant reduction of total CO_2 emissions occurs when the penetration share of FRES exceeds 50% of the global electricity demand. At 50% penetration share of FRES, power production from coal is lower than 17% of the total electricity demand.

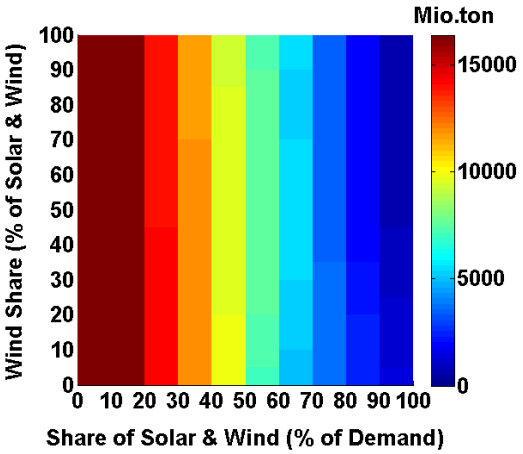

Fig. 4.47: Total annual CO_2 emissions in scenario “Link”

4.2.3.2.5 Total system costs

Total annual system costs are shown in Fig. 4.48. Over-installation of renewable power plants and backup capacities in baseline scenario implies higher system costs as compared to scenario “Link”. This effect is evident when the share of FRES is higher than 50% of the global electricity demand and if the renewable energy mix is dominated by solar energy. To clarify this effect, total system costs in baseline scenario are subtracted from the total costs in scenario “Link” and are represented as a percentage of total system costs in the former scenario in Fig.4.48.c. Furthermore, it is concluded that in both scenarios, increasing the share of wind power results in lower system costs. This effect is more evident if the penetration share of FRES is higher than 50%.

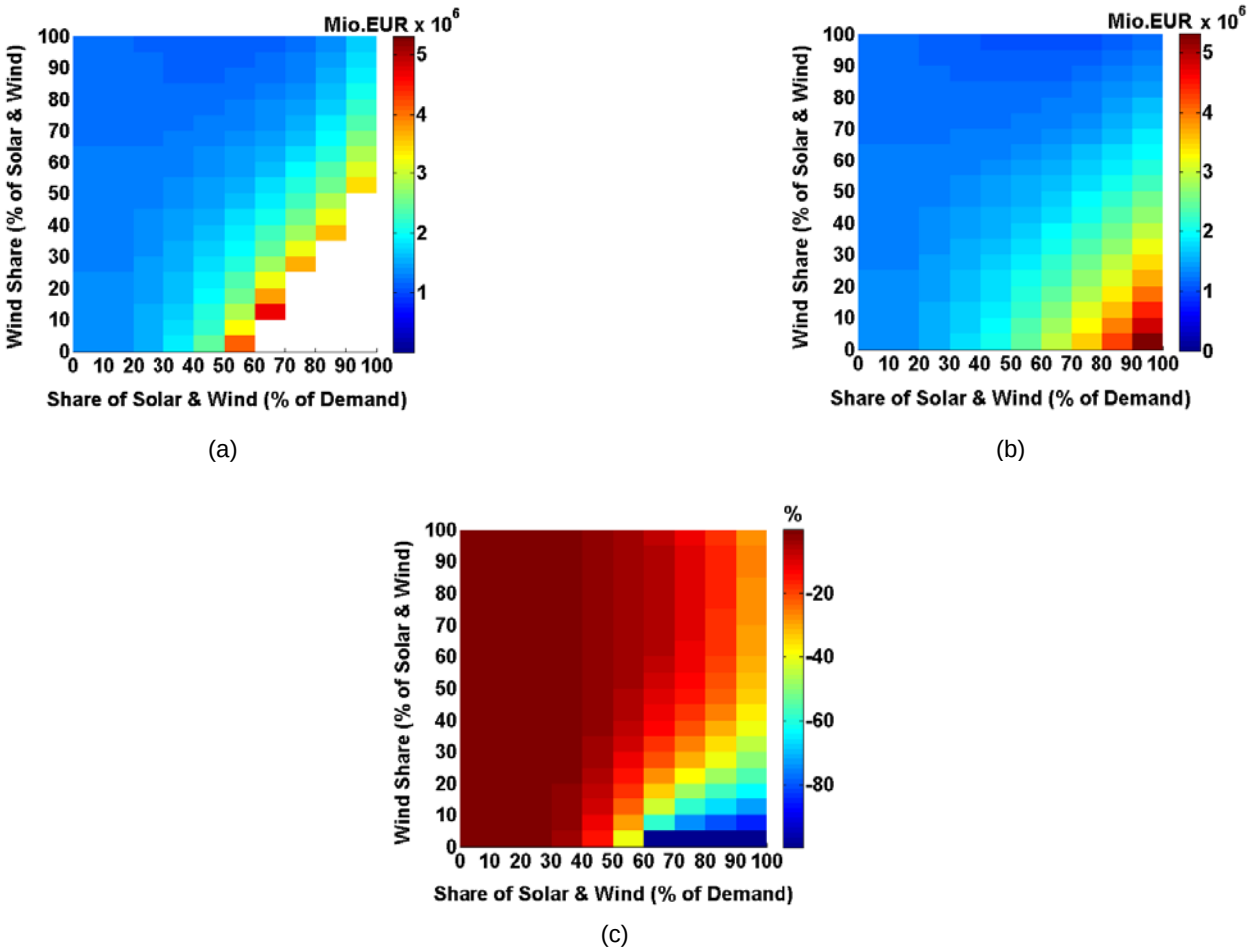

Fig. 4.48: Total annual system costs (a) Scenario “Base”; (b) Scenario “Link”; (c) Relative cost difference between “Link” and “Base”

4.2.3.2.6 Combined influence of inter-regional power transmission and energy storage

So far, optimization of the power transmission network structure or the capacity expansion of energy storage systems have been performed in separate scenarios named “Link” and “Storage”. In this part, the focus is laid on the combined influence of an optimal global grid and capacity expansion of energy storage systems.

To reduce the calculation time, specific scenarios are selected from the total parameter space. The capacity of inter-regional power transmission lines is increased step by step, starting from existing capacities and moving towards the optimal grid capacities, obtained from the scenario “Link”. The energy storage capacities are then optimized for each selected share of solar and wind power. Thus, in the following figures, the vertical axis represents the results of scenario “Storage”, where the capacity of energy storage systems is optimized and the capacities of inter-regional power transmission lines are fixed as today. In scenarios, locating at the right end of the horizontal axis, energy storage capacities are optimized while grid capacities are fixed at the optimal levels, obtained from the scenario “Link”. Other underlying assumptions remain unchanged as in previous subsections. A sensitivity study is also performed on the costs of energy storage systems. In baseline scenario, actual costs of the “HP-PS” technology are used (see Table 4.3). In another scenario, these are reduced by 40%.

Total storage output capacity and energy content of the reservoir are shown in Fig. 4.49 and Fig. 4.50. Reduction of the costs by 40% results in a significant increase of new capacities of energy storage systems. In most cases, the total storage capacity continuously declines when increasing the power transmission capacities. This effect is more evident at higher shares of FRES. It is finally concluded that huge capacities must be dedicated to energy storage to facilitate integrating a high share of FRES into a future global power system if capacity expansion of power transmission lines is not taken into account. However, with an ideal global grid, for instance, according to Fig. 4.50, the total storage capacity could be reduced by 89% at the highest integration share of wind power (*a=90% and b=100%*).

It can also be concluded that at any given share of FRES, the total storage capacity rises when increasing the share of solar energy. This can be described according to the fact that solar power plants are mainly installed near to the load centers; energy storage is then applied to buffer any temporal mismatch between the local demand and energy supply. However, wind is always blowing somewhere. The model prefers to transmit wind electricity from a generation site, where the produced electricity overweight the local demand, to a distant location that is short of generation, rather than storing wind energy for local usage in a later period. The power transmission grid is then mainly used to make an optimal usage of spatial de-correlations of short-term variations of wind power production.

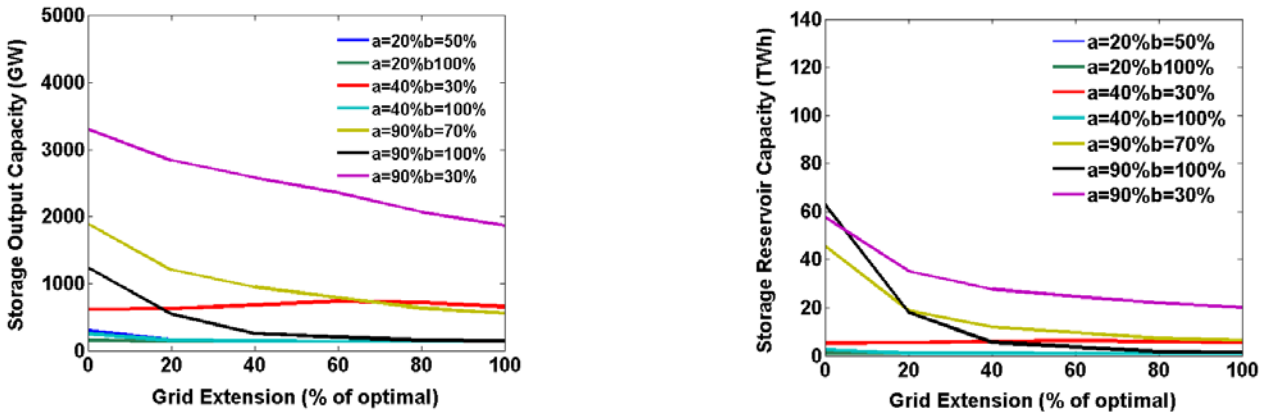

(a) (b)

Fig. 4.49: Storage capacity at actual costs (a) Storage output capacity; (b) Storage reservoir capacity (The worldwide capacity of "HP-PS" is 137 GW_{el} [96].)

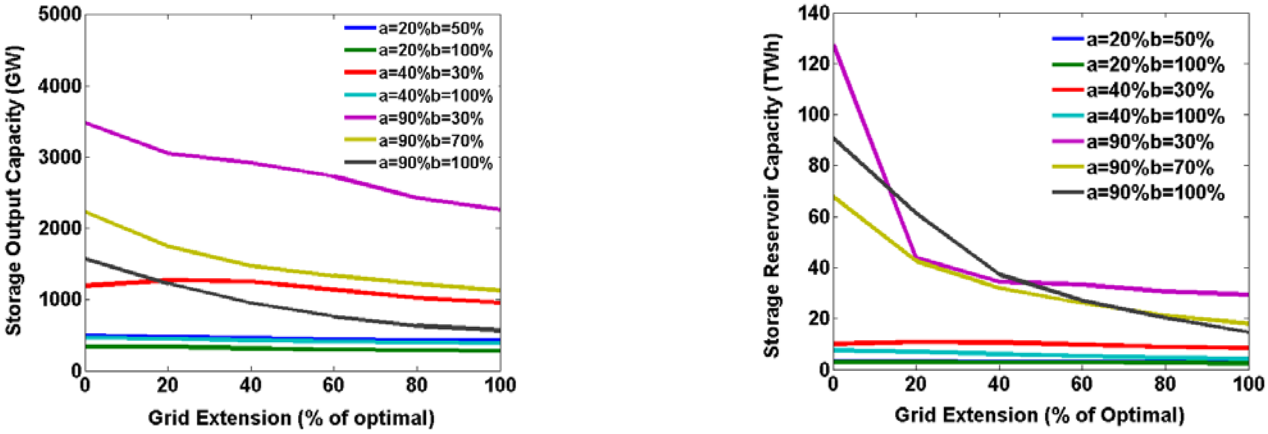

(a) (b)

Fig. 4.50: Storage capacity at reduced costs (a) Storage output capacity (b) Storage reservoir capacity (The worldwide capacity of "HP-PS" is 137 GW_{el} [96].)

According to Fig. 4.51.a, total discarded solar and wind power reduces when increasing the power transmission capacities. This effect is more evident if a high share of FRES is integrated into the power system, and if the renewable energy mix is dominated by wind energy. When these circumstances are satisfied, the reduced amount of discarded energy overweight the increasing level of power transmission losses. However, in other scenarios, total discarded solar and wind power plus the energy losses, occurring through power transmission and storage, continuously rises when increasing the grid capacities (see Fig. 4.51.b).

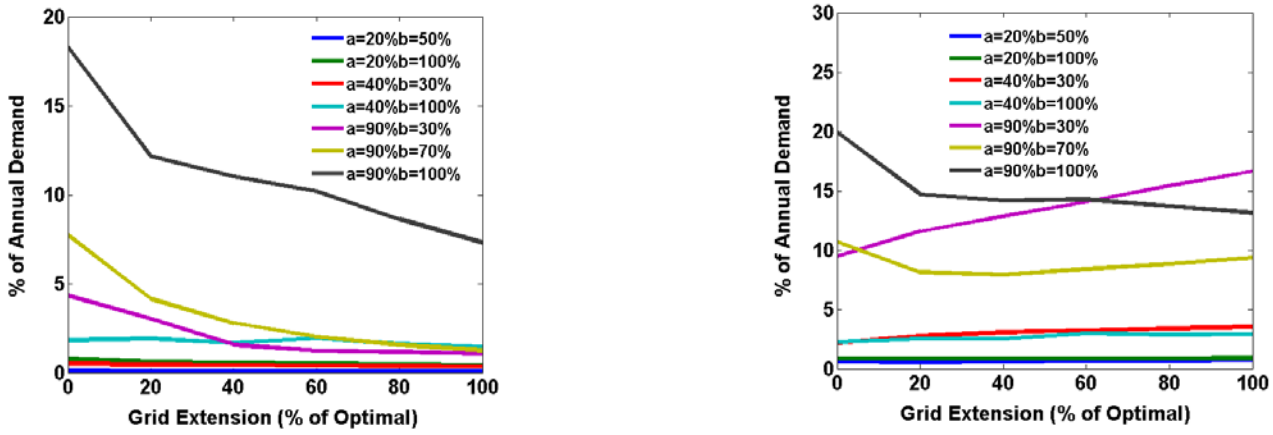

(a) (b)

Fig. 4.51: Discarded solar and wind power and energy losses (a) Total discarded solar and wind power; (b) Total wasted energy i.e. discarded solar and wind power plus power transmission and storage losses

Fig. 4.52 shows the new backup capacities and total solar and wind power generation capacities as a function of the total new capacity of inter-regional power transmission lines. When increasing the possibility for electricity exchange between the regions, the total capacity required for backup purposes as well as for solar and wind power generation reduces in all scenarios.

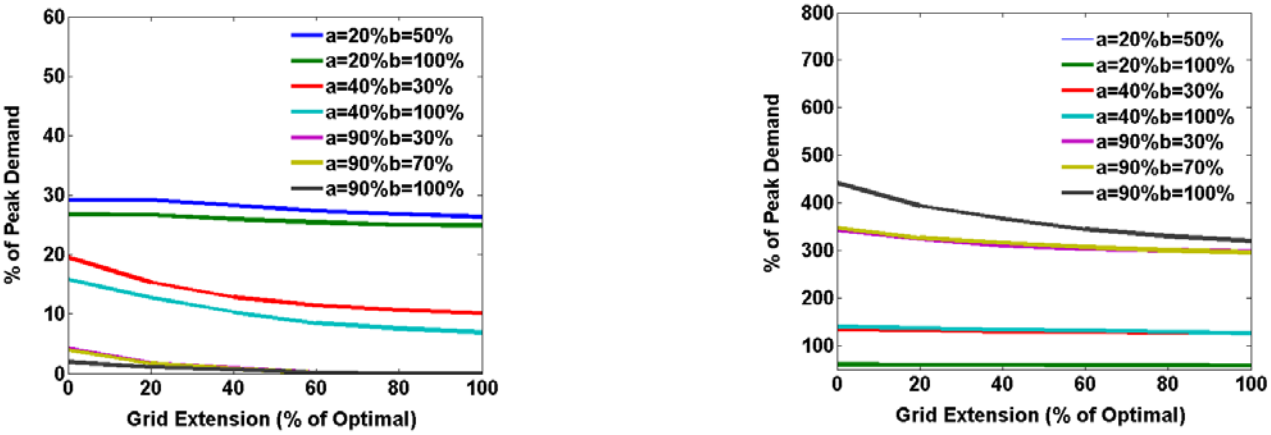

Fig. 4.52: Total power generation capacity (a) New backup capacity; (b) Solar and wind power generation capacity

Reduced utilization of fossil-fired power plants due to a higher generation from FRES leads to the reduction of CO_2 emissions. The combined influence of an optimal capacity expansion of energy storage systems and an optimal power transmission grid structure on total CO_2 emissions is visualized in Fig. 4.53. The influence of an optimal storage capacity adapted to the step-wise increase of power transmission capacities is compared with the results of scenario "Storage" and is illustrated in Fig. 4.53.b. It can be concluded that the grid extension results in additional CO_2 emissions abatement mainly at higher shares of FRES (*a>40%*), and its influence (steepness of the line) increases with further contribution of wind power.

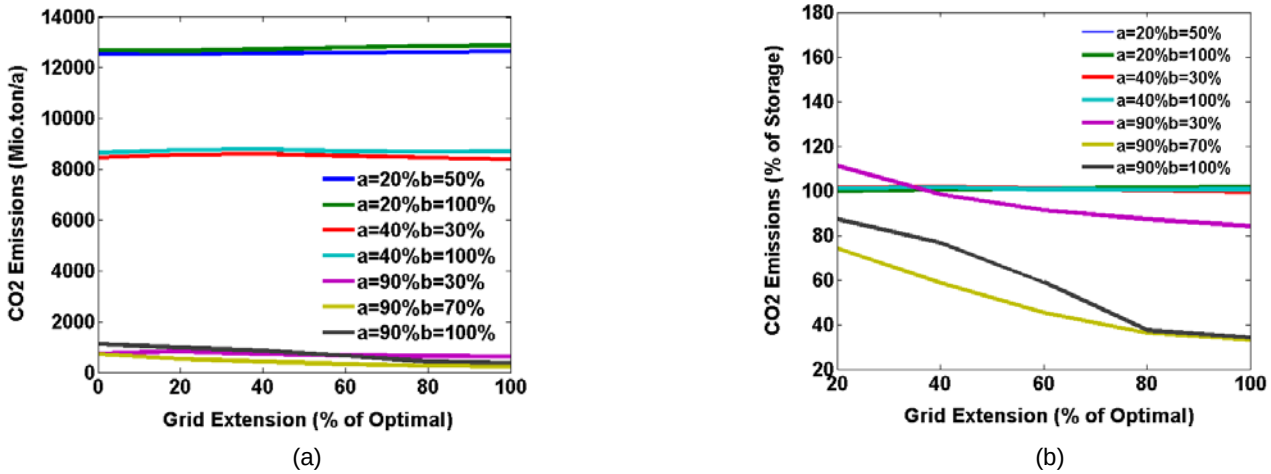

Fig. 4.53: Total annual CO_2 emissions (a) Absolute values; (b) Represented as a percentage of CO_2 emissions in scenario "Storage"

The relative system costs are shown in Fig. 4.54 as a function of total new inter-regional power transmission capacities. In Fig. 4.54.a, the costs are represented as a percentage of total system costs in baseline scenario (see Fig. 4.48.a. for absolute levels). Fig. 4.54.b shows the total system costs as a percentage of the costs, occurring in scenario "Storage". According to this, the influence of storage-only extension can be compared with the impact of an optimal

expansion of storage capacities adapted to an increasing capacity of inter-regional power transmission lines.

If only the storage capacities are optimized, total system costs can be reduced to 40% of the costs in baseline scenario when *a=90%* and *b=30%*. As demonstrated before, over-installation of renewable power plants and backup capacities in baseline scenario leads to a significant increase of total system costs mainly when the penetration share of FRES is higher than 50%, and if the renewable energy mix has a dominating share of solar energy. However, if the storage capacity is optimized, the total capacity of renewable and backup power plants can be reduced. This can be understood by comparing Fig. 4.52 with Fig. 4.43 and Fig. 4.45. This finally leads to the reduction of total system costs in scenario "Storage" as compared to the base case. When the storage capacity is optimized while the level of expansion is adapted to the step-wise increase of power transmission capacities, total system costs reduce even further from the costs, occurring in scenario "Storage". According to Fig. 4.54.b, this effect mainly occurs when the share of FRES is higher than 40% of the global electricity demand, and if the wind share is higher than the contribution of solar energy.

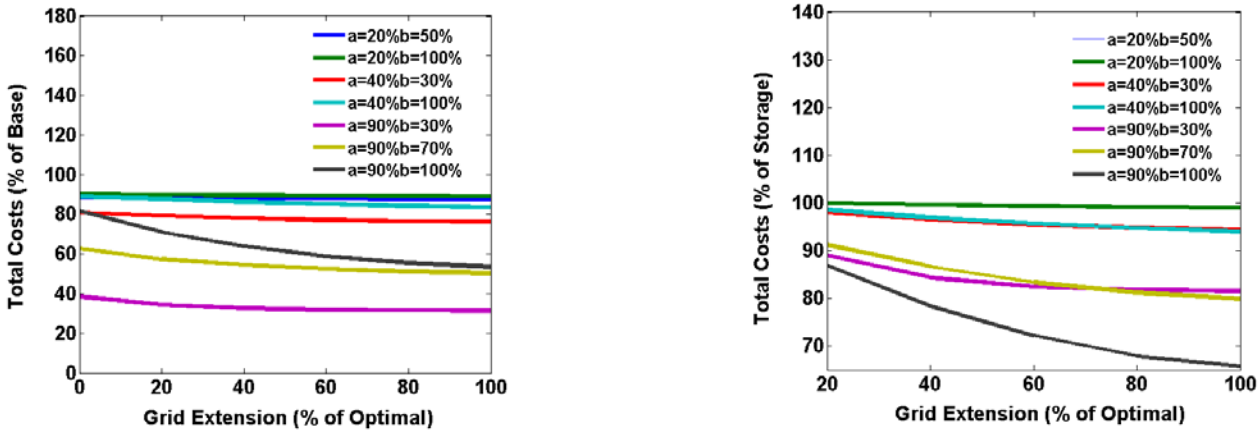

(a) (b)

Fig. 4.54: Relative total system costs (a) Represented as a percentage of total costs in scenario "Base"; (b) Represented as a percentage of total costs in scenario "Storage"

Finally, in Table 4.13, the combined influence of an optimal capacity expansion of energy storage systems and an optimal power transmission grid structure is compared with the influence of grid-only extension. In Table 4.13, different characteristics of the power system are compared between the scenarios "Link" and "Link-Storage". In the latter, the storage capacity is optimized while the inter-regional power transmission capacities are fixed at the optimal levels, obtained from the scenario "Link".

Table 4.13: Scenario “Link” vs. scenario “Link-Storage”

Scenario	Link			Link-Storage		
	Wasted energy incl. transmission/storage losses (% of annual load)	CO_2 emissions (% of Base)	Total costs (% of Base)	Wasted energy incl. transmission/storage losses (% of annual load)	CO_2 emissions (% of Base)	Total costs (% of Base)
a=20%b=50%	3.18	90.37	89.28	0.75	90.17	87.63
a=20%b=100%	3.26	91.82	91.31	0.91	92.56	89.07
a=40%b=30%	6.35	80.12	77.01	3.52	84.97	76.27
a=40%b=100%	5.56	91.92	84.45	2.90	92.34	83.58
a=90%b=30%	29.99	73.03	38.24	16.61	54.38	31.45
a=90%b=70%	14.63	35.18	51.26	9.35	20.74	50.24
a=90%b=100%	13.15	30.35	53.55	12.60	30.14	52.40

4.2.3.3 Conclusions

The developed methodology in chapter 2 has been applied to study the influences of an ideal global grid and energy storage systems to mitigate negative consequences caused by the power system integration of FRES. A parametrical study has been performed by varying the integration share of FRES and the renewable energy mix. This analysis has been made for a medium time horizon to determine the optimal energy mix, CO_2 emissions abatement, and system adaptation needs of a future global electricity generation system, which integrates different shares and combinations of solar and wind power. Towards this aim, the results of different scenarios with the possibility for extension of the power transmission network and/or energy storage facilities as well as a reference scenario based on the existing capacity of power transmission lines and the actual capacity of energy storage systems were compared.

Based on this analysis, the optimal geographic distribution of solar and wind power generation adapted to the available regulating systems is determined in order to integrate the corresponding share and combination of FRES in to a global electricity generation system while there is an optimal usage of different fluctuating patterns of solar and wind power production.

The first conclusion concerns the influence of a global grid and energy storage on the discarded solar and wind power. It has been shown that wasted energy rises rather exponentially when increasing electricity production from solar and wind energy. Extensive structural adaptations are then required to reduce this arising negative impact on power system’s operation. It has been shown that with capacity expansion of energy storage systems and a global grid, wasted energy significantly reduces. While the maximum wasted energy is significantly higher than 100% of the global electricity demand in baseline scenario, optimization of energy storage capacities leads to the reduction of the maximum wasted energy to 60% of the global electricity demand. An ideal global grid results in a higher reduction of the maximum wasted energy to 45% of the total electricity demand.

It is also concluded that the renewable energy mix, which has the minimum wasted energy, is highly influenced by available regulating systems. If power transmission capacities are optimized, wasted energy is minimized when the share of wind varies in a range from 60% to

100% of total solar and wind power production. However, in a scenario with the possibility for capacity expansion of energy storage systems, higher shares of solar energy become favorable. In this case, the minimum occurs when the share of wind varies in a range from 45% to 80% of total solar and wind power production.

It has been shown that the parallel optimization of energy storage capacities and the power transmission network structure results in additional benefits. For instance, when a high share of FRES is integrated into the power system and the renewable energy mix is characterized with a dominating share of solar energy (*a=90% and b=30%*), if both the storage capacity and the power transmission network structure is optimized, wasted energy could be reduced by 45% and 75% compared to grid-only extension and storage-only extension, respectively. Correspondingly, wasted energy could be reduced by 36% and 13% when the renewable energy mix has a dominating share of wind energy (*a=90% and b=70%*).

It was demonstrated that huge capacities are required for energy storage to facilitate integrating a high share of FRES into a future global power system when capacity expansion of power transmission lines is not taken into account. However, with an optimal global grid, the required storage capacity could be reduced by 89% at the highest integration share of wind power (*a=90% and b=100%*).

Another conclusion concerns the power transmission grid structure in a medium-term global power system, which integrates a high share of solar and wind power. The ideal global-link concept allows making an optimal usage of spatial de-correlations of fluctuating patterns of wind power production. For instance, inter-regional power transmission highways with a maximum capacity of 170 GW must be installed to satisfy 60% of the world electricity demand in year 2025 with FRES if the share of wind reaches to 85% of total solar and wind power production. When the share of solar energy is increased while no possibility exists for capacity expansion of power transmission lines, generation of wind power becomes more dispersed. The model decides to install high capacities for wind power production at the most promising sites and transmit the power through long distances. For instance, inter-zonal power transmission lines with a capacity of up to 780 GW must be installed to satisfy 60% of the world electricity demand in year 2025 with FRES if the share of wind reduces to 10%. It can finally be concluded that the grid integration costs of FRES are very low and remain mainly below 8% of the total investment and fixed costs of power generation and energy storage systems.

The backup capacity, required to integrate different shares and combinations of FRES, has also been determined by the optimization model. In baseline scenario, the new backup capacity remains mainly higher than 30% of the peak demand while in a globally-interconnected electricity supply structure it remains below 30% for a dominant share of the parameter space. However, over-installation of solar and wind power plants up to 700% of the global peak demand can not be avoided due to the short-term fluctuations and seasonal variations of FRES.

Another conclusion concerns the CO_2 emissions abatement due to an increasing generation from FRES. The electricity produced from FRES substitutes the fossil fuel power generation and leads to the reduction of CO_2 emissions. This is mainly caused by the reduced utilization of coal-fired power plants. In an ideal globally-interconnected supply structure, the minimum CO_2 emissions are as low as 620 million tons when 90% of the world electricity demand is satisfied with wind energy. Total CO_2 emissions are as high as 18553 million tons at a zero share of

renewable energies. At the highest feasible share of FRES and for a renewable mix, dominated by wind energy (*a=90% and b=70%*), if both the storage capacity and the power transmission grid structure is optimized, total CO_2 emissions reduce by 41% and 67% compared to grid-only extension and storage-only extension, respectively. Correspondingly, this could be reduced by 26% and 16% at the highest feasible share of FRES and for a renewable energy mix, which is dominated by solar energy (*a=90% and b=30%*).

Over-installation of renewable power generation capacities and significantly high capacities of backup power plants lead to a significant increase of total system costs in baseline scenario. An ideal global grid results in a considerable reduction of total system costs mainly when the penetration share of FRES is higher than 50% and the renewable energy mix has a dominating share of solar energy. At the highest feasible share of FRES and for a renewable energy mix, which is dominated by solar energy (*a=90% and b=30%*), if both energy storage capacities and the power transmission grid structure are optimized, total system costs could be reduced by 18% and 19% compared to grid-only extension and storage-only extension, respectively. Correspondingly, this could be reduced by 2% and 20% at the highest feasible share of FRES and for a renewable energy mix, which has a high share of wind energy (*a=90% and b=70%*).

Again, it is worth mentioning that the applied methodology does not include a load flow simulation. Furthermore, technical restrictions on the operation of power plants such as minimum operating level, minimum up and down time requirements, start-up conditions, and efficiency losses during partial load operation are not included in this optimization model at a detailed level as it is represented in a unit commitment problem. The ramp rates of power plants are respected on a technology basis to represent flexibility levels of power generation plants and to include the operational restrictions of the power system. Thus, discarded solar and wind power, required backup power, CO_2 emissions, and total system costs, which are obtained from this optimization model, must be considered as lower limits while the calculated feasible share of FRES represents an upper boundary. However, regarding the scale of the problem, these influences are very low in proportional terms (see section 2.5).

5 Summary, conclusions and recommendations

5.1 Summary and conclusions

The present electricity generation system is mainly centralized; the electricity demand is mainly satisfied with fossil fuels and nuclear power plants while cross-border exchange of electricity and energy storage play a minor role. These resources are exhaustible, and they are unequally distributed. Moreover, utilization of fossil fuels results in the emission of greenhouse gases, in particular CO_2. Thus, in pace with an increasing worldwide electricity demand, there is a growing need for sustainable power generation technologies such as solar and wind power generation systems. However, when integrating significant amounts of these fluctuating energy sources into the power system, challenges arise due to the uncontrollability of the primary energy source and its geographical dispersion.

The questions arise: what is the optimal share of solar and wind power that is feasible to integrate into a future global power system while maintaining a reliable electricity supply? How a prospective, renewable-based electricity generation system of the world should be designed and operated? Is an ideal globally-interconnected electricity supply structure an effective solution option to facilitate integrating a high share of FRES? What are the influences of energy storage systems?

This work is situated within the context of electricity generation system modeling and optimization. The focus of the research has been laid on worldwide impacts of large-scale integration of solar and wind power on the structure and operation of the power system. The influences of an ideal global grid and application of energy storage systems to mitigate negative consequences caused by the power system integration of FRES were investigated. In the following, different working packages are successively summarized, and conclusions are drawn.

In chapter 2, the model developed to optimize investment and production in electricity generation systems based on linear programming was described. The model in its basic form optimizes investment decisions in electricity generation systems while operational constraints of dispatchable power plants are not taken into account. This leads to the deviation of the obtained results from a realistic dispatch, obtained from a detailed operation optimization model, for instance, based on the MILP approach. The latter takes account of technical restrictions of power plants at a detailed level and on a unit basis. Specifically, regarding base load generation and wind power curtailment, the deviation can be significant. Therefore, additional linear constraints were proposed and incorporated in the developed LP investment and production optimization model to bring the solution in terms of operation closer to the technically-feasible solution, determined by the MILP approach. Technical restrictions are based on ramping constraints and start-up costs on a technology level. It has been demonstrated that the inclusion of these constraints brings the output from the LP approach very close to the generation proposed by the MILP approach. Furthermore, with the inclusion of technical constraints, investment decisions move further towards flexible power plant technologies when increasing the integration share of FRES. Curtailment of wind power and total operational costs increase as a result. Ramping constraints have the highest impact, and significant changes can be seen when a high share of wind power is integrated into a power system, which has a high capacity of non-flexible, base load power plants.

In chapter 3, different datasets, prepared to be used as input to the global electricity system optimization model, were elaborated. Geographic distribution and temporal variations of renewable energy sources and of electricity load, already installed capacities of power plants and their techno-economic parameters include the main input to the electricity system model. It was shown that the geographical spreading of wind power leads to a certain amount of smoothening and results in a less variable aggregated output power. The focus was also laid on the electricity load and additional smoothening effects captured in a globally-interconnected electricity supply structure due to spatial de-correlations of electricity demand. In the last part, different aspects of production, transportation and storage of hydrogen as a secondary energy carrier were described.

Finally, different applications of the electricity system optimization model and scenario results were presented. The developed methodology was applied to investigate optimal configuration of a global electricity supply system with a high share of FRES at different framework conditions.

As a starting point, the model in its basic form was applied to specifically investigate the benefits of dispersed generation in a prospective global electricity supply system with a dominant share of FRES. The target was to propose an ideal configuration for a long-term, renewable-based electricity supply system of the world not based on the actual levels of technology costs and technical restrictions but mainly according to the geographical and temporal dependencies of renewable energy sources and electricity demand.

Comparing the electricity generation system of today with the scenario results shows that a power system that integrates a high share of FRES cannot be operated as a centralized, fossil-fuel based electricity generation system. Extensive adaptations are required to mitigate negative consequences caused by the power system integration of FRES.

A globally-interconnected electricity supply structure is an ideal configuration to make an optimal usage of spatial de-correlations of fluctuating patterns of output power from solar and wind power generation systems. The scenario analysis shows that if the supply area consists of isolated regions, around five times the peak demand power generation capacity would be needed to satisfy 80% of the global electricity demand in 2050 with FRES. However, with an optimal global grid, the most promising sites for renewable power production are made accessible for wide area usage. As a result, the necessary backup power could be reduced by a factor of 4. If energy storage is also included, even less backup capacity is required. Moreover, inclusion of both energy storage and inter-regional power transmission leads to a significant reduction of discarded solar and wind power. In an ideal globally-interconnected electricity supply structure, excess production reduces by around 11% as compared to a baseline scenario without any possibility for energy transport or storage. If energy storage is additionally included, discarded energy reduces by 18-46%.

The future scenarios, having the possibility for inter-regional energy transport, are characterized with significant energy flows. Inter-regional power transmission highways with a maximum capacity of 1260 GW_{el} are installed, and 60-80% of total produced electricity is inter-regionally transported. In one scenario, inter-continental energy exchange between North Africa and Europe, South- and North- America, Australia and South East Asia is possible only through transportation of renewable hydrogen while the rest of area is interconnected via HVDC power transmission lines. In this scenario, the maximum hydrogen transport capacity reaches to

850 GW_{H2} to apply the significant potential of solar and wind energy centralized in Australia to satisfy the electricity demand in South East Asia. Australia is characterized with a significant potential of solar and wind electricity production, but it is subject to high seasonal variations.

Regarding the addressed question concerning the required share of renewable energies in a future global power system to meet the proposed global emissions reduction targets, in the next step, the focus was laid on CO_2 emissions of the world electricity sector. The electricity system optimization model was applied to study complex interactions of different factors, influencing CO_2 emissions of the power system, while realistic levels of technology costs are taken into account and technical restrictions of power plants are respected on a technology level.

At first, the global model was examined versus a real power production mix to validate its appropriateness for modeling electricity generation systems. It was then calibrated through steps to minimize the deviation of simulation results from real estimates. The calibrated model was then applied to quantify the potential for reducing emissions in response to a global carbon price by means of fuel switching. It was concluded that total emissions would be reduced by 5% (several hundreds of million tons) if a global carbon price of 18 €/ton existed in year 2006.

Another general conclusion concerns the influences of large-scale integration of FRES on the CO_2-certificate price. It was shown that the reduction of CO_2-price strongly correlates with the contribution of wind power. When a time horizon from 2020 to 2040 is taken into account, optimization results show that wind energy is extensively employed to meet ambitious emissions reduction targets. In year 2020, total wind power capacity reaches to 4570 GW and rises to 15285 GW by 2040. Extension of wind power at this level allows limiting CO_2 emissions from the global electricity supply sector to 6107 million tons in 2020, i.e. 35% reduction from the emissions of year 2000; this reduces to 2067 million tons by 2040 while the CO_2-price rises to 61 €/ton. However, this can only be achieved if capacities of inter-regional power transmission lines are expanded far beyond the existing capacities. If an optimal extension of the power transmission network is not possible, over-installation of power generation capacities up to 18% is unavoidable to satisfy the proposed CO_2-limit in year 2040. In this case, the CO_2-price significantly rises to 147 €/ton by the end of the time horizon.

A parametrical study was then performed by varying the integration share of FRES and the renewable energy mix. The optimization model was applied to study the required system adaptation in order to mitigate negative consequences caused by the power system integration of various shares of solar and wind power and to achieve a specific level of CO_2 emissions abatement.

The first conclusion concerns the influence of an ideal global grid and energy storage on the mitigation of discarded solar and wind power. It was demonstrated that wasted energy rises rather exponentially when increasing the electricity production from FRES. Massive structural changes are then required to minimize this negative impact on the operation of the power system. It was shown that with an optimal capacity expansion of energy storage systems or inter-regional power transmission interconnections, wasted energy can be significantly reduced. While the maximum wasted energy is significantly higher than 100% of the global electricity demand in baseline scenario, optimization of energy storage capacities leads to the reduction of the maximum wasted energy to 60% of the global electricity demand. An ideal global grid leads to a further reduction of the maximum wasted energy to 45% of the global electricity demand.

It is also concluded that at any given share of FRES, wasted energy is minimized at a specific combination of solar and wind power, which is highly dependent on available regulating systems. If the power transmission grid structure is optimized, the optimal energy mix in terms of minimal wasted energy occurs when the share of wind varies in a range from 60% to 100% of total solar and wind power production. However, in a scenario with a possibility only for capacity expansion of energy storage systems, higher shares of solar energy become favorable. In this case, the minimum occurs when the share of wind varies in a range from 45% to 80% of total solar and wind power production. This shows how we can benefit from different fluctuating patterns and seasonal characteristics of solar and wind power production through an optimal geographic distribution of FRES adapted to the available regulating systems.

Another conclusion concerns the power transmission grid structure in a medium-term global electricity supply system with a high share of solar and wind power. The ideal global-link concept allows making an optimal usage of spatial de-correlations of wind power. For instance, inter-regional power transmission highways with a maximum capacity of 170 GW are installed to satisfy 60% of the world electricity demand in 2025 with FRES when the share of wind reaches to 85% of total solar and wind power production. If the share of solar energy is increased while no possibility exists for capacity expansion of energy storage systems, generation of wind power becomes more dispersed. The model decides to install high capacities for wind power production at the most promising sites and transmit the power through long distances. For instance, inter-regional power transmission lines with a maximum capacity of 780 GW are installed to satisfy 60% of the world electricity demand in year 2025 with FRES if the share of wind is 10%. Finally, it can be concluded that the grid integration costs of FRES are very low and remains mainly below 8% of total investment and fixed costs of power generation and storage systems.

The influence of an increasing power production from FRES on the CO_2 emissions abatement was also quantified. It was demonstrated that in an ideal globally-interconnected structure of a future global power system, the minimum CO_2 emissions are as low as 620 million tons if 90% of the world electricity demand is satisfied with wind energy. Total CO_2 emissions are as high as 18553 million tons at a zero share of solar and wind power.

It is concluded that over-installation of renewable power plants and huge backup capacities, occurring in baseline scenario, leads to a significant increase of total system costs. An ideal global grid results in a considerable reduction of system costs mainly when the share of FRES is higher than 50% of the global electricity demand and for a renewable energy mix, which is dominated by solar energy.

Summarily, the modelling approach, developed and applied in this thesis, is a combination of an adequately precise geographical coverage with a high temporal resolution; it is adequate to properly mimic geographical dependencies of energy supply and demand as well as short-term intermittent patterns of FRES. It optimizes investment decisions in electricity generation systems while it takes into account technical restrictions of power plants at a technology level. As a global, multi-regional electricity system optimization model, it can mimic complex interactions of different system components within large sets of interconnected power systems. Through minimization of overall system costs, promising sites for renewable power production, required backup power, and optimal operation schedule of power plants are determined. The optimal

capacity for energy storage and for inter-zonal transmission of electricity and hydrogen is determined under different framework conditions. CO_2 emissions and the CO_2-price can also be quantified by this optimization model. Examination of the model results versus a real power generation mix and comparison of the obtained results with the solution, found by different methodologies and electricity system models, validate the model formulation and its database.

It is worth mentioning that in the developed LP investment and production optimization model, power transmission lines are modeled as trade-based interconnections; thus, load flow constraints are neglected. The model lacks a detailed representation of technical restrictions for power system integration of FRES such as minimum operating levels, minimum up and down time constraints, start-up conditions, and upward/downward reserve power requirements. Negative consequences on the operation of the power system mainly caused by the limited predictability of FRES are not the main focus of this study. These mainly include additional start-up costs and efficiency losses of conventional power plants at partial load operation. Potential consequences on the results are the overestimation of the feasible integration share of FRES and their economical and environmental benefits.

However, as the optimization is performed on a global level, and, thus, covers a large scale, deviation of the obtained results from the results of a detailed operation optimization model, which respects technical restrictions of power plants on a unit basis, are very low in proportional terms. These influences were described in section 2.5.

5.2 Recommendations for further research

The first part of recommendations for further research is related to the enhancement of the applied modeling approaches. In the developed methodology, power transmission lines are modeled as trade-based interconnections. Neglecting load flow restrictions can lead to suboptimal results. Further research in this topic using power flow models is necessary. Another option is to increase the level of technical detail in the optimization model. Additional technical constraints on the operation of thermal power plants can be taken into account. However, one always should try to retain the appropriate balance between the research objective and the required level of technical detail. Another option could be modeling the uncertainty of different input parameters such as fuel prices, CO_2-price, and time series of wind power capacity factor.

The second part of recommendations for further research is related to the improvement of the accuracy. The main option to increase the realism of simulations might be the increase of geographical resolution, i.e. reducing the size of model regions. However, one always should choose an appropriate level of geographical detail taking into account the increase of calculation time and the achieved improvements in the obtained results. So far, no transportation costs of fossil fuels have been included, and fuel prices are uniform through all model regions. Thus, another possible point of improvement might be to include fossil fuel prices on a country basis or region specific. Another possibility is an improvement of the used time series to represent temporal variations of electricity demand and renewable energy supply. Effort should be made to include electrical load profiles of countries, for them no data have been made accessible so far. One could also try to improve the accuracy of the used meteorological data by applying other datasets, having a higher level of geographical detail and temporal

resolution. It might be a much further enhancement if the data also include the possible impacts of climate change on the available renewable energy supply in the long-term.

The third part of recommendations for further research is related to the improvement of the optimization performance. The major drawback of the applied mathematical approach, linear programming, is the long calculation time and a high usage of physical memory. Further research is necessary to propose and apply other optimization techniques to reduce the calculation time. One should, however, find a compromise between the reduced calculation time and the deviation of the obtained results from the global optimum found by a deterministic approach such as LP.

The fourth part of recommendations for further research is related to the extension of modeling scope. The focus in this thesis has been mainly laid on the optimization of investment decisions in electricity generation systems influenced by an increasing power production from fluctuating renewable energy sources. In the developed linear investment planning model, technical restrictions of dispatchable power plants are modeled at a technology level. Thus, modeling operational characteristics of electricity generation systems at a detailed level was not covered in this study. Indeed, on a time horizon ranging from hours to weeks, wind and solar power influence the commitment and economic dispatch of conventional generation units. They reduce utilization of thermal power plants while these units are crucial to compensate for the variability and limited predictability of these uncontrollable energy sources. Models can be developed to optimize commitment and dispatch of power generation units and address questions, which are specifically related to the impacts of fluctuating energy sources on the operational aspects of the power system.

Bibliography

[1] Nakicenovic, N.: World Energy Outlook 2007: CO_2 Emissions Pathways Compared to Long-term CO_2 Stabilization Scenarios in the Literature and IPCC Assessment Report 4, IIASA and Technische Unversität Wien, Austria, 2007.

[2] Intergovernmental Panel on Climate Change (IPCC): Special Report on Emission Scenarios - A Special Report of Working Group III, 2000.

[3] Intergovernmental Panel on Climate Change (IPCC): Fourth Assessment Report (AR4), 2007.

[4] Wheeler, D., Ummel, K.: Calculating CARMA - Global Estimation of CO_2 Emissions from the Power Sector, Center for Global Development, Working Paper No. 145, pp. 1-37, 2008.

[5] Manne, A., Richels, R.: On Stabilizing CO_2 Concentrations - Cost-Effective Emission Reduction Strategies, International Journal of Environmental Modeling and Assessment, Vol. 2, pp. 251-265, 1997.

[6] van Vuuren, D.P., Hof, A.F., den Elzen, M.G.J.: Meeting the 2° C target - From Climate Objective to Emission Reduction Measures, Netherlands Environmental Assessment Agency (PBL), Bilthoven, Netherlands, 2009.

[7] European Photovoltaic Industry Association (EPIA) and Greenpeace International: Solar Generation 6 - Solar Photovoltaic Electricity Empowering the World, 2010.

[8] European Photovoltaic Industry Association (EPIA): Global Market Outlook for Photovoltaic until 2014, 2010.

[9] Bosatra, M., Fazi, F., Lionetto, P.F., Travagin, L.: Utility Scale PV and CSP Solar Power Plants Performance - Impact on the Territory and Interaction with the Grid, Power-Gen Europe, Amsterdam, Netherlands, 2010.

[10] Global Wind Energy Council (GWEC) and Greenpeace International: Global Wind Energy Outlook, 2009.

[11] Global Wind Energy Council (GWEC) and Greenpeace International: Global Wind Energy Outlook, 2010.

[12] Brückl, O.: Global Technical Potential of Electricity Production from Wind Energy, Internal Final Report for BMW AG Study, Institute for Energy Economy and Application Technology (IfE), Technische Universität München, Germany, 2005.

[13] Tzscheutschler, P.: Global Technical Potential of Solar Thermal Electricity, PhD Thesis, Institute for Energy Economy and Application Technology (IfE), Technische Universität München, Germany, 2005.

[14] Hoogwijk, M.M.: On the Global and Regional Potential of Renewable Energy Sources, PhD Thesis, Universiteit Utrecht, Netherlands, 2004.

[15] Dreier, Th.: Ganzheitliche Systemanalyse und Potenziale Biogener Kraftstoffe, Internal Final Report, Institute for Energy Economy and Application Technology

(IfE), Technische Universität München, Germany, 2000.

[16] Lehner, B., Czisch, G., Vassolo, S.: The Impact of Global Change on the Hydro Power Potential of Europe: A Model-based Analysis, Journal of Energy Policy, Vol. 33, pp. 839-855, 2005.

[17] Auer, J., Haslauer, E.M., Kress, B.: Globales Geothermie Potential, Internal Final Report for Research Studio iSpace Salzburg, Austria, 2008.

[18] Nitsch, M., Giersdorf, J.: Biotreibstoffe in Brasilien, Diskussionsbeiträge des Fachbereichs Wirtschaftswissenschaft der Freien Universität Berlin, Germany, 2005.

[19] Archer, C.L., Jacobson, M.Z.: Evaluation of wind power, Journal of Geophysical Research, Vol. 110, D12110, doi: 10.1029/2004JD005462, 2005.

[20] Rafikin, J.: Die H_2 Revolution, Campus Verlag, ISBN 3593370972, 2002.

[21] Delarue, E.: Modeling Electricity Generation Systems - Development and Application of Electricity Generation Optimization and Simulation Models with Particular Focus on CO_2 Emissions, PhD Thesis, Katholieke Universiteit Leuven, Belgium, 2009.

[22] Ummels, B.C.: Wind Integration - Power System Operation with Large-Scale Wind Power in Liberalised Environments, PhD Thesis, Technische Universiteit Delft, Netherlands, 2009.

[23] Ventosa, M., Baíllo, Á., Ramos, A., Rivier, M.: Electricity Market Modeling Trends, Journal of Energy Policy, Vol. 33, No. 7, pp. 897-913, 2005.

[24] Han, W.E., Ward, D.J.: Internal Final Report on EFDA TIMES Model Electricity Sector Update Task, EURATOM/UKAEA Fusion Association, Culham Science Centre, Abingdon, UK, 2007.

[25] Labriet, M., Loulou, R., Kanudia, A.: Global Energy and CO_2 Emission Scenarios - Analysis with a 15-Regions World MARKAL Model, Advances in Global Change Research, Vol. 22, pp. 205-235, 2005.

[26] Biberacher; M.: Modelling and Optimization of Future Energy Systems Using Spatial and Temporal Methods, PhD Thesis, University of Augsburg, Germany, 2004.

[27] Czisch, G.: Szenarien zur zukünftigen Stromversorgung - Kostenoptimierte Variationen zur Versorgung Europas und seiner Nachbarn mit Strom aus erneuerbaren Energien, PhD Thesis, University of Kassel, Germany, 2005.

[28] Padhy, N.P.: Unit commitment - A Bibliographical Survey, IEEE Transactions on Power Systems, Vol. 19, No. 2, pp. 1196-1205, 2004.

[29] Hobbs, B.F., Rothkopf, M.H., O'Neill, R.P., Chao, H.: The Next Generation of Electric Power Unit Commitment Models, International Series in Operations Research and Management Science, Vol. 36, pp. 1-328, 2001.

[30] Sen, S., Kothari, D.P.: Optimal Thermal Generating Unit Commitment - A Review, International Journal of Electrical Power and Energy Systems, Vol. 20, No. 7, pp. 443-451, 1998.

[31] Yamin , H.Y., Shahidehpour, S.M.: Unit Commitment Using a Hybrid Model between Lagrangian Relaxation and Genetic Algorithm in Competitive Electricity Markets, Journal of Electric Power Systems Research, Vol. 68, pp. 83-92, 2003.

[32] Dantzig, G.B., Thapa, M.N.: Linear Programming, Springer Series in Operations Research, 1997.

[33] Nemhauser, G.L., Wolsey, L.A.: Integer and Combinatorial Optimization, Wiley-Interscience Series in Discrete Mathematics and Optimization, 1999.

[34] Haase, T.: Anforderung an eine durch Erneuerbare Energien geprägte Energieversorgung - Untersuchung des Regelverhaltens von Kraftwerken und Verbundnetzen, PhD Thesis, University of Rostock, Germany, 2006.

[35] Heitmann, N.: Solution of Energy Problems with the Help of Linear Programming, Master Thesis, University of Augsburg, Germany, 2005.

[36] Streiffert, D., Philbrick, R., Ott, A.: A Mixed Integer Programming Solution for Market Clearing and Reliability Analysis, IEEE Power Engineering Society General Meeting, Vol. 3, pp. 2724-2731, 2005.

[37] Carrion, M., Arroyo, J.M.: A Computationally Efficient Mixed Integer Linear Formulation for the Thermal Unit Commitment Problem, IEEE Transactions on Power Systems, Vol. 21, No. 3, pp. 1371-1378, 2006.

[38] Chang, G.W., Aganagic, M., Waight, J.G., Medina, J., Burton, T., Reeves, S., Christoforidis, M.: Experiences with Mixed Integer Linear Programming Based Approaches on Short-term Hydro Scheduling, IEEE Transactions on Power Systems, Vol. 16, No. 4, pp. 743-749, 2001.

[39] Wood, A.J., Wollenberg, B.F.: Power Generation, Operation, and Control, 2nd ed., Wiley-Interscience, New York, 1996.

[40] Chung-Ching, S., Yuan-Yih, H.: Fuzzy Dynamic Programming: and Application to Unit Commitment, IEEE Transactions on Power Systems, Vol. 6, pp. 1231-1237, 1991.

[41] Kumar, S., Palanisamy, V.: A Dynamic Programming Based Fast Computation Hopfield Neural Network for Unit Commitment and Economic Dispatch, Journal of Electric Power Systems Research, Vol. 77, No. 8, pp. 917-925, 2007.

[42] Ouyang, Z., Shahidehpour, S.M.: A Hybrid Artificial Neural Network - Dynamic Programming Approach to Unit Commitment, IEEE Transactions on Power Systems, Vol. 7, pp. 236-242, 1992.

[43] Padhy, N.P.: Unit Commitment Using Hybrid Models - A Comparative Study for Dynamic Programming, Expert System, Fuzzy System and Genetic Algorithms, International Journal of Electrical Power & Energy Systems, Vol. 23, pp. 827-836, 2001.

[44] Ongsakul, W., Petcharaks, N.: Unit Commitment by Enhanced Adaptive Lagrangian Relaxation, IEEE Transactions on Power Systems, Vol. 19, pp. 620-628, 2004.

[45] Virmani, S., Adrian, E.C., Imhof, K., Mukherjee, S.: Implementation of a Lagrangian-Relaxation based Unit Commitment Problem, IEEE Transactions on

Power Systems, Vol. 4, pp. 1373-1380, 1989.

[46] Zhai, Q.Z., Guan, X.H., Cui, J.: Unit Commitment with Identical Units - Successive Sub-problem Solving Method based on Lagrangian Relaxation, IEEE Transactions on Power Systems, Vol. 17, pp. 1250-1257, 2002.

[47] Rosenthal, R.E.: GAMS A User's Guide, GAMS Development Corporation, Washington, 2008.

[48] International Energy Agency (IEA) and Nuclear Energy Agency (NEA): Projected Costs of Generating Electricity, 2010.

[49] Institute for Energy Economy and Application Technology (IfE): Kraftwerk Datenbank, Technische Universität München, Germany, 2008.

[50] Bofinger,S., von Bremen, L., Knorr, K., Lesch, K., Rohrig, K., Saint-Drenan, Y.M., Speckmann, M.: Raum-zeitliche Erzeugungsmuster von Wind- und Solarenergie in der UCTE- Region und deren Einfluss auf elektrische Transportnetze, Institut für Solare Energieversorgungstechnik, ISET e.V., Kassel, Germany, 2008.

[51] De Vos, K., De Rijcke, S., Rombauts, Y, De Saint Quentin, S., Dedecker, J., Driesen, J.: WINDBALANCE - Balancing Wind Energy in the Grid: an Overall, Techno-economic and Coordinated Approach, Belgian Science Policy, Brussels, Belgium, 2010.

[52] Roth, H., Kuhn, Ph.: Technik- und Kostenszenarien der Strombereitstellung in Deutschland bis 2040, Institute for Energy Economy and Application Technology (IfE), Technische Universität München, Germany, 2008.

[53] VGB PowerTech Service GmbH: Tätigkeitsbericht 2007/2008, Essen, Germany, 2008.

[54] De Jonghe, C., Delarue, E., Belmans, R., D'haeseleer, W.: Determining Optimal Electricity Technology Mix with High Level of Wind Power Penetration, Journal of Applied Energy, Vol. 88, pp. 2231-2238, 2011.

[55] Shahidehpour, M., Wang, C.: Ramp-rate Limits in Unit Commitment and Economic Dispatch Incorporating Rotor Fatigue Effect, IEEE Transactions on Power Systems, Vol. 9, pp. 1539-1545, 1994.

[56] Maddaloni, J., Rowe, A., Van Kooten, G.: Wind Integration into Various Generation Mixtures, Journal of Renewable Energy, Vol. 34, pp. 807-14, 2009.

[57] Abrell, J., Kuntz, F., Weigt, H.: Start me Up - Modeling of Power Plant Start-Up Conditions and Their Impact on Prices, Electricity Market Working Papers, Chair for Energy Economics and Public Sector Management, Technische Universität Dresden, Germany, 2008.

[58] Kuntz, L., Müsgens, F.: Modelling Start-Up Costs of Multiple Technologies in Electricity Markets, Journal of Mathematical Methods of Operations Research, Vol. 66, No. 1, pp. 21-32, 2007.

[59] Scillings, C., Pereira, E., Perez, R., Meyer, R., Trib, F., Renne, D.: High Resolution Solar Energy Resource Assessment within the UNEP Project SWERA, World Renewable Energy Congress VII, Cologne, Germany, 2002.

[60] Bishop, J.K.B., Potylitsina T., Rossow, W.B.: Documentation and Description of Surface Solar Irradiance Data Sets Produced for SeaWiFS, NASA Grant, Department of Applied Physics, Columbia University, USA, 2000.

[61] World Radiation Data Center (WRDC), http://wrdc-mgo-nrel.gov.

[62] Duffie, J.A., Beckman, W.A.: Solar Engineering of Thermal Processes, John Wiley and Sons, New York, 2006.

[63] International Energy Agency (IEA)/ Organization for Economic Cooperation and Development (OECD): Potential for Building Integrated Photovoltaics, Paris, 2001.

[64] Solar Millennium AG: The Parabolic Trough Power Plants Andasol 1 to 3 - The Largest Solar Power Plants in the World - Technology Premiere in Europe, Erlangen, Germany, 2008.

[65] Sander and Partner GmbH: World Wind Atlas (WWA), http://www.sanderpartner.ch, 2002.

[66] Glasserman, P.: Monte Carlo Methods in Financial Engineering, Springer-Verlag, New York, 2004.

[67] van Kuik, G.A.M.: The Lanchester-Betz-Joukowsky Limit, Journal of Wind Energy, Vol. 10, pp. 289-291, 2007

[68] Lysen, E.: Introduction to Wind Energy: A Publication of SWD, Utrecht Centre for Energy research, Utrecht University, Netherlands, 1982.

[69] Wieringa, J.: Does Representative Wind Information Exist? Journal of Wind Engineering and Industrial Aerodynamics, Vol. 65, pp. 1-12, 1996.

[70] Beune, R., Nobel, F.A.: System Balancing in the Netherlands - Methods to Secure Peak Load Capacity on Deregulated Electricity Markets, Stockholm, Sweden, 2001.

[71] Norgaard, P., Holttinen, H.: A Multi-Turbine Power curve Approach, Nordic Wind Power Conference, Chalmers University of Technology, Sweden, 2004.

[72] Seguro, J.V., Lambert, T.W.: Modern Estimation of the Parameters of the Weibull Wind Speed Distribution for Wind Energy Analysis, Journal of Wind Engineering and Industrial Aerodynamics, Vol. 85, pp. 75-84, 2000.

[73] TenneT TSO GmbH, http://www.tennettso.de/Transparenz/Veröffentlichungen, 2009.

[74] 50Hertz Transmission GmbH, http://www.50hertz-transmission.net/Kennzahlen/Windenergie, 2009.

[75] EnBW Transportnetze AG, http://www.enbw.com, 2009.

[76] Amprion GmbH, http://www.amprion.net/Kunden/Netzkennzahlen, 2009.

[77] European Environmental Agency (EEA): Europe's Onshore and Offshore Wind Energy Potential - An Assessment of Environmental and Economical Constraints, EEA Technical Report, 2009.

[78] Global Wind Energy Council (GWEC) and Greenpeace International: Global Wind Energy Outlook, 2006.

[79] ENERCON GmbH: ENERCON Windenergieanlagen Produktübersicht, http://www.enercon.de, 2010.

[80] Greenpeace and European Wind Energy Association (EWEA): Wind Force 12 - A Blueprint to Achieve 12% of the World's Electricity from Wind Power by 2020, Greenpeace, Amsterdam, Netherlands, EWEA, Brussels, Belgium, 2005.

[81] European Wind Energy Association (EWEA): Wind Energy - the Facts. Vol. 1: Technology, http://www.ewea.org/fileadmin/ewea_documents/documents/publications/WET/Facts_Volume 2.pdf, 2009.

[82] Heide, D., von Bremen, L., Greiner, M., Hoffmann, C., Speckmann, M., Bofinger, S.: Seasonal Optimal Mix of Wind and Solar Power in a Future Highly Renewable Europe, Journal of Renewable Energy, Vol. 35, pp. 2483-2489, 2010.

[83] Stacy, F.D., Loper, D.E.: Thermal History of the Earth: a Corollary Concerning Non-linear Mantle Rheology, Journal of Physics of the Earth and Planetary Interiors, Vol. 53, pp. 167-174, 1988.

[84] Diskson, M.H., Fanelli, M.: What is Geothermal Energy?, Istituto di Geoscienze e Georisorse, CNR , Pisa, Italy, 2004.

[85] Pollack, H.N., Hurter, S.J., Johnson, J.R.: Heat flow from the Earth's interior-Analysis of the global data set, Reviews of Geophysics, Vol. 31, No.3, pp. 267-280, 1993.

[86] Armstead, H.C.H.: Geothermal Energy - Its Past, Present, and Future Contributions to the Energy Needs of Man, 2nd Ed., London, UK, 1983.

[87] Stefansson, V.: The Renewability of Geothermal Energy, Proceedings of World Geothermal Energy, Japan, 2000.

[88] Bertani, R., Green, E.: Long-term Projections of Geothermal Electric Development in the World, GeoTHERM Conference, Offenburg, Germany, 2009.

[89] Fridleifsson, I.B., Ruggero, B., Huenges, E., Lund, J.W.: The Possible Role and Contribution of Geothermal Energy to the Mitigation of Climate Change, O. Hohmeyer and T. Trittin (Eds.), IPCC Scoping Meeting on Renewable Energy Sources, Proceedings, Luebeck, Germany, 2008.

[90] Lund, J.W.: The USA Geothermal Country Update, Journal of Geothermics, Vol. 32, pp. 409-418, 2003.

[91] International Energy Agency (IEA): Renewable Energy Essentials - Geothermal, 2010.

[92] International Institute for Applied Systems Analysis (IIASA): Greenhouse Gas Initiative (GGI) Database, http://www.iiasa.ac.at/web-apps/ggi, 2009.

[93] International Energy Agency (IEA): IEA Energy Technology Essentials - Biomass for Power Generation and CHP, 2007.

[94] Benders, G., Hoogwijk, M., van den Broek, R.: The contribution of Biomass in the

Future Global Energy System: a Review of 17 Studies, Journal of Biomass and Bioenergy, Vol. 25, pp. 1-28, 2003.

[95] European Renewable Energy Council (EREC): Renewable Energy Technology Road Map 20% by 2020, Brussels, Belgium.

[96] UDI World Electric Power Plants Data Base (WEPP): Data Base Description and Research Methodology, Platts, UDI Products Group, Washington, USA, 2009.

[97] ENTSO-E European Network of Transmission System Operators for Electricity, Statistical Database, http://www.entsoe.eu/resources/data-portal, 2009.

[98] Döll, P., Alcamo, J., Henrichs, Th., Kaspar, F., Lehner, B., Rösch, Th., Siebert, S.: The Global Integrated Water Model WaterGAP 2.1, Center for Environmental Systems Research, University of Kassel, Germany, 2001.

[99] Hans-Burkhard Horlacher, H.: Globale Potenziale der Wasserkraft, Externe Expertise für das Wissenschaftlicher Beirat der Bundesregierung Globale Umweltveränderungen (WGBU) - Hauptgutachten "Welt im Wandel: Energiewende zur Nachhaltigkeit", Heidelberg, Germany, 2003.

[100] International Energy Agency (IEA): World Energy Outlook, Paris, 2008.

[101] UK National Grid Company, http://www.nationalgrid.com/uk, 2009.

[102] Nordel, http://www.nordel.org, 2009.

[103] Zickermann, Y.: Approximation of Typical Load Curves for Different Continents and Climate zones, Studienarbeit, Institute for Energy Economy and Application Technology (lfE), Technische Universität München, Germany, 2005.

[104] Estonian Power Transmission System Operator Elerging OÜ, http://www.elering.ee, “Personal Communication”, 2009.

[105] Energy Information Administration (EIA): International Electricity Data, http://www.eia.gov/electricity/data, 2010.

[106] United Nations (UN): Energy Statistics Database, http://www.unstats.un.org/unsd/energy/edbase, 2010.

[107] Ihle, J., Owens, B.: Integrated Coal and Wind Power Development in the US Upper Great Plains, Boulder, CO: Platts Research and Consulting, 2004.

[108] International Energy Agency (IEA): World Energy Outlook, Paris, 2007.

[109] Woyte, A., Purchala, K., Meibom, P., Larsen, H., Kleinschmidt, Ch., Moldovan, N.: Trade Wind - D 7.5 Power Market Design with a High Wind Power Share - Simulations and Analysis, 2008.

[110] European Transmission System Operators (ETSO): Capacity Publications and Procedures, 2001.

[111] European Transmission System Operators (ETSO): Definitions of Transfer Capacities in Liberalised Electricity Markets, 2001.

[112] Angloher, J., Dreier, TH.: Techniken und Systeme zur Wasserstoffbereitstellung, Internal Final Report, Institute for Energy Economy and Application Technology

(IfE), Technische Universität München, Germany, 1999.

[113] Bossel, U.: The Physics of Hydrogen Economy, European Fuel Cell News, Vol. 10, No. 2, 2003.

[114] Ultra High Voltage DC Systems, ABB Power Technologies AB Grid Systems - HVDC, http://www.abb.com/hvdc.

[115] Ivy, J.: Summary of Electrolytic Hydrogen Production, National Renewable Energy Laboratory, Colorado, USA, 2004.

[116] Nitsch, J.: Potenziale der Wasserstoffwirtschaft, Gutachten für den Wissenschaftlichen Beirat der Bundesregierung Globale Umweltveränderungen (WBGU), Stuttgart, Germany, 2002.

[117] Hawkins, S., Joffe, D.: Technological Characterization of Hydrogen Production Technologies, PSI, UK, 2005.

[118] Bossel, U.: Does a Hydrogen Economy Make Sense?, Proceedings of the IEEE, Vol. 94, No. 10, pp. 1826-1837, 2006.

[119] Hawkins, S., Joffe, D.: Technological Characterization of Hydrogen Storage and Distribution Technologies, PSI, UK, 2006.

[120] Hawkins, S., Joffe, D., Hughes, N.: Hydrogen Fuel Cells for Stationary Power - Technological Characterization and Market Assessment, UKSHEC Social Science Working Paper No. 24, PSI, UK, 2005.

[121] Amos, W.A.: Costs of Storing and Transporting Hydrogen, National Renewable Energy Laboratory (NREL), Colorado, USA, 1998.

[122] Heitmann, N., Hamacher, Th.: Stochastic Model of German Electricity System, Optimization in the Energy Industry, Energy Systems, Vol. 3, pp. 365-385, 2009.

[123] Mathur, J., Bansal, N.K., Wagner, H.J.: Investigation of Greenhouse Gas Reduction Potential and Change in Technological Selection in Indian Power Sector, Journal of Energy Policy, Vol. 31, pp. 1235-1244, 2003.

[124] Newcomer, A., Blumsack, S.A., Apt, J., Lave, L.B., Morgan, M.G.: Short Run Effects of a Price on Carbon Dioxide Emissions from U.S. Electric Generators, Environmental Science and Technology, Vol. 42, No. 9., pp. 3139-3144, 2008.

[125] International Energy Agency (IEA): World Energy Outlook, 2002.

[126] World Alliance for Decentralized Energy (WADE): Projected Costs of Generating Electricity (2005 Update), WADE's Response to the Report of the International Energy Agency and the Nuclear Energy Agency, 2005.

[127] Royal Academy of Engineering: The Cost of Generating Electricity, A Study Carried Out by BP Power for the Royal Academy of Engineering, 2004.

[128] International Energy Agency (IEA) and Nuclear Energy Agency (NEA): Projected Costs of Generating Electricity, 2005.

[129] International Energy Agency (IEA): World Energy Outlook, 2006.

Appendices

A Model structure

General structure of the electricity system optimization model (LPIPOM) is shown in Fig. A.1.

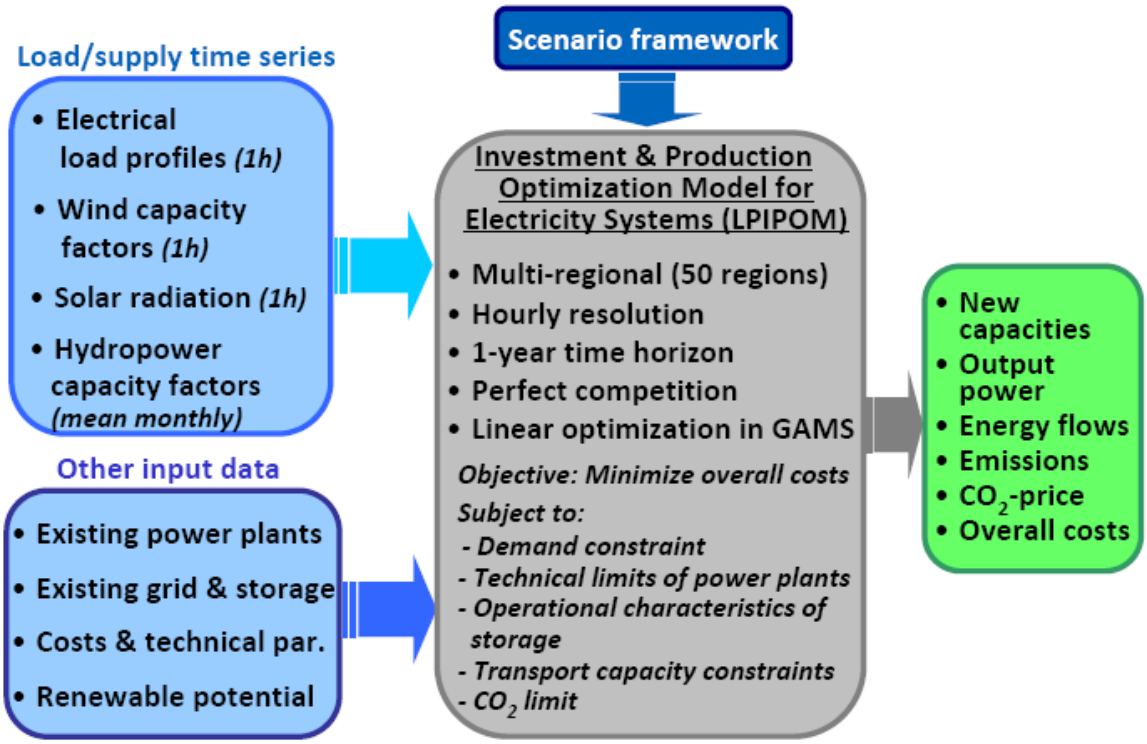

Fig. A.1: Overview of model's structure

This global multi-regional electricity system optimization model comprises of 50 regions. Model regions are represented in Table A.1.

Table A.1: Description of model regions

Model region	Region name	Comprising countries (ISO 2-digit)
R1	SAM-S	AR, CL, UY, BO, PY
R2	BR-E	BR-East & South
R3	BR-W	BR-North & West
R4	SAM-N1	PE, EC
R5	SAM-N2	CO, VE, AG, AN, AW, BB, DM, DG, GP, KN, LC, MQ, MS, TT, VC, GD, VG
R6	SAM-N3	GF, GY, SR
R7	CAM	GT, BZ, SV, HN, NI, CR, PA, BS, CU, DO, HT, JM, PR, VI, KY, TC
R8	MEX	MX
R9	USA-W	US-West
R10	USA-E	US-East

R11	AK	AK
R12	CAN-W	CA-West
R13	CAN-E	CA-East
R14	GL	GL
R15	NAF-NE	EG, LY
R16	NAF-NW	DZ, MA, TN
R17	AF-NM	SD, TD, CF
R18	AF-W1	ML, NE
R19	AF-W2	EH, CV, MR
R20	AF-W3	BJ, BF, CI, GH, NG, TG
R21	AF-W4	LR, SL, GN, GW, SN, GM
R22	AF-M	CM, GQ, GA, CG, ST
R23	AF-S1	CD, TZ, UG, RW, BI, ZM, AO
R24	AF-E1	ER, ET, DJ, KE
R25	AF-E2	SO
R26	AF-S2	MW, MZ, ZW, KM, YT, MG
R27	AF-S3	NA, BW
R28	ZA	ZA,LS, SZ
R29	AS-W1	AM, GE, AZ, TR
R30	AS-W2	SY, IQ, IL, LB, JO, KW, CY, PS
R31	AS-W3	SA, AE, YE, OM, QA, BH
R32	CAS	KG, KZ, TJ, TM, UZ
R33	AS-S	IN, LK, MV, AF, PK, IR
R34	AS-E1	MN, CN-West
R35	AS-E2	CN-East, JP,KP, KR, HK, TW
R36	AS-SE1	MM, KH, LA, TH, VN, BO, BT, NP
R37	AS-SE2	BN, TL, ID, MY, PH, SG, PG
R38	RU-W	RU-West
R39	RU-M	RU-Central
R40	RU-E	RU-East
R41	RU-FE	RU-Far East
R42	AUS	AU
R43	NZ	NZ
R44	EU-1	EE, LV, LT, BY, UA, MD, PL,CZ
R45	EU-2	SK, AT, HU, SI, HR, RS, BG, BA, ME, MK, AL, GR, RO
R46	EU-3	DE, NL, BE, LU, FR, DK
R47	EU-4	CH, LI, MC, SM, IT, MT
R48	EU-5	AD, ES, PT, GI
R49	EU-6	NO, SE, FI
R50	EU-7	IE, GB, IS

B Geographical potential of renewable electricity production and demand

B1 Geographical potential of solar electricity production

The suitable and limited suitable area for solar electricity production has been determined based on the study, conducted in [13], and it was adapted to the geographical structure of the optimization model. Derived values are given in Table B1.1.

Table B1.1: Available area for installation of solar power plants (centralized PV and CSP)

Model region	Suitable area (km^2)	Limited suitable area (km^2)
R1	1514299	562903
R2	1446333	274180
R3	231887	30225
R4	75590	117546
R5	390888	63515
R6	19188	6671
R7	38711	12286
R8	386569	201349
R9	353354	366906
R10	856989	345112
R11	129241	216127
R12	91633	597865
R13	112048	1834897
R14	123	57839
R15	20387	1208982
R16	93332	1718113
R17	1883374	1317132
R18	684106	839163
R19	91593	439175
R20	1189485	193183
R21	247269	128472
R22	272408	51972
R23	1069180	468931
R24	632495	315879
R25	397203	117521
R26	392612	223394
R27	686924	203492
R28	181602	186242
R29	38910	47238

R30	171488	311583
R31	114626	708553
R32	1243082	499852
R33	392398	796775
R34	687620	1217411
R35	314829	228829
R36	121638	71258
R37	95502	21236
R38	108541	32014
R39	70608	107946
R40	172204	870180
R41	119295	309361
R42	5860548	153438
R43	26948	33570
R44	4388	2366
R45	2359	2344
R46	2246	1939
R47	7478	7192
R48	18791	30261
R49	9134	15807
R50	2531	13303
World	23073987	17581528

B2 Geographical potential of wind electricity production

Available area for installation of wind turbines in on- and off- shore sites has been determined based on the study, conducted in [12], and it was adapted to the geographical structure of the optimization model. Derived values are given in Table B2.1.

Table B2.1: Available area for installation of wind turbines

Model region	**Suitable onshore area (km^2)**	**Suitable offshore area (km^2)**
R1	3350945	315620
R2	3190609	352254
R3	258550	38219
R4	354414	28489
R5	542742	161960
R6	24954	136968
R7	141084	335865

R8	840909	193036
R9	1083726	20319
R10	3066711	445496
R11	491704	397393
R12	1127563	50013
R13	2267358	256423
R14	98839	29073
R15	2530522	85496
R16	2577673	58915
R17	4020437	23552
R18	2417837	0
R19	1304442	41449
R20	1654469	57107
R21	494985	196749
R22	359238	53671
R23	2242904	50680
R24	1376685	109467
R25	601035	21690
R26	1237241	99315
R27	1330920	5527
R28	952630	25749
R29	393261	17750
R30	657460	109122
R31	2445004	392775
R32	3283773	0
R33	3081050	291955
R34	3616506	6150
R35	1377180	598525
R36	619836	709270
R37	384742	1679673
R38	1311301	149527
R39	485193	57107
R40	1430944	21724
R41	289131	208814
R42	7222291	964640
R43	107064	51739
R44	1044831	216151
R45	401992	109173
R46	633556	385499
R47	116347	70150
R48	325378	36772
R49	59836	260404

R50	255447	173383
World	69483251	10100799

B3 Geographical potential of geothermal electricity production

The geographical potential for geothermal electricity production has been quantified using the geographic distribution of geothermal heat flow based on the study conducted in [17]; it was then adapted to the geographical structure of the optimization model. The lower boundary of temperature difference between the geothermal heat source and the ambient temperature is assumed at 170 K while the regions are categorized according to the required drilling depth. The first category includes the sites, where the desired temperature difference is reached at depths of lower than 4000 m; therefore, ΔT (4000 m) ≥ 170K. For the second category, the condition is ΔT (4000 m≤ z≤6000 m) ≥ 170K while for the third category, ΔT (6000 m≤ z≤10000 m) ≥ 170K. Table B3.1 shows the derived values for model regions.

Table B3.1: Geographical potential of geothermal electricity production

Region	Δ T=170K at z≤4000 m			ΔT=170K at 4000≤z≤6000 m			ΔT=170K at 6000≤z≤10000 m		
	Δ T (K/km)	Area (km^2)	Q (GW)	Δ T (K/km)	Area (km^2)	Q (GW)	Δ T (K/km)	Area (km^2)	Q (GW)
R1	-	-	-	30	434008	32	23	4205072	250
R2	-	-	-	-	-	-	21	7457340	400
R3	-	-	-	-	-	-	21	3468277	180
R4	-	-	-	-	-	-	21	1327105	68
R5	-	-	-	-	-	-	20	1777819	89
R6	-	-	-	-	-	-	21	298940	15
R7	-	-	-	-	-	-	20	125060	7
R8	-	-	-	-	-	-	23	1409739	80
R9	-	-	-	30	96624	72	26	1226437	80
R10	-	-	-	30	48234	36	25	4478936	274
R11	48	974546	116	32	59423	5	23	155845	10
R12	40	1474915	146	31	684324	53	23	1017444	61
R13	62	427921	68	31	504928	38	23	1121616	63
R14	80	1876196	364	30	53337	4	24	120451	7
R15	-	-	-	-	-	-	25	2362066	147
R16	-	-	-	-	-	-	25	2746953	173
R17	-	-	-	-	-	-	23	4359448	249
R18	-	-	-	-	-	-	24	2353400	138
R19	-	-	-	-	-	-	24	1141403	68
R20	-	-	-	-	-	-	22	1799425	97
R21	-	-	-	-	-	-	22	502486	28
R22	-	-	-	-	-	-	22	997176	54
R23	-	-	-	-	-	-	21	5223652	278

R24	-	-	-	-	-	-	22	1678316	93
R25	-	-	-	-	-	-	22	389654	22
R26	-	-	-	-	-	-	22	1485121	81
R27	-	-	-	-	-	-	24	1329189	81
R28	-	-	-	33	285	0.023	24	1165797	70
R29	-	-	-	29	126375	9	26	590633	37
R30	-	-	-	-	-	-	24	742019	47
R31	-	-	-	-	-	-	22	2342793	141
R32	35	268869	23	30	2498153	193	26	1102490	71
R33				29	8063	1	25	4738061	288
R34	34	134041	11	31	3203213	246	25	3628765	228
R35	36	188254	17	31	1089178	83	24	2611368	153
R36	-	-	-	-	-	-	22	2755907	147
R37	-	-	-	-	-	-	20	826463	41
R38	39	1443851	139	31	541824	42	23	632236	38
R39	43	1551706	161	31	335006	26	23	152929	9
R40	47	5555164	616	31	855072	68	25	274498	17
R41	46	3559150	408	32	826047	65	22	610189	35
R42	38	126	0.012	-	-	-	24	6751197	415
R43	-	-	-	31	114	0.009	20	61561	3
R44	35	316854	28	32	778525	63	24	229933	13
R45	-	-	-	31	478526	38	26	350351	23
R46	35	96260	8	32	538748	43	21	233749	12
R47	-	-	-	30	58384	4	24	112682	7
R48	-	-	-	30	3528	0.27	23	389148	25
R49	41	188461	19	30	111795	8	23	426353	24
R50	39	29434	3	30	90777	7	20	167716	9
World	14	18085748	2127	15	12990483	1104	22	81250136	4696

B4 Electricity demand

Proportion of the minimum electricity demand to the peak load is given in Table B4.1 for selected countries and model regions. Increase of this proportion represents the smoothed pattern of an aggregated ELP compared to the ELP of a single country or a model region.

Table B4.1: Proportion of minimum electricity demand to peak load

Model region/Country/Continent	Annual Min / Annual Max
ZA	0.53
R15	0.54
R16	0.54
R17	0.54

R18	0.54
R19	0.53
R20	0.54
R21	0.53
R22	0.53
R23	0.63
R24	0.53
R25	0.53
R26	0.53
R27	0.54
R28	0.53
AFR	0.68
GB	0.36
IT	0.38
DE	0.43
FR	0.36
RO	0.44
GR	0.33
SI	0.28
AT	0.41
PL	0.44
CZ	0.44
ES	0.40
PT	0.38
NO	0.28
SE	0.30
FI	0.36
IS	0.42
R44	0.44
R45	0.46
R46	0.44
R47	0.40
R48	0.41
R49	0.32
R50	0.36
EU	0.44
CO	0.39
R1	0.39
R2	0.39
R3	0.39
R4	0.39
R5	0.39

R6	0.39
R7	0.40
SAM	0.48
World	0.58

C Model calibration

Changes have been made in the underlying assumptions of the electricity system optimization model through the calibration process in order to minimize the deviation of model's results from the real net generation mix of the year 2000. These are represented in Table C.1.

Table C.1: Underlying assumptions of calibrated model

Model region	Demand scaled to match to real net power generation	AVF COAL-ST (% of max. capacity)	AVF LIG-ST (% of max. capacity)	Fuel price ratio Gas to oil / Coal to oil
R1	√	84	85	0.80/0.36
R2	√	84	85	0.80/0.36
R3	-	84	85	0.80/0.36
R4	√	84	85	0.80/0.36
R5	√	63	85	0.80/0.36
R6	√	84	85	0.80/0.36
R7	√	84	85	0.80/0.36
R8	√	84	85	0.80/0.36
R9	-	84	85	0.80/0.36
R10	-	75	77	0.80/0.36
R11	-	84	85	0.80/0.36
R12	√	84	85	0.80/0.36
R13	√	70	85	0.80/0.36
R14	-	84	85	0.80/0.36
R15	-	84	85	1.5/0.36
R16	-	65	85	1.4/0.36
R17	√	84	85	0.80/0.36
R18	-	84	63	0.80/0.36
R19	-	84	85	0.80/0.36
R20	√	84	85	0.80/0.36
R21	√	84	85	0.80/0.36
R22	√	84	85	0.80/0.36
R23	-	84	85	0.80/0.36
R24	√	84	85	0.80/0.36
R25	√	84	85	0.80/0.36
R26	-	50	85	1.0/0.36
R27	-	50	85	0.80/0.36
R28	-	84	85	0.80/0.36
R29	√	84	85	0.80/0.36
R30	√	84	85	1.0/0.36
R31	-	84	85	1.0/0.36
R32	√	60	85	0.80/0.36
R33	√	70	84	1.2/0.36
R34	-	65	70	1.3/0.36
R35	-	65	70	1.3/0.36
R36	√	70	84	1.2/0.36
R37	-	75	50	1.0/0.36
R38	√	84	85	0.80/0.36
R39	√	84	85	0.80/0.36
R40	√	84	85	0.80/0.36
R41	√	84	85	0.80/0.36
R42	-	84	62	0.80/0.36

R43	-	84	53	0.80/0.36
R44	√	70	85	0.80/0.36
R45	-	70	75	0.80/0.36
R46	√	70	85	0.88/0.36
R47	-	70	85	0.88/0.36
R48	√	84	85	0.80/0.36
R49	√	70	85	0.80/0.36
R50	-	70	85	0.88/0.36

D Techno-economic parameters of power plants

Development of techno-economic parameters of power plants over a time horizon from 2020 to 2040, are determined based on data from [24, 49]; these parameters are represented in Table D.1 and Table D.2; projected fuel prices are given in Table D.3.

Table D.1: Investment costs of new power plants (All costs are in US$ (2008).)

Technology	Investment 2020 ($/kW$_{el}$)	Investment 2025 ($/kW$_{el}$)	Investment 2030 ($/kW$_{el}$)	Investment 2035 ($/kW$_{el}$)	Investment 2040 ($/kW$_{el}$)
BIO-ST	3426	3426	3426	3426	3426
COAL-ST	1596	1596	1596	1596	1596
GAS-GT	471	471	471	471	471
GAS-CC	630	630	630	630	630
GEO-ST	4000	4000	4000	4000	4000
LIG-ST	1828	1828	1828	1828	1828
OIL-CC	630	630	630	630	630
OIL-GT	567	567	567	567	567
SOL-CSP	3678	3240	2802	2616	2429
SOL-PV	5751	4703	3655	3412	3168
URA-ST	2283	2283	2283	2283	2283
WIND	1036	1016	995	975	955
WIND-O	1767	1736	1706	1675	1645

Table D.2: Conversion efficiency of new power plants

Technology	Efficiency 2020 (%)	Efficiency 2025 (%)	Efficiency 2030 (%)	Efficiency 2035 (%)	Efficiency 2040 (%)
BIO-ST	40	41	41	41	41
COAL-ST	46	46.5	47	47	47
GAS-GT	39	39.5	40	40	40
GAS-CC	61	61.5	62	62	62
GEO-ST	20	20	20	20	20
LIG-ST	45	45	45	45	45
OIL-CC	54	54	55	55	55
OIL-GT	34.5	35	35	35	35
SOL-CSP	25	25	25	25	25
SOL-PV	20	20	20	20	20
URA-ST	34	34	34	34	34
WIND	96	96	96	96	96
WIND-O	93	93	93	93	93

Table D.3: Projection of fossil fuel prices (All costs are in US$ (2008).)

Technology	2020 ($/MWh$_{th}$)	2025 ($/MWh$_{th}$)	2030 ($/MWh$_{th}$)	2035 ($/MWh$_{th}$)	2040 ($/MWh$_{th}$)
Crude oil	78.40	84.90	91.39	94.64	94.64
Hard coal	16.20	16.72	17.14	17.49	17.49
Lignite	5.22	5.38	5.52	5.63	5.63
Natural gas	52.17	55.34	59.31	61.29	61.29
Uranium	3.08	3.08	3.08	3.08	3.08

Nomenclature

Abbreviations

AC	Alternative Current
AFR	Africa
AM	America
AUS	Australia
B	Base
BIG/GT	Biomass Integrated Gasification Gas Turbine
BP	Backup Power
CARMA	Carbon Monitoring for Action
CC	Combined Cycle
CSAM	Central and South America
CSP	Concentrating Solar Power
DC	Direct Current
DP	Dynamic Programming
ED	Economic Dispatch
el	Electrical
ELCYS	Electrolysis Systems
ELP	Electrical Load Profile
ENTSO-E	European Network of Transmission System Operators for Electricity
EU	Europe
FCELL	Fuel cell
Fix	Fixed cost
FRES	Fluctuating Renewable Energy Sources
FLH	Full Load Hours
GAMS	General Algebraic Modeling System
GAOR	Ground Area Occupation Ratio
GGI	Greenhouse Gas Initiative
GH_2	Gasified Hydrogen
GHG	Greenhouse Gas
GIS	Geographic Information System

GMT	Greenwich Mean Time
GT	Gas Turbine
HHV	High Heat Value
HP	High Peak
HVDC	High Voltage Direct Current
IEA	International Energy Agency
IGCC	Integrated Gasification Combined Cycle
IIASA	International Institute for Applied Systems Analysis
Inv	Investment cost
IPCC	Intergovernmental Panel on Climate Change
IPOM	Investment and Production Optimization Model
ISCCP	International Satellite Cloud Climatology Project
LCOE	Levelised Cost of Electricity
LDC	Load Duration Curve
LH_2	Liquefied Hydrogen
LP	Linear Programming
LR	Lagrangian Relaxation
M	Mid
Max	Maximum
MILP	Mixed Integer Linear Programming
Min	Minimum
MIP	Mixed Integer Programming
NAM	North America
NCAR/NCEP	National Center for Atmospheric Research and National Center for Environmental Prediction
NTC	Net Transfer Capacity
OECD	Organization for Economic Co-operation and Development
OHL	Overhead Line
O&M	Operation and Maintenance
OPM	Operation Optimization Model
P	Peak
PJM	Pennsylvania, New Jersey, Maryland Interconnection
PS	Pumped Storage

PV	Photovoltaic
R	Region
RMS	Root Mean Square
RUS	Russia
SAM	South America
sc	Start-up costs
SeaWiFS	Sea-viewing Wide Field-of-view Sensor
SRES	Special Report on Emission Scenarios
SSIDS	Surface Solar Irradiation Data Set
ST	Steam Turbine
Std	Standard deviation
Std-var	Standard deviation of hourly variations
th	Thermal
TTC	Total Transfer Capacity
TRM	Transmission Reliability Margin
TSO	Transmission System Operator
UC	Unit Commitment
UCTE	Union for the Co-ordination of Transmission of Electricity
URA	Uranium
Var	Variable Cost
WRDC	World Radiation Data Center
WWA	World Wind Atlas

Main symbols

Sets

i	Index of technologies in LPIPOM
j	Index of power generation units in MILPOPM
PrFRES	Renewable power plants including wind onshore, wind offshore, PV, CSP
PrOt	Other generation processes (e.g. electrolysis)
PrPG	Power generation technology
PrSto	Energy storage Technology
PrTr	Energy transport technology

PrWIND	Onshore and offshore wind turbines
t	Index of time steps (in hours)
tm	Index of time steps (in hours)
x	Index of model regions
y	Index of model regions

Model Parameters

A	Variable O&M costs at minimum output of power plant [$/h]
a	Share of fluctuating renewable energies in total electricity demand [-]
AVF	Availability factor [-]
b	Share of wind power in total electricity from FRES [-]
C0	Previously installed power plant capacity [MW_{el}]
C0St	Previously installed storage reservoir capacity [MWh_{el}]
C0Stin	Previously installed storage input capacity [MW_{el}]
C0Stout	Previously installed storage output capacity [MW_{el}]
co2Up	CO_2 emissions upper limit [ton]
CTr0	Previously installed transport capacity [MW_{el}]
cUp	Capacity upper limit of power plant technology [MW_{el}]
cUpSt	Capacity upper limit of storage reservoir [MWh_{el}]
cUpStin	Capacity upper limit of storage input [MW_{el}]
cUpStout	Capacity upper limit of storage output [MW_{el}]
cUpTr	Capacity upper limit of transport interconnection [MW_{el}]-[MW_{H2}]
D	Hourly electricity load [MW_{el}]
F	Specific variable O&M costs between Pmin and Pmax of power plant [$/$MWh_{el}$]
k^{Fix}	Specific fixed O&M costs [$/($MW_{el}$.a)]-[$/(MW_{el}.a)/km]-[$/$MWh_{el}$]
k^{Inv}	Specific annual investment costs [$/($MW_{el}$.a)]-[$/(MW_{el}.a)/km]-[$/$MWh_{el}$]
k^{Var}	Specific variable O&M costs [$/$MWh_{el}$]-[$/MWh_{th}]
kCO2e	CO_2-price [$/ton]
kemf	Emission factor of power plant [ton/MWh_{th}]
mdt	Minimum down time of power plant [h]
mut	Minimum up time of power plant [h]

Pmax	Maximum output of power plant [MW_{el}]
Pmin	Minimum output of power plant [MW_{el}]
r(x,y)	Distance between regions x and y [km]
ramp	Ramp rate of committed or non-committed capacity [% of maximum capacity/h]
rampc	Ramp rate of committed capacity [% of maximum capacity/h]
rampnc	Ramp rate of non-committed capacity [% of maximum capacity/h]
ResLoad	Hourly electricity load minus power produced from FRES [MW_{el}]
SC	Specific start-up costs of power plant [$/$MW_{el}$]
Supim	Wind power capacity factor [-]; Hydropower capacity factor [-]; Solar irradiation [W/m^2]
T	Final time step [h]
t0	Initial time step [h]
tf	Last time step of simulated seasonal period [h]
ts	First time step of simulated seasonal period [h]
Trl	Transport losses [% of transported energy /km]
W	Weighting factor of simulated time steps [-]
η	Conversion Efficiency [-]
α	Constant parameter [-]
β	Constant parameter [-]

Model Variables

C	Total generation capacity [MW_{el}]-[MW_{H2}]
CN	Newly installed generation capacity [MW_{el}]-[MW_{H2}]
CNSt	Newly installed storage reservoir capacity [MWh_{el}]-[MWh_{H2}]
CNStin	Newly installed storage input capacity [MW_{el}]-[MW_{H2}]
CNStout	Newly installed storage output capacity [MW_{el}]-[MW_{H2}]
CNTr	Newly installed transport capacity [MW_{el}]-[MW_{H2}]
CSt	Total storage reservoir capacity [MWh_{el}]-[MWh_{H2}]
CStin	Total storage input capacity [MW_{el}]-[MW_{H2}]
CStout	Total storage output capacity [MW_{el}]-[MW_{H2}]
CTr	Total transport capacity [MW_{el}]-[MW_{H2}]
delta	Output power between Pmin and Pmax of a power generation unit [MW_{el}]

E^{in}	Hourly input energy (inflow) [MW_{th}]-[MW_{el}]
E^{out}	Hourly output energy (outflow) [MW_{el}]-[MW_{H2}]
$E^{out\text{-}d}$	Shut down capacity [MW_{el}]
$E^{out\text{-}up}$	Started capacity [MW_{el}]
EL	Wasted energy (energy loss) [MWh_{el}]
EP	Excess electricity production [MWh_{el}]
ESt	Stored energy [MWh_{el}]-[MWh_{H2}]
ESt^{in}	Hourly input energy (inflow) to storage system [MW_{el}]-[MW_{H2}]
ESt^{out}	Hourly output energy (outflow) from storage system [MW_{el}]-[MW_{H2}]
EStints	Interseasonally stored energy [MWh_{el}]-[MWh_{H2}]
EStTot	Total stored energy [MWh_{el}]-[MWh_{H2}]
ETr^{in}	Hourly input energy (inflow) to transport interconnection [MW_{el}]-[MW_{H2}]
ETr^{out}	Hourly output energy (outflow) from transport interconnection [MW_{el}]-[MW_{H2}]
flex-down	Ramp-down limit of power plant technology [MW_{el}]
flex-up	Ramp-up limit of power plant technology [MW_{el}]
k^{st}	Start-up costs in MILPOPM [$/h]
obj	Total system operation costs (objective function in MILPOPM) [$]
s	State variable of a power generation unit to indicate whether it is committed or not: 1 if committed, 0 if not
sc	Total technology start-up costs in LPIPOM [$]
windcurt	Hourly discarded wind power [MW_{el}]
z	Total system investment, fixed, and operation costs (objective function in LPIPOM) [$]

Other symbols

Af	Annuity factor [-]
Area	Swept area of turbine rotor blades [m^2]
CO2P	CO_2-price [$/ton]
c_p	Power coefficient of wind turbine [-]
$c_{p,Betz}$	Lanchester-Betz-Joukowsky limit [-]
$c_{p,max}$	Maximum power coefficient of wind turbine [-]
CF_{Wind}	Wind power capacity factor or normalized output power [-]

ef	Emission factor of power plant [ton/kWh_{th}]
ELIFE	Economic lifetime [a]
FIXOM	Specific fixed operation and maintenance costs [\$/(kW_{el}.a)]
FLH	Annual full operating hours [h/a]
fP	Fuel price [\$/kWh_{th}]
GP	Gross hydropower potential [TWh_{el}/a]
H_x	Hub height [m]
H_{Ref}	Reference Height [m]
I_{Diff-H}	Diffuse horizontal solar irradiation [W/m^2]
I_{Dir-H}	Direct horizontal solar irradiation [W/m^2]
I_{Dir-N}	Direct solar irradiation on a surface perpendicular to the beam [W/m^2]
$I_{Dir,ts}$	Direct solar beam on a tilted surface [W/m^2]
I_{GH}	Global horizontal solar irradiation [W/m^2]
i_{inc}	Surface-solar incidence angle [°]
INV	Specific investment costs [\$/kW_{el}]
l	Time interval between Wed and Wed-i [h]
LCOE	Levelised cost of electricity [\$/kWh_{el}]
m	Time interval between Wed and Wed-j [h]
P_R	Nominal power of wind turbine [W_{el}]
$P_{T,el}$	Output power of wind turbine [W_{el}]
P_{Wed}	Electricity load on Wednesday (unknown) [MW_{el}]
P_{Wed-i}	Electricity load on Wednesday (known) [MW_{el}]
P_{Wed-j}	Electricity load on Wednesday (known) [MW_{el}]
P_{Wind}	Energy content of wind [W_{el}]
r	Discount rate [%/a]
t	Time step [h]
v	Wind speed upstream the rotor (at hub height) [m/s]
v_{cut-in}	Cut-in wind speed [m/s]
$v_{cut-out}$	Cut-out wind speed [m/s]
v_R	Rated wind speed [m/s]
v_{Ref}	Wind speed at reference height [m/s]
VAROM	Specific variable operation and maintenance costs [\$/kWh_{el}]

z_0	Roughness length of the terrain [m]
β_s	Solar altitude [°]
ρ_{air}	Density of air [kg/m^3]
η_T	Conversion efficiency of wind turbine [-]
η	Conversion efficiency [-]

Units

a	year
E	Exa, 10^{18}
G	Giga, 10^9
h	hour
J	Joule
K	Kelvin
k	kilo, 10^3
kg	kilogram
Mio	Million, 10^6
m	meter
m	mili,10^{-3}
P	Peta, 10^{15}
ppmv	Part per million volume
s	second
T	Tera, 10^{12}
t CO_2-eq	ton CO_2 equivalent
W	Watt
W_p	Watt-peak
Wh	Watt-hour

List of figures

List of tables